Development and modification of glass membranes for aggressive gas separations

Doctorial Thesis

by

Arne Lindbråthen

Submitted in partial fulfilment of the requirements for the academic degree:

Doktor Ingeniør

Norwegian University of technology and science (NTNU)

Faculty of Natural Sciences and Technology

Department of Chemical Engineering

Trondheim, Norway

December 2004

ABSTRACT

Chlorine as a chemical is widespread in industry and found in a great variety of processes ranging from water purification to plastic production. In this thesis, a magnesium production factory was chosen as an example because it involved both chlorine - air separation and hydrogen –hydrogen chloride separation.
Previously, various types of membrane materials have been tested out for their applicability in the chosen process. The materials previously tested either lacked sufficient membrane performance or sufficient membrane stability. As an attempt to improve both the membrane performance and stability, glass membranes are used in this thesis.
Glass membranes are prepared from a borosilicate glass, via a phase separation followed by an acid leaching route. By choosing the appropriate phase separation temperature and acid to glass ratio, the membrane can be produced with an average pore diameter of 2 nm (or 4 nm).
However, the 2 nm average pore size is still too large to separate gases with separation selectivities beyond the selectivities predicted from Knudsen diffusion theory. If the pores are narrowed, the selectivity may be raised while the flux hopefully is maintained. The narrowing of the pores was done by a silane coupling to the surface OH-groups on the glass. The silane coupling agent is of the dimethyl-acyl-chlorosilane type, where the length of the acyl chain varies from 1 carbon up to 18 carbons. Glass fibres are also tested in this work, which are produced without phase separation and their average pore size is smaller than the surface-modified glasses.

To be able to compare the performance of the various membranes, permeance measurements are performed and these measurements are evaluated by the separation power (product of the selectivity and the permeability of the fastest permeating compound). Because of the harsh chlorine or hydrogen chloride environment, to which the membranes are exposed in this work, the membrane stability is at least as important s factor as the perm-selectivities. To evaluate this, both short- and long-term aggressive gas exposures are performed using a special designed durability

chamber. From the combination of the perm-selectivities and the durability tests, the following conclusions may be drawn (evaluated at 30°C and 1 bar):
Firstly, the pure glasses have a relatively poor stability (for chlorine gas) and the perm-selectivity is too low (for both separations in question). Secondly, the C8 and C12 modified glass membranes have a relatively satisfactory perm-selectivity for chlorine separation, but the durability in chlorine is poor. Thirdly, the long-chained C18 modified glass membrane has a relatively satisfactory perm-selectivity but a fair to low chlorine stability. If the C18 membrane is applied in the hydrogen chlorine separation the perm-selectivity is a bit low, but the stability is sufficient. However, this membrane is the best choice for a low temperature HCl selective membrane.
Finally, to improve the chlorine stability, a perfluorinated version of a C10 modification is tried out. This membrane has excellent chlorine stability, and the perm-selectivity is fair. This membrane is the best choice for a chlorine selective membrane.
The stability of the fibres is comparable to that found for the pure glass tubes. However, the permeabilities in the glass fibres are several orders of magnitude lower than for the glass tubes. The pore size in the fibre is so narrow that separation occurs according to a molecular sieving mechanism. The mounting of the fibres into a lab-sized module is tricky and the permeabilities are at the border of detection, so the results obtained here should only serve as trends.

ACKNOWLEDGEMENTS

First of all, I would like to thank my supervisor professor May-Britt Hägg for first introducing me to membrane technology, then employing me as a membrane researcher and finally, for persuading me to start on my doctoral degree. Your unquestioned believe in me has been an inspiration over all these years.

Secondly, sincere thanks go to Dr. ing. Magnar Ottøy, for being my assistant supervisor, for being my office mate in Porsgrunn and for many fruitful detailed membrane discussions.

I also appreciate the excellent collegial relations present in the MEMFO group. Special thanks to Dr. ing. stipendiate Jon Arvid Lie for joining in on the move of location from Porsgrunn to Trondheim, without him the moving to Trondheim would have been a tough task. A special thank also goes to Ph.D. student David Grainger for proof reading this thesis. It is mostly appreciated to have a native English speaking guy to turn to in cases of language doubts.

Thanks also to the glass blower at Norsk Hydro Research centre in Porsgrunn, Mr. Sørensen, for assembling excellent modules and the durability chamber from my rather vague drawings.

Finally, thanks goes to Prof Yazawa and Dr. Koraoka (currently at Himeji Institute of Technology, Himeji, Japan and at the Faculty of Maritime Sciences at the Kobe University, Kobe, Japan, respectively) for preparing most of the membranes (except for some of the C1 and C18 membranes and all of the C18 (low coverage) and Pf-C10(2nm) surface modified glass membranes,which I prepared during my research stay in Japan), for fruitful discussions and for kindly receiving and hosting me during my research stay. I mostly appreciate the special training I got in making glass membranes and to surface modify them, and the way they integrated me into their research group.

LIST OF SYMBOLS

Notation:

A = Total surface area according to the BET-method [m^2/mol]
a = Energy fraction factor [-]
a_m = Molecular cross sectional area
A(T) = Temperature dependent adsorption [cm^3(STP)/g]
C = Constant
C_R = Resistance coefficient [kg/(s m^2)]
c = Constant in the BJH-method.
c = Concentration [mol/m^3]
D_{ab} = Diffusion coefficient [m^2/s]
dc/dx = Concentration gradient [mol/(m^3·m)]
d_p = Average pore diameter [m]
Ea = Activation energy [J/mol]
E = Energy barrier for surface migration [J/mol]
e = Probability factor [-]
g_d = Probability factor[-]
h = Planck's constant [$6.63 \cdot 10^{-34}$ J s]
k = Boltzmann's constant [$1.38 \cdot 10^{-23}$ J/K]
L = Avogadro's constant [$6.03 \cdot 10^{23}$ 1/mol]
l = Membrane thickness [m]
J_a = Flux [mol/(m^2 s)]
Mw = Molecular weight [kg/mol]
N = Molar flux [mol/(m^2 s)]
n^a = Amount adsorbed [mol]
p = Partial pressure [bar]
P = Permeability [m^3 (STP) m/(m^2 bar h)]
P/l = Permeance [mol/(m^2 Pa s) or m^3 (STP) /(m^2 bar h)]
PD = Permeability decay [-]
q = Adsorption enthalpy [J/mol]
Q = Partition function [-]
R = Gas constant [8.314 J/(mol K)]
r = Radius [m]
r = Rate of partial desorption (or hopping rate) [mol/(m^2 s)]
S = Entropy [J/(mol K)]
SP = Separation power [m^3 (STP) m/(m^2 bar h)]
S_W = Specific surface area [m^2/kg]
T = Temperature [K]
t = Multilayer thickness [m]
V = Volume [m^3]
x = Amount adsorbed [mol/kg]
z = Net flux direction [m]

Greek letters

α = Selectivity [-]
Δ = Denotes a finite difference
θ = Surface coverage [-]
θ = Time lag [s]
λ = Surface free mean path [m]
$\bar{v}$ = Average molecular velocity [m/s]
ν = Jump frequency factor [1/s]
ν^l = Molar volume of liquid condensate [m^3/mol]
ρ = Density [kg/m^3]
σ = Surface tension of liquid [J/m^2]
τ = Tortuosity [-]
ψ = Relative contribution of the SSF to the total flow. [-]

Subscripts

A,a = General compound
app = Apparent
d = Diffusion
k = Kelvin
K = Activated Knudsen mechanism
Kn = Knudsen mechanism
l = Membrane outlet (low pressure side)
i = Gas type
m = Monolayer
n = Integer index of pressure decrement.
MS = Molecular sieving
p = Pore
S = Surface
ssf = Selective surface flow
Tot = Total
X = Direction
Z = Direction
0 = Membrane inlet (high pressure side)
0 = Pre exponential term
1 = First principal radius
2 = Second principal radius

Superscripts

o = Saturated
0 = Activated compound

CONTENTS

ABSTRACT II
ACKNOWLEDGEMENTS IV
LIST OF SYMBOLS V
CONTENTS VII
1 INTRODUCTION AND BACKGROUND 1
1.1 Outline of the thesis 1
1.2 Brief introduction to membrane technology 2
1.3 Aggressive gases used in industry 3
1.4 References 5
2 PREPARATION OF GLASS MEMBRANES 6
2.1 Glass materials in general 6
2.1.1 Soda-lime glasses 6
2.1.2 Lead glasses 7
2.1.3 Borosilicate glasses 7
2.2 Microporous glass membranes 8
2.2.1 Phase separation 8
2.2.2 Theory of immiscibility 9
2.2.3 Phase separation in borosilicate glasses 11
2.2.4 Acid leaching 12
2.2.5 Applications for porous glass 13
2.3 Glass hollow fibres 14
2.4 Preparation of porous glass membranes 15
2.4.1 Phase separation 15
2.4.2 Acid leaching 16
2.4.3 Surface modification 16
2.4.4 Modification procedure 17
2.5 References 18
3 TRANSPORT MECHANISMS 20
3.1 General mass transport 21
3.2 Knudsen Flow 22
3.3 Surface diffusion 22
3.3.1 2D-gas model 24
3.3.2 Site-to-site hopping model 25
3.3.3 Liquid-like sliding layer model 26
3.4 Molecular Sieving 26
3.5 Combined mass transfer 27
3.6 References 28

4 MEMBRANE CHARACTERISATION 29
4.1 Background 29
4.2 N_2 adsorption /desorption 30
4.3 Stereology (Microscopy) 36
4.3.1 Scanning electron microscope 36
4.3.2 Atomic force microscope 39
4.4 IR spectroscopy 41
4.5 References 44
5 EXPERIMENTAL 46
5.1 N_2 adsorption 46
5.1.1 Procedure 46
5.2 Stereology analysis 48
5.2.1 Scanning Electron Microscopy 48
Procedure 48
5.2.2 Atomic Force Microscopy 49
5.3 FTIR spectroscopy 49
Procedure 50
5.4 Permeance measurements 50
5.4.1 Pure gas permeances 51
Membrane module design 52
Procedure for pure gas permeance measurements 54
5.4.2 Permeance measurements with simultaneous UV –radiation of the glass membrane tubes 56
Reaction procedure 57
5.4.3 Permeance measurements of the glass fibres 58
Mounting procedure 58
5.4.4 Mixed-gas permeation test 59
Procedure 60
5.5 Sorption measurements 60
5.5.1 Single point adsorption measurement 62
5.5.2 Isotherm measurements 62
5.6 Diffusion coefficient estimation 63
5.7 Membrane gas exposure in durability chamber 64
Gas exposure procedure 64
5.8 References 65
6 RESULTS AND DISCUSSION 66
6.1 Chlorine - air separation 66
6.1.1 Unmodified glass membrane 4 nm average pore size 66
Stereology images 66
FTIR with HATR accessory spectrum 70
Permeance measurement 71
6.1.2 Unmodified glass membrane 2 nm average pore size 72
Pore size distribution from N_2 adsorption 72

Permeance measurements 74
6.1.3 C1 surface-modified glass membrane 75
Permeance measurements 75
Combined chlorine permeance and UV radiation measurements 76
6.1.4 C8 surface-modified glass membrane 78
Permeance measurement 78
6.1.5 C18 surface-modified glass membrane 79
Permeance measurements 79
Knudsen flow in C18 modified glass membrane 81
Combined UV and chlorine reaction 83
FTIR with HATR accessory spectroscopy 88
6.1.6 C18 and C1 surface-modified glass membrane 93
6.1.7 C12 surface-modified glass membrane 95
Permeance measurements 95
6.1.8 Sum-up of the results on the aliphatic surface-modified glass membranes 96
6.1.9 Perfluorinated C10 surface-modified glass membrane (4 nm base) 97
Pore size distribution from N_2 adsorption 98
Elemental analysis 100
FTIR with HATR accessory spectroscopy 101
Permeance measurements 103
6.1.10 Perfluorinated C10 surface-modified glass membrane (2 nm base) 105
Pore size distribution from N_2 adsorption 106
Permeability measurements, pure gases 107
Mixed gas permeation measurements 109
Sorption measurements 110
Temperature dependence of the chlorine adsorption 116
Estimation of the degree of SSF 118
Diffusion coefficient determinations 123
6.1.11 Glass hollow fibre 125
Permeance measurements 125
6.1.12 Sum-up for the chlorine air separation 127
6.2 Hydrogen chloride – Hydrogen separation 131
6.2.1 C18 surface-modified glass membrane (Low surface coverage) 131
Permeance measurements 131
6.2.2 C1+C18 surface-modified glass membrane 135
Permeance measurements 135
6.2.3 Pf-C10 surface-modified glass membrane 135
Permeance measurements 135
6.2.4 Pf-C10 (2 nm) surface-modified glass membrane 137
Sorption measurements 137
Temperature dependence for the HCl adsorption 140
6.2.5 Glass hollow fibre 141
6.2.6 Sum up of the HCl / H_2 –separation 143
6.3 References 145
7 CONCLUSION 146
FURTHER WORK 148
LIST OF APPENDICES 149

1 INTRODUCTION AND BACKGROUND

1.1 Outline of the thesis

In chapter 1 a brief introduction to membrane technology and examples of the widespread use of chlorine as a chemical agent is summarised and given in a separate section of this chapter, followed by a specific industrial example.
Chapter 2 discusses glasses in general, theory of phase separation and the production of both ultramicroporous glass and hollow fibres.
The expected transport mechanisms in porous membranes are discussed thoroughly in chapter 3. In this chapter a newly developed theory of combined transport between the Knudsen and selective surface flows is introduced, in which the degree of selective surface flow, SSF, can be estimated based on the helium permeance and a assumption that SSF and Knudsen flows are additive.
Characterisation of the membrane materials is of crucial importance for the prediction and the understanding of the membrane performance and chapter 4 discusses the theoretical background of the applied techniques. These includes: Liquid N_2 adsorption /desorption, stereology (Atomic force microscopy (AFM), scanning electron microscope (SEM) and field emission scanning electron microscope (FESEM)) and Fourier transform infrared spectroscopy (FTIR).
In chapter 5 the experimental procedures are outlined for the mentioned characterisation techniques and in addition the procedures for the permeance, sorption and gas exposure measurements are given.
In chapter 6 the various membranes are discussed for their suitability both in the chlorine / air and hydrogen chloride / hydrogen separations. These comparisons are based on both the membrane perm-selectivity and the durability.
The conclusion follows where the usefulness of the material tested are discussed both relative to the given example and compared to other possible gas compositions. Finally, tasks that ought to be further investigated are suggested but for which the available time in this project has been too limited to pursuit.
Parts of this thesis have been submitted as two articles for publication in Journal of Membrane Science. These articles are presented in appendix 1 and 2.

1.2 Brief introduction to membrane technology

Membranes are a relatively new technology only a little more than a century old. However, the last few decades there has been a burgeoning interest in membranes for industrial separations. The membrane industry is still a rapidly growing industry, and large scale membrane processes have replaced and are replacing conventional separation processes.

Membrane systems have captured the attention, and increasingly, the markets related to hydrocarbon processing, chemical purification, pharmaceutical and biotechnology processing, water desalination, and liquid-waste processing. Membrane separation has in general, several advantages compared to other separation technologies /Mulder/:

- Separation can be carried out continuously.
- Energy consumption is generally low.
- Membrane processes are easily combined with other separation processes (Hybrid processing).
- Separation conditions are generally milder than competing separation processes.
- Easy to scale-up.
- Membrane properties are variable and can be adjusted.
- No additives are required.

However, there are some drawbacks:

- Short membrane lifetime.
- Low selectivity or flux (or combination).
- Up-scaling is more or less linear.

A membrane being a thin film, acts as a semipermeable barrier between two fluid phases. The separation is possible because the membrane controls the rate of movement of a specific compound from one of the fluid phase into the other. The two phases can be gas- gas and the process is then called gas separation, which is the process discussed here. For the separation to take place, a driving force is required. This diving force is the difference in the chemical potential for a given component

and in gas separation it is manifested by partial pressure difference across the membrane. /Mulder/

The membranes used in gas separation can be classified according to material class, morphology and whether they are dense or microporous. These classification parameters are also important to be able to predict and / or identify the most probable transport mechanism by which the membrane separates. The transport theories are further discussed in chapter 3.
Thus the glass membranes developed in this project can be classified as inorganic symmetric microporous membranes.

1.3 Aggressive gases used in industry

In this thesis, aggressive gases refer to chlorine (Cl_2) and hydrogen chloride (HCl). Chlorine has the main focus in this work, but aspects of HCl separation are also discussed. According to /Ullmann's; vol 8/ the total world wide capacity of chlorine in 1998 was $4.8 \cdot 10^9$ kg annually. It is also stated that in Western Europe, 1995:

- Almost two million jobs were related to chlorine.
- 55% of European chemical turnover depended on chlorine.
- 85% of pharmaceuticals are made using chlorine.
- 98% of the drinking water is purified by chlorination.

These numbers demonstrate the economical importance of the chlorine industry. In this variety of industries there is a great potential for improvement and simplification of the separation processes of chlorine from other gases. The ultimate goal of the current work has been to incorporate membrane technology for recovery of chlorine from various gas mixtures, both for economical and environmental reasons. Special attention has been given to the IG Farben process for magnesium production for historical reasons. A general flow-sheet of the IG Farben process for magnesium production is shown in figure 1 /Hagg (Sep.&Purif. Techn)./ as an example and the chlorine membrane module is added in figure 1.

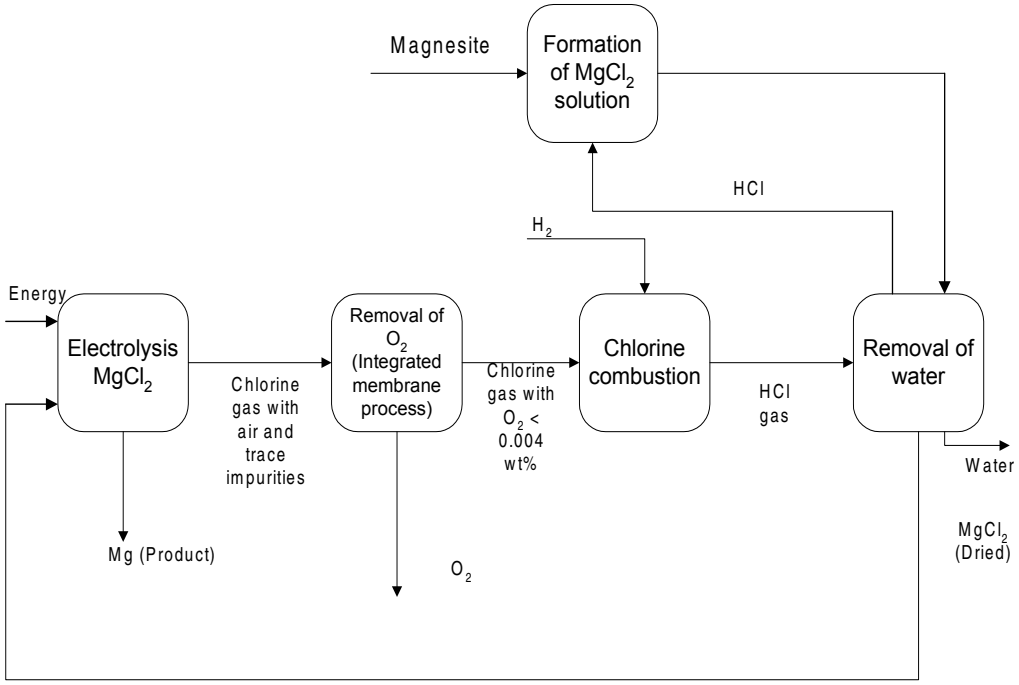

Figure 1: Simplified flow sheet of the IG-Farben Mg production process with integrated membrane modules /Hagg (Sep. &Purif. Techn)./

The IG Farben process includes purification of both Cl_2 and HCl gas and is thus is an excellent example of aggressive gas separation. Here Cl_2 must be separated from air and HCl gas from H_2. The chlorine – air stream contains about 90% Cl_2 by volume, and it is crucial to have most of the oxygen removed (as indicated in figure 1) before Cl_2 is reacted with hydrogen downstream. Likewise, excess hydrogen (about 7% by volume) should be recovered from the gas stream after the HCl (dry gas) is formed. /Ullmann's; vol 20/ For the chlorine separation a temperature around 80°C is preferred, but down to 30°C is acceptable. The temperature in the gas stream after HCl is formed is very much higher (300-400 °C), hence the separation could theoretically be performed at very high temperature. These process conditions indicate very clearly the demands that have to be met for an efficient membrane separation material; likewise it indicates that the transport mechanisms which will be governing the two basic separations (Cl_2 – air and HCl – H_2) will be very different. Previously, different membrane materials were tested out for their suitability in chlorine separation. These materials include: Teflon®, PDMS, Fluorel®, Carbon molecular sieves and glass membranes. The permeabilities and durability of these materials are reported by /Hägg; vol 170/, /Hägg; vol 177 / and /Eikeland et al/.

Based on the findings in these works the focus was set on glass membranes and optimization of the material for the separations in question.

1.4 References

Eikeland M. S. et al.: "Durability of Poly(dimethylsiloxane) When Exposed to Chlorine Gas", J. of Applied Polymer Sci., vol. 85, 2458-2470 (2002)

Hägg, M.-B.: "Membrane Purification of Cl_2 Gas I. Permeabilities as a Function of Temperature for Cl_2, O_2 N_2, H_2 in Two Types of PDMS Membranes", J. Membrane Sci., 170, 2000, 173-190.

Hägg, M.-B.: "Membrane Purification of Cl_2 Gas II. Permeabilities as a Function of Temperature for Cl_2, O_2 N_2, H_2 and HCl in Perfluorinated, Glass and Carbon Molecular Sieve Membranes", J. Membrane Sci.,177, 2000, 109-128.

Hägg, M.-B.: “Purification of chlorine gas with membranes- an integrated process solution for magnesium production”, Sep. & Purif. Tech., 21, (2001), 261-278

Mulder, M.: “Basic Principles of Membrane Technology” 2nd ed., Kluwer Academic publishers, 1996.

Ullmann's Encyclopedia of Industrial Chemistry: "Chlorine", Vol. 8, 6.ed. Wiley-VCH, 2000, 265-270.

Ullmann's Encyclopedia of Industrial Chemistry: "Magnesium", Vol. 20, 6.ed. Wiley-VCH, 2002, 315-325.

2 PREPARATION OF GLASS MEMBRANES

2.1 Glass materials in general

Glass as a material has been known to Humans since ancient times. Glass materials can be formed by natural "processes" such as volcano eruptions, meteorite crashes and lightning. When glass is referred to as a material, it is a collective term for an infinite number of different materials /Pfaender /.

Many definitions of glass exist: "Glass is an inorganic product of melting, which when cooled without crystallisation assumes a solid state" or alternatively "a frozen liquid is called glass"/Pfaender /.

Glass can consist of almost the entire periodical system of elements but some elements are more frequently present, as oxides of silicon, boron, germanium, phosphorous and arsenic. In the following sections the most common types of glass are listed and described briefly.

2.1.1 Soda-lime glasses

A typical composition of a soda-lime glass is 71-75 wt% SiO_2 (in the form of sand), 12-16 wt% Na_2O (in the form of soda ash) and 10-15 wt% CaO (in the form of limestone).

These glasses are by far the most industrially produced glasses and are used for bottles, jars, drinking glasses and window glass. These glasses have several chemical and physical advantages such as good light transmission that makes them very suitable as flat glass used in windows. In addition, having a smooth and nonporous surface these glasses are excellent containers for food and drinks.

These glasses have, in general, a high value of the thermal expansion coefficient; thus the resistance to sudden temperature changes is relatively poor. /Pfaender /

Figure 2 gives a 2-D sketch of the lattice of SiO_4 arrangements in: crystal structure, fused silica and sodium silicate glass /Pfaender /.

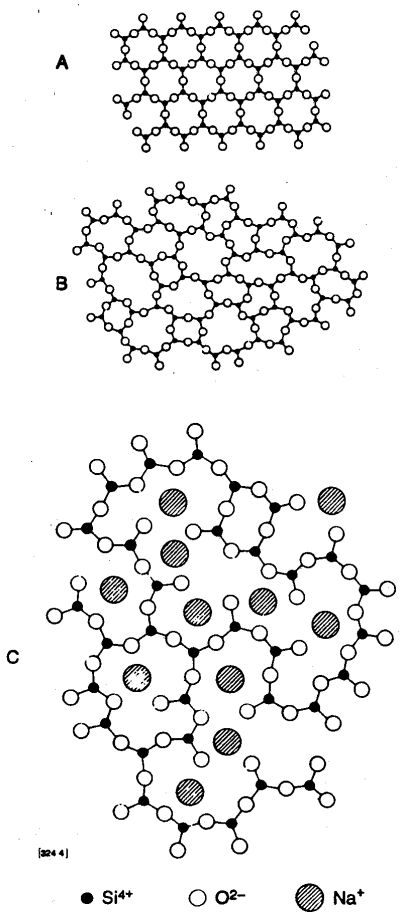

Figure 2: SiO_4 lattice arrangement in: A) crystal structure, B) fused silica and C) sodium silicate glass. The fourth oxygen - silicon bond is pointing towards or away from (alternately) the reader. /Pfaender /

2.1.2 Lead glasses

If a larger part of the lime in soda-lime glasses is replaced by lead oxide, the resulting glass is popularly called lead crystal. Such glass contains typically 54-65 wt% SiO_2, 18-38 wt% PbO, 13-15 wt% Na_2O or K_2O and various other oxides. Glasses with a lead content less than 18wt % PbO are called crystal glass.
These glasses are used as drinking glasses, vases, bowls or decorative items /Pfaender /.

2.1.3 Borosilicate glasses

This group has a higher percentage of SiO_2 than the soda-lime and lead glasses. The typical composition for borosilicate glass is as follows: 70-80 wt% SiO_2, 7-13 wt% B_2O_3 (boron oxide), 4-8 wt% Na_2O (or K_2O) and 2-7 wt% Al_2O_3 (Aluminum oxide). These glasses have a high resistance to chemical corrosion and temperature changes.

Pyrex® glass, used in any chemical laboratory, is an example of a borosilicate glass. It is also found in casserole and baking dishes /Pfaender /.
Since the glass membranes are synthesized from a borosilicate precursor, more details are given in the following chapters.

2.2 Microporous glass membranes

This section discusses the theory governing phase separation and acid leaching in borosilicate glass. Several applications for microporous glasses are also presented.

2.2.1 Phase separation

There are two types of phase separation originating from stable and metastable immiscibility.
The stable immiscibility occurs when the glass separates into two or more distinct phases at a temperature higher than the liquidus* temperature. When such a phase-separated glass is cooled, the resulting glass shows distinct regions of different compositions. These manifest themselves as milkiness in the cooled glass /Lewis (ed.)/.
On the other hand metastable immiscibility occurs at temperatures below the liquidus temperature. It is the metastable immiscibility that is important in the production of microporous glass membranes. Figure 3 explains the difference between stable and metastable immiscibility for phase separation in the CaO-SiO_2 (a) and NaO_2-SiO_2 (b) systems respectively.

*The liquidus temperature is the multicomponent equivalent to the melting temperature.

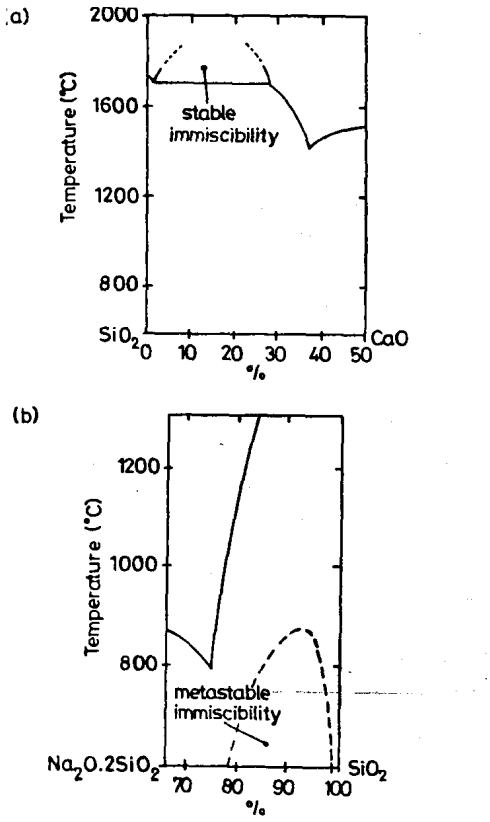

Figure 3: Phase separation in the CaO-SiO_2 (a) and Na_2O-SiO_2(b) systems. (data extracted from /Phillips and Muan/, /Kracek/, /Haller et al./ and published by /Lewis (ed.)/)

2.2.2 Theory of immiscibility

In general, if the free energy change of mixing is greater than the sum of the free energy for each phase isolated, then the system will tend to phase separate. Greater in this context means a larger negative value.

A simplified view of this concept is that in order to get phase separation of the glass, the temperature has to be lower than a (system given) critical temperature, and any natural occurring local deviation in the composition of the glass has to be large enough so that an internal energy barrier is passed.

More technically, if a binary mixture of component X and Y exists at a temperature above the critical temperature then a free energy composition curve as indicated in figure 4a) results. Here the melt will be uniform and as a single phase because of the balancing of the decrease in the energy of the system due to increasing order and the increase in energy due to disordering. The increase in the energy due to disordering is temperature dependent. As indicated in figure 4a), if an inhomogeneity Ci

develops in a melt of composition C_0 then the change in free energy will be given as the gap between the tangent to the curve (tangent at C_0) and the energy curve at point C_i. This gap is called ΔF in figure 4a). If ΔF is located below the energy curve then ΔF >0 and no demixing will occur. In general, if $\delta^2F/\delta C^2 > 0$ then ΔF>0 for all points on the curve. /Lewis/

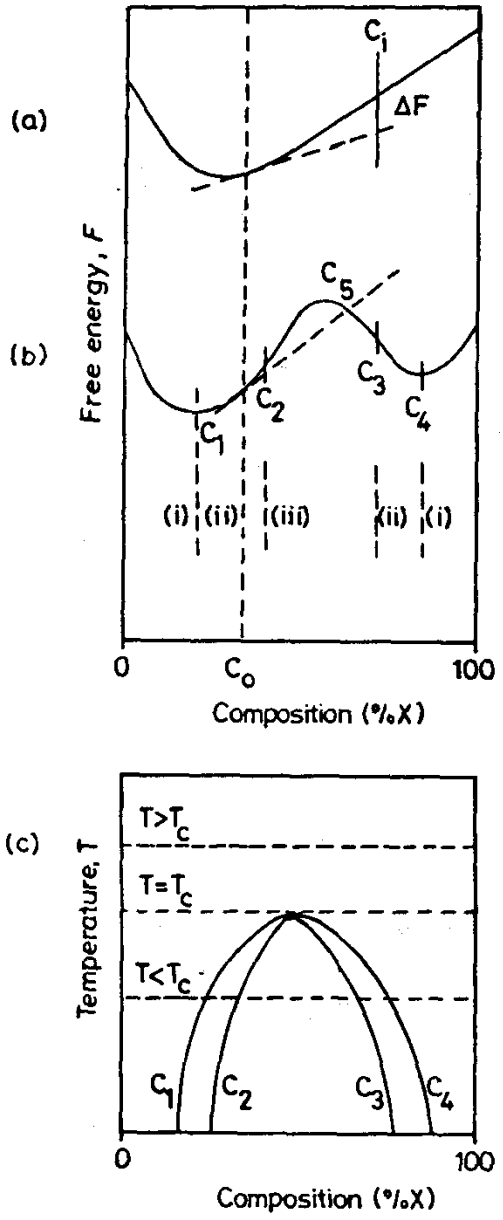

Figure 4: Free energy -composition curve for a binary system; where a) corresponds to a temperature above the critical temperature Tc. b) indicates a typical behaviour below the critical temperature. c) gives the corresponding temperature composition curve for the same system. /Lewis (ed.)/

If the temperature is reduced so that T <Tc, then the energy curve will be of the form presented in figure 4b). This curve can be divided into three regions /Lewis/:
For compositions $C_0<C_1$, $C_3<C_0<C_4$ and $C_0>C_4$ then $\Delta F>0$ and as explained above phase separation is impossible.
For compositions $C_1<C_0<C_2$ where C_2 is the point of inflection ($\delta^2F/\delta C^2 =0$) and C_1 is the local minimum ($\delta F/\delta C =0$) and if a region of inhomogeneity develops with a composition $C_i<C_5$ where C_5 is the intersection of the tangent at point C_0 and the energy curve (Same argument as in 4 a), then in that case $\Delta F>0$ and the region of inhomogeneity will be unstable and tends to redissolve. On the other hand if $C_i>C_5$ then $\Delta F<0$ and a change in the composition of the inhomogeneity towards that of C_4 gives a decrease in the free energy. This means that separation is energetically favourable for compositions in this domain. The phase separation in this domain takes place according to a nucleation and growth process. This process is activated and thus needs to overcome a given energy barrier in order to happen. This process is called binodal phase separation and as a result droplet type microstructures are formed in a continuous matrix.
For compositions $C_2<C_0<C_3$ any development of an inhomogeneity is energetically stable since $\delta^2F/\delta C^2 <0$. In this region there is no barrier in the formation of an inhomogeneity and any fluctuation will grow and the system tends to phase separate into two phases of composition C_1 and C_4. This is the region of spinodal phase separation and the resulting structure is a finely interconnected continuous one.
If track is kept of the compositions C_1, C_2, C_3 and C_4 at varying temperatures, the critical temperature, Tc, is the temperature where C_1 and C_4 coincide. Figure 3c) gives the composition and temperature diagram for the binary system. The binodal phase separation can then occur between C_1 and C_2 and between C_3 and C_4. Spinodal phase separation will occur between C_2 and C_3.

2.2.3 Phase separation in borosilicate glasses

Borosilicate glasses have been known to phase separate at appropriate conditions (as indicated in figure 5) for a long time. A well-known example is the Vycor process developed by Hood and Nordberg in the end of the 1930s for the production of high silica content glass via a microporous glass route. The Vycor process thus involves

all the same steps in the production of microporous glass membranes, plus an additional sintering step. The sintering step causes the porous structure to collapse and a non-porous material of high silica content is the result. Figure 5 gives the phase diagram for the system Na_2O-B_2O_3-SiO_2 where the "horizontal hatched" areas show the immiscibility regions.

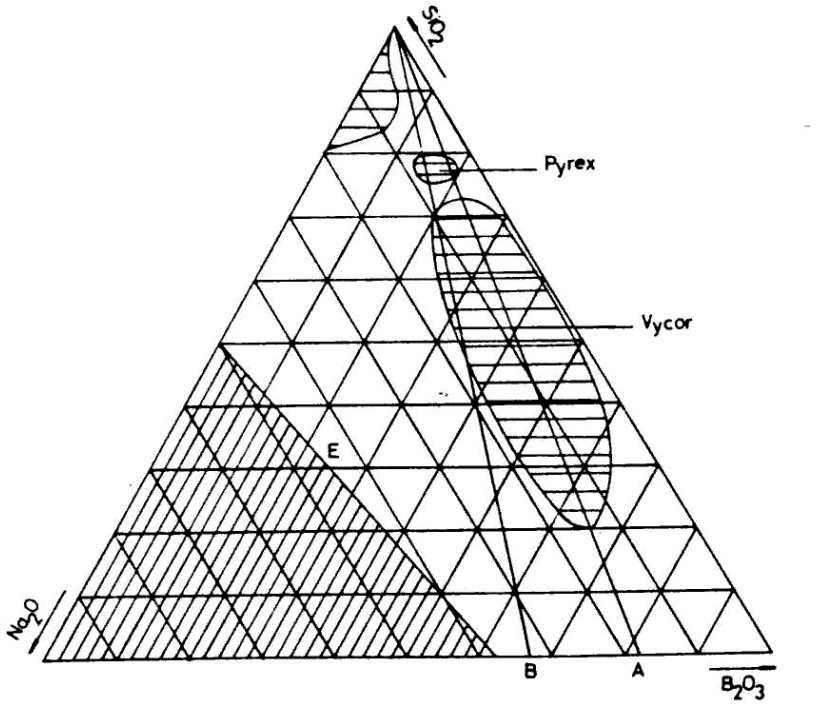

Figure 5: Phase diagram for the system Na_2O-B_2O_3-SiO_2 /Schnabel and Vaulont/.

The tendency of borosilicate glasses to phase separate can be controlled by the addition of small amounts of compounds like Al_2O_3. Al_2O_3 is known to retard the phase separation considerably. The actual reason for this effect is uncertain /Doremus/.

The composition of the borosilicate used as a precursor in the production of the microporous glass was: 65.1%SiO_2, 25.4% B_2O_3 and 9.4 % Na_2O, which places the glass in the upper left of the "Vycor" immiscibility region in figure 4.

2.2.4 Acid leaching

Acid leaching is typically carried out with 3N HCl or 5N H_2SO_4 at a temperature of about 100 °C. The leaching proceeds at a rate of approximately 1 mm/day. The

leaching properties of the borosilicates can be improved by the addition of S, Sb_2O_3, ZrO_2 or TiO_2. /Lewis (ed.)/

In the initial stages of leaching the H_3O^+ ions replace the Na^+ ions and a swelling of the glass results. This swelling can induce intolerable stresses in the glass and lead to breakage. As the leaching proceeds the B_2O_3 is removed and the remaining silica skeleton shrinks.

An enhanced leaching of the glass can be achieved by adding small quantities of P_2O_5, V_2O_5, MoO_3 or WO_3 to the starting glass. These compounds are known to shift the immiscibility region and cause the borate rich phase to contain less silica. /Lewis (ed.)/

2.2.5 Applications for porous glass

Several applications for porous glass are reported in the literature /Lewis(ed) and references within/:

- Gas separation membranes.
- Reverse osmosis membranes.
- Resistance thermometers.
- Substructure of highly critical magnetic superconducting materials.
- Material for the encapsulation of nuclear waste.
- Refractory foams.
- Enzyme immobilisation and catalyst support.

In this thesis only the gas separation application will be covered.

Our Japanese research associates (currently at Himeji Institute of Technology, Himeji, Japan and at the Faculty of Maritime Sciences at the Kobe University, Kobe, Japan) have reported permeability results for various types of glass membranes and glass template silica membranes. N_2, He, CO_2, CH_4, C_2H_6, C_3H_8, n-C_4H_{10} and i-C_4H_{10} permeabilities were measured through several different surface-modified glass membranes /Kuraoka et al.(2001)/

They have also reported the methanol vapour flux through a silica membrane prepared by the CVD- method (porous glass used as a template.) /Kuraoka et al.(1999)/

Hägg has published initial results on the separation of chlorine gas from air using unmodified glass membranes (2 and 4 nm pore size base) and one surface-modified glass membrane. /Hägg/ Additional results for the perm-selectivity of chlorine over nitrogen in newly tested glass membranes are presented in chapter 6.

2.3 Glass hollow fibres

The advantage of having the glass membrane in fibre form compared to tubes or flat sheet form is the higher packing density (m^2 membrane surface / m^3 installation) for the fibres packed into a module than the flat sheet or tubular modules. The fibres also have a better ability to withstand larger pressure differences than the tubes or the flat sheet membranes.

Our Japanese research associate has tested out several methods in fibre production and several glass materials. Glass hollow fibres can be produced by one of two main routes:

- Redrawing of glass tubes into glass fibres.
- Fibres spun directly from the melt.

The fibres were made from:

- A silica alkaline base (77.8 mol% SiO_2 and 22.2 mol% Na_2O or K_2O). In this case the membrane fibre was redrawn from a tube. The fibre was made ultramicroporous by ion exchange of the alkaline metal ions by H_3O^+. Although the N_2 adsorption isotherm and the thereby calculated pore size distribution showed no sign of larger pores, the perm-selectivity was still low. Kuraoka et al. concluded that this most likely was due to micro cracks formed during the acid leaching (ion exchange). /Kuraoka K. et al.(1998)/
- A borosilicate base with or without trace amount of aluminium. Compositions given: 62.5 SiO_2, 28.3B_2O_3, 9.2Na_2O (all wt%) for the aluminium free and 62.5 SiO_2, 27.3B_2O_3, 7.2Na_2O, 3.0Al_2O_3 (all wt%) for the one with trace amounts of aluminium. The fibre was redrawn from a tube as well and made ultramicroporous by acid leaching. No additional phase separation was performed but a phase separation is still likely to occur (to some extent) by cooling of the fibre during the redrawing process. These fibres are reported to have molecular sieving properties and the aluminium free fibre has a larger selectivity than the

fibre containing aluminium. /Kuraoka K. et al. (2000)/. However, no permeation data are reported, hence no complete comparison can be made. Fibres of this type have been tested both in the chlorine and hydrogen chloride purification projects and the obtained perm selectivity results are reported in chapters 6.1.11 and 6.2.5, respectively.

2.4 Preparation of porous glass membranes

Glass membranes can be manufactured with two different average pore sizes depending among other on the composition of the starting glass. In general the methods are similar, but since only the synthesis leading to an average pore size of 4 nm is patented, only this process will be the discussed here.

The starting glass is a commercially available handmade glass tube from Akagawa Glass Co. Ltd. Japan. These tubes come in different diameters ranging from 0.2-10 mm and wall thicknesses from 0.03 to 2 mm. The glass tubes used in this thesis has an inner diameter of 4 mm and a wall thickness of 0.5mm. The tubes are cut in lengths of approximately 30cm using a hack file (30 cm is thus the length of the active part of the surface-modifying reactor.)

2.4.1 Phase separation

The glass tubes are placed in alumina tubes to prevent the glass from fusing into each other and to prevent them from being spatially deformed during heat treatment. An excess of boron oxide (B_2O_3) is added as powder into the furnace in an alumina bowl in order to prevent any boron loss from the glass tubes during the heat treatment. The temperature is then raised from room temperature to 585 ºC slowly over three hours. The temperature is then kept stable at 585 ºC for 72 hours. The glass now contains two phases of different composition as discussed in chapter 2.2.3. One phase is rich in SiO_2 and the other is rich in B_2O_3-Na_2O. The temperature of the furnace is decreased slowly over three hours down to room temperature.

However, the glass is not yet mesoporous. To obtain this the glass has to be leached with an acid.

2.4.2 Acid leaching

The surfaces of the glass tubes are rinsed with a HF solution (4/1 ratio water / 46% HF). The glass tubes are then immersed into a 1N HNO_3 solution and heated to 98ºC and kept at that temperature for 24 hours. The glass tubes are then rinsed with distilled water and the synthesis is completed.

This acid treatment has now removed the B_2O_3-Na_2O rich phase completely, resulting in a porous network of pore diameters of approximately 30nm. SiO_2 remaining in the boron rich phase after the phase separation is only slightly soluble in the acid, and this solubility is very pH dependent /Tanaka/. At the optimal acid to glass ratio this pH dependent solubility will cause colloid-sized SiO_2 particles to be formed in the solution with a diameter that also is strongly pH dependent. However, since the solubility of the SiO_2 is low the colloid particles precipitate easily on any available surface of the glass tube, including inside the 30 nm pores. If the right set of parameters is chosen, the colloid particles that fill the original 30 nm pore will leave a porous network of voids between the random spaced spheres resulting in "new" pores with an average diameter of 4 nm /Tanaka/.

2.4.3 Surface modification

A pore of 4 nm is too large to separate gases efficiently since this is clearly in the Knudsen transport regime. (See chapter 3.2) To narrow the pores, silane coupling surface modification is performed. This modification involves specific reaction with the surface –OH groups, as shown in figure 6 /Kuraoka, K. et al. 2001/.

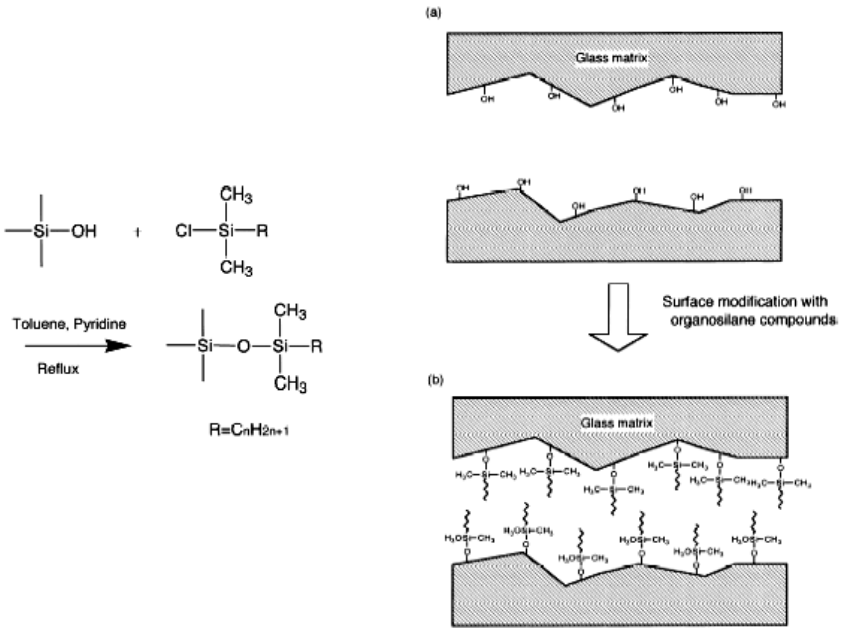

Figure 6: Conceptual drawing of the silane-coupling surface modification reaction / Kuraoka, K. et al. 2001/.

2.4.4 Modification procedure

The membrane is dried at 170 ºC, under vacuum, for 3 hours to remove capillary-condensed and -adsorbed water from the pores. The reactor is then cooled to room temperature. The porous glass has -OH end groups evenly distributed over all surfaces, both internal surfaces (in the pores) and external surfaces. By titration of the glass tube with a suitable acid and indicator, the –OH density can be estimated. According to research performed at AIST, Kansai Japan, the average –OH density in a 4 nm glass membrane is approximately 5 µmol –OH groups / m^2.
The surface area of the pores in a glass tube is 200 m^2/g of membrane. /Kuraoka et al. (2001)/. Thus the -OH density is 1mmol/g. From the consideration of the –OH density it is easy to calculate that the stoichiometric amount of the silane coupling compound needed is approximately 2.5 mmol for a 20cm long glass membrane (outer diameter 5mm, and wall thickness 0.5mm). However, since the pores are narrow and the diffusion times may be long, at least 200 % excess is used.
The glass surface has a high affinity for water so it is important to use dehydrated grade toluene as a solvent for the modifying compound. The reaction of the surface

modifying compound with the –OH sites produces HCl, which needs to be removed in order to achieve a high conversion in the reaction. The acidic HCl is removed by adding pyridine (dehydrated grade) to the reactor 5 minutes after the reaction is started. The reactor is run at 110 ºC with vapour reflux for 20 hours. After the reaction is completed, the reactor is cooled down and the solution removed.
Fresh toluene is added and another 3 hour reflux at 110 ºC follows. The membrane is then removed from the reactor and dried at room temperature over-night.
As indicated in figure 6, all reactants are based on the Cl-Si$(CH_3)_2$-R template where R is an acyl group of varying length and all R's tested are described in table 1.

Table 1: Chemical structure for the modification used in the silane coupling reaction and the abbreviations used as synonyms.

Abbreviation	Silane compound used (R in Cl-Si$(CH_3)_2$-R)	Comment
Pure 4 nm	None	"4 nm" refers to the average pore size distribution
Pure 2 nm	None	"2 nm" average pore size distribution
C1	CH_3	
C8	C_8H_{17}	
C12	$C_{12}H_{25}$	
C18	$C_{18}H_{37}$	
C1+C18	CH_3 and $C_{18}H_{37}$	C18 modified first and then C1 modified
Fibre	None	
Pf-C10(4 nm)	$(CH_2)_2$-$(CF_2)_7$-CF_3	4 nm is the pore size of the precursor
Pf-C10(2 nm)	$(CH_2)_2$-$(CF_2)_7$-CF_3	2 nm is the pore size of the precursor

2.5 References

Doremus, R. H.: ""Glass science", John Wiley & Sons Inc., New York, 2nd ed., (1994) Chapter 4("Phase separation") pp 49-72.

Haller,W. et al., J.Am.Ceram.Soc.,57 (1974), p120.

Hägg, M-B: "Membrane purification of Cl_2 gas II. Permeabilities as function of temperature for Cl_2, O_2, N_2 and HCl in perfluorinated, glass and carbon molecular sieve membranes", J. Memb. Sci., 177, (2000), pp 109-128.

Kraceck,F., J.Am.Ceram.Soc.,61, (1939), p2869.

Kuraoka, K., Chujo, Y. and Yazawa,T.: "Hydrocarbon separation via porous glass membranes surface-modified using organosilane compounds" J. Memb. Sci., 182, (2001), pp 139-149.

Kuraoka, K. et al.: "Preparation of molecular sieving glass hollow fiber membranes based on phase separation" J. Memb. Sci., 175, (2000), pp 215-223.

Kuraoka, K. et al.: "Permeation of methanol vapor through silica membranes prepared by the CVD method with the aid of evacuation." J. Memb. Sci., 160, (1999), pp 31-39.
Kuraoka, K. et al.: "Trial for preparation of glass capillary membranes by elution of alkali metal ions" Separation science and technology, 33, (1998), pp 297-309.

Lewis, M. H. (Editor): "Glasses and Glass-Ceramics", Chapman & Hall Chapter 6 ("Application of microporous glasses") (1989) pp203-225.

Phillips,B. and Mulan,A., J.Am.Ceram.Soc., 42, (1959), p414.

Pfaender, Heinz G.: "Schott Guide to Glass" Chapman & Hall 2nd ed. Chapter 2.

Schnabel, R. and Vaulont, W.: "High pressure techniques with porous glass membranes" Desalination, 24, (1978), pp 249-272.

Tanka, H et al.: "Precipitation of colloidal silica and pore size distribution in high silica porous glass." Journal of non-Crystalline Solids, 65, (1984), pp301-309.

3 TRANSPORT MECHANISMS

Three "families" of glass membranes have been investigated in the current work: pure glass tubes, surface-modified glass tubes and glass hollow fibre. These glasses have an average pore size distribution from 4 nm down into the sub-nanometer range, respectively. The average pore distribution is important since it gives an indication of which transport mechanism is to be expected to be dominant for a given separation in a defined material. Figure 7 generalizes the dependence of pore size and the most probable transport mechanism in porous membranes.

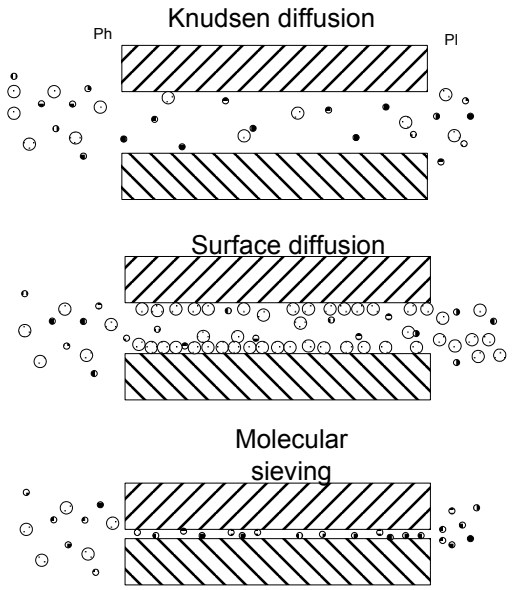

Figure 7: Transport mechanisms for microporous membranes. Feed or high pressure side is on left hand side of the figure.

The mechanisms are briefly characterised as follows:

- Knudsen diffusion; the square root of the ratio of the molecular weights will give the separation factor.
- Selective surface diffusion; governed by a selective adsorption of the larger (non-ideal) or "chemically attractive" components on the pore surface. In a mixed gas situation an additional increase in the selectivity might be achieved if the pores initially are so narrow that an adsorbed monolayer covering the internal pore walls causes the free pore entrance to be smaller than the diameter of the non-adsorbed molecule.

- Molecular sieving; the smallest molecules will permeate, the larger being retained. For evaluation of the gas properties, reference is made to Table 2.

Table 2: Various properties for selected gases /Reid/

Gas	Lennard-Jones diameter, σ [Å]	T_C [K]	Mw_A [g/mol]
Cl_2	4.22	417	70.9
N_2	3.79	126	28.0
O_2	3.47	155	32.0
HCl	3.34	324	36.5
H_2	2.82	33.3	2.02

3.1 General mass transport

Fick's law gives the mass flux through any area perpendicular to the flow direction: (The general transport equations can be found in any basic textbook on transport as /Geankoplis/)

$$J_A = -D_{AB}\frac{dc_A}{dx} \tag{3.1}$$

Where J_A is the mass flux [mol(A)/(m^2·s)], D_{AB} is the diffusion coefficient [m^2/s] and dc_A/dx is the concentration gradient for component A over the distance x [mol/(m^3·m)].

Fick's law can be integrated over the membrane thickness to yield the following expression, given that the diffusion is independent of the concentration:

$$J_A = \frac{D_{A,memb}(c_{0,A} - c_{l,A})}{l} \tag{3.2}$$

Where l is the membrane thickness [m] and $c_{0,A}$ and $c_{l,A}$ are the concentrations [mol/m^3] on the inlet and the outlet of the membrane, respectively. The $D_{A,memb}$ will vary according to which transport mechanism is dominating (as indicated in figure 7).

The permeance, P/l, for a given gas type (A) is defined by:

$$P_A/l = \frac{J_A}{\Delta p_A} \tag{3.3}$$

Where P/l is the permeance (also referred to as permeability flux) [mol/(m^2 Pa s) or m^3(STP)/(m^2 bar h)] and p_A is the partial pressure difference of "A" across the membrane [bar].

3.2 Knudsen Flow

The Knudsen flow is characterized by the mean free path of the molecules being wider than the pore size /Geankoplis/. Thus collisions between the molecules and the pore walls are more frequent than intermolecular collisions. The "classical" Knudsen equation is:

$$D_{Kn,A} = \frac{d_p}{3}\bar{v}_A = \frac{d_p}{3}\sqrt{\frac{8RT}{\pi Mw_A}} = 48.5 \cdot d_p\sqrt{\frac{T}{Mw_A}} \tag{3.4}$$

Where d_p = average pore diameter [m], $\bar{v}_A$ = average molecular velocity [m/s], Mw = molecular weight [kg/mol], and T = temperature [K].

Previously, a lower limit for the significance of the Knudsen mechanism was set to d_p > 20 Å. However, recent findings of /Gilron and Soffer/ indicate that the Knudsen mechanism can be significant for pore sizes as small as dp~5Å. The Knudsen flow in this region takes slightly different form as indicated in the following expression derived as transport through a series of constrictions /Burggraaf/:

$$D_{A,K} = g_d d_p\sqrt{\frac{8RT}{\pi Mw_A}}\exp(-\frac{\Delta E_a}{RT}) \tag{3.5}$$

Where g_d is the probability that a molecule can make a jump in the right direction, given the jump length is d_p and the velocity is $\bar{v}_A$.

They have also demonstrated the influence of varying pore diameter through a single pore, yielding a resistance in series model for the transport.

3.3 Surface diffusion

The mechanism of surface diffusion is disputed and several different approaches have been proposed in the literature. Theories ranging from viewing the low surface

coverage adsorbed gas as a 2D gas, through a hopping model into a more "liquid like" sliding layer theory. Which of the mechanisms is dominating the surface diffusion coefficient will be influenced by a number of factors including the homogeneity of the surface, the temperature vs. the adsorption enthalpy and the surface concentration, c_s./Gilliland et al. 1974/.

All three regimes can be described by a 2D analogue of Fick's law (given here for a single component):

$$J_{x,s} = -D_s \frac{dc_s}{dx} \tag{3.6}$$

Where $J_{x,s}$= is the flux (evaluated as molecules crossing a hypothetical line in the surface perpendicular to the direction x) [mol/(m s)], D_s is the surface diffusion coefficient [m^2/s] and dc_s/dx is the surface concentration gradient in the x-direction [mol /(m^2·m)].

An important feature about surface transport is that is not necessary for the molecule to hit the pore entrance in order to be transported according to this mechanism. Molecules also hitting the external surface will contribute as indicated in figure 8 /Burggraaf/. This approach is similar to water in a sink where, if the plug is removed, all the water is going down the drain and not only the water directly above the drain inlet.

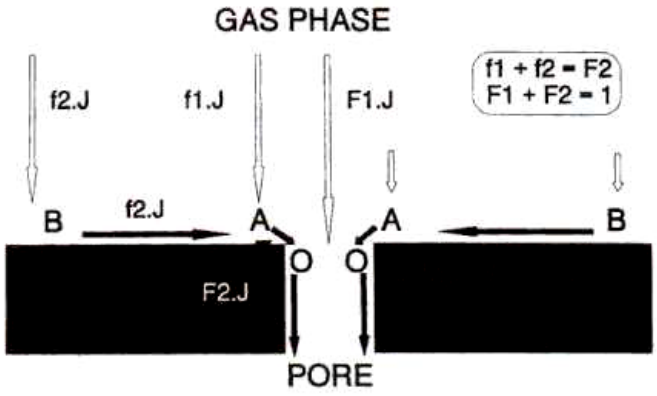

Figure 8: Schematic model of gas permeation in microporous membranes. The flux consist of two contributions: Direct hit of the pore entrance and adsorption on the external surface./Burggraaf/

3.3.1 2D-gas model

According to /Gilliland 1974/ the following expression may be used to determine if the surface transport is dominated by the 2D-gas model:

$$q / RT < 1 / a \tag{3.7}$$

Where q is the adsorption enthalpy [J/mol] and a is an energy fraction factor. The energy barrier for surface migration, E, is then defined as:

$$E = a\,q \tag{3.8}$$

Figure 9 gives a visualisation of various energy barriers for surface migration./Dacey/.

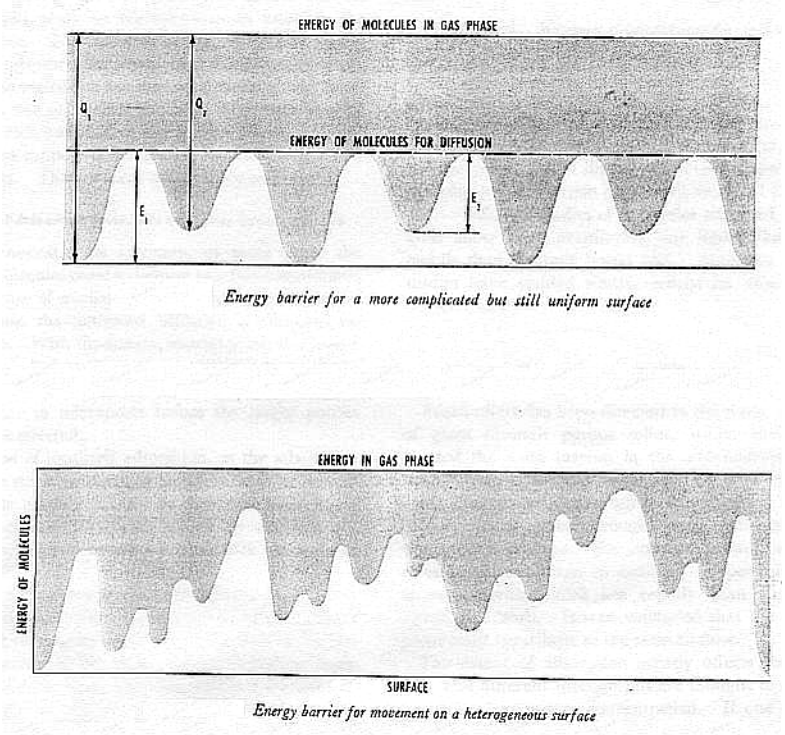

Figure 9: Energy barriers for surface migration on: A complicated but uniform surface (upper halve) and a heterogeneous surface. /Dacey/

The 2D-gas is characterised by a surface mean free path, λ_s, inversely proportional to the surface concentration, c_s, and this λ_s value can be much larger than the spacing between adjacent surface sites.

If the c_s is low then a random walk diffusion of independent molecules can be expected and the D_s would be given as:

$$D_s = \frac{1}{4}\nu\lambda_s^2 \tag{3.9}$$

Where υ is a jump frequency factor (This factor has a temperature dependence according to Arrhenius law, $\upsilon=\upsilon_0 \cdot \exp(-aq/(RT))$ [1/s].

3.3.2 Site-to-site hopping model

If the q/RT part of eq. (3.7) is increased then λ_s will no longer be controlled by collisions between adsorbed molecules. As q/RT increases, λ_s decreases and becomes equal to the spacing between adjacent sites and a hopping mechanism is observed. A more detailed description is given by / Weaver and Metzner / based on the following assumptions:

- The adsorbed gas and gas phase are in thermodynamic equilibrium.
- Adsorbed molecules migrate over the surface by small hops.
- These hops have a random direction.

This yields the following expression:

$$N_A = -\frac{S_w \rho}{2\pi\tau^2}\left[r\frac{\partial\lambda^2}{\partial z} + \frac{\pi}{2}\lambda^2\frac{\partial r}{\partial z}\right] \tag{3.10}$$

Where: N_A is molar flux [mol/(m^2 s)], S_W= Specific surface area [m^2/kg], ρ= density of the material [kg /m^3], τ_g= tortuosity [-], λ= mean average jumping distance [m], r= Rate of partial desorption (or hopping rate) [mol/(m^2 s)] and z= net flux direction [m].

The partial desorption rate or the hopping rate, can according to /Glasstone et al/, be expressed as:

$$r = \frac{c_s}{S_w}\frac{Q^0}{Q}\frac{kT}{h}e^{\left(-\frac{E_{a,hm}}{R\cdot T}\right)} \tag{3.11}$$

Where Q and Q^0 are the partition functions for the non-activated and activated species, respectively, k is Boltzmann's constant [$1.38\cdot10^{-23}$ J/K], h is Planck's constant [$6.63\cdot10^{-34}$ J·s] and $E_{a,hm}$= activation energy for surface migration [J/mol]

3.3.3 Liquid-like sliding layer model

If the surface concentration is increased, the chance of a molecule hitting another molecule increases and this interaction will bear some similarity to diffusion in a liquid. Thus, the region of the sliding layer prevails.
Based on the given assumptions /Gilliland et al. 1958/:

- Thermodynamic equilibrium between the gas and adsorbed phase.
- No shear stresses between the adsorbed layer and the gas phase.

The following equation was derived:

$$\frac{N_A}{A} = \frac{RT\rho_{app}}{\tau^2 C_R S_w l}\int_{p_2}^{p_1}\frac{x^2}{p}dp \qquad (3.12)$$

Where: x = amount adsorbed [mol/kg], C_R= resistance coefficient [kg/(s m^2)] and l is the membrane thickness [m].

3.4 Molecular Sieving

Molecular sieving is the dominating transport mechanism when the pore size is comparable to the molecular dimensions, 3-5 Å. The dimensions of a molecule are usually described with either the Lennard-Jones radii (Table 2) or the Van der Waals radii. For separation by molecular sieving, this is not a satisfactory way of giving the molecular size; a shape factor should also be included /Singh and Koros/. This can be understood by viewing oxygen and nitrogen molecules as two fused spheres with different projected diameters parallel or perpendicular to the covalent bonding (i.e., the bonding between the atoms in O_2 and N_2). Consider a pore with a diameter of 3.8 Å, here an oxygen molecule may pass through the pore independent of it rotation. However, nitrogen may or may not then pass the pore depending on how the molecule rotates; this explains the increase in the selectivity in favour of O_2 /Singh and Koros/.
The sorption selectivity has little influence on the separation when molecular sieving is considered. An Arrhenius type of equation is still valid for the activated transport, but attention should be drawn to the pre-exponential term, D_0. From the transition state theory this factor may be expressed as shown in equation 13 /Glasstone et.al./:

$$D_0 = e\lambda^2 \frac{kT}{h} \exp\left(\frac{S_{a,d}}{R}\right) \tag{3.13}$$

Where k and h are Boltzmann's and Planck's constants, respectively; $S_{a,d}$ is the activation entropy for diffusion. This means that a change in entropy will have a significant effect on the selectivity when molecular sieving is considered. Singh and Koros have discussed this thoroughly /Singh and Koros/. The flux may be described as in equation 14 where $E_{a,MS}$ is the activation energy for diffusion in the molecular sieving media.

$$J_A = \frac{\Delta p}{RT \cdot l} D_0 \cdot \exp\left(\frac{-E_{a,MS}}{RT}\right) \tag{3.14}$$

The sorption will in this case have little influence, and thus the selectivity for separation will increase with increasing temperature because of the increased diffusion rate of the permeating component. Likewise, it will become more difficult for the larger molecule to pass the narrow slit when the temperature increases.

3.5 Combined mass transfer

If the selective surface flow (SSF) and the Knudsen flow is assumed to be additive in the glass membranes and helium gas are assumed to be solely transported by Knudsen flow the following expression may be derived:

$$\begin{aligned} &\alpha_{Tot,i,He} = \frac{J_{Tot,i}}{J_{Tot,He}} = \frac{J_{Kn,i} + J_{ssf,i}}{J_{Kn,He}} = \alpha_{kn,i,He} + \frac{J_{ssf,i}}{J_{Kn,He}} \Leftrightarrow \\ &1 - \frac{\alpha_{Kn,i,He}}{\alpha_{Tot,i,He}} = \frac{J_{ssf,i}}{J_{Tot,i}} \end{aligned} \tag{3.15}$$

Where J is the permeance [m^3(STP)/(m^2 bar h)], $\alpha_{Kn,i/j}$ is the selectivity based on the Knudsen flow [-] and $\alpha_{i/j}$ is the (total) selectivity [-]. From the general Knudsen transport mechanism theory the $\alpha_{Kn,i/j}$ is given as the square root of the inverse ratio of the molecular weights.

This means that based on the assumptions used it is possible to derive an expression for the degree of contribution from SSF to the overall transport

$$\psi_i = 1 - \frac{2\sqrt{\frac{1}{Mw_i}}}{\alpha_{tot,i/He}} \tag{3.16}$$

Where ψ is the degree of SSF which is equal to J_{SSF}/J_{Tot} [-]

3.6 References

Burggraaf, A .J.: "Single gas permeation of thin zeolite (MFI) membranes: theory and analysis of experimental observations", J. Membrane Sci., Vol.155, 1999, 45-65.

Dacey, J. R.: "Surface diffusion of adsorbed molecules" Ind.&Eng. Chem, 57, no.6, 1965, 27-33.

Geankoplis, C.: "Transport processes and unit operations" 3rd ed., Prentice Hall, 1993.

Gilliland, E. R. et al.: "Rates of flow through microporous solids" A.I.Ch.E. Journal Vol 4, no 1, 1958, 90-96.

Gilliland, E. R. et al.: "Effect of concentration on the diffusivity of physically adsorbed gases", Ind. Eng. Chem. Fundam., Vol.13 no.2, 1974, 95-100.

Gilron, J. and Soffer, A.: "Knudsen Diffusion in Microporous Carbon Membranes with Molecular Sieving Character", J. Membrane Sci., Vol.209, 2002, 339-352.

Glasstone, S., Laidler, K.J. and Eyring, H.: "The Theory of Rate Processes", 1st Edition, McGraw-Hill Book Co., Inc. New York, NY, 1941.

Reid, R.C et al.: "The Properties of Gases and Liquids", 4th Edition, McGraw-Hill, New York, 1987.

Singh, A. and Koros, W. J.: "Significance of Entropic Selectivity for Advanced Gas Separation Membranes", Ind. Eng. Chem. Res., 35, 1996, 1231-1234.

Weaver, J. A. and Metzner, A. B.: "The surface transport of adsorped molecules" A.I.Ch.E. Journal Vol 12, no 4, 1966, 655-661.

4 MEMBRANE CHARACTERISATION

4.1 Background

The pore size distribution in a porous membrane is of fundamental interest. Different methods for pore size determination based on different physical properties of the porous membrane exist. As given in /Burggraaf/, these can be summed up in the following figure:

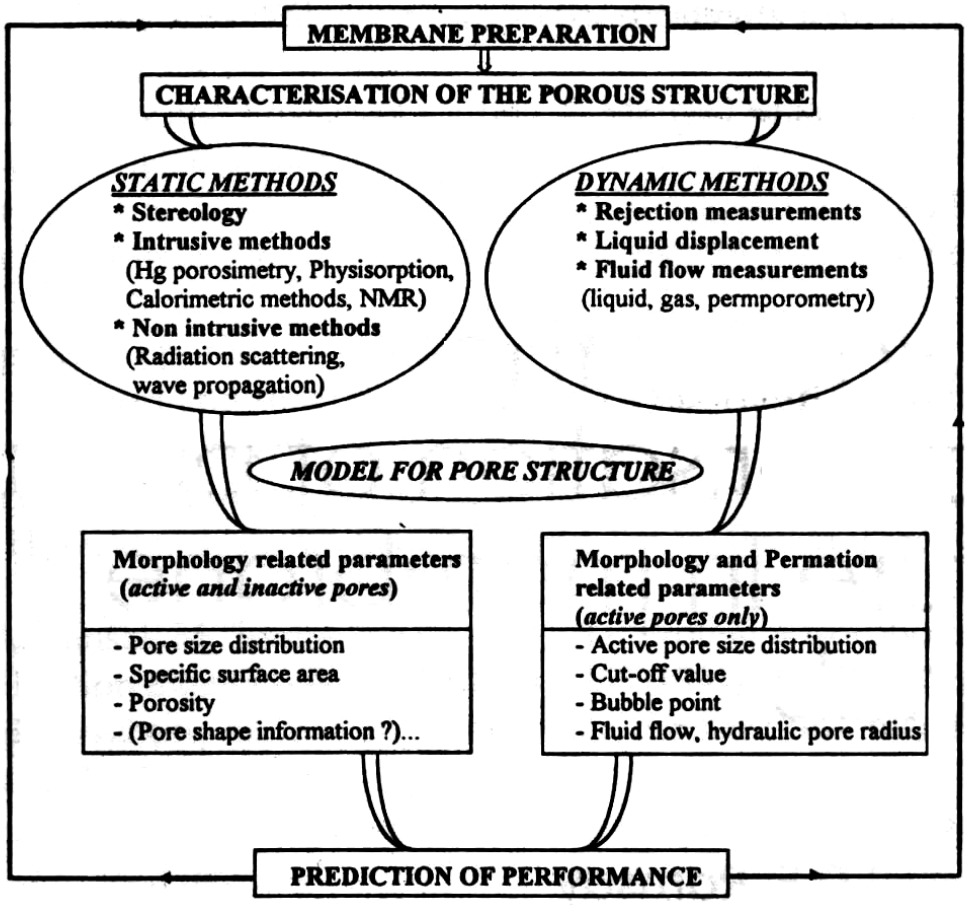

Figure 10: Methodology for membrane characterization. /Burggraaf/

Since the various methods are based on different physical parameters, the obtained pore size should be expected to differ.

Two different methods are selected for the pore size distribution determination:

- N_2 adsorption / desorption at 77 K
- Stereology (microscopy): Due to the small pore size of the glass membranes various methods were tried, including scanning electron microscopy (SEM), atomic force microscopy (AFM) and field emission scanning electron microscopy (FESEM).

For the general understanding of the different glass membranes, the Fourier transform infrared spectroscopy (FTIR) spectrum was recorded. The IR-spectrum is believed to be important in the validation of the surface stability of the surface-modified glass membrane.

4.2 N_2 adsorption /desorption

The measurement of N_2 adsorption/desorption isotherms has the advantage of being non-destructive at least for powders. Membranes would not be destroyed in the sense that only a small amount of sample is necessary to perform the measurement. The measurement is easy to perform, but the analysis and interpretation of the measured isotherms may be difficult.

Adsorption may be defined as an enrichment of one or several components in an interfacial layer /Sing/. The intermolecular forces involved in adsorbing a component to a surface are the same as those responsible for condensation of vapours. These forces include attractive dispersion forces, short-range repulsive forces and specific molecular interactions (e.g. polarization, dipole/ dipole and dipole /quadropole). If the formation of a chemical bond between the absorbent and the absorbate occurs, a so-called chemisorption has taken place. This is an almost irreversible process, and it is not useful in determining the pore size distribution. When desorption is taking place, it may follow a different path from the adsorption; a hysteresis curve results. Many adsorbents with high surface area are porous and it is useful to distinguish between internal and external surface area.

For porous membranes in gas separation, the internal surface and the pore distribution is important.

The IUPAC, /Sing/ recommends the following classification of porous material:

- Macropores: pores with widths exceeding 50 nm.
- Mesopores: pores with widths between 2 and 50 nm.
- Micropores: pores with widths smaller than 2 nm.

The monolayer capacity is an important parameter in adsorption and it is defined as the amount of adsorbate needed to cover the surface with a complete monolayer. This is closely related to the surface coverage, θ, which is defined as the ratio of the amount adsorbed to the monolayer capacity. The surface area of the absorbent can be calculated from the monolayer capacity if the effective area of one molecule in the monolayer is known.

The majority of adsorption isotherms may be classified into one of the six general types shown in figure 11.

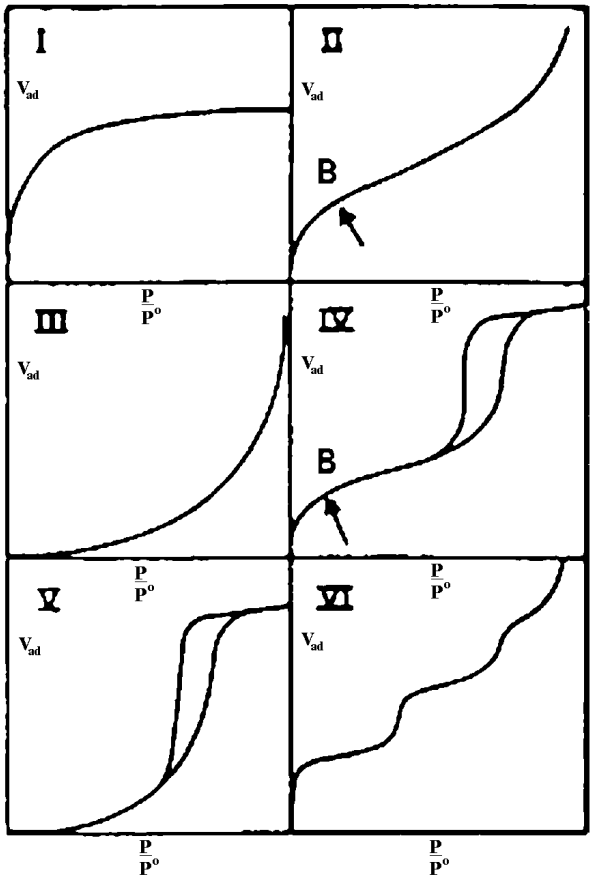

Figure 11: Types of physisorption isotherms /Sing/

Of these isotherms, no.2 and no.4 are important in this work. The point "B" marked on isotherm 2 and 4 is taken as the completion of the monolayer. Isotherm no.2 is

easily fitted to the BET-equation (equation 4.1), and the region below the point B is used to obtain the correct constants in the BET-equation.
The hysteresis given in isotherm no IV in figure 11 is often subdivided to belong to one of the four general shapes indicated in figure 12.

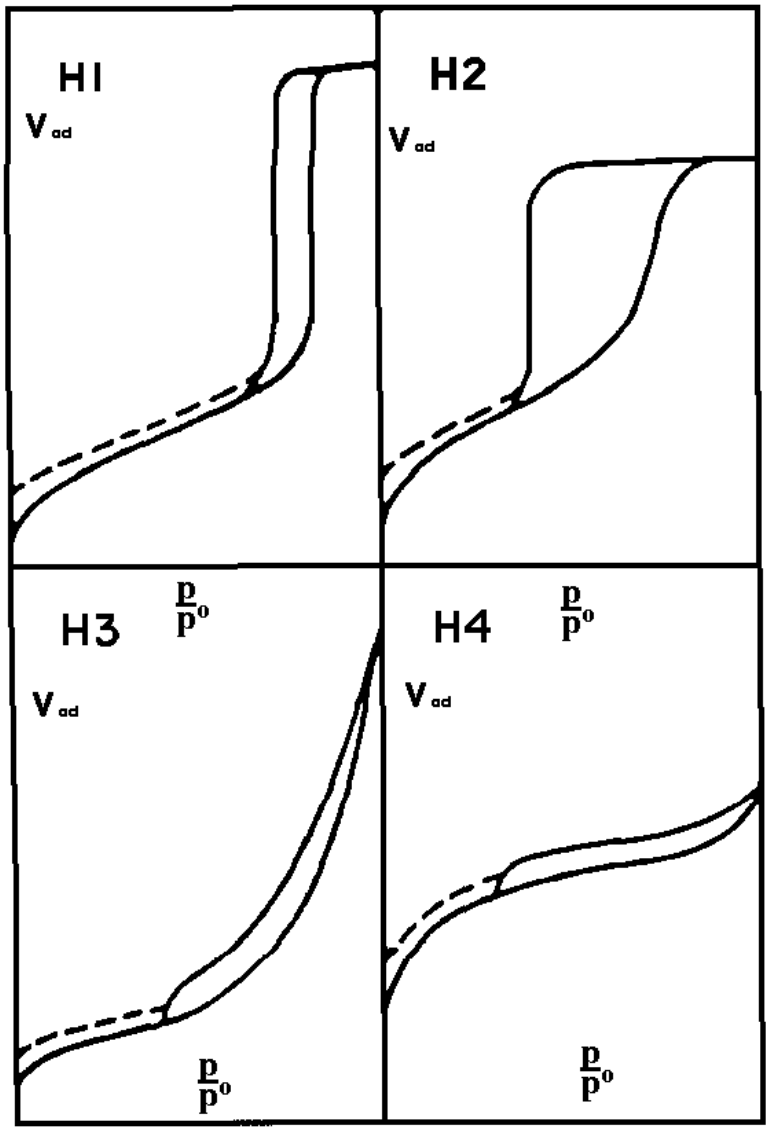

Figure 12: Types of hysteresis loops /Sing/

The hysteresis appearing in the multilayer range of adsorption isotherms is usually associated with capillary condensation. The shapes of these hysteresis loops can be associated with the pore shape at least to a certain extent. H1 in figure 12 is associated with agglomerates, H2 is associated with "ink bottle" pores, or porous network. Type H3 and H4 are associated with slit like pores, where the H4 is characteristic for micropores.

The Brunauer-Emmett-Teller or BET method has become the most widely used gas adsorption isotherm for the determination of the surface area of porous material /Sing/.

The BET-equation is given as follows (in its linear form):

$$\frac{p}{n^a\left(p^0-p\right)}=\frac{1}{n_m^a\cdot C}+\frac{(C-1)}{n_m^a\cdot C}\cdot\frac{p}{p^0} \tag{4.1}$$

Where n^a is the amount adsorbed at the relative pressure p/p^0 and n_m^a is the monolayer capacity. According to the BET theory, C is a constant that can be related to the enthalpy of adsorption of the first adsorbed layer. However, /Sing/ states that it is now generally accepted that the C-value can be used to characterize the shape of the isotherm but that the C-value is at best an indication of the magnitude of the adsorption enthalpy. A high value of C (~ 100) is associated with a sharp bend in the isotherm, thus making the determination of the point "B" trivial. However, if C is ~ 20 the point "B" cannot be identified as a single point. If p/n^a (p^0-p) is plotted versus p/p^0 and a linear curve results, then equation 4.1 is obeyed and the measurements can be described by the BET-theory. The range of linearity is restricted to a limited part of the isotherm, usually for p/p^0 values in the 0.05 –0.30 range. The calculation of the surface area requires the knowledge of the average coverage area of a N_2 molecule in the complete monolayer. Then the BET-area can be calculated according to:

$$A_s(BET)=n_m^a\cdot L\cdot a_m \tag{4.2}$$

Where A_s(BET) is the total surface area according to the BET-theory [m^2/mol], L is Avogadros constant, $6.02\cdot10^{23}$ [mol^{-1}] and a_m is the molecular cross sectional area[m^2]. a_m has the value of 0.162 nm^2 for close-packed N_2 molecules at 77K./Sing/

The pore size distribution is the distribution of pore volumes with respect to pore size. This calculation usually involves a number of assumptions such as pore shape, mechanism of pore filing, the validity of the Kelvin Equation etc.

The Kelvin Equation is given as follows:

$$\frac{1}{r_1}+\frac{1}{r_2}=-\frac{RT}{\sigma^{lg}\nu^l}\ln\left(\frac{p}{p^0}\right) \tag{4.3}$$

Where r_1 and r_2 are the principal radii of curvature for the liquid meniscus in the pore [m], σ^{lg} is the surface tension of the liquid condensate [J/m^2] and υ^l is the molar volume of the liquid condensate [m^3/mol].
If the shape of the pores is assumed to be cylindrical then the principal radii (defined in eq. 4.3) are equal, leading to:

$$\frac{1}{r_1}+\frac{1}{r_2}=\frac{2}{r_k} \tag{4.4}$$

Where r_k is the Kelvin radius [m].
Equation 4.3 substituted into eq. 4.4 and solved for r_k gives the following expression:

$$r_k=\frac{2\sigma^{lg}\nu^l}{RT\ln\left(p^0/p\right)} \tag{4.5}$$

Of course the multilayer thickness of the adsorbed layer has to be taken into account, thus the radius of the pore can be expressed as:

$$r_p=r_k+t \tag{4.6}$$

Where t is the multilayer thickness [m].

The pore size distribution is usually calculated from the desorption branch of the isotherm. If cylindrical open ended pores are considered, then the change in the different layers according to eq.7 can be sketched as a function of relative pressure as done in figure 13.

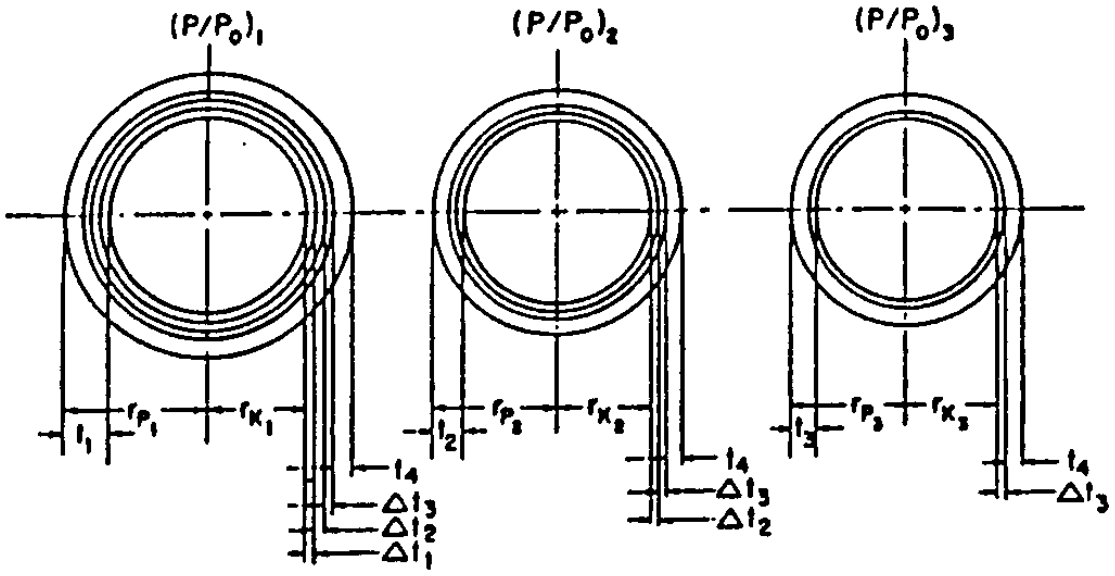

Figure 13: Schematic representation of the assumed desorption mechanism in the Barrett, Joyner and Halenda, BJH,-theory. Showing the thinning of the physical adsorbed layer for three pores over the first three pressure decrements. /Barrett, E et.al./

In figure 13, the relative pressure $(P/P^0)_1$ differs infinitesimally from unity so substantially all pores are filled with liquid. The largest pore has a radius of r_{p1}, and upon its surface is a physical adsorbed layer of thickness t_1. Within this physically adsorbed layer the inner capillary has an effective capillary radius equalling r_k from which the evaporation occurs as the relative pressure, (P/P^0), is lowered.
By summing up the incremental decreases (n steps) in the thickness of adsorbed layer a volume desorption distribution may be obtained/Barrett et.al./. This volume distribution method is known as the BJH-method. Only the working equation is given here:

$$V_{pn} = R_n \Delta V_n - R_n \ \Delta t \sum_{i=1}^{n-1} A_{pi} c_i \tag{4.7}$$

Where $R_{n=1}$ is defined by the following expression:

$$R_1 = \frac{r_{p1}^2}{\left(r_{k1} + \Delta t_1\right)^2} \tag{4.8}$$

The constant c is defined by the following ratio:

$$c = (\overline{r}_p - t_{\overline{r}}) / \overline{r}_p \tag{4.9}$$

V_{pn} is the pore volume [m^3], Vn is the observed degassed volume at a given relative pressure decrease [m^3], $\overline{r}_p$ is the average pore radii [m] and A is the average area for desorption in an emptied pore [m^2].
Thus by using equations 8 and 9, the desired plot of V_{pn} vs. r_p, the pore size distribution is produced.

4.3 Stereology (Microscopy)

Stereology can be defined as a kind of "inspection" method to "look" at the surface and to count and measure the dimensions of the pores from images of the surface. One of the greatest advantages of various stereological analysis is that they are easy to perform. Unfortunately the method also has some severe drawbacks:
Firstly, no distinctions are made between transport active pores and dead end pores. Secondly, since the surface under inspection is only a small fraction of the total membrane surface it is crucial to find a representative patch. This will be very important in determining an average pore size distribution.

4.3.1 Scanning electron microscope

Instead of using visible light to inspect surfaces, it is possible to use electrons (which are both particles and waves according to the particle wave dualism in quantum mechanics). The advantage of using an electron wave is that it has a much shorter wavelength and thus a better spatial resolution than visible light. As a rule of thumb, the smallest distinguishable detail on the surface is roughly half of the wavelength of the radiation used. This means that the resolution of a regular scanning electron microscope, SEM, is in the range of 5 nm. They come in three different operational modes: Regular, Field emission scanning electron microscope (FESEM) and transmission electron microscope TEM. In this work the Regular SEM and FESEM have been used.
A SEM operates according to the following principle, as indicated in figure 14.

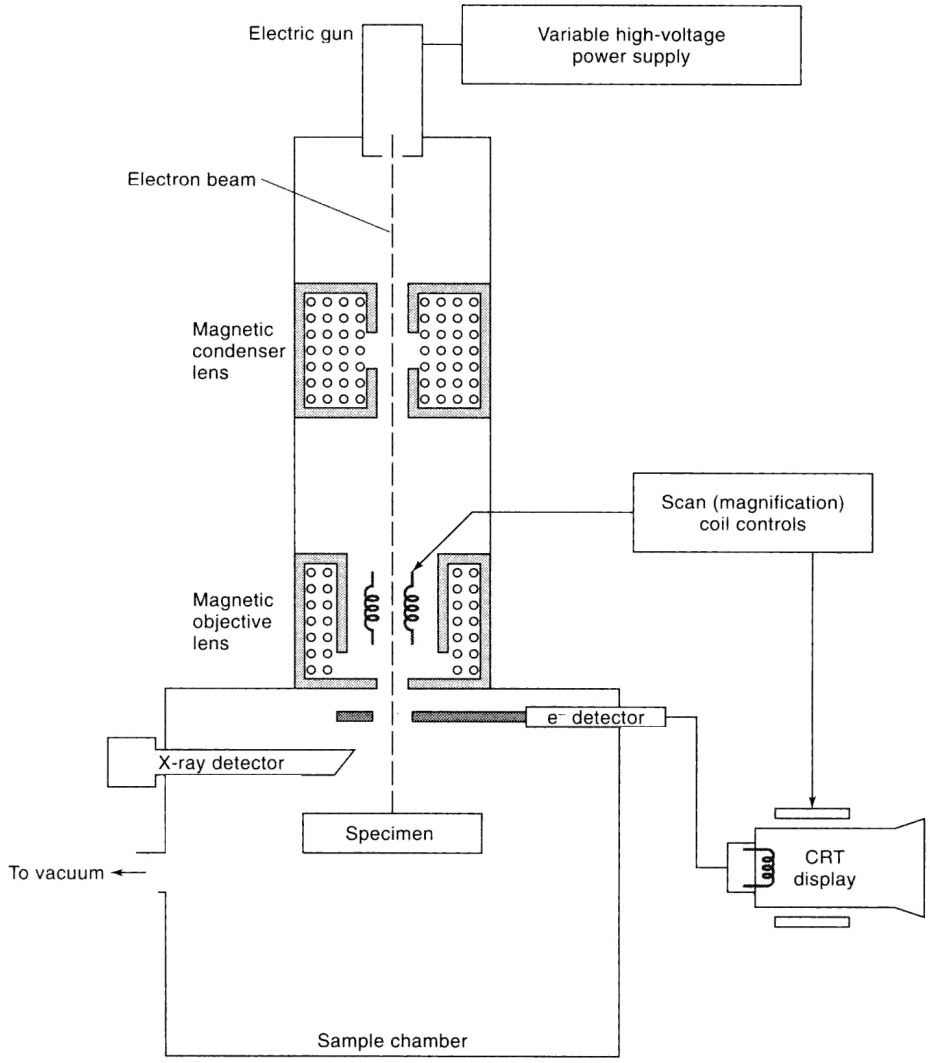

Figure 14: Principal sketch of a SEM /Skoog/

The electrons are generated by the electric gun or filament as seen on top in figure 14. This particular filament is the main difference between SEM (Thermo ionic source) and FESEM (cold cathode). The cold cathode electron source enables the use of a lower accelerating voltage in the FESEM and thus a lesser need of metallization of the specimen /Burggraaf/. This is a great advantage since the metallization might bury interesting surface morphology such as the pores.

The electron beam is focused on the specimen using a set of magnetic lenses, as illustrated in figure 14. As the electron beam strikes the specimen, it would interact with it and cause an ionization of the specimen. Many types of electrons emitted from or interfering with the sample exist. This is illustrated in figure 15:

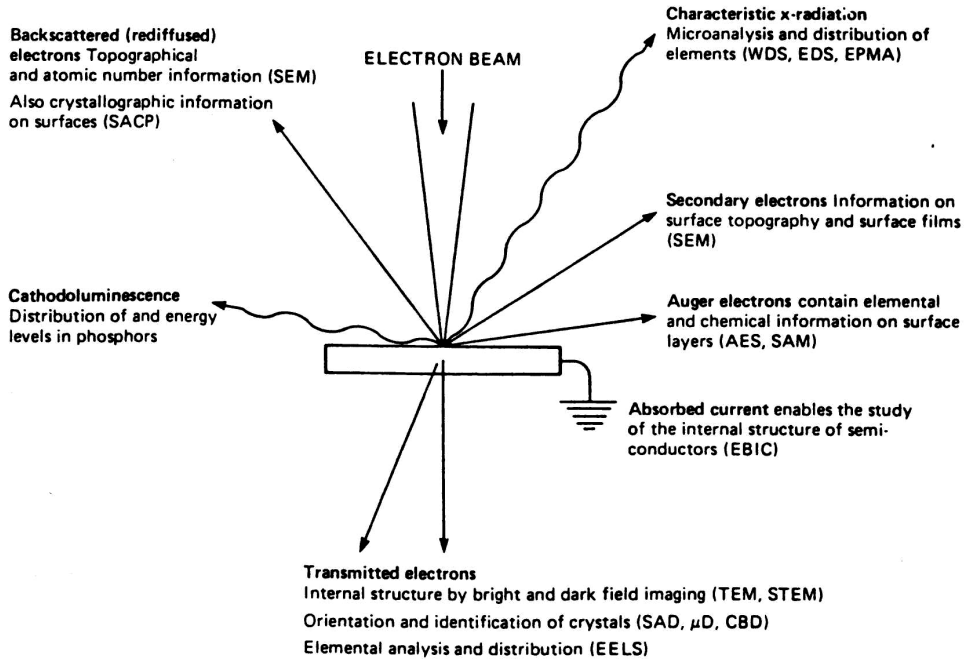

Figure 15: Different electrons available for detection in SEM and related techniques. /Einarsrud/

One form of electron or other secondary phenomenon emitted from the sample according to figure 15, is detected with the appropriate detector and the result is transmitted to a computer. Thus by letting the beam scan the surface systematically, an image of the surface is obtained. Depending on the type of detections (according to figure 15) different characteristics of the sample can be highlighted. The use of the characteristic X-radiation, upper right in figure 15, is of special importance since it enables the chemical composition of the sample to be determined by the elemental analysis option. The principle of the detection is as follows: /Einarsrud/
X-rays can originate from two distinct mechanisms when electrons interfere with the sample:

1. Retardation of the electrons in the electrostatic field around the atomic nucleus generates a continuous spectrum of wavelengths, i.e. retardation radiation.
2. Characteristic X-ray radiation is emitted when an exited element (atom) relaxes to the ground state or a lower energy state.

Only the second mechanism is element specific and thus the one discussed here. In the cases where the primary electrons have sufficient energy they can eject electrons from the K, L or M shell as indicated in figure 16.

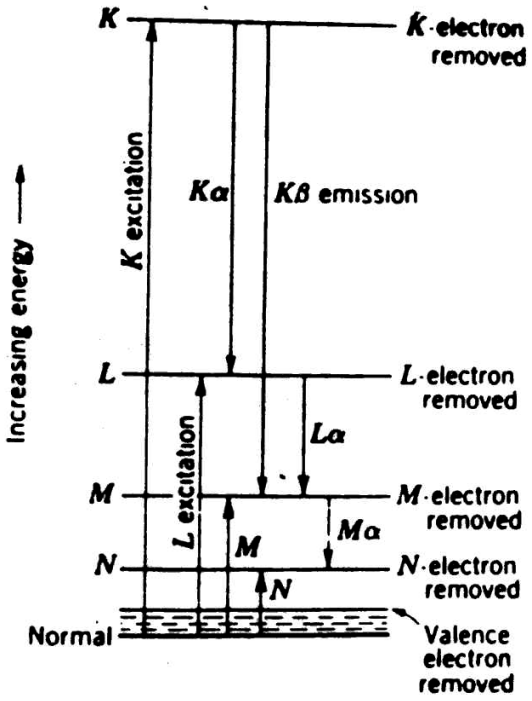

Figure 16: Schematic overview of a energy level diagram. /Einarsrud/

When the exited atom returns to the ground level electrons from a higher orbital will replace the lost electron. The energy difference between the orbitals is then emitted as a photon with a specific wavelength in the X-ray region of the electromagnetic continuum. Since the energy levels in figure 16 are element dependent, the emitted x-ray radiation will be characteristic for that element. Thus this characteristic x-ray can be used both in qualitative and quantitative chemical composition analysis. However, since the incoming electrons from the SEM are highly focused, a pattern of analysis has to be chosen which may be a point, a line or a limited area.
The lightest elements, i.e. hydrogen, helium and lithium have characteristic peaks outside the regular x-ray detection area and they can therefore not be detected.

4.3.2 Atomic force microscope

Atomic force microscopy is one technique among the scanning probe microscopy (SPM) "family". In AFM a microscopic tip is allowed to interact with a small part of the surface that is investigated. The AFM have some great advantages compared to SEM techniques, which include /Burggraaf/:

- AFM has a higher resolution
- AFM is non-destructive
- AFM requires no sample pre-treatment
- AFM spectroscopy is performed at atmospheric pressure.

The main components in the AFM are given in figure 17.

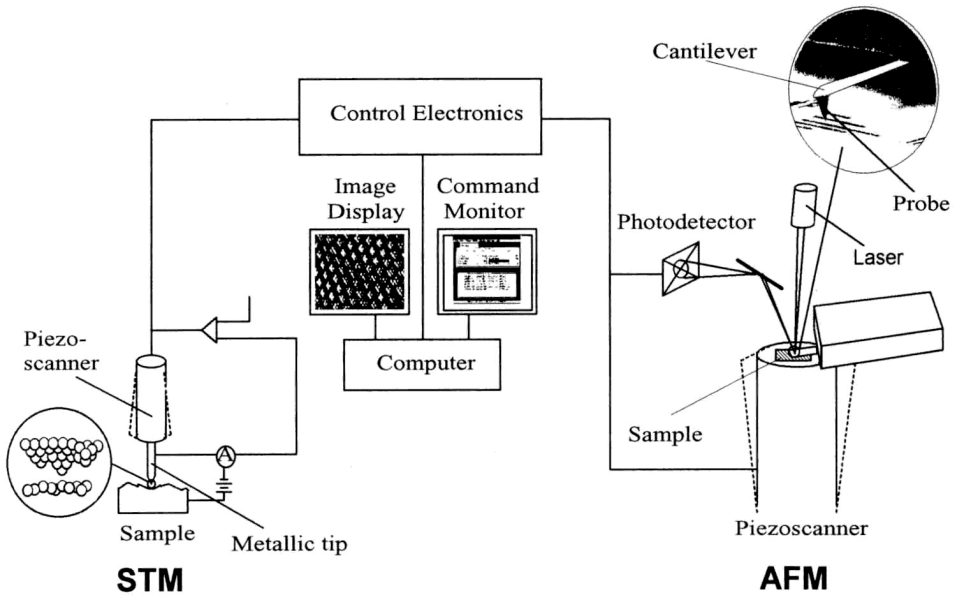

Figure 17: Schematic overview of the main components in SPM with AFM on the right hand side. /Magonov/

It is important that the tip (cantilever) is able to move freely over the surface and thus a too-bulky surface may cause the cantilever to get jammed on the surface. If that happens the cantilever will break and it must be replaced.
AFM spectroscopy is mainly performed in two different modes: The contact mode and the tapping mode. In both modes the surface is scanned with a sharp probe and the difference is whether the probe is in physical contact with the sample (contact mode) or oscillating from a distance of a few nanometres towards contact with the surface (tapping mode)
As indicated in the upper right corner of figure 17 (zoomed in), a fine tip is attached to the cantilever that scans the surface with a given constant force. The interaction between the tip and the sample causes an extremely small change in the lever position that is measured by laser interferometry. The output from the laser interferometry thus provides an image of the topography of the sample. The

oscillation amplitude in the tapping mode can be adjusted by the user to fit soft material and to give high resolution images.

4.4 IR spectroscopy

Generally it is the chemical bonding in a molecule that absorbs IR (Infra Red)-radiation. For this absorption to occur it is necessary that a difference in the dipole moment of the two atoms sharing the chemical bond exists. This means that diatomic symmetrical molecules like N_2, O_2 or Cl_2 do not absorb in the IR region but simple unsymmetrical molecules like HCl do. The absorption of IR-radiation is only possible when the frequency of the radiation is in resonance with the natural vibrations of the bounds in the molecule. This natural frequency is determined by which kind of atoms are connected by the bond and only slightly influenced by the other atoms in the distance of more than two bond lengths (meaning that couplings over long distances have little effect.). Different types of vibrations are identified in figure 18.

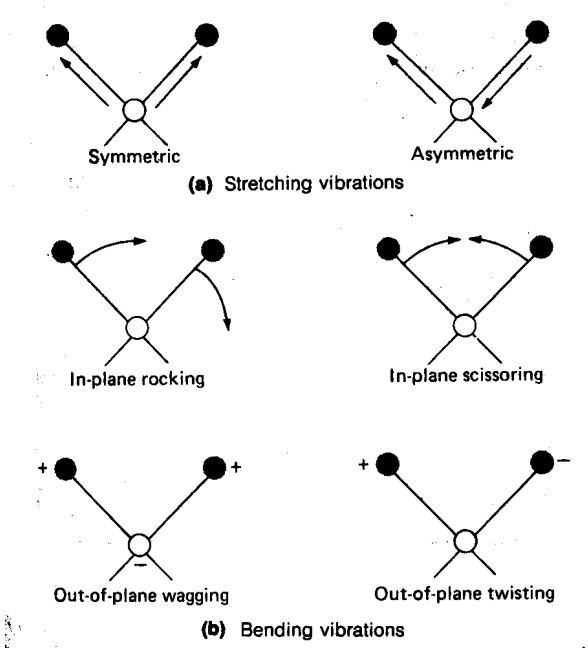

Figure 18: Vibration modes that are IR active. "+" indicates motion of the atom out of the paper plane towards the reader. /Skoog/

Not all of these vibrations lead to separate bands in the IR-spectrum because the corresponding intensity may be too low to detect or other bands from other chemical

groups in the molecule may interfere. The spectrum usually consists of two separate areas: The ”fingerprint” area (frequencies from 400 cm^{-1} to 1500 cm^{-1}) and the ”Group band” area (frequencies from 1500 cm^{-1} to 3500 cm^{-1}). I.e. two isomeric compounds like 1-butanol and 2-butanol would have identical spectra in the group band range and different spectra in the fingerprint range. Good identification frequencies are those that do not change much in frequency as their chemical environment changes. As an example the C=O frequency is identified as an intense peak around 1600 cm^{-1}-1700 cm^{-1} both in ketones and acids. Tables of characteristic frequencies are available in any book about IR spectroscopy, i.e. /Skoog/ or /Silverstein/

An IR-spectrum can (in theory) be acquired in two different modes:

- One frequency at a time (typical double beam accessory).
- All frequencies measured instantaneously (Fourier Transform Infra Red spectroscopy, FTIR).

Because of the much shorter sampling times required by FTIR it is almost solely in use. In the following only FTIR will be discussed. A typical FTIR instrument consists of a moving mirror assembly as indicated in figure 19:

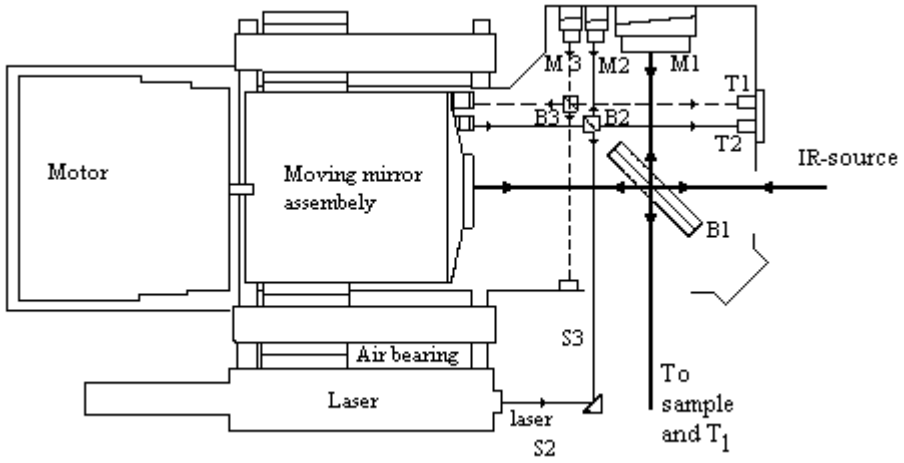

Figure 19: Moving mirror assembly in a FTIR /Skoog/.

As can be seen from figure 19, all the mirrors are semitransparent and a tree beam systems exists. This tree beam system consists of a laser system used to measure the exact position and speed of the moving mirror, a white light system to measure the exact location of the Zero retardation and of course the IR system /Skoog/. The IR

beam consists of all frequencies and interferes with the sample. After the IR-beam has interfered with the sample an interferogram, as indicated in figure 20, is measured in the time continuum:

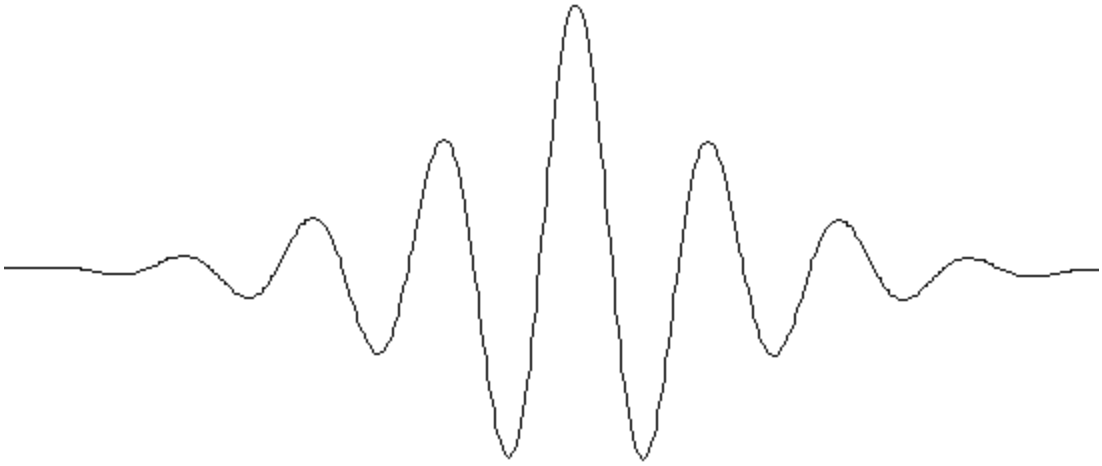

Figure 20: Typical IR time continuum interferogram detected by a FTIR instrument. The largest peak in the middle corresponds to zero retardation. /Skoog/

This interferogram, which is a plot of the intensity vs. time, is then Fourier transformed and a familiar intensity vs. wave number (or frequency) results.

In general, there are several modes of use developed for samples of varying nature. For dense material the following methods can be used to obtain a spectrum:

- Standard transmittance measurements. Requires, of course, that the sample is at least partially IR-transparent.
- KBr tablet method. This is also a transmittance measurement but the sample can be less IR-transparent than what is required by the standard method. This method is capable of measuring powder samples.
- Diffuse reflectance measurement. This is, at the name indicates, a reflective method. The method is excellent for powder samples.
- (Horizontal) Attenuated Total Reflectance, HATR, measurement. Another reflective method that can be used for both solids and powder.

Since SiO_2- glasses are IR-opaque below 2000 cm^{-1} the standard transmittance method is hard to use for qualitative purposes. In this work the HATR technique has been used. The HATR technique is very simple to perform once it is properly

calibrated and aligned. There is no need of sample preparation if the surface is flat and clean from contaminants. Figure 21 shows a sketch of a typical HATR accessory

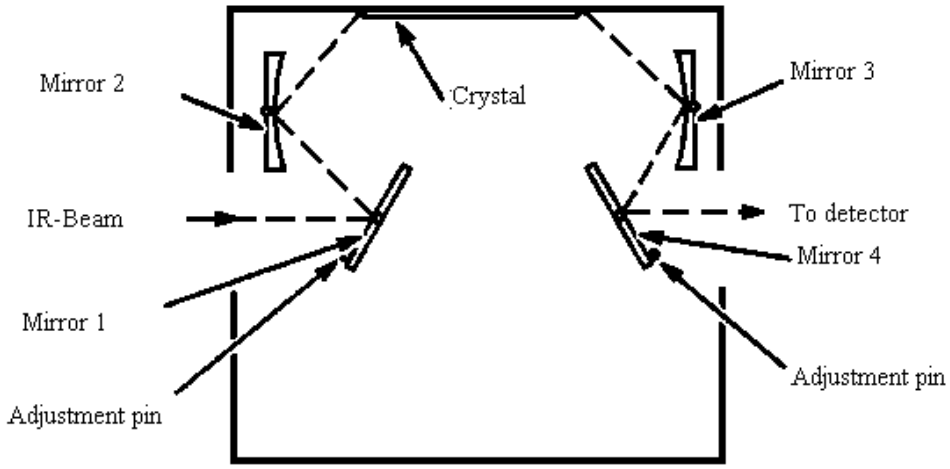

Figure 21: Principal sketch of a HATR-accessory. /Perkin Elmer/

Various mirrors reflect, as given in figure 21, the IR-beam originating from the instrument, until it enters a ZnSe-crystal. Inside the crystal, the beam is totally internally reflected at each of the crystal surfaces (an odd number of times in total). However, it has been shown that the IR-beam extends a bit outside the surface, in the range of several μm or a few wavelengths, before it re-enters the crystal /Skoog and Perkin Elmer/. Thus if a solid IR-opaque sample is brought in close contact with the crystal, an IR-spectrum could be obtained. To ensure close proximity between the sample and the crystal, it is of importance that the sample is either in powder form or uniformly plane. The IR beam then continues towards the detector.

4.5 References

Barrett, E. P., Joyner, L. G. and Halenda, P. P.: "The determination of pore volume and area distributions in porous substances. I. Computations from nitrogen isotherms", J. Am. Chem. Soc., 73, 373, 1951.

Burggraaf, A.J. and Cot, L.: "Fundamentals of inorganic membrane science and technology", Elsevier science B.V., Amsterdam, 1996.

Einarsrud, M. -A.: ”Scanning elektron mikroskopi og mikroanalyse” Compendium NTH 1992 (in Norwegian only).

Magonov, SN & Whangbo, M-H: “Surface analysis with STM and AFM”, VCH Verlagsgeschellshaft mbH, Weinheim,1996.

Perkin Elmer: “Horizontal ATR accessory”, part no. 0993 4080 (instruction manual) C- edition, Nov 1996.

Silverstein, R.M. and Webster F.X.: “Spectrometric identification of organic compounds”, 6th ed., John Wiley & sons Inc, 1998

Sing, K.S.W (Chairman): “Reporting physisorption data for gas /solid systems with special reference to the determination of surface area and porosity” Pure and Appl. chem. Vol. 57, no.4, pp 603-619. IUPAC, 1985

Skoog, D. A. and Leary J. J.: “Principles of instrumental analysis” Saunders college publishing Fort Worth 4th edition 1992.

5 EXPERIMENTAL

5.1 N_2 adsorption

The apparatus used in the N_2 adsorption measurements was a Belsorp 28 manufactured by Bel Japan Inc. This instrument has the ability to run three samples simultaneously. The sample holder for this apparatus is sketched in figure 22.

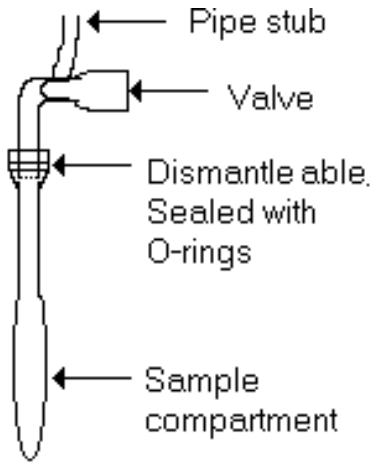

Figure 22: Portable and separable sample holder for adsorption measurements.

As indicated in the figure, the sample holder is separable at the junction in the middle. This makes it easier to place the sample in the sample holder (drawn in the lower part in figure 22). The junction is sealed with a double set of Viton® o-rings. The valve is of great importance in order to keep an inert atmosphere with a defined gas pressure in the sample compartment. This is of crucial importance when the mass of the outgassed sample is to be determined, since the sample holder then had to be disconnected from the apparatus and weighted on a standard lab balance.

5.1.1 Procedure

A sample holder without a sample, was evacuated for approximately 5 minutes (P_{tot}<1 mmHg (<1.33 mbar)) and then filled with 1 bar of helium. The valve indicated in figure 22 is then closed and the sample holder was disconnected from the evacuation line and weighed. The mass is determined by a balance with accuracy in

the 0.1 mg range. The method required approximately 0.5 g of sample, which correspond to ca. 3 cm of glass tube. The sample holder is dismantled at the junction, and the sample is added. The sample holder was then re-connected. As indicated in figure 23, the sample was connected by an Ultra-torr ® coupling to the preheat treatment line of the Belsorp 28 (the right hand part of figure 23, marked with (41)).

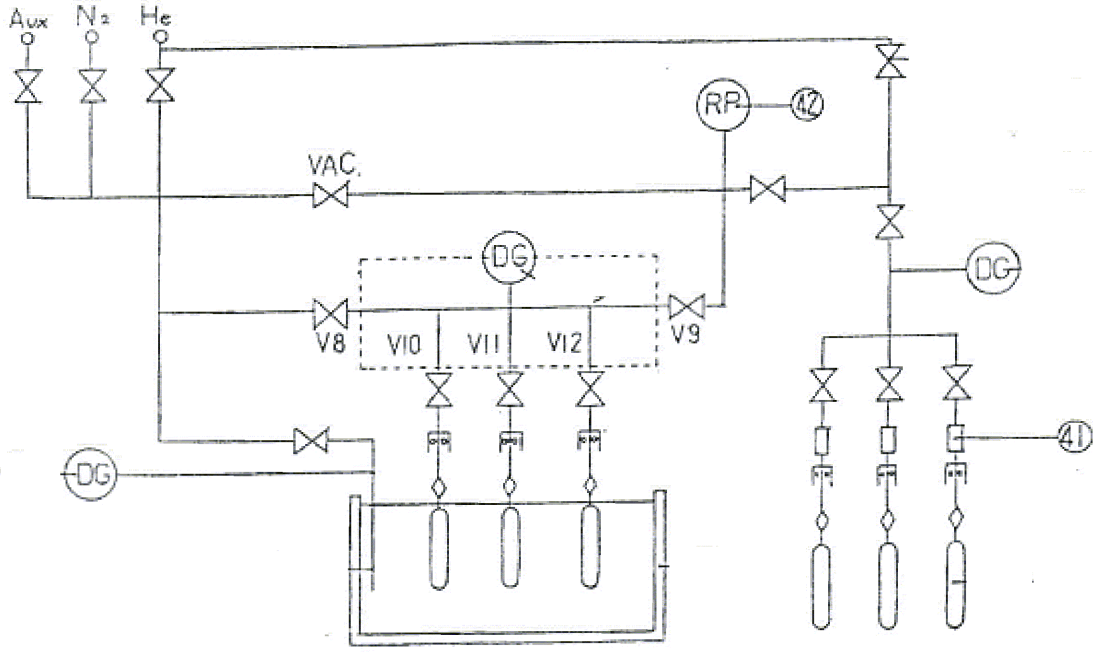

Figure 23: Flow sheet of the Belsorp 28. /Bel Japan/

The preheat treatment was according to the following scheme: The sample was evacuated and heated to 80ºC (during 2 hours, rate= 25 ºC/h) and then kept at this temperature for 5 hours. The sample was cooled to room temperature at the same rate. Helium was fed into the sample holder up to 1 bar and the valve shown in figure 22 was closed. The sample holder with the degassed sample was weighed and the sample mass calculated. The holder was connected to the N_2-adsorption part (left hand side of figure 23) and the valve was opened upon the PC software request. The Belsorp 28 has a well-regulated level system for keeping the liquid N_2 level almost constant, which is important for reproducible isotherms. This system is not included in the figure but it consists of a reservoir tank for liquid N_2 and a precise level sensor. The apparatus is automatically controlled by a PC and the factory standard setup has been used in the measurements reported here. The PC software has options where

the user can make a best fit of the BET isotherm to the measured isotherm and, for mesoporous material, to calculate the pore size distribution according to the BJH method.

5.2 Stereology analysis

5.2.1 Scanning Electron Microscopy

The method for mounting the specimens is identical for all the different SEM-techniques, except for the transmittance-SEM and is depending on the electric conducting ability of the specimen. It is crucial to ensure that excess electrons at the surface of the sample are efficiently drained, thus preventing a charge build-up that causes the SEM image to lose contrast. If the sample is an electric insulator, as with glass, then it is best to coat the sample with a gold layer. This was done in the field emission scanning electron microscopy (FESEM) tests but not in the standard SEM.

Trained personnel were hired to capture the FESEM images. The author was not present during the analysis, so the choice of mounting technique and other optimizations are uncertain.

Procedure

The regular SEM images were obtained the following way, using a Hitachi S-3500N apparatus:
Small pieces of the glass membranes, approximately 10mm^2/piece, were glued with carbon glue onto the sample holder. The samples had either the concave and convex side of the surface facing up. The carbon glue is electrically conductive, thus it helped to ensure both that the sample was spatially fixed during the subsequent evacuation and that the sample was sufficiently grounded to prevent charge build-up. The glue was hardened for 24 hours after mounting before the measurement was performed. In order to obtain a detailed and high quality SEM image, several parameters must be optimized simultaneously, including the contrast, the hue, the astigmatism, the accelerating voltage, the working distance, the proper pressure and detector choices (see figure 15) and the sample tilt angle. The best image often

results from a series of optimizations corresponding to a series of increasing magnifications.
The elemental analysis was performed on the sample while it was evacuated inside the SEM. To analyze the surface, or in this case the pores, a specific sample pattern must be specified. A single point sample was chosen in this work.

5.2.2 Atomic Force Microscopy

AFM needs virtually no sample preparation as long as the sample can be spatially fixed. Although in practice, flat samples of a size of a few mm^2 are generally recommended.
The images were obtained the following way with a Nanoscope III from Digital Instruments, using the contact mode (in air):
The sample was fixed with the convex side pointing upwards from the sample holder using tape with glue on both sides. The sample was a small fraction of a cylinder wall and the corresponding cylinder length was carefully aligned with the tapping direction of the AFM. This was necessary otherwise the tip may get jammed on the surface. A PC controlled the AFM with software that automatically tried to optimize the parameters that influence the image quality. This optimization seemed to yield fair quality pictures at moderate to high magnifications. However, the AFM is very sensitive to vibrations and the current setup is judged to be insufficient.
To perform the AFM analysis the author got help from a trained person, but the author was present to influence the process of finding an interesting patch of the sample.

5.3 FTIR spectroscopy

A Perkin-Elmer Universal ATR (attenuated total reflectance) has been used in these measurements. This work discusses the use of HATR only. In general if spectra from different samples are to be compared it is important that the samples have identical concentrations or that a peak in the spectra of the various samples used is unchanged and can serve as an internal standard. The choice of a suitable peak is difficult, especially since the peak intensities in the reflectance spectra are different from the transmittance spectra /Skoog/. In general, the best way of obtaining reproducible spectra from the HATR technique is to ensure that the sample is

powdered and evenly distributed over the whole measuring crystal. To ensure a reproducible penetration depth of the IR-beam, a gentle constant force should be applied to the sample.
However, the sample as a whole could not be powdered since that would ruin it as a future membrane, thus only a small piece was available to be powdered. This was not sufficient to cover the whole measuring crystal so the spectra obtained here should only be used for indicative analysis purposes.

Procedure

Two different approaches were tried:

1. Spectra obtained directly of the membrane material: A background spectrum with an empty measuring crystal was recorded. Then a piece of the sample with an area of ca. 10 mm^2 was placed directly on top of the measuring crystal without applying any force. This was not enough sample to cover the entire surface, but it should be sufficient to give a qualitative spectrum of the membranes.
2. Spectra obtained from glass plates. These glass plates, ca. 15x25x1 mm, were treated almost like the glass tubes, meaning they were acid leached, surface modified and chlorine exposed, but they were not phase separated (meaning that boron will be present to a larger extent in the glass plates than in the glass tubes) : A background spectrum with an empty measuring crystal was recorded. Then a plate was placed directly on top of the measuring crystal and a constant force applied (46 [no unit given by the producer]). In chapter 6 the spectra obtained by using the plates are clearly marked in the corresponding figure captions

5.4 Permeance measurements

In general there are two different approaches for measuring the permeance [m^3(STP)/(m^2 bar h)] (or the permeability[m^3(STP) m/(m^2 bar h)] if the thickness can be determined) for a gas through a membrane./Mulder/ The simplest approach is to apply a pressure, above atmospheric pressure, on the high-pressure side of the membrane and then measure the flux of gas penetrating the membrane. This flux can

be measured by a bubble flow meter or if more accuracy is desired, by a mass flow meter. The second alternative is a closed set-up (as the permeation apparatus in figure 24) where the low-pressure side of the membrane is evacuated using a vacuum pump. The permeance is then calculated from the linear steady state pressure increase on the vacuum side as the test proceeds (a derivation of how the permeance can be calculated from the stable pressure increase for the closed set-up is found in appendix 3).

5.4.1 Pure gas permeances

In the case of the aggressive gases studied in the current project, the bubble (or mass flow) method is not a desired setup because:

1. It is more susceptible to gas leakages since a higher pressure is needed on the high pressure side of the membrane to obtain the same pressure gradient as in the closed set-up.
2. It would require a continuous disposal handling procedure for the aggressive gases.
3. The moisture from the ambient air can back-diffuse into the apparatus, react with the chlorine or hydrogen chloride and lead to very harsh corrosive conditions.

These disadvantages are more easily controlled in the closed vacuum set-up where the gas can be let out in a batch process and the apparatus can be filled with dry nitrogen if it is to be left idle for a longer period, thus minimizing the corrosive attack on the apparatus. Another advantage of the closed setup is that it is possible to cover several orders of magnitude of permeances by simply allowing the test time to increase. Contrarily to what is the case by using a mass flowmeter, there is no need for changing to a lower scaled pressure transducer as the permeance slows down.

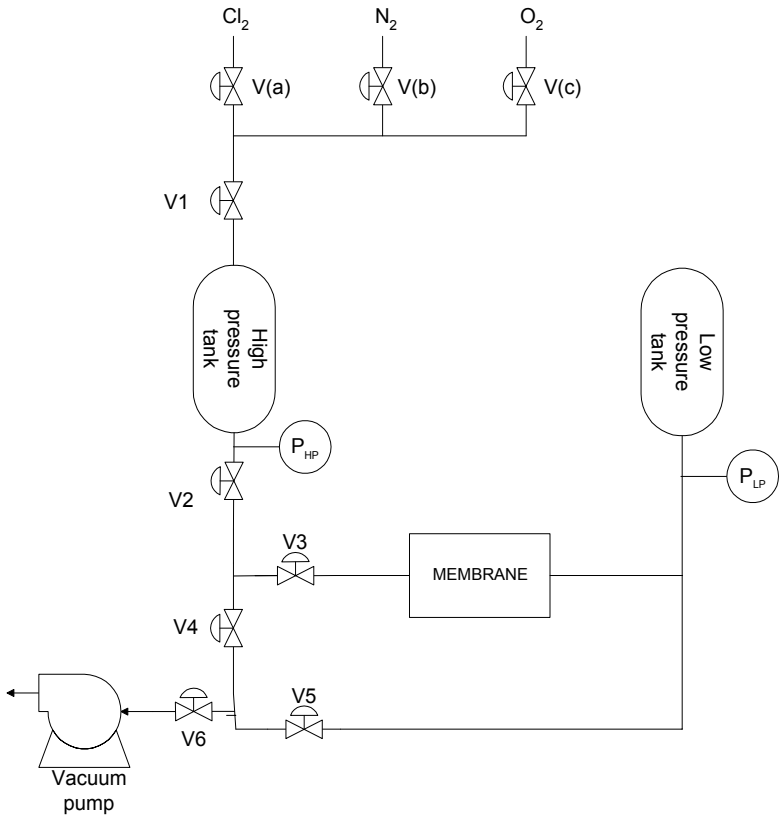

Figure 24: Flow-sheet of the closed set-up permeance apparatus used for pure gas measurements in this thesis.

In such a closed set-up it is important that the pressure transducers are of high quality, meaning that they have small errors and can sustain the aggressive environment. Both the MKS 121AA (0-5000 mbar range) used on the high pressure side, P_{hp} in figure 24, and the MKS Baratron 626 (0-100 mbar range) used on the low pressure side, P_{lp} in figure 24 meet these requirements. It is of vital importance that the deviation in the linearity of the response of the permeance pressure transducer is as low as possible in terms of obtaining a reproducible permeance in successive runs. This rig was designed and built by the MEMFO research group prior to this project was started.

A detailed analysis of the experimental errors in the permeation apparatus are given in appendix 3.

Membrane module design

The only drawback in the closed permeance set-up is that the module in which the membrane is to be mounted has to be vacuum proof. This was in particular a

problem in designing a suitable module for testing the brittle glass membrane. A sketch of the first useable module designed is drawn in figure 25:

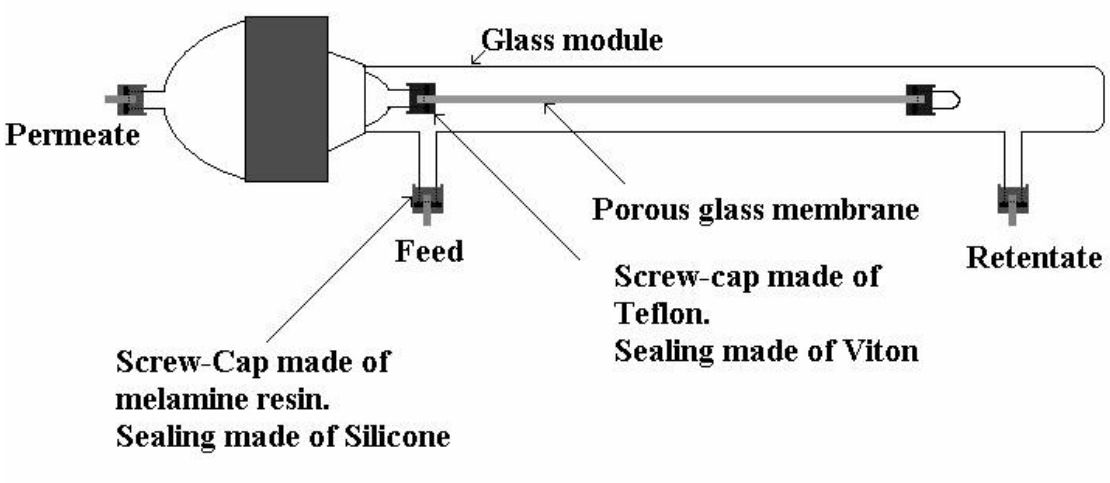

Figure 25: "Original" module design for the permeability measurements

The silicone rubber gaskets used in the module was a problem since the silicone rubber deteriorates after relatively short time exposures to chlorine or hydrogen chloride. A new and improved module was designed as shown in figure 26.

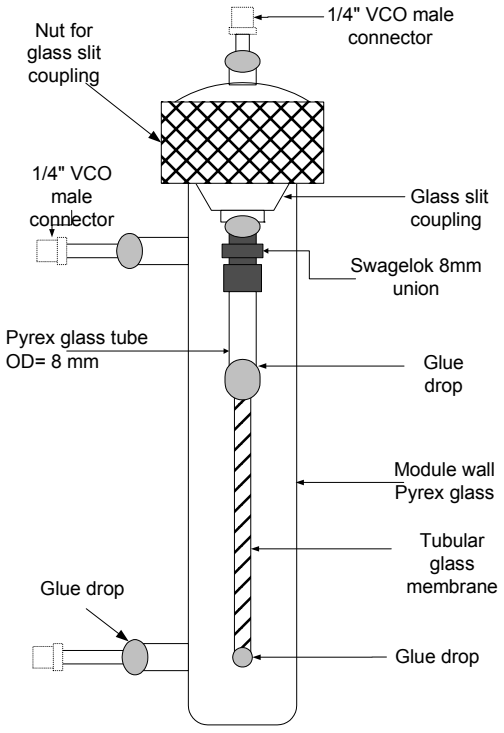

Figure 26: Detailed sketch of the module developed for the permeance measurements.

The advantage of using an extra Pyrex® glass tube into which the glass membrane is glued is that the wall thickness of the extra Pyrex® tube will be greater compared to the wall thickness of the glass membrane. The glass membranes are synthesized from hand-drawn glass tubes where the deviation in the diameter is much larger than in the factory made commercial Pyrex® glass. This causes the Teflon® ferrules in the Swagelok® union to be vacuum-tight against the glass at a much lower applied force than if a smaller diameter union should have been used directly with the membrane.
The glue used is Araldite® AV 138M with the hardener HV 989. This glue has excellent wetting abilities for both glass types and the glue is also stable against the aggressive gases, for temperatures up to 80°C over long time. The glue forms a gas-tight seal when hardened, which is highly important when it shall be used in permeance experiments.

Procedure for pure gas permeance measurements

Before a glass membrane was used for the first time, it must be conditioned by heating under vacuum up to 80°C. This temperature must be kept for two hours. This conditioning procedure was required because of slightly different reasons for the pure and surface-modified membranes: The pure microporous glass is hygroscopic, so adsorbed water will be present in the pores (the membrane was rinsed with water after the acid leaching to remove excess acid and water will adsorb from the ambient air during storage). This causes some pores to be (partial) plugged, thus the permeance will be lower than it needs to be. The surface-modified membranes have excess organic vapours (mostly toluene) in the pores originating from the surface modification procedure, and water is also adsorbed from the ambient air during storage, thus giving a lower than expected permeance and poorer stability.

After the regeneration procedure and prior to each new gas tested, the membrane was evacuated overnight (at least 12 hours) at a vacuum pressure below 1 mbar.

All the valves indicated in figure 24 are ball valves (Whitey Ball 33 series valve, Whitey is a sub-division of Swagelok®) and they were all semi-automatically operated by a pneumatic system which was controlled by a computer using the LabView program. LabView was also used to log the pressures from the two

pressure transducers (indicated in figure 24) each second and to save the pressure data into a computer file.

A measurement started by creating a new log file in LabView, which then automatically closed all the valves. The high pressure tank was filled with the desired test gas up to the desired test pressure (plus 10% extra because the small flashes caused by the gas filling the volumes between V2 and V3, between V3 and the module and the high pressure side of the module). The test was started by opening V2 and then V3 (figure 24). After a sufficient test time (experience based) the logging was stopped and the apparatus evacuated.

The pressure data file created by LabView was then further analyzed in Matlab. For the Matlab analysis three scripts were written to be able to:

1. Plot the vacuum pressure as a function of the elapsed experiment time. From this plot the start and end points of the time range in which the pressure increase was linear has to determined. (A linear pressure increase corresponds to steady state permeance through the membrane. This is actually only correct in the start of an experiment because as time elapses the pressure on the high pressure side is decreasing and the pressure on the low pressure side is increasing, thus leading to a decrease in the driving force across the membrane. This will cause the vacuum pressure vs. time to deviate from the straight line at higher vacuum pressures and longer times, giving a typical S-shaped curve.)
2. Calculate the slope dp/dt. This was done in Matlab by a linear least-square best fit of the logged pressure data in the linearity region determined in step one. Information about the membrane area and the test temperature must then be entered so that the program could calculate the permeance [m^3(STP)/(m^2 bar h)]. In many cases this was all the information the test performer required, but if the time-lag was wanted step 3 was also required.
3. Determine the time-lag from the transient state at the start of a permeance measurement. The only additional information required to be able to perform these calculations was to determine the stable base line (or start line). The time-lag is then the cross point between an extrapolation of the best fit found in step 2 and the base line.

The equations for determining the permeance in a closed set-up, copy of the Matlab script and estimations of the errors in the apparatus are given in appendix 3.
In the cases where several pressures of one gas were measured, the membrane was evacuated for at least one hour between each measurement and the permeance measurements were always performed in sequence, starting with the lowest pressure and ending with the highest.

In the cases where the permeance is measured at several temperatures for a specific gas, the membrane is evacuated for at least two hours after the temperature has stabilized on the new level.

5.4.2 Permeance measurements with simultaneous UV – radiation of the glass membrane tubes

Since the reason for trying a combination of permeance measurement with simultaneous UV-radiation is not obvious, a brief explanation follows:
Chlorine is known to be quite a "reactive" reagent, and as documented in chapter 6, effort has been put into proving the various materials to be chlorine stable. UV-radiation shorter than a specific wavelength (492 nm, estimated from the chlorine-chlorine bound energy) has the ability to break the chlorine -chlorine bound in chlorine gas into two chlorine radicals. This is summed in equation 5.1:

$$Cl_2 + h\nu \rightarrow 2Cl\bullet \qquad (5.1)$$

The chlorine radical is believed to have a significantly larger reaction rate with the membrane material than chlorine gas (Given identical process conditions). If the chlorination reaction ceases before the transport properties are too damaged, then the original surface modifying compound could be used despite some deterioration of the material.

The UV radiation catalyzed chlorination setup is drawn schematically in figure 27. The module used in these experiments is slightly altered from the module drawn in figure 26.

In addition to what is drawn in figure 27, a sheet of aluminium foil was wrapped around the module and used to shield the environment from the UV-radiation and to focus as much radiation as possible on the membrane surface.

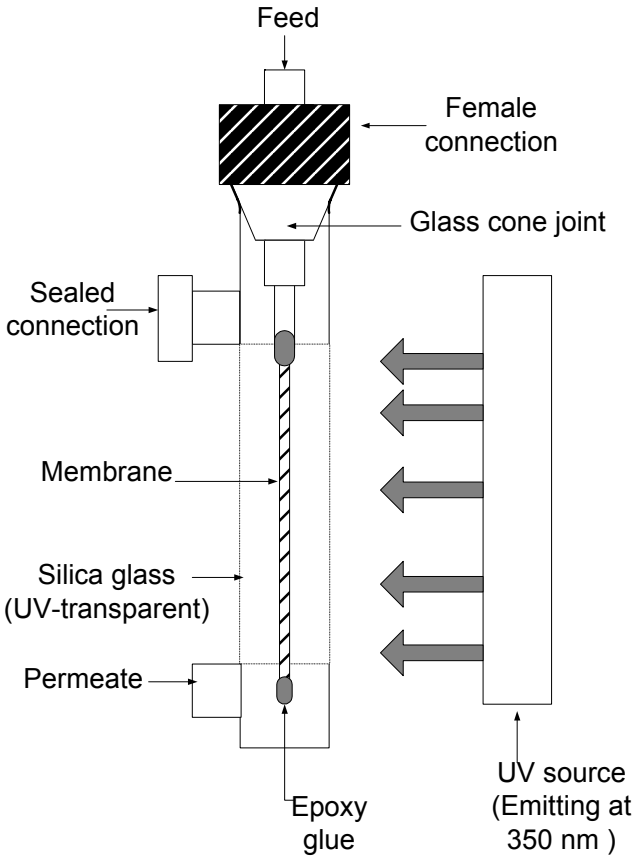

Figure 27: Experimental setup of the chlorine exposure with UV-radiation.

Reaction procedure

Prior to the gluing, the length of the Pyrex® glass had to be adjusted so that the active membrane area was aligned with the UV-transparent Silica glass region of the module as indicated in figure 27.

The membrane module was turned 60° each 1/6 of the total exposure time to ensure the most homogeneous radiation exposure over the whole active membrane area.

This combined test started as a regular permeance test but after approximately 1000 seconds the aligned UV-source was switched on. The absolute pressure on the low-pressure side was then typically 7 mbar.

5.4.3 Permeance measurements of the glass fibres

The permeance measurements of the fibres are quite tricky and believed to be less accurate than the measurement performed with the tubes due to several factors that are heavily entangled:

- The fibres were relatively short. They were approximately 10 cm in length and had an outer diameter of 0.05mm. This led to a small active membrane area per fibre.
- Small membrane areas have a low flux and thus the leakage of the cabinet limited how small fluxes could be measured.
- Gluing of several fibres into a module was difficult since the fibres tend to cluster, thus leading to a narrow hole between them from which the glue seems to be more easily drained.
- Using small droplet of glue to seal of the dead end of the fibre was also difficult since the capillary forces of the glass-glue interface were so strong that the droplet of glue could actually migrate against the gravitational force.
- Build-up of static charges during the gluing process did in the worst case lead to a fibre bundle that was impossible to mount into the module.

Mounting procedure

As an attempt to minimize the effects described above, the following procedure was implemented: As for the membrane tubes, the 8mm outer diameter Pyrex glass tube was used as a fibre bundle template. However, in order to prevent the fibres from clustering during the glue hardening process, the gluing was performed in two stages:

1. The glass tube was glue sealed at one end and left to harden over-night.
2. The following day three holes were drilled through the glue seal. A fibre was thread through each hole and a new rim of glue applied to seal the old seal and the fibre. The dead end of each fibre was sealed individually by dipping the end into the glue.

In some cases the glue drop migrated up the fibre during the hardening process and in those cases the end had to be glued over again. From this point on, the procedure was identical to the "tube measurement" permeation procedure.

5.4.4 Mixed-gas permeation test

To be able to analyze the mixed gases, a modification of the permeation equipment is necessary. Figure 28 gives a sketch of the set-up for mixtures:

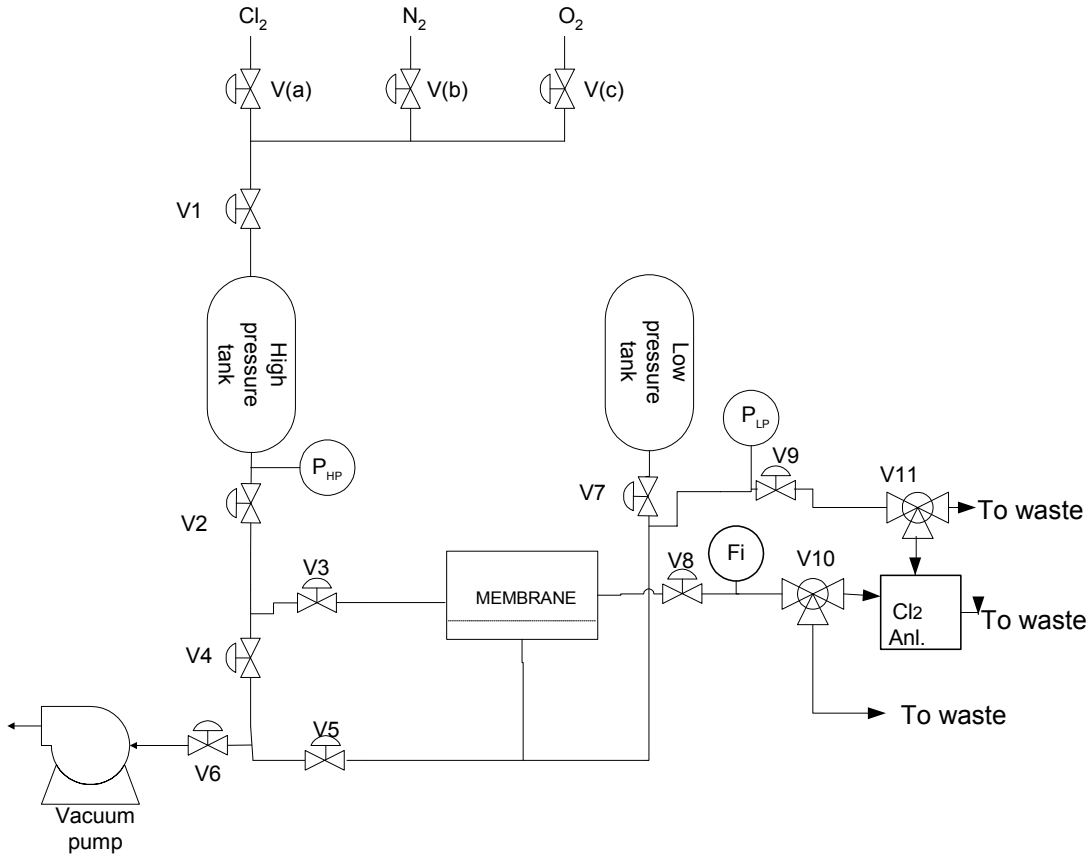

Figure 28: Mixed-gas permeation set-up.

In figure 28 the valve V7 is of particular interest, since it allows the low pressure tank to be shut down during the permeation test thus, decreasing the fill-up time of the low-pressure side 20-folds.

The low-pressure transducer used in this setup was a 1000 mbar MKS 121AA transducer. Since the set-up was "loosing" gas through the spectrophotometer (Cl_2 Anl. in figure 28) and through the retentate, it was necessary to apply as high pressure as possible. The spectrophotometer used was a Sigrist, Sipro 2001 process-photometer. To handle the chlorine waste, three strong alkaline solutions were prepared (approximately 1 Molar NaOH) through which the gas was bubbled.

Procedure

The apparatus was evacuated for at least 2 hours between each test.
The gases were mixed in the high pressure tank using a simple additive partial pressure approach, (The mole fraction of each component was assumed equal to the partial pressure of that component). Chlorine was always added first. The measurement started by closing all valves (except the two three ways valves, V10 and V11) followed by the opening of valvesV2, V3 and V7. The valve V8 was used to set the cut rate (the ratio of the permeate flow over the feed flow). The flow rate was rather difficult to set to a low enough level to obtain any significant cut rate thus the cut rate in the experiments was close to 0 (lower than 0.1). However, the smallest stable retentate flow possible was used. Since it took ca. one hour to perform the permeation recording and another hour to fill the low pressure side, the retentate was analyzed first. In order to speed up the filling of the low-pressure side and to save gas, the valve V7 was closed after the recording of the permeation test. This increased the filling rate of the low-pressure side by a factor of 20. As the low-pressure indicator indicated that the low- pressure side was at atmospheric pressure the stream to the analyzed was changed to measure the permeate. After a stable readout of the analyzer was achieved, that for low chlorine contents took hours, a final high retentate flow (volumetric flow at least one magnitude higher than previously used) was measured. This last measurement was taken as a measure for the real feed composition.

5.5 Sorption measurements

The sorption of a gas on a material can in general be determined by two main methods: /Mulder/

- An accurate balance can be used to measure the weight increase during the sorption process and thus by plotting the mass increase as a function of time, the sorption isotherm is obtained. This is known as the gravimetric method.
- The sorption can be calculated from the pressure decrease in the sorption chamber after the initial gas flash. This is known as the volumetric method.

Because the aggressive gases are believed to possibly be ruining the balance in the gravimetric method, the simpler volumetric set-up has been chosen. Figure 29 gives the flow scheme of the single chamber adsorption set-up used in this thesis.

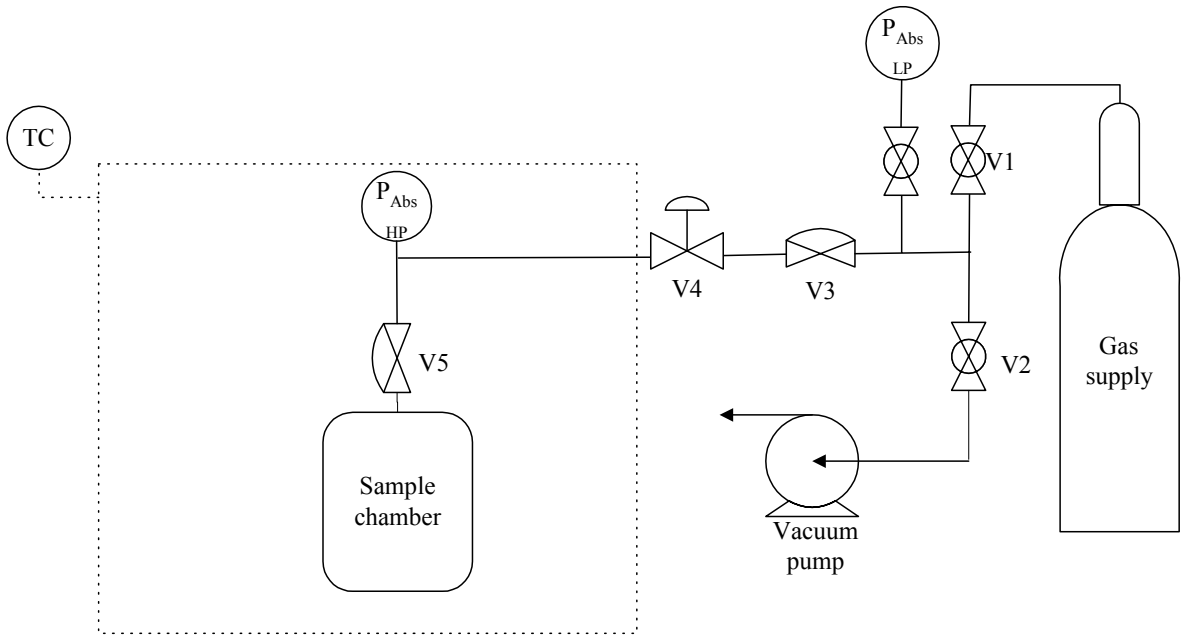

Figure 29: Flow scheme of the apparatus for the adsorption measurements

In the adsorption set-up or during an adsorption measurement there are some important factors to be aware of:

- The volumes of the of the sample cell, the pressure transducer, the tubes and valves have to be carefully volume calibrated in order to be able to calculate the adsorption properly.(detailed procedure given in appendix 4.1)
- The pressure transducer should be kept inside the temperature-regulated chamber in order to avoid unnecessary temperature gradients.
- The valve tagged as V4 in figure 29 should be of very high quality. This valve is the barrier between the sample and the rest of the world and a leak here can erroneously be interpreted as an adsorption.
- The amount of sample used has to be adjusted in relation to the available sample cell volume so that the resulting pressure decrease from the adsorption will be detectable on the pressure transducer.
- Long enough desorption times must be applied and the evacuation time should, as a rule of thumb, be at least twice the expected time it takes to obtain a stable adsorption measurement.

The sample chamber is made from high quality steel consisting of a volume of 17 cm^3 that can be easily accessed through a Svagelok® ¾" VCR (metal gasket face seal fitting) blind nut.

5.5.1 Single point adsorption measurement

The sample was evacuated at least overnight prior to each test. The maximum pressure test available in the set-up is a consequence of the pressure range of the pressure transducer. The flash resulting from having the sample chamber evacuated and the vis-à-vis volume (the volume of the tube, including the pressure transducer between V4 and V5 in figure 29) at the maximum detectable pressure gave a maximum test pressure of approximately 50 % of the maximum pressure. In the current set-up this meat that 3 bar was the maximum test pressure.
The equations used in the calculation of the sorption coefficient are given in appendix 4.2 and an estimation of the total apparatus error is given in appendix 4.3

5.5.2 Isotherm measurements

The adsorption isotherm has been measured, first starting with the lowest test pressure and adding on points without evacuation between them. When all the points on the adsorption isotherm were measured, the sample was evacuated for at least two days. This evacuation was done for two reasons: Firstly, the error of measurement was propagated during the series so it was important to reset the errors. Secondly, the determination of the start point of the adsorption (i.e. the pressure calculated from the flash calculation) required that the pressure reading was absolute, thus the pressure transducer output should be readjusted to zero.
The points on the desorption branch was obtained by starting with the highest pressure and then subtracting flashes (i.e. applying a vacuum or a lower than test cell pressure on the volume of the tube, including the pressure transducer between V4 and V5 in figure 29)

5.6 Diffusion coefficient estimation

Estimations of the total diffusion coefficient can be obtained by two different methods:

1) The diffusion can be calculated from the following well known equation /Mulder/:

$$P = D \cdot S \tag{5.2}$$

Where P= permeability [m^3(STP)m/(m^2 bar h)], D is the diffusion coefficient [m^2/h] and S is the sorption coefficient [m^3(STP)/(m^3 bar)].

Thus the diffusion coefficient can be calculated as the ratio between P and S at a given pressure and temperature.

2) The diffusion can be estimated from the time-lag in the start of the gas permeation measurement. Figure 30 gives a brief sketch of how this is done /Mulder/. The θ-value obtained from the plot, relates to the diffusion according to equation 3 /Mulder/:

$$\theta = \frac{l^2}{6D} \tag{5.3}$$

Where θ is the time-lag [s] and l is the membrane thickness [m].

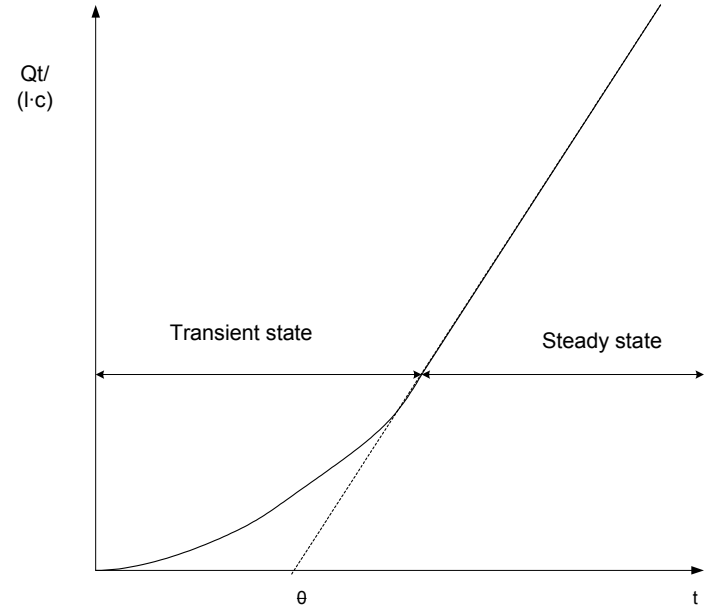

Figure 30: Time-lag measurements in gas permeation measurements /Mulder/.

5.7 Membrane gas exposure in durability chamber

In order to save run time on the permeance equipment, a durability chamber was designed by the MEMFO research group. In this chamber the membrane can be stored under a controlled specific atmosphere. Although there might be a difference in the response of the membrane upon a static exposure in the durability chamber compared to a dynamic long-time permeance test, this would at least give important information about the chemical stability of the membrane material. Figure 31 gives a sketch of the durability chamber used.

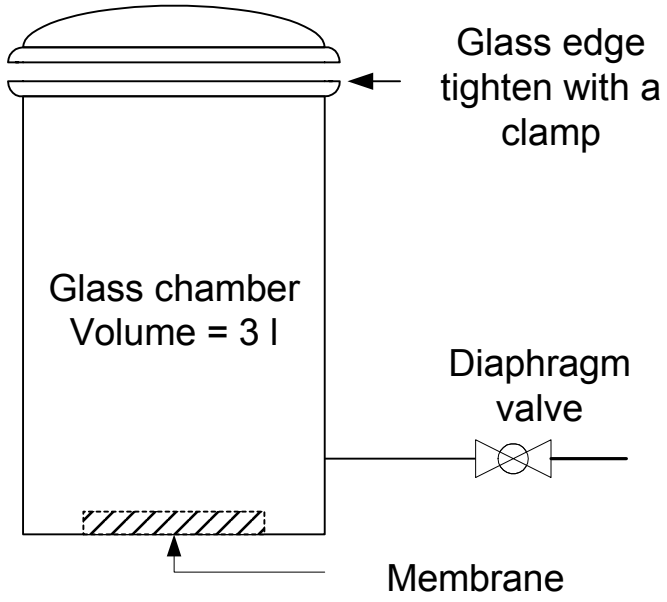

Figure 31: Sketch of the durability chamber.

The relative large chamber volume of three litres is chosen to ensure that the gas atmosphere would not change significantly even in the cases where the membrane is reacting with the gas.

Gas exposure procedure

A membrane for which the permeances for nitrogen and at least one other inert gas have been measured was placed in the durability chamber. A thin film of grease (Molycote® BG 87) was evenly distributed on the glass edges indicated in figure 31 before they were squeezed together by a clamp. The chamber was then mounted in the permeance apparatus replacing the indicated membrane in figure 24. Since the chamber only had one inlet, the high pressure connection to the module was sealed. This allowed the inspection of the degree of vacuum during evacuation by the low-

pressure transducer. It also ensured that the correct pressure was applied in the exposure through the reading of the high-pressure transducer.
After the chamber was sealed, the surrounding equipment was evacuated and the diaphragm valve opened very slowly. The chamber was evacuated for at least 12 hours before the exposing gas was slowly fed into the chamber until the desired pressure was reached. After shutting the valve on the chamber, the surrounding apparatus was emptied for gas and the chamber was disconnected from the apparatus. The outlet valve on the chamber was sealed with a blind nut and the chamber was placed in a vented heating cabinet for a given period of time.
When the desired test period had ended the durability chamber was connected to the permeation apparatus as described in the previous section and the surrounding equipment was emptied of air. Since chlorine and hydrogen chloride are poisonous gases, it was important to ensure that the gas was not vented into the atmosphere during evacuation. This was ensured by keeping the rate of evacuation low (narrow opening of the diaphragm valve) and simultaneously dissolving the effluent chlorine or hydrogen chloride from the vacuum pump in water by use of a water jet pump. The chamber was evacuated over night and when opened the membrane was immediately mounted into the module (figure 26) and coupled onto the permeance apparatus. The membrane was evacuated for at least 24 hours before the first permeation test after the exposure was performed.

5.8 References

Bel Japan: “Belsorp (28) SA user manual” Bel Japan, Inc. Osaka Japan; Home page: http://www.nippon-bel.co.jp/index_e.html

Mulder, M.: “Basic Principles of Membrane Technology” 2nd ed., Kluwer Academic publishers, 1996.

Skoog, D. A. and Leary J. J.: “Principles of instrumental analysis” Saunders College publishing Fort Worth 4th edition 1992.

Silverstein, R.M. and Webster F.X.: “Spectrometric identification of organic compounds”, 6th ed., John Wiley & sons Inc, 1998.

6 RESULTS AND DISCUSSION

The process of obtaining chlorine or hydrogen chlorine stable materials is iterative, and the results from the various measurements are reported in the order in which the materials were received from our Japanese partners. Tables summarising the results, are given for each membrane material.

In the chlorine stability evaluation, this table includes the following variables: the permeance for N_2, the O_2/N_2 selectivity, the Cl_2/N_2 selectivity, the N_2 permeability decay and the Cl_2 exposure time.

For the evaluation of material stability towards chlrine, the table includes the following variables: permeance for N_2, H_2/N_2 selectivity, HCl/H_2 selectivity, N_2 permeability decay and HCl exposure time.

The detailed experimental results are given in corresponding appendices.

6.1 Chlorine - air separation

The main focus of this thesis has been on chlorine – air separation since this was a successor of previous project work, as explained in chapter 1; ”Introduction and background”.

6.1.1 Unmodified glass membrane 4 nm average pore size

As explained in chapter 2.4, “Preparation of porous glass membranes” glass membranes can be produced with two different pore sizes, and both can be pore tailored by surface modifications.

On the unmodified 4 nm glass tube, extensive characterisation techniques have been applied, both to obtain a basic understanding of the material and to characterise the pores.

Stereology images

Figure 32 shows the field emission scanning electron microscopy, FESEM, photo of the pure 4 nm glass membrane surface.

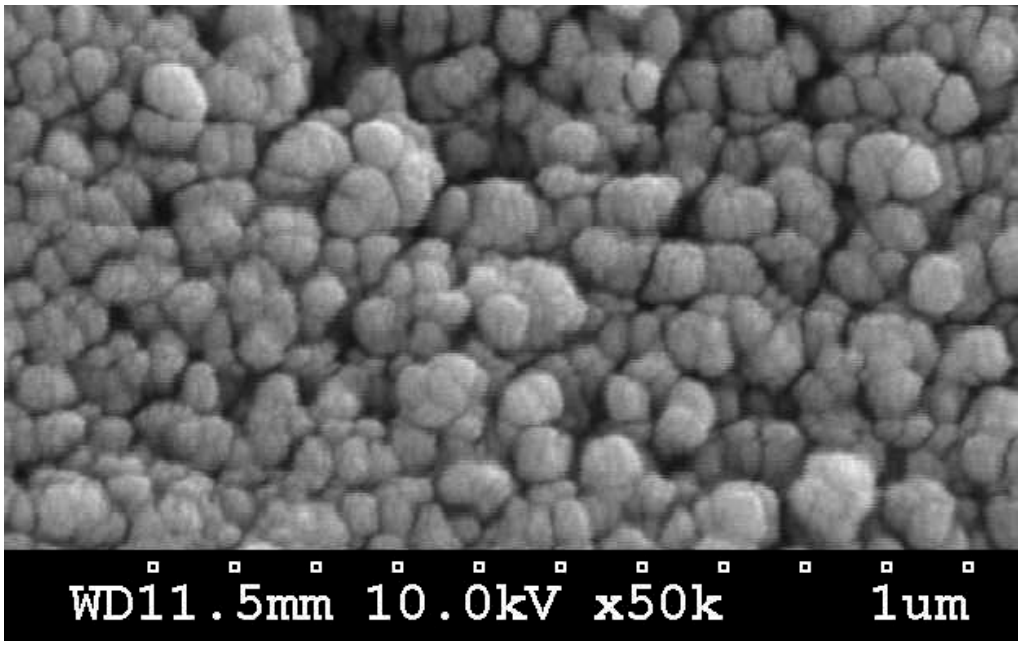

Figure 32: FESEM photo of the pure 4 nm glass surface.

The corresponding atomic force microscopy, AFM, picture is given in figure 33.

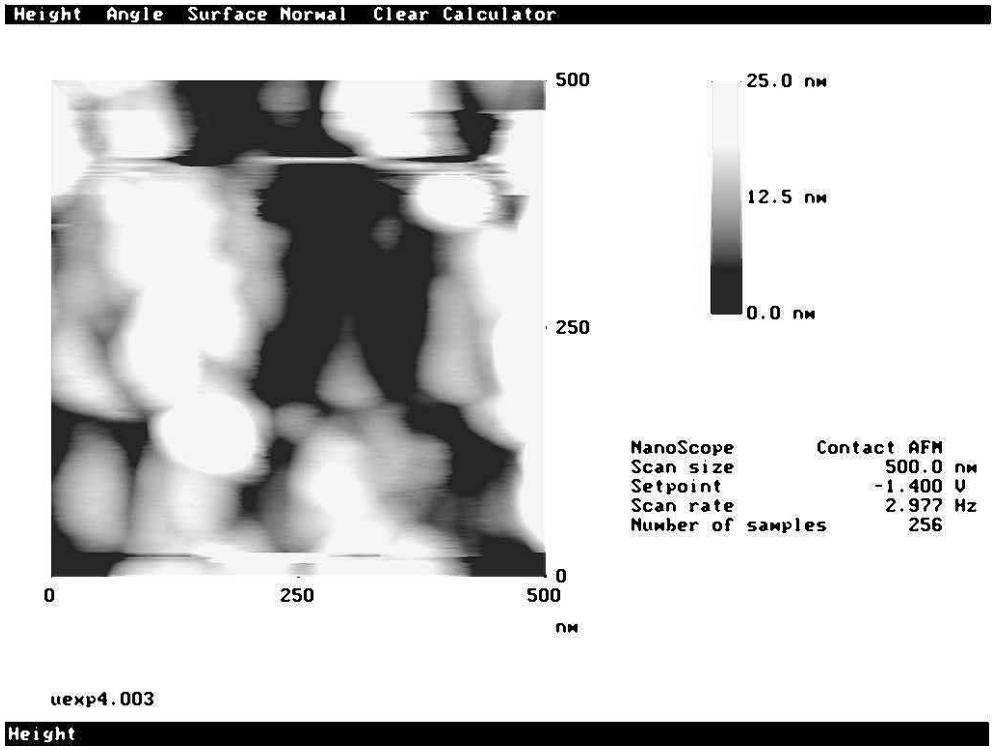

Figure 33: AFM picture of the pure 4 nm glass surface.

Elemental analysis was successfully performed using a SEM instrument, but standard SEM images could not be obtained of the 4 nm glass tube. The chemical composition is discussed at the end of the section.

The FESEM of the unmodified 4 nm glass is shown in figure 32. Compared to the scale indicated in the bottom of the FESEM image, a 4 nm pore would have a length corresponding to 2% of the distance of any to closest point on the small squared scale line. The pores may not be visible in the image at first glance, but a pore entrance will exist wherever three (or more) spheres meet. The porosity can be estimated by counting the number of pore entries on a randomly chosen patch corresponding to a given area, i.e. 0.25 μm^2. The pore counting started by selecting a random patch and this selected patch of the picture was magnified using the zoom function in the MS Paint computer program. The pores were then manually counted. An estimate based on a random patch in figure 32 yielded a porosity of approximately 600pores/μm^2 (1.8%, if the pore entries are assumed to be circular with a diameter of 4 nm). This is 13.3 times lower than the estimate based on the liquid N_2 absorption measurement on the unmodified 4 nm glass tube performed by AIST Kansai. The underestimation from the FESEM-determination could be (partly) explained by the following factors:

1. The estimation was based on the assumption that an average representative patch of the FESEM picture chosen at random also is a random part of the glass tube as a whole. So even if the picture does not show any significant structure deviation, it is only a minute fraction compared to the surface used in the adsorption measurement. Ca. 1μm^2 surface area is shown in the FESEM picture compared to the 4 cm^2 of outer external sample area measured on in the adsorption measurement. This means that the chosen random patch may deviate from the "average patch". The fact that the FESEM image is a projection of the topology of the surface, may cause some pore entries to be buried under the uppermost colloid particles (the particles that are most bright white in figure 32).
2. The counting of the pores leads to the inevitable question of whether there are none, one or several pores starting in the regions where more than three colloid spheres collide, resulting in a shadowed slit-like pattern (upper left corner in figure32). In the present estimate, a conservative approach has been chosen, that only on the short-ends of the slit a pore starts.
3. Although the selected patch of the picture was magnified using the zoom function in the MS Paint computer program (this would of course only increase the size of the picture and not the resolution or information in the

image), it is hard to "keep on track" when counting the pores. A further increase of the magnification by the FESEM would perhaps make it easier to determine which are pore entries and which are not. This would however make the search for the average patch even harder.

The AFM picture in figure 33 is of a rather low quality, which is partly due to the lack of an anti-vibration table. Even minor vibrations from the floor (for example somebody walking) would cause disturbances in the AFM-pictures. Another effect causing the blur in the picture, is the high magnification (x240 000) combined with a curved sample that has a surface roughness comparable in magnitude with the current magnification.
Ideally, a new picture should be captured using a properly aligned instrument, but since the information gained from an AFM picture is assumed to be identical to the information acquired by the FESEM picture this was not followed up further. However, if an estimation of the porosity should be made from figure 33, the problem would be what to "do" with the relatively large black area in the middle of the image. The problem would be the same as discussed for the FESEM image, namely to find a representative patch, and of cause to decide where three (or more) colloid particles actually meet. Thus, if the numbers of pores in the "black hole" are estimated from the curvature of the circumference of the "hole", or alternatively the area of the "black hole" is subtracted from the area of the total image, it would yield a porosity of 100 pores / μm^2 and 60 pores / μm^2, respectively. Compared to the FESEM estimated porosity, the AFM estimated porosity is an order of magnitude lower. Almost needless to say, this estimate is very small compared with the liquid N_2 adsorption calculations.

By elemental analysis performed using the regular SEM, the pure 4 nm glass tube was analyzed to consist of (Expressed as atomic percent):
69.1% O, 3.00% Al and 27.9% Si.
This is a bit different than measured by our Japanese research associate; they have determined the pure glass to consist of:
Na_2O=0.21, B_2O_3=2.94, SiO_2=96.5 and Al_2O_3=0.13 (in wt%) (Additionally, traces of Fe_2O_3 may occur)

This composition transformed into atomic percent yields: 66.3% O, 0.05% Al, 0.014% Na, 1.69% B and 31.8% Si.

The reason for the discrepancy in the composition may be that the elemental analysis was performed on a single point randomly chosen on the glass surface. Thus there is no guarantee that the "average" point was found.

FTIR with HATR accessory spectrum

The horizontal attenuated total reflectance IR-spectrum of the pure 4 nm glass membrane is given in figure 34.

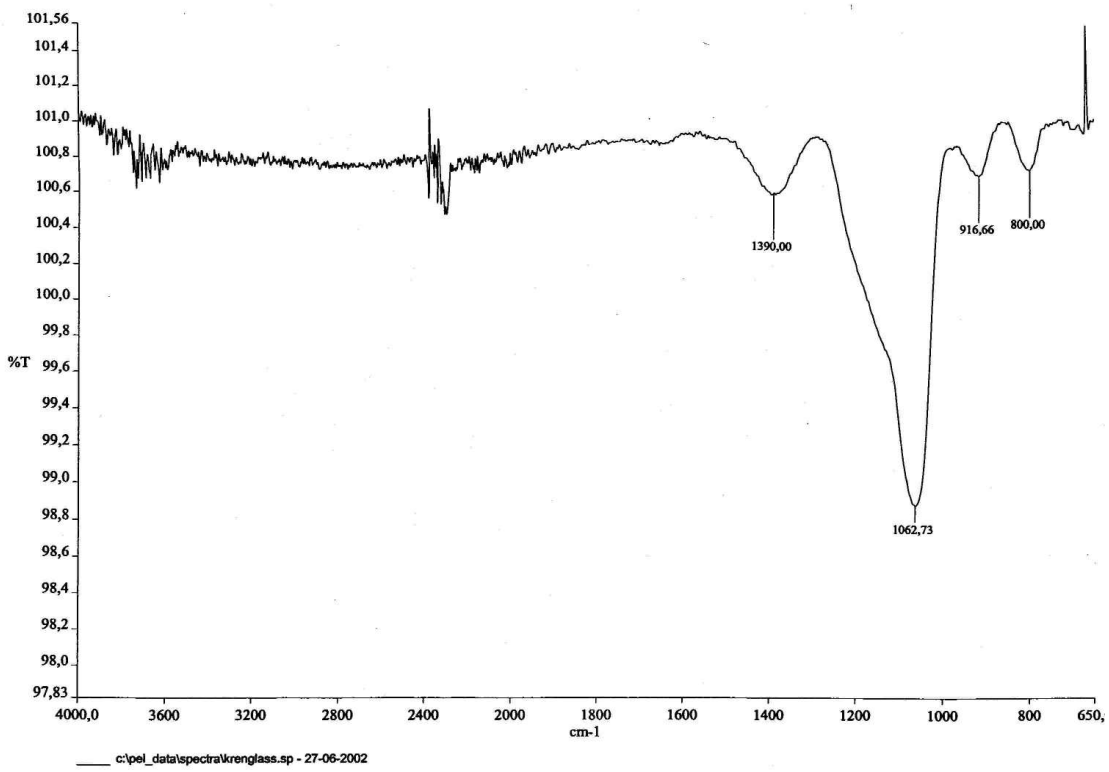

Figure 34: HATR FTIR spectrum of 4 nm glass membrane.

In this spectrum, there are four peaks which are assigned to the following fundamental vibrations: /Silverstein/:

1390 cm^{-1} can be associated with the HO- in the plane deformation vibration frequency. If any boron still is present after the acid leaching, the B-O vibration is also found in this range.

1063 cm^{-1} (including the shoulder at 1150 cm^{-1}) are the Si-O-Si chain coupled stretch frequencies.

917 cm^{-1} is assigned to the Si-OH stretch vibrator frequency (or Si-OB)

The peak at 800 cm^{-1} is identified as a Si-O-Si chain stretch frequency.

All these adsorption bands are in agreement with the expected chemical composition and known physical structure of the pure 4 nm glass.

Permeance measurement

Detailed permeance data are given in appendix 5-1 and a sum-up table only is presented here. The permeability decay is calculated according to the following equation:

$$PD(t) = \frac{P/l_{before} - P/l_{after}}{P/l_{before} \cdot t_{exposure}} \quad (6.1)$$

Where: PD(t) is the permeability decay as a function of time [s^{-1}] (In this work measured using nitrogen gas), P/l is the permeance [m^3 (STP)/(m^2 bar h)] and $t_{exposure}$ is the chlorine exposure time [s].

In the captions of the tables for the permeance results, it is indicated whether the tests are performed using the old module or the new module (as described in section 5.4.1). The reason for emphasising this is that the membrane seemed to be discoloured to a much larger extent during chlorine exposures in the old module. This discolouration was most severe near the silicone rubber gaskets, thus it is possible that it is caused by degradation products from the gasket. No obvious quantifiable measure of this effect has been detected on the perm-selectivities measured by either module.

Table 3: Permeance results for pure gases on the pure 4 nm glass membrane at 30°C. (Tests performed with old module).

Parameter	Value [Unit]
P/l_{N2}	0.1871 [m^3 (STP)/(m^2 bar h)]
$\alpha_{O2/N2}$	0.81 [-]
$\alpha_{Cl2/N2}$	1.2 [-]
PD(t)	3.8 [10^{-5}/s]
Cl_2 exposure time	3050 [s]

Compared to the corresponding theoretical Knudsen flow selectivities of 0.93 and 0.63 for oxygen relative to nitrogen and chlorine relative to nitrogen, respectively, the results from table 3 indicate that the O_2/N_2 selectivity is lower than that predicted from the theoretical Knudsen value. The reason for this increase in the expected N_2 permeance or decrease in expected O_2 permeance is unclear. The increase in the Cl_2/N_2 selectivity in table 3 compared to the theoretical Knudsen value indicates that the surface selective flow is making a significant contribution to the total transport, even in the pure glass.

The "large" permeability decay is an indication that the chlorine stability for the pure 4 nm glass membrane is seemingly poor, but this large permeability decay may to a large extent be due to adsorbed chlorine in the pores. The selectivity is too low to be of any commercial interest. No further tests were carried out with the pure 4 nm glass membrane.

6.1.2 Unmodified glass membrane 2 nm average pore size

As explained in chapter 2.4, the first logical step to optimize the perm-selectivity of the membrane was to decrease the average pore size. The pore sizes of pure glass can be made as narrow as 2 nm and this section discuss this membrane.

Pore size distribution from N_2 adsorption

N_2 adsorption and desorption measurements have been performed for the pure 2 nm (expected pore size). Figure 35 shows the resulting pore size plot, based on the BJH method and calculated from the desorption branch. The adsorption isotherm and BET-plot are given in appendix 6-1and 6-2, respectively.

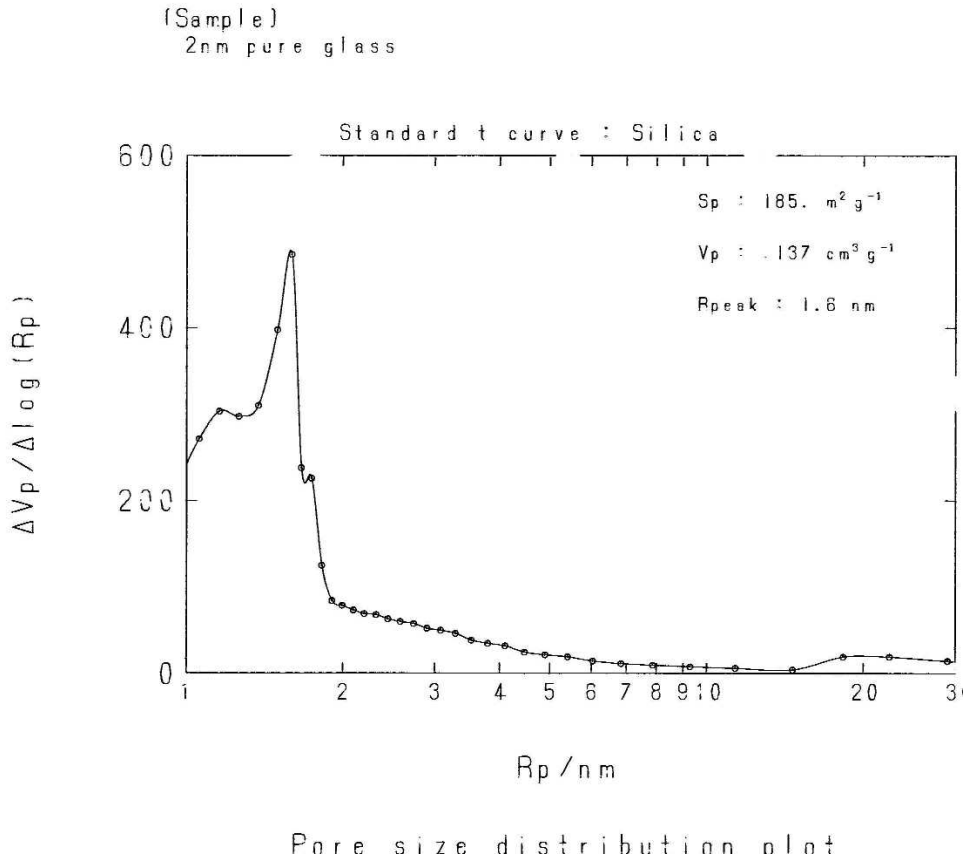

Figure 35: pore size distribution of the "2 nm" pure glass membrane.

There are four important aspects to be discussed about the pore size distribution in figure 35;

1. The believed average pore diameter of 2 nm is an underestimate and a better estimate is 3 nm (2·1.6). However, according to our Japanese research associate, this membrane has the smallest average pore size that the phase separation and acid leaching process can create.
2. The pore size distribution shows a tail up to Rp ~ 7 nm. The tail is undesired since it may cause problems in optimising the perm-selectivity of the membrane. If the transport is modelled to consist of two independent and additive contributions from the Knudsen flow and the surface flow, then the optimal membrane will consist of a narrow pore with a large internal pore surface. In such an optimal pore the contribution of the Knudsen flow could be minimized and the total selectivity would be given by the surface flow selectivity alone. However, in reality the tail of the pore size distribution will cause the average pore size to be smaller than necessary in order to obtain a

desired selectivity and thus leading to a lower permeability than it would have been in an ideal porous membrane without a pore size distribution.

3. The pore distribution has a shoulder at Rp ~ 1.2 nm. This is not believed to cause any problems in the perm-selectivity optimization.
4. The small peak at Rp ~ 20 nm is expected and is originating from the pore size of the mesoporous phase separated glass, as explained in chapter 2.4.2. These large pores are not believed to be empty throughout the membrane, but rather filled with the colloidal silica particles to some extent.

Permeance measurements

More detailed permeance data, including some indication about the pressure and temperature dependencies for this material, is given in appendix 6-3.
The measured permeances and stability evaluations are summed up in table 4.

Table 4: Permeance results for pure gases for the pure 2 nm glass membrane at 30°C. (Tests performed with old module).

Parameter	Value [Unit]
P/l_{N2}	0.0915 [m^3 (STP)/(m^2 bar h)]
$\alpha_{O2/N2}$	0.96 [-]
$\alpha_{Cl2/N2}$	2.4 [-]
PD(t) *	5.3 [10^{-5}/s]
Cl_2 exposure time *	7660[s]

* This membrane has been exposed to chlorine gas at two different pressures (1 and 3 bar) and four temperature levels (30, 60, 80 and 90 °C).

The results in table 3 and 4 can be compared by means of the separation power which is defined in equation 6.2:

$$SP=P_{Cl_2} \bullet \alpha_{Cl_2,N_2} \quad (6.2)$$

Where SP is the separation power [m^3(STP)m/(m^2 bar h)], P_{Cl2} is the chlorine permeability [m^3(STP)m/(m^2 bar h)] and $\alpha_{Cl2,N2}$ is the chlorine / nitrogen selectivity [-]
By inserting the corresponding values from table 3 and 4, the 4 nm glass has a SP $1.35 \cdot 10^{-4}$ [m^3(STP)m/(m^2 bar h)] and the 2 nm glass has a SP of $2.58 \cdot 10^{-4}$ [m^3(STP)m/(m^2 bar h)], respectively.

If the previously mentioned theory stating that the Knudsen and surface flows are additive in the glass membranes are correct, this means that in order to double the separation power by reducing the pore diameter by half, two scenarios are possible:

1. The total specific membrane area is equal for the two membranes since the basic Knudsen flow equation, equation 3.4, states that the Knudsen diffusion coefficient is linear with the pore diameter.
2. The limiting step in the surface flow is the "collection of the molecules" on the "external" surface according to figure 8.

Our Japanese research associate has published specific surface area and pore volume for the 4 nm pure glass /Kuraoka et al. 2001/. For the pure 4 nm glass, the specific surface area is 162.0 m^2/g and the pore volume is 0.143 cm^3/g. If these values are compared with the data given in figure 34, (specific surface area of 185.0 m^2/g and the pore volume is 0.137 cm^3/g), the first argument is favoured.
The nitrogen permeability decay after chlorine exposure calculated for this material is rather large, indicating that the material is unstable. However, the chlorine exposure was performed in steps of increasing temperature, thus the reaction rate is expected to have been much higher during the elevated temperature intervals. Detailed exposure times and exposure temperatures are given in appendix 6-3.

6.1.3 C1 surface-modified glass membrane

The first surface-modified membrane to be tried out was the one with C1. The modification is based on the 4 nm pure glass tube, and after the modification the actual effective pore size is believed to become close to that of the pure 2 nm glass.

Permeance measurements

To test the stability of this material, both short-time and long-time chlorine exposures have been performed.
Table 5 and 6 sums up the permeance results measured on this material. (Two different samples)

Table 5: Permeance results for pure gases for the C1 surface-modified glass membrane at 30°C, short chlorine exposure. (Tests performed with new module).

Parameter	Value [Unit]
P/l_{N2}	0.0288 [m^3 (STP)/(m^2 bar h)]
$\alpha_{O2/N2}$	0.97
$\alpha_{Cl2/N2}$	2.6 [-]
PD(t)	3.2 [10^{-5}/s]
Cl_2 exposure time	3 600 [s]

Table 6: Permeance results for pure gases for the C1 surface-modified glass membrane at 30°C, long chlorine exposure. (Tests performed with new module).

Parameter	Value [Unit]
P/l_{N2}	0.0484 [m^3 (STP)/(m^2 bar h)]
$\alpha_{O2/N2}$	0.94 [-]
$\alpha_{Cl2/N2}$	3.1 [-]
PD(t)	0.019 [10^{-5}/s]
Cl_2 exposure time	86 400[s]

More detailed permeance data for this material is given in appendix 7

If the results from table 5 and 6 are compared, it can be seen that the permeation decay is still significant even after a prolonged chlorine exposure. Comparison of table 5 and 6 with table 4 reveals that the C1modified membrane is comparable with the pure 2 nm membrane both in perm-selectivity and durability.

Combined chlorine permeance and UV radiation measurements

As an attempt to speed up the decay, which is believed to be due to chlorine reacting with the glass surface or the surface modification compound, the membrane was exposed to UV-radiation during an ordinary permeance measurement. This attempt is based on the following assumptions:

UV-radiation shorter than a specific wavelength (492 nm, estimated from the chlorine- chlorine bound energy) has the ability to break the chlorine -chlorine bound in chlorine gas into two chlorine radicals. This can be summed in equation 3:

$$Cl_2 + h\nu \rightarrow 2Cl\bullet \quad (6.3)$$

The chlorine radical is believed to have a significantly larger reaction rate than chlorine gas (Given identical process conditions).
Table 7 reports the results of the 1 hour combined chlorine exposure and UV-radiation reaction.

Table 7: Combined permeance and UV reaction (1 hour) for pure gases for the C1 surface-modified glass membrane results at 30°C. (Tests performed with UV- module).

Parameter	Value [Unit]
P/l_{N2}	0.0265[m^3 (STP)/(m^2 bar h)]
$\alpha_{O2/N2}$	1.0[-]
$\alpha_{Cl2/N2}$ (Initial, before the UV-source was switched on)	2.8[-].
PD(t)	0.76[10^{-5}/s]
Cl_2 exposure time	4500[s] (Reaction time included)
$\alpha_{O2/N2}$ (After reaction)	0.97
$\alpha_{Cl2/N2}$ (After reaction)	2.7

The permeability decay after 1 hour combined UV and chlorine exposure is comparable to that found in tables 5 and 6, and the perm-selectivity is not significantly altered. As a second test, the reaction time was increased to 6 hours on the same membrane sample.

Table 8: Combined permeance and UV reaction (6 hours) results for pure gases for the C1 surface-modified glass membrane at 30°C. (Tests performed with UV- module).

Parameter	Value [Unit]
P/l_{N2}	0.0248[m^3 (STP)/(m^2 bar h)]
$\alpha_{O2/N2}$	0.97[-]
$\alpha_{Cl2/N2}$ (Initial, before the UV-source was switched on)	2.7[-].
PD(t)	0.75 [10^{-5}/s]
Cl_2 exposure time	22 100 [s] (Reaction time included)
$\alpha_{O2/N2}$ (After reaction)	0.95
$\alpha_{Cl2/N2}$ (After reaction)	2.9

There are two interesting aspect to discuss concerning the results reported in table 7 and 8:

- The permeability decay is constant during the combined exposure meaning that the permeability decay is independent of the reaction time. This is taken as an indication that the combined exposure follows a different reaction rate law than the regular chlorine exposures since all regular chlorine exposures shows a decrease of the value of the permeability decay as a function of the exposure time.
- The membrane seems to maintain its selectivity towards the measured gases. Thus the surface flow ability of the surface is not ruined by the treatment.

6.1.4 C8 surface-modified glass membrane

Permeance measurement

Table 9 sums-up the perm-selectivity and stability measurement for the C8 modified glass membrane:

Table 9: Permeance results for pure gases for the C8 surface-modified glass membrane at 30°C. (Tests performed with old module)

Parameter	Value [Unit]
P/l_{N2}	0.00175[m^3 (STP)/(m^2 bar h)]
$\alpha_{O2/N2}$	1.3[-]
$\alpha_{Cl2/N2}$	9.4[-]
PD(t)	12 [10^{-5}/s]*
Cl_2 exposure time	6 950 [s]

* The membrane was very discoloured

More detailed permeance data for this material is given in appendix 8.

The membrane became very discoloured during the permeance measurement. A colour change of the membrane may be associated with a chemical change of the glass surface. However, the reaction with chlorine could be between the sealant and chlorine, depositing products on the glass surface only. In that case the value of the permeability decay will be an overestimate.

Ideally, a second membrane sample should have been tested, but since the membrane perm-selectivity does not seem to be much improved compared to the other material tested, this membrane was not further investigated.

6.1.5 C18 surface-modified glass membrane

Permeance measurements, pure gases

Reviewing the specific surface areas and pore volumes reported for this material, the pores are almost blocked with this long surface modifying compound./K.Kuraoka et al./ Based on the assumption that the surface diffusion and Knudsen (both the activated and the classical) flows are additive, the selectivity of this membrane is expected to be high and the permeance low, which is indeed the case of the results given in the following tables. Table 10 gives the results from short-time chlorine exposure using the old module.

Table 10: Permeance results for pure gases for the C18 surface-modified glass membrane at 30°C. Short chlorine exposure. (Tests performed with old module).

Parameter	Value [Unit]
P/l_{N2}	0.00255[m^3 (STP)/(m^2 bar h)]
$\alpha_{O2/N2}$	1.7[-]
$\alpha_{Cl2/N2}$	24 [-]
PD(t)	12 [10^{-5}/s]
Cl_2 exposure time	1850 [s]

More detailed permeance data for this material is given in appendix 9-1.

Table 11 reports the long-term chlorine exposure of the C18 using the old module.

Table 11: Permeance results for pure gases for the C18 surface-modified glass membrane at 30°C. Long chlorine exposure* (Tests performed with old module).

Parameter	Value [Unit]
P/l_{N2}	0.00452[m^3 (STP)/(m^2 bar h)]
$\alpha_{O2/N2}$	1.2 [-]
$\alpha_{Cl2/N2}$	12.1 [-]
PD(t)	0.079 [10^{-5}/s]
Cl_2 exposure time*	1 209 600[s]

* Exposure performed in the durability chamber.

The results reported in table 11 do not comply with those in table 10; the permeance is a bit too high and the selectivities are too low. One possible reason for is deviation is that the surface modifying compound (dimethyl-octadecyl-chlorosilane) comes in solid form as a powder, which is highly hygroscopic. A reaction with ambient water is devastating because OH from water can substitute the chlorine in the surface modifying compound.

To gain a better understanding of the differences between the modules, a medium-term exposure test performed with the new module is given in table 12.

Table 12: Permeance results for pure gases for the C18 surface-modified glass membrane at 30°C. (Tests performed with new module).

Parameter	Value [Unit]
P/l_{N2}	0.00194[m^3 (STP)/(m^2 bar h)]
$\alpha_{O2/N2}$	1.2 [-]
$\alpha_{Cl2/N2}$	21 [-]
PD(t)	0.63 [10^{-5}/s]
Cl_2 exposure time	86 400[s]

No obvious change in the membrane performance is seen by changing the modules, but the membrane in the new module became much less discoloured.
As initially expected the permeance of this material is low and the selectivity is relatively high. However, the chlorine stability seems to be too low.

Knudsen flow in C18 modified glass membrane

To investigate the validity of the assumption that helium gas is transported according to the Knudsen flow theory, additional helium permeance tests have been performed on the C18 membrane. Based on the Knudsen flow transport theory discussed in chapter 3.2, two different modes of Knudsen transport exist, yielding the diffusion coefficient given in the equations 3.4 and 3.5. Given Fick's law (equation 3.1) integrated over the membrane thickness and substituting the ideal gas law for the concentrations yield:

$$J_A = \frac{D_{A,(Knudsen)}}{RTl}\Delta p_A \qquad (6.4)$$

Where: $D_{A(Knudsen)}$ is the Knudsen diffusion coefficients [m^2/s] according to the equations 3.4 or 3.5.
If equation 3.4 (classical Knudsen diffusion) is substituted into equation 4, the following temperature dependence for the permeance may be derived:

$$J_A = \frac{48.5 \cdot d_p \sqrt{\frac{T}{Mw_A}}}{RTl} \Delta p_A = \frac{48.5 \cdot \Delta p_A \cdot d_p}{Rl \cdot \sqrt{Mw_A}} \cdot \frac{\sqrt{T}}{T} \Leftrightarrow \quad (6.5)$$

$$J_A = K_{Kn} \cdot \sqrt{\frac{1}{T}}$$

Thus, if the permeance is plotted as a function √1/T, a straight line with the slope K_{Kn} should be obtained and the line should pass through the origin. Figure 36 gives the corresponding least-square fit for helium according to a classical Knudsen regime in the C18 membrane.

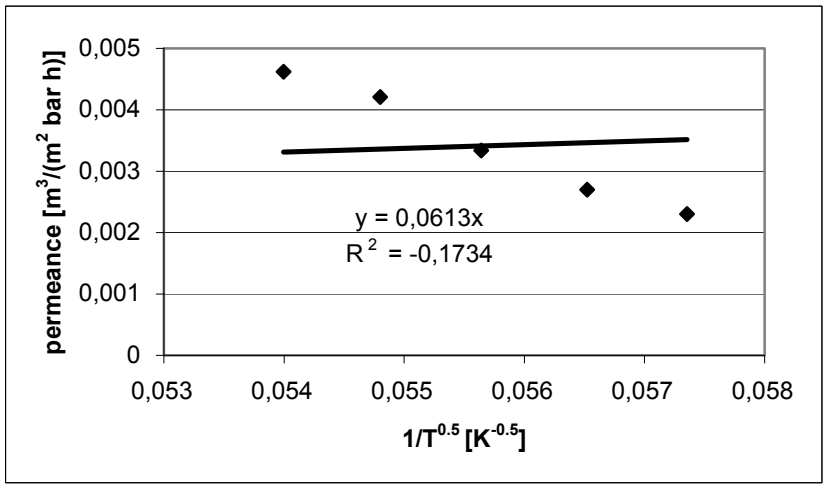

Figure 36: Least-square fit for helium according to a classical Knudsen flow in the C18 membrane.

According to figure 36 this is no typical classical Knudsen behaviour, thus a fit according to the activated Knudsen mechanism was tried out. If equation 3.5 is substituted into equation 6.4 the following temperature dependence for the permeance may be derived:

$$J_A = \frac{\gamma_d d_p \sqrt{\frac{8RT}{\pi Mw_A}} \exp(-\frac{\Delta E_a}{RT})}{RTl} \Delta p_A = \frac{\Delta p_A \gamma_d d_p \sqrt{8R}}{R \cdot l \sqrt{\pi Mw_A}} \cdot \frac{\sqrt{T} \cdot \exp(-\frac{\Delta E_a}{RT})}{T} \Leftrightarrow \quad (6.6)$$

$$J_A = K_K \cdot \frac{1}{\sqrt{T}} \cdot \exp(-\frac{\Delta E_a}{RT}) \Leftrightarrow \ln(\sqrt{T} \cdot J_A) = -\frac{\Delta E_a}{R} \frac{1}{T} + \ln(K_K)$$

The consequence of equation 6.6 is that if activated Knudsen is obeyed, then a plot of ln(√T·permeance)versus the reciprocal temperature should yield a straight line with a

slope equal to -ΔEa/R and a constant (the crossing point of the line with the y-axis) equal to ln(K_K). Figure 37 gives the corresponding least-square fit for helium according to an activated Knudsen regime in the C18 membrane.

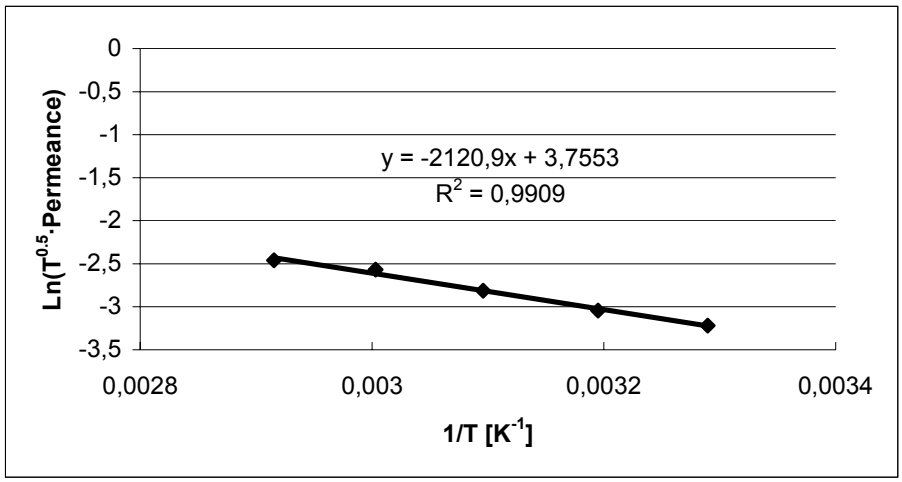

Figure 37: Least-square fit for helium according to an activated Knudsen flow in the C18 membrane.

Thus it is obvious from the regression coefficient in figure 37 that the fit of the experimental permeances to the activated Knudsen mechanism is perfect. This means that the helium transport in the C18 modified glass membrane is according to the activated Knudsen mechanism.

Combined UV and chlorine reaction

As for the C1 modified membrane described in section 6.1.3, the combined UV and chlorine reaction was tried out to investigate if also for the C18 modified membrane the permeability decay will come to an end given the chlorination was completed. A chlorination substitution reaction of the surface modification hydrogen (or the "end-methyl" group) in the C18 surface modification is believed to occur during the chlorine exposure, leading to almost plugging of the pores. The effect of this plugging is what is measured as the permeability decay. Examples of different types of attack points for the chlorine substitution is indicated as underlined atoms or groups in figure 38:

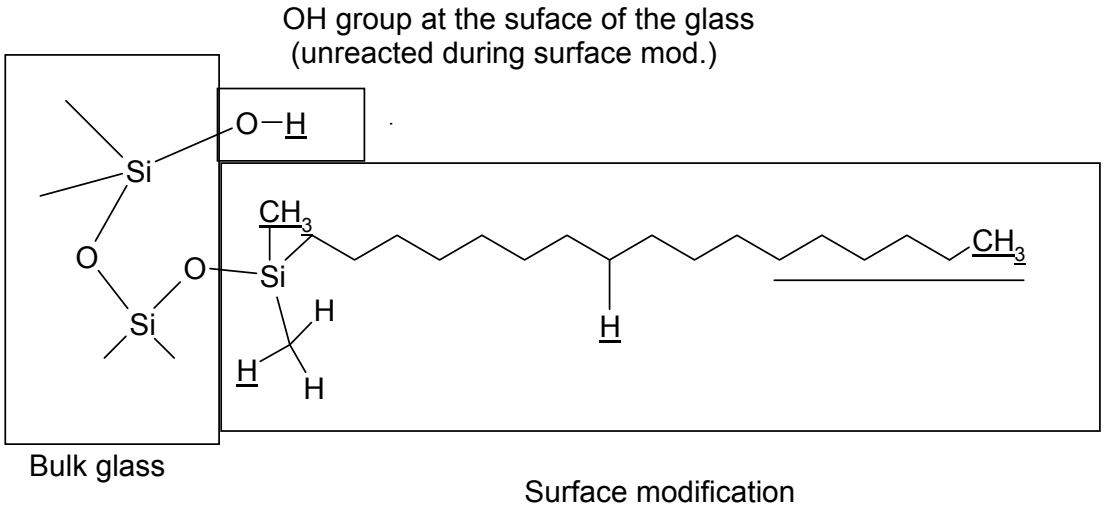

Figure 38: Surface-modified glass membrane with different possible chlorine reaction sites.

As a first test a short time (10 minutes) test was tried out and the results of this attempt is reported in table 13.

Table 13: Combined permeance and UV reaction (10 minutes) results for pure gases for the C18 surface-modified glass membrane at 30°C. (Tests performed with UV- module).

Parameter	Value [Unit]
P/l_{N2}	0.000230 [m^3 (STP)/(m^2 bar h)]
$\alpha_{O2/N2}$	1.1[-]
$\alpha_{Cl2/N2}$ (Initial, before the UV-source was switched on)	35[-].
PD(t)	-1.8[10^{-5}/s]
Cl_2 exposure time	8600[s] (Reaction time included)
$\alpha_{O2/N2}$ (After reaction)	0.93
$\alpha_{Cl2/N2}$ (After reaction)	0.94

Although the permeance for nitrogen is actually increased after the treatment, leading to negative permeability decay, both the oxygen nitrogen and the chlorine nitrogen selectivities have decreased to below unity. One possible explanation may be that the surface diffusion contribution to the total transport is lost. When the chlorine reacts with the surface modification it occupies some of the surface sites permanently

(process known as chemisorption), which can effect the surface diffusion regardless of which detailed surface diffusion mechanism it follows: In the hopping mode, when chlorine molecules associated with the neighbouring sites have to "jump over" the reacted chlorine and thus significantly increases the spacing between neighbouring free sites. This will significantly decrease the number of molecules having enough energy to sustain the jump.
For the liquid-like condensed layer, the fixed chlorines may act as "anchors" retarding the sliding layer process.

Since there was actually a negative permeation decay for the 10 minute exposure test a longer, 6 hour combined exposure test, was performed and the results from this test is reported in table 14.

Table 14: Combined permeance and UV reaction (6 hours) results for pure gases for the C18 surface-modified glass membrane at 30°C. (Tests performed with UV- module).

Parameter	Value [Unit]
P/l_{N2}	0.000251 [m^3 (STP)/(m^2 bar h)]
$\alpha_{O2/N2}$	1.5[-]
$\alpha_{Cl2/N2}$ (Initial, before the UV-source was switched on)	45[-].
PD(t)	2.2 [10^{-5}/s]
Cl_2 exposure time	21 600 [s] (Reaction time included)
$\alpha_{O2/N2}$ (After reaction)	0.93
$\alpha_{Cl2/N2}$ (After reaction)	0.86

The permeability decay in this case is very high, especially when the relatively long exposure time is taken into consideration. As can be estimated from figure 39, giving the plot of the low pressure side pressure versus time during the combined exposure, the chlorine flux is deceased by two orders of magnitude.

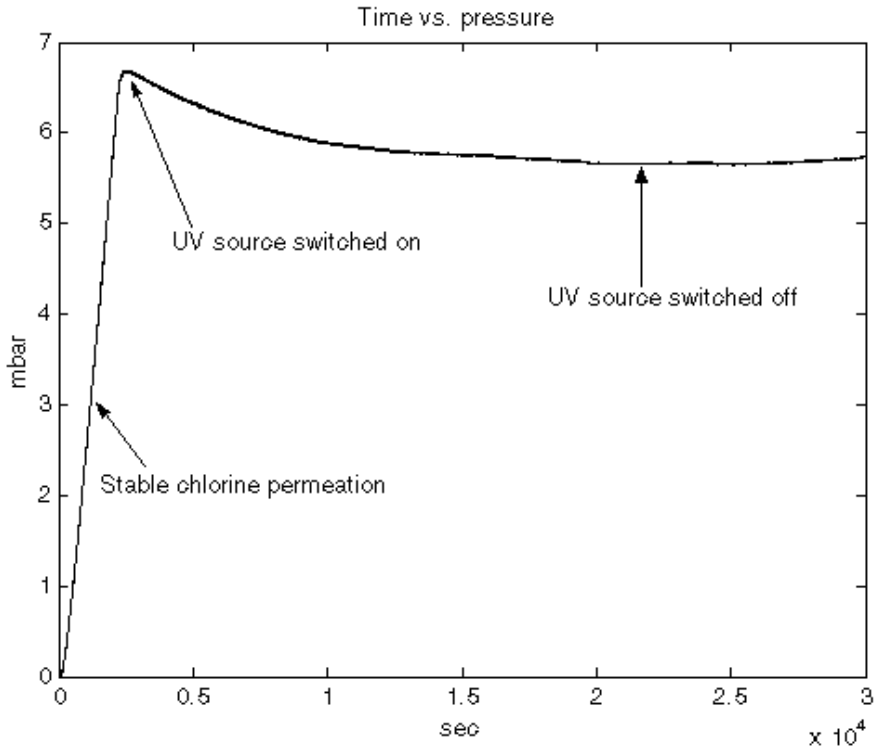

Figure 39: The low pressure side pressure versus time during the combined UV and chlorine exposure.

In figure 39, the times for switching the UV-source on and off are indicated. An interesting fact to be seen from figure 39 is that the reaction is consuming chlorine faster than what is provided through the membrane as the reaction develops, causing a minimum in the figure. This is interpreted as the reaction being limited by access to chlorine gas and in order to improve this, a special low surface coverage C18 modified glass membrane was tried in a subsequent test. The preparation of this membrane type is slightly different than the regular procedure described in section 2.4.4, namely that the capillary-condensed water is removed under vacuum at 400°C rather than the normal 170°C. This will cause some of the surface -OH groups on the glass surface to condense into water and an oxygen bridge to form according to the following reaction:

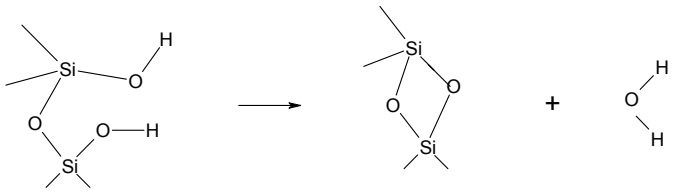

The results of the 6 hour combined UV and chlorine reaction for the low surface coverage C18 membrane is given in table 15.

Table 15: Combined permeance and UV reaction (6 hours) results for pure gases for the C18 surface-modified glass membrane (Low surface coverage) at 30°C. (Tests performed with UV- module).

Parameter	Value [Unit]
P/l_{N2}	0.000928 [m^3 (STP)/(m^2 bar h)]
$\alpha_{O2/N2}$	1.5 [-]
$\alpha_{Cl2/N2}$ (Initial, before the UV-source was switched on)	22[-].
PD(t)	4.2 [10^{-5}/s]
Cl_2 exposure time	23 400 [s] (Reaction time included)
$\alpha_{O2/N2}$ (After reaction)	0.73
$\alpha_{Cl2/N2}$ (After reaction)	0.23

The times for switching the UV-source on and off are indicated in figure 40 which gives the pressure at the low pressure side versus time.

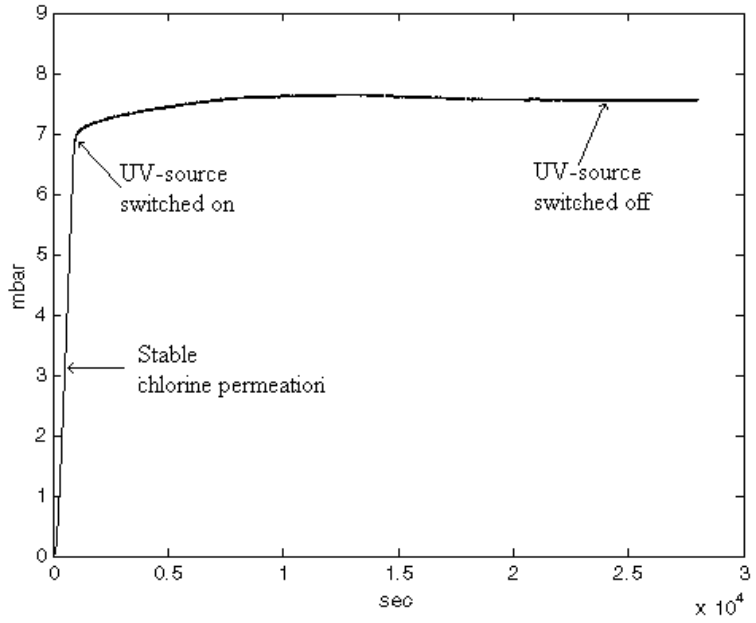

Figure 40: The low pressure side pressure versus time during the combined UV and chlorine exposure.

As can be seen from figure 40, the membrane is now able to deliver gas fast enough, so that the reaction itself is rate determining.
However, as table 15 indicates, the permeation decay for the low surface coverage C18 membrane is large (taken into consideration the relatively long reaction time used) and the chlorine nitrogen selectivity drops two orders of magnitude whereas the nitrogen permeance is decreased by 98 %.

The membrane characteristics indicate that the transport is changed from being a surface flow membrane, to becoming a molecular sieving membrane. The substitution of groups, as shown in figure 38, may cause different effects depending on where the attack is occurring, i.e. if a hydrogen atom is substituted by a chlorine atom then the surface modification will become spatially bigger, causing the pores to be more filled (and possibly more compacted in the surface-modified layer).

FTIR with HATR accessory spectroscopy

The use of glass plates as substitute for the actual membrane tubes in the IR HATR spectroscopy has both advantages and disadvantages. The advantages include:

- The glass plates ensure that the contact between the HATR measuring crystal and the glass plate is good.
- The glass plates are less porous than the tubular membranes and they are therefore less brittle and can withstand a applied pressure, thus a constant force can be applied on the glass plate squishing it onto the measuring crystal and leading to better reproducibility in the spectra

The major disadvantage is:

- Since the HATR is most likely to detect the outer surface and not the inside of the pores and there is a possibility that the reaction rate with the gasses and the surface or surface modification may be overestimated on the planar surface than in the narrow pores due to the lack of steric hindrance on the outer surface.

Figure 41 gives the FTIR HATR spectra of the: A) acid leached glass plate, B) Glass plate chlorine exposed for 9 weeks at 30°C and 1 bar, and C) Glass plate UV- and chlorine exposed for 1 hour.

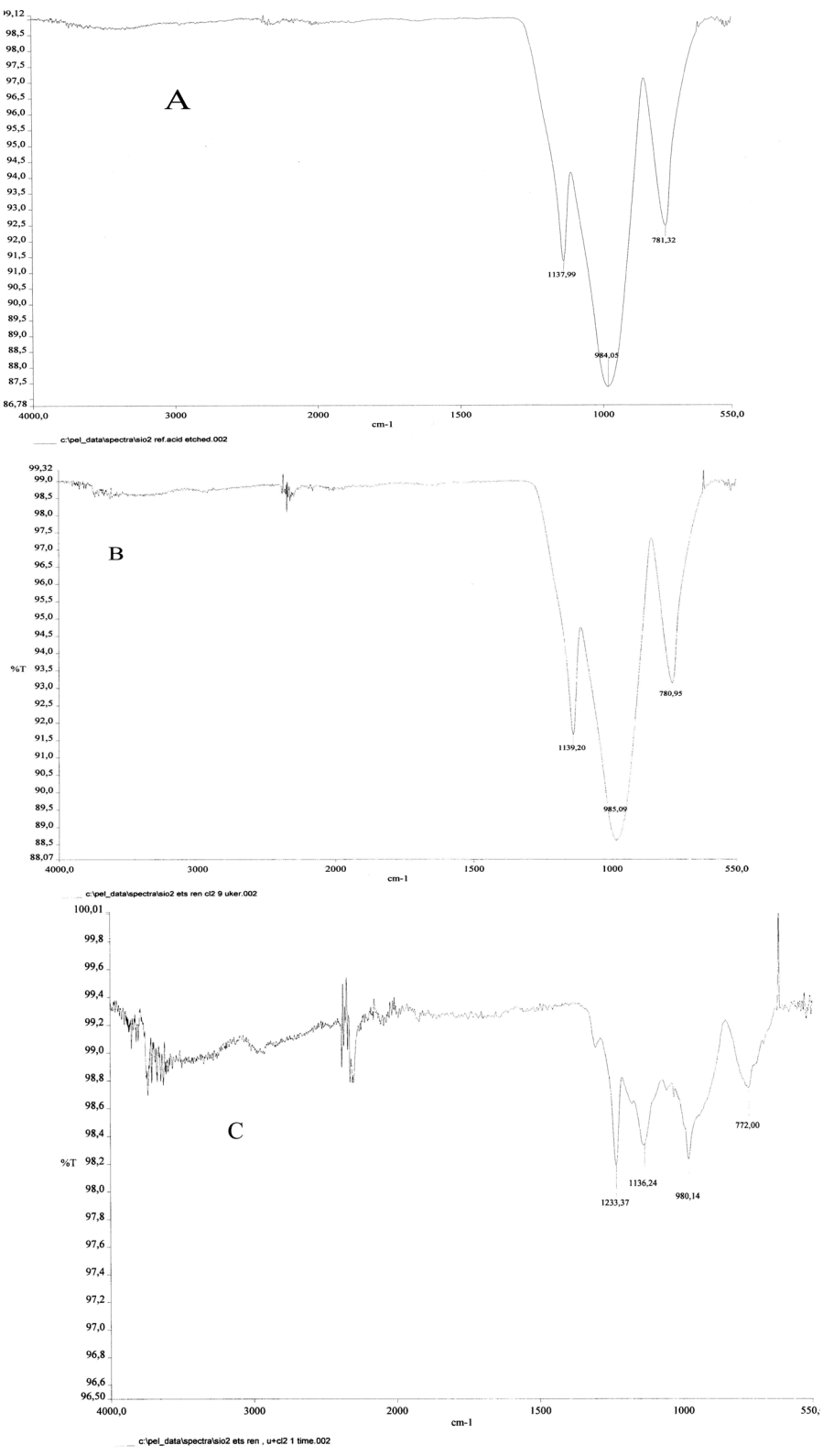

Figure 41: FTIR HATR spectra of borosilicate glass plates: A) Acid leached, B) Chlorine exposed for 9 weeks at 30°C and 1 bar C) UV- and chlorine exposed, 1 hour.

Figure 42 gives the FTIR HATR spectra of the: A) unexposed C18 modified glass plate, B) C18 modified glass plate UV- and chlorine exposed for 1 hour

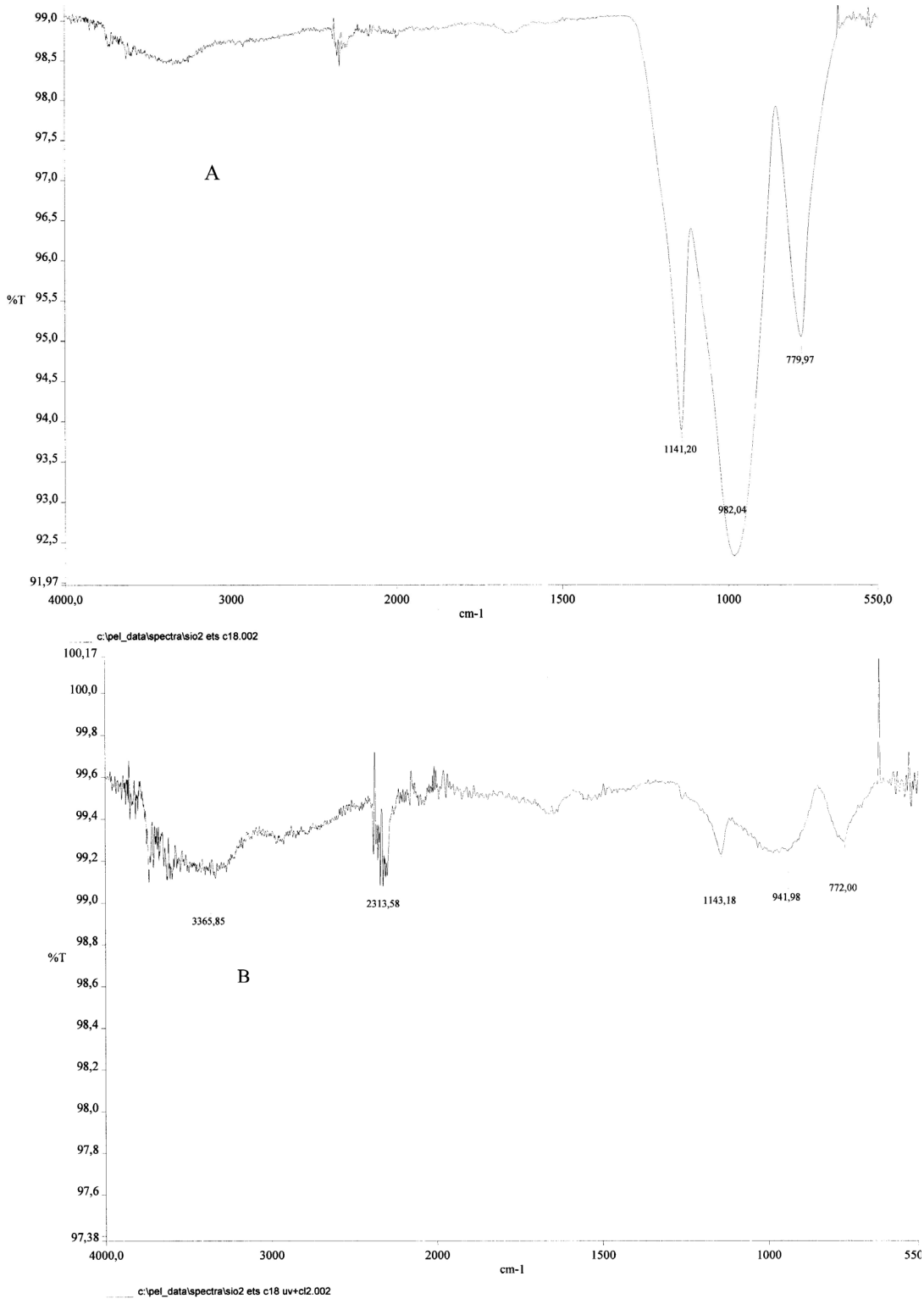

Figure 42: FTIR HATR spectra of surface-modified glass plates: A) C18 modified glass plate, B) UV- and chlorine exposed, 1 hour, C18 modified glass plate.

The FTIR spectra given in figure 41 A) and B) are identical, except for a change in the intensity for the small peak at 2300cm^{-1}. If the spectra in figure 41 are compared to the spectrum of the 4 nm unmodified glass membrane, obtained in figure 34, it is obvious that the two glasses are not chemical identical. However, the interpretations of the peaks are similar, and the following fundamental frequencies are identified from the spectra in figure 41 A):

The band at 780 cm^{-1} is identified as a Si-O-Si chain stretch (possibly confounded by the vitreous boron oxide, B_2O_3). The 985 is possibly the Si-OH stretch (slightly low) (may be confounded with the Si-OB stretch) the frequency and the peak at 1140 cm^{-1} is the Si-O-Si chain coupled stretch frequency (possibly confounded by the vitreous boron oxide, B_2O_3). The small peak at ~2300 cm^{-1} is possibly an overtone of the 1140 band.

The fact that the unexposed spectrum figure 41 A) and the spectrum of the chlorine exposed sample, figure 41 B) are identical is taken as an indication that the chlorine has not chemically reacted with the glass (at least not to any extent detectable by the FTIR). Any chlorine gas adsorbed on the surface is not detectable by IR since chlorine does not possess a permanent dipole moment.

If the UV- and Cl_2 exposed glass spectra, figure 41 A) (or B)) and C), respectively, are compared, three aspects need to be discussed:

1. A new peak is appearing in the spectra of the UV- and Chlorine exposed glass, figure 41 C) at 1233 cm^{-1}
2. The tree remaining peaks have their peak positions shifted towards lower wavenumbers.
3. The relative intensities of the tree remaining peaks are changed as shown in table 16.

Table 16: Relative peak intensities in FTIR spectra of glass plate before chlorine exposure, after chlorine exposure and after combined UV- and chlorine exposure.

Spectra \Peak	~1230 cm^{-1}	~1140 cm^{-1}	~980 cm^{-1}	~780 cm^{-1}*
Before exposure Figure 41 A)	-	1.17	1.89	1
Chlorine exposed Figure 41 B)	-	1.25	1.78	1
UV- and Chlorine exposed Figure 41 C)	1.96	1.74	1.89	1

* The peak at 780 cm^{-1} is the reference peak in the relativity calculations. The peak intensities are estimated solely by the peak height

The new peak at 1233 cm^{-1} in figure 41 C) is the most intense in the whole spectrum, but the association of the peak to a fundamental frequency is a bit uncertain. However, as a working hypothesis, it is assumed that chlorine has reacted with the surface HO-groups of the glass and formed >Si-O-Cl. In that case the fundamental frequency will be shifted towards a lower wavenumber because chlorine has a larger molecular mass than hydrogen (can be derived from a simple harmonic oscillator approach). Chlorines does under normal circumstances only adsorb below 700 cm^{-1}. The chlorination reaction is leading to the decrease in peak intensity of the 1140, 980 and 780 cm^{-1} peaks, possibly because a certain amount of IR-active bounds previous detected are lost during the combined UV-and chlorine reaction. The appearance of the peak at 1230 cm^{-1} may then be due to the decreasing of the confounding Si-O-Si coupled chain stretch frequency, revealing the vitreous boron oxide peak normally found at 1260 cm^{-1}. Even though the theory introduced here might be erroneous, the large difference between the chlorine exposed glass and the UV- and chlorine exposed glass leave no doubt that the glass has reacted with chlorine during this treatment. The normal chlorine exposure seems to be much less reactive than the combined exposure which indeed was the purpose of the combination.

The spectra of the C18 modified glass plates as given in figure 42 A) and B) are almost identical to the corresponding spectra recorded for the pure glass (figure 41 A) and C)). However, two aspects of the spectra in figure 42 need to be discussed:

1. The expected C-H aliphatic stretch peak at ~2900 cm^{-1} is absent.
2. The new peak at 1230 cm^{-1}, found in the pure glass plate spectrum in the case of combined UV- and Chlorine exposure, do not appear in the corresponding C18 modified glass plate test.

The absence of the expected C-H aliphatic stretch peak at ~2900 cm^{-1} may be due to the problem with the surface modifying agent being a bit too old as discussed on page 80, thus leading to a lesser degree of surface modification than expected. This means that the surface modifying compound is not detected by the IR since the surface concentration may be below the detection limit.
The absence of the peak at 1230 cm^{-1} may be explained by the hypothesis of chlorine preferably substituting onto the OH- groups on the glass surface, because the surface modification reaction uses surface OH groups of the glass, thus making them inaccessible to the chlorine radicals formed during the combined UV- and chlorine exposure. The chlorine radicals might react with the surface modifying compound, but this is not detected, since the surface modifying compound was not detected as a whole. However, if the reaction occurs in the surface modifying compound this may lift the IR- focal point up from the glass surface leading to the decrease in the reflectance as found in figure 42 B).

6.1.6 C18 and C1 surface-modified glass membrane

One significant contribution to the relatively large permeance decay for the C18 modified glass membrane, may originate from chlorine reacting with unreacted OH group on the glass surface. The reason for this may be that the number of free surface OH group is especially high in the case of this long-chained surface modification because of spatial hindrance in the middle of the pore (this can be pictured as wheel spokes starting at the rim and ending on the hub where the number of spokes per area are higher than at the rim.). As an attempt to improve this, the membrane was first modified by C18 and then subsequently a C1 modification was

performed. The C1 modification is assumed to modify in between the C18 modification leading to fewer free surface –OH groups.
Table 17 gives the pure gas permeances and selectivities for this membrane.

Table 17: Permeance results for pure gases for the C1+C18 surface-modified glass membrane at 30°C. (Tests performed with old module).

Parameter	Value [Unit]
P/l_{N2}	0.000818[m^3 (STP)/(m^2 bar h)]
$\alpha_{O2/N2}$	1.1[-]
$\alpha_{Cl2/N2}$	11[-]
PD(t)	6.0 [10^{-5}/s]
Cl_2 exposure time	3 600 [s]

More detailed permeance data for this material is given in appendix 10-1

The nitrogen permeance, as reported in table 17, is low for the C1+C18 membrane. This is expected since the C1+C18 surface modification can be viewed as a stuffed C18 modification. The more filled pores may be the reason for the lowering of the selectivities compared to the C18 modification, since to much fill pores may slow down the SSF contribution to the overall transport.
If the permeability decay in table 17 is compared with the permeability decays in table 3, 5 and 10, it is relatively clear that the stability is slightly improved by the addition of C1. A long-term static chlorine test was performed to investigate whether the improvement in the stability is still significant after prolonged exposure times. Table 18 sums up the results for this long-term static chlorine exposure.

Table 18: Permeance results for pure gases for the C1+C18 surface-modified glass membrane at 30°C. Long-term exposure (Tests performed with old module).

Parameter	Value [Unit]
P/l_{N2}	0.000774 [m^3 (STP)/(m^2 bar h)]
$\alpha_{O2/N2}$	1.2 [-]
$\alpha_{Cl2/N2}$	n/a[-]
PD(t)	0.13 [10^{-5}/s]
Cl_2 exposure time	432 000 [s]

More detailed permeance data for this material is given in appendix 10-1

The long-term stability of the C1+C18 modification is at least as stable as the pure C18 modification.

6.1.7 C12 surface-modified glass membrane

The difference between the C8 and the C18 is rather large, so the C12 falls as a natural midpoint in the stability and perm-selectivity evaluations.

Permeance measurements

The results of the permeance measurements are summarized in table 19:

Table 19: Permeance results for pure gases for the C12 surface-modified glass membrane at 30°C (Tests performed with old module).

Parameter	Value [Unit]
P/l_{N2}	0.00580 [m^3 (STP)/(m^2 bar h)]
$\alpha_{O2/N2}$	1.3 [-]
$\alpha_{Cl2/N2}$	7.2 [-]
PD(t)	12 [10^{-5}/s]
Cl_2 exposure time	6 600 [s]

More detailed permeance data for this material is given in appendix 11

The perm-selectivity for this material is good, but the stability is the worst found. The reason why this membrane has the poorest stability is not easy to interpret.

However, one possible reason may be that this modification length has many attachment sites for the chlorination, as indicated in figure 38, but the pores are still not filled completely, so in this membrane neither the lack of attachment point nor spatial hindrance are limiting the decay.

6.1.8 Sum-up of the results on the aliphatic surface-modified glass membranes

Since experimental results have been presented for seven different materials, this chapter sums up the perm-selectivities and stabilities for all of them. Table 20 lists the perm-selectivities and the stability for the membranes tested so far

Table 20: Permeance results for pure gases for the surface-modified glass membrane at 30°C. Short chlorine exposures.

Parameter	Pure 4 nm	Pure 2 nm	C1	C8	C18	C18+C1	C12
P/l_{N2} [m^3 (STP) /(m^2 bar h)]	0.187	0.0912	0.0288	0.00175	0.00255	0.000818	0.00580
$\alpha_{O2/N2}$	0.81	0.96	0.97	1.3	1.7	1.1	1.3 [-]
$\alpha_{Cl2/N2}$	1.2	2.4	2.6	9.4	24	11	7.2 [-]
PD(t) [10^{-5}/s] [s]	3.8	5.3	3.2	12	12	6	12
Cl_2 exp. time [s]	3050	7660	3600	6950	1850	3600	6 600

If the perm-selectivity is evaluated by the separation power, as given in equation 6.2, the following order is obtained ranged from best to poorest: C18, pure 2 nm, C1, C12, pure 4 nm, C8 and C1+C18. Simultaneously, the stability must be as good as possible meaning that the permeability decay should be as low as possible. Since the chlorine exposure times varied in the experiments and the permeability decay is most likely an exponential function of the exposure time, the permeability decays can not be directly compared. However, if the perm decay rate (permeability decay divided

by the exposure time) is plotted versus the exposure time in a log-log plot, then the comparison is relatively straightforward as given in figure 43:

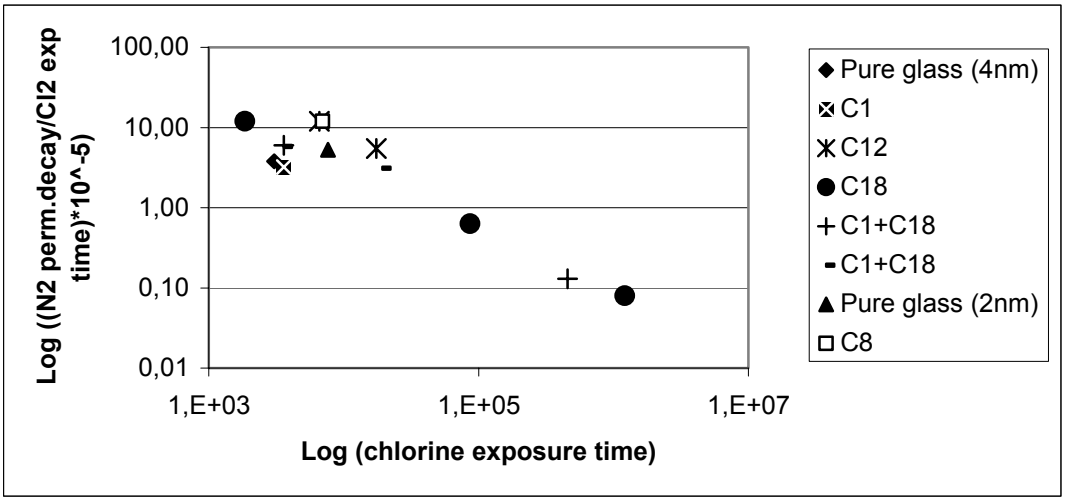

Figure 43: The permeability decay rate as a function of the chlorine exposure time for the chlorine exposed surface-modified glass membranes

Figure 43 also includes the long term chlorine exposures. For those membranes that several points are known, then is it possible to calculate the slope and intersection with the ordinate axis for a line connecting these points. The most stable membrane in figure 43 is then the one with the lowest value for the intersection and most negative slope. For the pure 4 nm glass, pure 2 nm glass and C8 surface-modified membranes only one point is determined, and an average slope is assumed for comparison purposes. The stability plot indicates that the most stable membrane is the C1 followed by the pure 4 nm glass, C1+C18, C18, pure 2 nm glass (This membrane was chlorine exposed at higher temperatures), C8 and C12.
As an attempt to improve the stability and hopefully the perm-selectivity, perfluorinated surface modification was tried out as discussed in the next section.

6.1.9 Perfluorinated C10 surface-modified glass membrane (4 nm base)

Based on knowledge from other materials investigated for their durability in chlorine separation, it is quite clear that the Teflon® and Fluorel® are stable towards both chlorine and hydrogen chloride gases. This is not surprising since the C-F bounds

have a higher enthalpy (489 KJ/mol) than the C-Cl bounds (339 KJ/mol) /Aylward and Findlay/ and fluorine is more electronegative than chlorine. In search of a suitable surface modifying compound, it was necessary to find a long "fully" fluorinated silane. The (Heptadecafluoro-1,1,2,2-tetrahydrodecyl) dimethylchlorosilane, Cl-Si$(CH_3)_2$-$(CH_2)_2$-$(CF_2)_7$-CF_3, was the best suited compound commercially available. Compounds with all, or a majority, of their hydrogen substituted with fluorine are called perfluorinated in the common naming system, (however, this is not according to current rules of the IUPAC).
This modification is abbreviated as Pf-C10 later on in this thesis.

Pore size distribution from N_2 adsorption

Figure 44 and 45 gives the pore size distribution in the Pf-C10 (4 nm base) before and after long-term chlorine exposure, respectively.

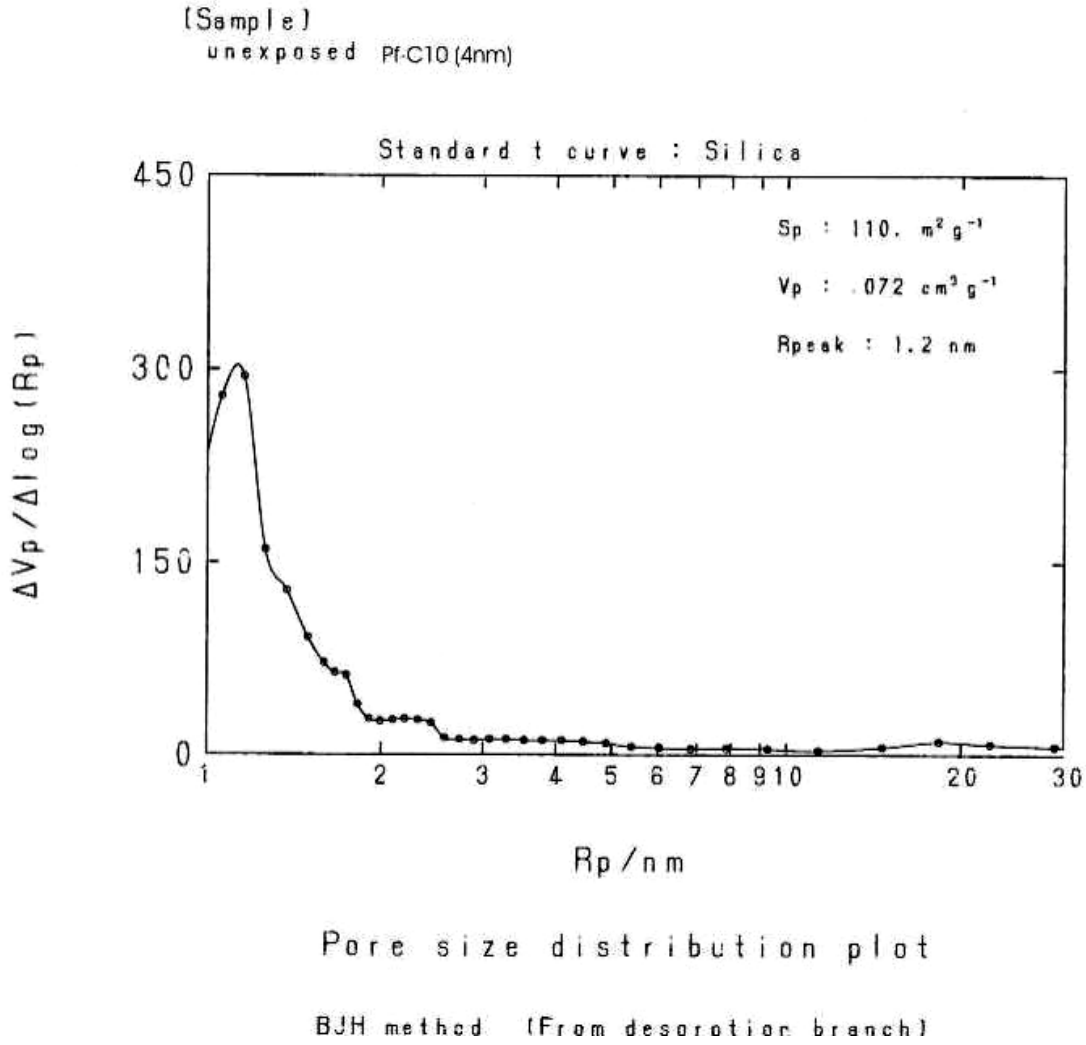

Figure 44: Pore size distribution plot for the Pf-C10 4 nm base surface-modified glass membrane. Unexposed sample

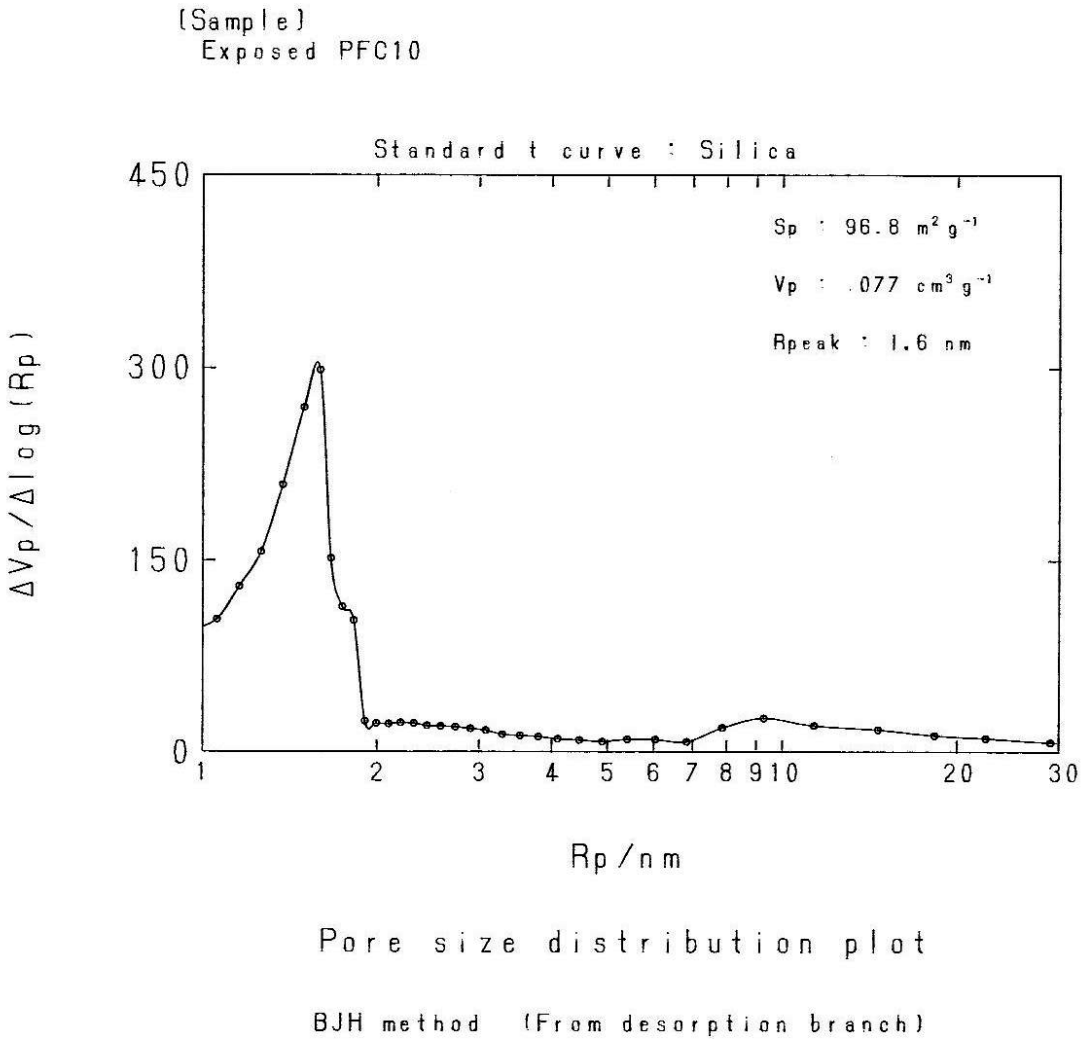

Figure 45: Pore size distribution plot for the Pf-C10 (4 nm base) surface-modified glass membrane. Long-time chlorine exposed sample.

The corresponding adsorption isotherms and BET-plots are given in appendix 12-1 and 12-2 for the unexposed and the long-time chlorine exposed samples, respectively.

The pore size distributions given in figures 44 and 45 are, by all means, identical for pore radii greater than 2 nm. However, below 2 nm the peak shape is different. The peak of the exposed sample has a narrower maximum peak than the unexposed sample and the unexposed sample has a shoulder in the pore size distribution for the smallest pore radii. A theory consistent with these observations may be that the chlorine exposure causes the smallest pores to be filled by adsorbed chlorine that is not removable at the preheat temperature used, or that the chlorine is chemically

bound in the smallest pores, thus shifting the average pore to a higher value. One complicating matter is that the exposed and the unexposed samples are two different samples measured at the same time, and not the same sample measured before and after the chlorine exposure. This means that the values obtained for the total V_p and S_p should be used as indications only, since the actual porous network may differ significantly between the two samples.

Elemental analysis

One motivation for performing the elemental analysis is to investigate how easy it is to identify the surface modification. Table 21 gives a comparison of the element distribution of the theoretical base glass and the Pf-C10 membrane (before and after chlorine exposure).

Table 21: Element composition of the Pf-C10 surface-modified glass compared to the reference glass. All values are atomic percent.

↓Membrane \ Element→	C	O	F	Al	Na	B	Si
Reference glass (Theoretical composition)		66.3		0.050	0.150	1.70	31.8
Unexposed PF-C10	4.30	66.7	3.10				25.9
Exposed PF-C10 (42 days @ 1 bar 30 °C)	2.80	64.3	2.30	0.200			30.4

It is indeed interesting to see that no elemental chlorine could be detected, even after long-time chlorine exposure. However, it is believed that the capillary forces are more favourable for chlorine condensation inside the pores and possibly increased chlorine reactivity, than on the outer surface of the glass.

FTIR with HATR accessory spectroscopy

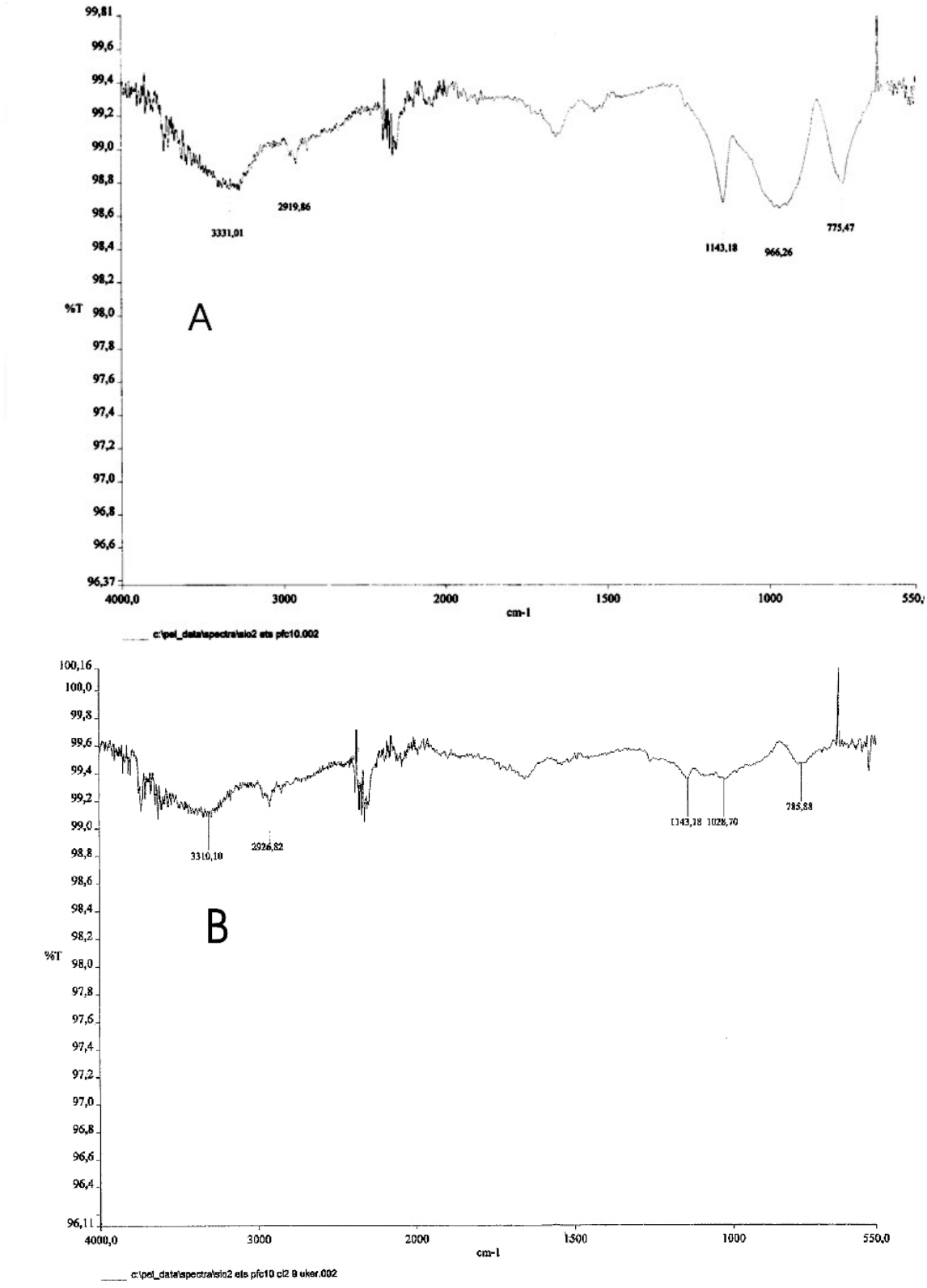

Figure 46: FTIR HATR spectra of Pf-C10 surface-modified borosilicate glass plates: A) unexposed sample, B) Chlorine exposed for 9 weeks at 30°C and 1 bar.

Contrary to what was experienced for the C18 modified glass plate, the perfluorinated surface glass, figure 46 A), is actually showing a small C-H stretch peak at 2950 cm^{-1} (this is not surprising since each surface modifying molecule contains 4 C-H bounds). A more intriguing fact about the spectra in figure 46 A) is that the strong $–CF_2$- stretch in the 1350-1120 cm-1 is not readily detected. However the relative intensities of the three peaks at 1139, 984 and 781 cm-1 are shifted compared to the values calculated for the pure glass plate in table 16. Table 22 gives a comparison of the relative intensities of the untreated, unexposed Pf-C10 modified and chlorine exposed Pf-C10 modified (9weeks@ 1bar and 30 °C) glass plates.

Table 22: Relative IR-peak intensities of the untreated, unexposed Pf-C10 modified and chlorine exposed Pf-C10 modified (9weeks@ 1bar and 30 °C) glass plates.

Spectra \Peak	~2920 cm^{-1}	~1140 cm^{-1}	~980 cm^{-1}	~780 cm^{-1}*
Before exposure pure glass Figure 41 A)	-	1.17	1.89	1
Unexposed Pf-C10 glass Figure 46 A)	0.28	1.17	1.39	1
Chlorine exposed Pf-C10 glass Figure 46 B)	1.16	1.66	1.66	1

*The peak at 780 cm^{-1} is the reference peak in the relativity calculations. The peak intensities are estimated solely by the peak height.

The decrease of the relative intensity of the peak at 980 (assigned to the Si-OH stretch) for the unexposed Pf-C10 glass plate compared to the pure glass plate in table 22, can be explained by the fact that the surface modification reaction is using surface OH-groups, thus the concentration of them will decrease when the surface is modified, hence the decrease in the relative intensity.

However, it is more difficult to explain the relative intensities calculated from the IR-spectrum of the chlorine exposed Pf-C10 glass plate. One explanation might be that adsorbed chlorine in the surface modification is masking the glass structure below. If

this layer is thick enough, only a minute fraction of the IR-radiation is penetrating, leading to the loss in the characteristic peak ratios since the sizes of the peaks is approaching the detection limit of the instrument.

Permeance measurements

The initial permeance results for the perfluorinated surface-modified glass membrane are summed up in table 23:

Table 23: Permeance results for pure gases for the Pf-C10 surface-modified glass membrane (4 nm base) glass membrane at 30°C (Tests performed with new module)

Parameter	Value [Unit]
P/l_{N2}	0.00796 [m^3 (STP)/(m^2 bar h)]
$\alpha_{O2/N2}$	1.2 [-]
$\alpha_{Cl2/N2}$	2.6 [-]
PD(t)	1.5 [10^{-5}/s]
Cl_2 exposure time	3 600 [s]

More detailed permeance data for this material is given in appendix 12-3.

If the results in table 23 are compared with those in table 19 (C12 membrane), then it can be seen that the nitrogen permeability and the oxygen /nitrogen selectivity are comparable, whereas the chlorine/nitrogen selectivity is significantly lower. The stability seems to be significantly increased. All these observations are easily explained, if the transport is assumed to consist of two additive contributions from surface and Knudsen flows: The pore size of the Pf-C10 membrane is obviously somewhere between the C8 and the C12 membrane, so it is logical for the nitrogen and oxygen to have similar permeances in these three materials since the Knudsen flow permeance, which is pore size dependent, has a significant contribution on the total permeance for these gases. For chlorine however, the effect of the perfluorinated surface modifying compound is a lower chlorine attraction (this was, after all one reason for choosing this modifying compound), thus a decrease in the chlorine permeation results.

The permeances, selectivities and permeability decay after the long-term chlorine exposure of the Pf-C10 membrane are given in table 24.

Table 24: Permeance results for pure gases for the Pf-C10 surface-modified glass membrane (4 nm base) glass membrane at 30°C, long-time chlorine exposure*. (Tests performed with new module).

Parameter	Value [Unit]
P/l_{N2}	0.00650 [m^3 (STP)/(m^2 bar h)]
$\alpha_{O2/N2}$	1.3 [-]
$\alpha_{Cl2/N2}$	3.6 [-]
PD(t)	0.0026 [10^{-5}/s]
Cl_2 exposure time	3 682 800 [s]

* Test performed in the durability chamber

More detailed permeance data for this material is given in appendix 12-3.
If the permeability decay in table 24 is compared with those obtained by the other membranes it is clear that the stability of the Pf-C10 (4 nm base) is superior compared to the other materials, but the perm-selectivity is very low.

6.1.10 Perfluorinated C10 surface-modified glass membrane (2 nm base)

Although the Pf-C10 (4 nm base) had superior stability towards chlorine gas compared to all other materials tested, the perm-selectivity was rather poor. As an attempt to increase the perm-selectivity the 2 nm glass was used as base material for surface modification.

In order to prove whether the Pf-C10 (2 nm base) is the proper choice of membrane material or not, comprehensive research was performed on this membrane.

Including:

- Pore size distribution from N_2 adsorption
- Permeability measurements
    - Pure gases
        - Knudsen flow regime determination
    - Mixed gases
- Sorption measurements
    - Nitrogen and oxygen adsorption
    - Chlorine adsorption
        - Adsorption / desorption isotherms (given as a Henry's Law equivalent versus absolute pressure)
        - Adsorption / desorption isotherms (given the "normal" way: sorption versus relative pressure
        - Adsorption temperature dependence
- Estimation of the degree of SSF(Requires the combination of the permeances and sorption) for N_2, O_2 , He, HCl, Cl_2, Xe, CO_2, H_2, SF_6, CO and R22 (CHF_2Cl)
- Diffusion coefficient determinations (Estimated two ways: From D = P/S and from the time-lag, θ)

Pore size distribution from N_2 adsorption

Figure 47 shows the pore size distribution plot for the Pf-C10 (2 nm base) surface-modified glass membrane.

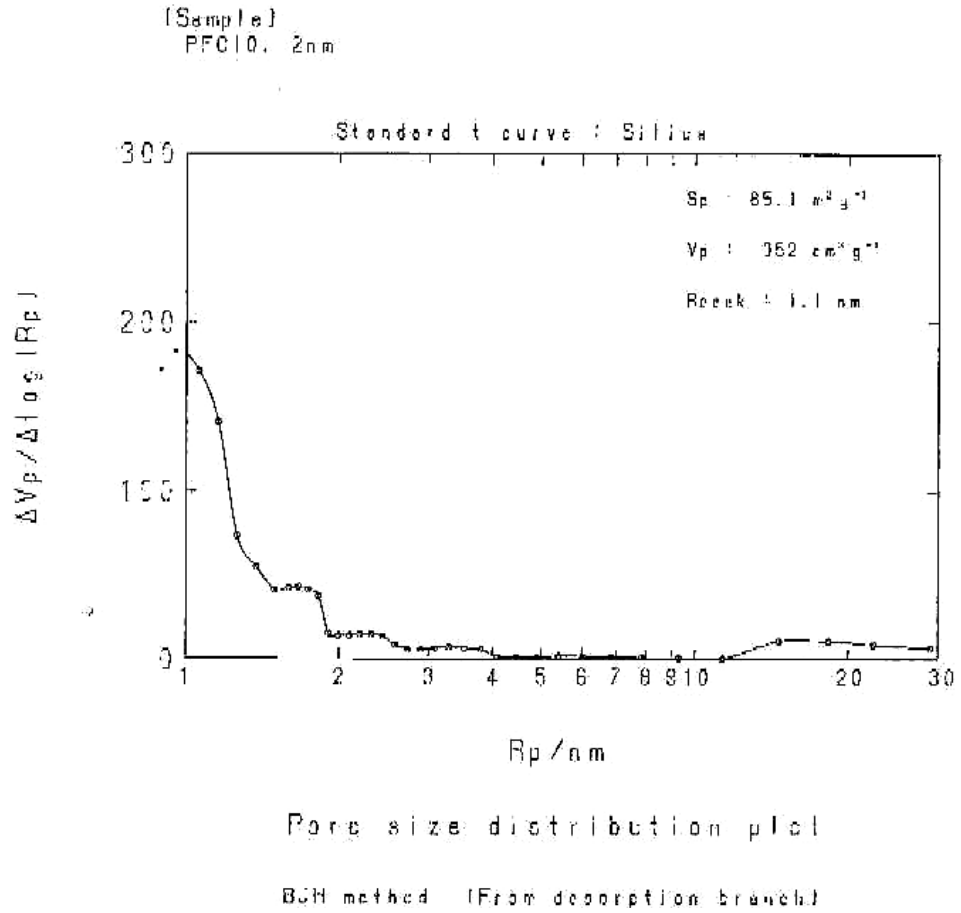

Figure 47: Pore size distribution plot for the Pf-C10 (2 nm base) surface-modified glass membrane.

The corresponding adsorption isotherm and the BET-plot are given in appendix 13-1 and 13-2, respectively.

If the pore size distribution plots in figure 44 and 47 are compared, they are more or less identical for pore sizes wider than 2 nm. The 2 nm base membrane has a more distinct shoulder at ca. 1.8 nm than the 4 nm base membrane. As is the intention, the peak in the pore size distribution in figure 47 is shifted towards a narrower pore size than in figure 44. As discussed in the 2 nm pure membrane section, the pore volumes are more or less constant in the 2 and 4 nm base membrane, leading to a doubling of the separation factor in the 2 nm membrane compared to the 4 nm membrane. Here the difference between the pore volumes is larger and this will most probably not

lead to that great an increase in the separation power. However, if the 2 nm base membrane is compared to the pure 2 nm membrane in figure 35, it is clear that the tail of in the distribution is heavily reduced in the Pf-C10 modified membrane compared to the pure 2 nm membrane. The lack of the tail in the pore size distribution may lead to an increase in the separation factor so it is difficult to predict which effect will be the strongest.

Permeability measurements, pure gases

The measured permeances, selectivities and permeability decay for the Pf-C10 (2 nm) membrane are reported in table 25.

Table 25: Permeance results for pure gases for the Pf-C10 surface-modified glass membrane (2 nm base) at 30°C (Tests performed with new module).

Parameter	Value [Unit]
P/l_{N2}	0.00576 [m^3 (STP)/(m^2 bar h)]
$\alpha_{O2/N2}$	1.3 [-]
$\alpha_{Cl2/N2}$	5.7 [-]
PD(t)	1.8 [10^{-5}/s]
Cl_2 exposure time	7 000 [s]

More detailed permeance data for this material is given in appendix 13-3

The performance and stability seem to be very promising for this membrane. Compared to the reported permeances for the C12 modification, in table 19, it can be seen that the permeances are more or less identical, but the stability is an order of magnitude better.

In order to better evaluate the long-term stability, a static chlorine exposure was performed using the durability chamber. The results of this test are reported in table 26.

Table 26: Permeance results for pure gases for the Pf-C10 surface-modified glass membrane (2 nm base) at 30°C.Long exposure* (Tests performed with new module).

Parameter	Value [Unit]
P/l_{N2}	0.00496 [m^3 (STP)/(m^2 bar h)]
$\alpha_{O2/N2}$	1.4 [-]
$\alpha_{Cl2/N2}$	9.4 [-]
PD(t)	0.0085[10^{-5}/s]
Cl_2 exposure time	5 441 000 [s]

* The exposure was performed in the durability chamber.

The membrane stability seems to be very promising, so the permeances for many gas types were measured at 30° to be able to get a better picture of the membrane performance. These results are presented in the "Estimation of the degree of SSF" section on page 118.

Knudsen flow

As for the C18 membrane, a fit of the helium permeances as a function of the temperature was tried, according to both the classical and the activated Knudsen mechanisms. From these fits, it is clear that the temperature dependence is by far best explained by an activated Knudsen mechanism. The fit according to the activated Knudsen mechanism is given in figure 48.

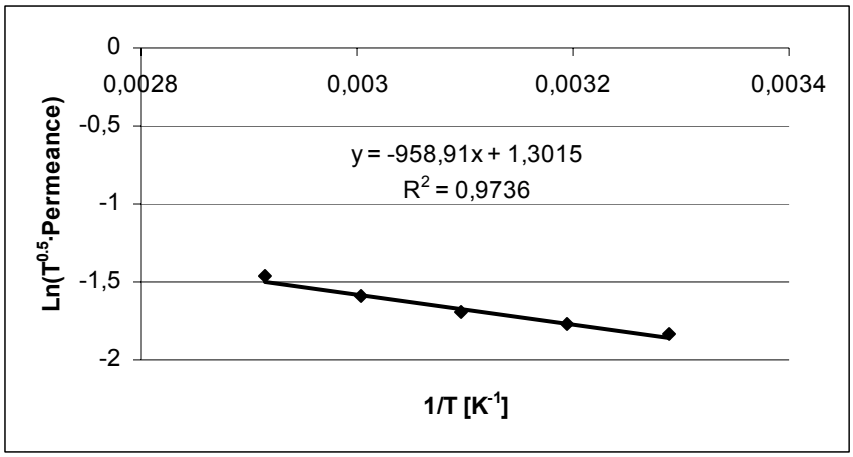

Figure 48: Least-square fit for helium according to activated Knudsen mechanism in the Pf-C10 (2 nm) membrane.

If the equation for the regression line in figure 44 is compared with the equation obtained in figure 36 it is evident that the activation energy is 50% lower than for the 18 membrane.

Mixed gas permeation measurements

As an evaluation of the selectivities obtained for the Pf-C10 membrane, a few screening mixed gas experiments have been performed. The results of these experiments are given in table 27.

Table 27: Mixed gas permeation tests for the Pf-C10(2 nm) surface-modified glass membrane.

% Cl2 in feed	Feed pressure [bar]	permeate pressure [bar]*	%Cl_2 in retentate	% Cl_2 in permeate	Permeance* [m^3(STP)/ (m^2 bar h)]	$\alpha_{Cl2/N2}$ based on eq. 6.7
0, pure N_2	3.7	-	-	-	0.0106	-
18	4->3.8	1	18.1	29.7	0.0135	1.9
57	3.8->3.4	1	57.2	82.4	0.0244	3.5
90	4->3	1	91.1	97.7	0.0308	5.8
100, pure Cl_2	3.8	-	-	-	0.0388	-
						Pure gas based: 3.7

*The permeate pressure was 1 bar during the flow composition analysis. However, the permeances are measured with vacuum on the low-pressure side.

Where the selectivities are calculated according to the following equation:

$$\alpha_{Cl_2/N_2} = \frac{y_{Cl_2,perm} / y_{N_2,perm}}{x_{Cl_2,ret} / x_{N_2,ret}} \qquad (6.7)$$

Where y is the permeate mole fraction [-] and x is the retentate mole fraction [-].

The mixed gas permeation tests show that an increase in selectivities compared to the pure gas case may be expected for feeds richer than ca. 60 vol% in chlorine. The relatively low pure gas selectivity reported in table 26, compared to the reported value in table 25, is assumedly due to long-term storage in a desiccator in the mean time. (The membrane was also used in the degree of SSF measurements reported in the section after the following.)

Sorption measurements

When the transport in a membrane is to be classified /identified, it is of crucial importance to measure the adsorption. Adsorption measurements will enable the

diffusion coefficient to be determined and possibly to identify which of the SSF mechanism theories is best fitted by the performed experiments.

Nitrogen and oxygen adsorption

The results of the nitrogen and oxygen measurements are given in table 28.

Table 28: Nitrogen and oxygen adsorption on the Pf-C10(2 nm) glass membrane at 30 °C

Gas type	Test pressure [bar]	Adsorption [sccm/(g bar)]	Comment
N_2	1.00	0.0732	
N_2	1.04	0.0789	
O_2	1.48	0.0872	
O_2	0.938	0.0887	
O_2	0.688	0.0877	Additive isotherms
O_2	0.999	0.0764	
N_2	0.995	0.0820	Stored in N_2 atmosphere for 14 days after this test.
N_2	1.04	0.0879	
N_2	0.983	0.0930	
N_2	1.58	0.0670	New regeneration prior to this test.
N_2	1.21	0.0779	
O_2	1.37	0.0881	
O_2	1.02	0.0834	

Chlorine adsorption

The chlorine adsorption was measured as a sequence of flashes (the first column of table 29). This means that no evacuation of the sample was performed between the subsequent runs. To keep track of systematic deviations in the pressure transducer, the apparatus and the sample were evacuated (pressure >1mbar) for a minimum of 24 hours after the highest pressure level of the increasing pressure series. After resetting the zero level of the pressure transducer, two new flashes were performed.

The results from these measurements are given in italic font in the bottom rows (first column) of table 29. The subsequent desorption measurements are given in the second column in table 29.

Table 29: Chlorine gas adsorption on the Pf-C10(2 nm) at 30 °C; first run.

Adsorption Pressure [bar]	Adsorbed[cm^3(STP)/(g bar)]	Desorption Pressure [bar]	Desorbed [cm^3(STP)/(g bar)]
0.0315	16.4	2.89	3.67
0.0920	12.9	2.13	3.93
0.209	10.0	1.68	4.11
0.348	7.25	1.15	4.31
0.465	6.79	0.811	4.42
0.689	6.42	0.565	4.28
0.956	5.85	0.377	3.75
1.41	5.09	0.232	2.25
1.89	4.66		
2.88	3.97		
3.82	3.52		
2.10	*4.17*		
3.37	*3.60*		

The measurements were repeated to examine the stability and reproducibility of the measurements. The second run was performed the same way as the first and the results are reported in table 30.

Table 30: Chlorine gas adsorption on the Pf-C10(2 nm) at 30 °C; second run

Adsorption pressure [bar]	Adsorbed [cm^3(STP)/(g bar)]	Desorption pressure [bar]	Desorbed [cm^3(STP)/(g bar)]
0.0305	13.5	2.92	3.70
0.138	10.6	1.86	3.92
0.281	9.55	1.47	4.09
0.449	8.60	1.07	4.33
0.707	7.80	0.719	4.51
1.07	6.96	0.512	3.73
1.47	6.03	0.320	2.45
2.98	4.26	0.205	($-7.0\cdot10^{-5}$ mol)*
3.84	3.99	0.15	($-5.5\cdot10^{-5}$ mol)*
2.11	*4.32*		
3.35	*3.68*		

* The last two desorption results are given in moles because accumulated errors in the calculations otherwise causes the results to be negative This is a consequence of the calculation method that sequentially subtracts the amount desorbed from the previous result obtained. It is possible to calculate the desorption the other way around, but the problem is then to determine the starting desorption level.

The results presented table 29 and 30 are plotted in figure 49 and 50, respectively, to ease the readability of the results.

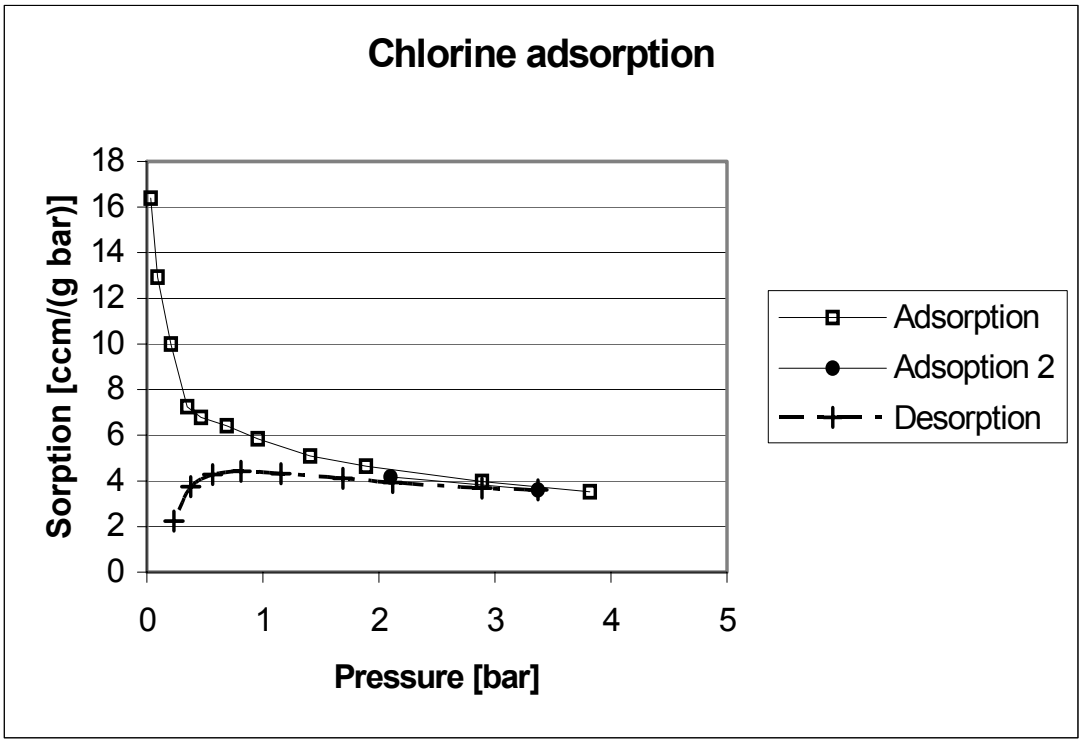

Figure 49: Adsorption and desorption (first run) at 30°C given as [cm³(STP)/(g bar)] as a function of pressure.

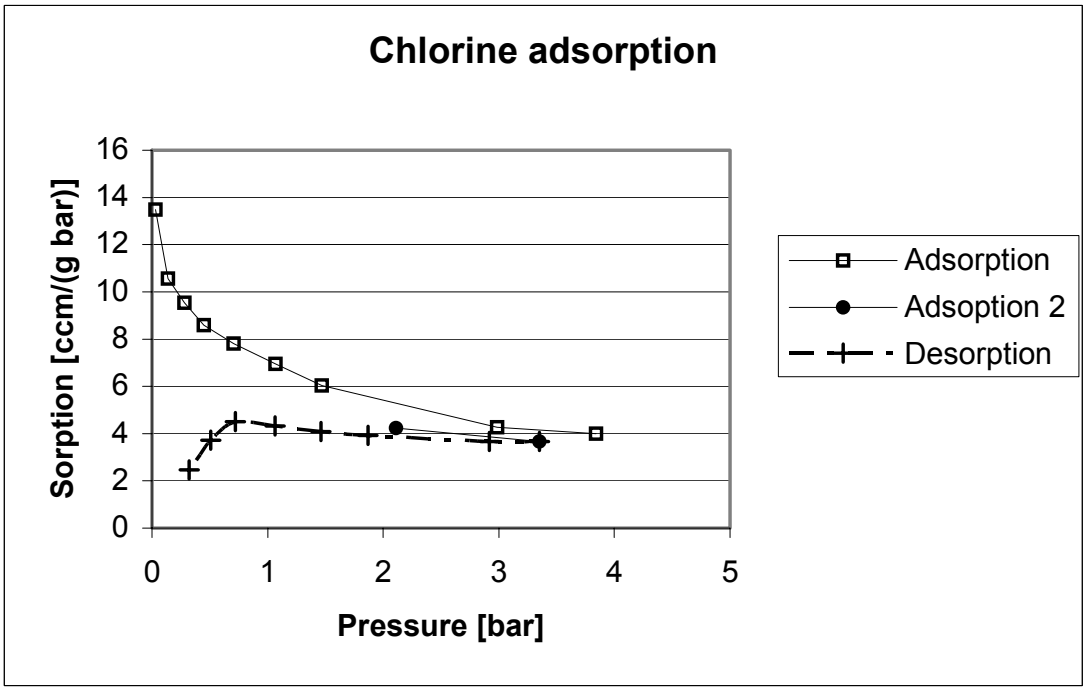

Figure 50: Adsorption and desorption (second run) at 30°C given as [cm³(STP)/(g bar)] as a function of pressure.

The adsorption given in the unit [cm^3(STP)/(g bar)], can be compared to the Henry's law constant and it is clear from figures 49 and 50, that the rate of adsorption monotonically decreases as a function of the applied pressure. This behavior can be explained if the glass surface is believed to consist of specific adsorption sites that may have different potential (adsorption) energies (characteristic for a heterogeneous surface). In that case the most energy-favorable sites will fill first, and the energy released by adsorption will decrease as a function of the degree of the surface coverage.

For the desorption branch the same energy argument can be used, namely that the most energy-favorable adsorption sites will be desorbed at the end of the desorption process, and at the same time, the surface coverage will of course decrease as the desorption continues, thus leading to a smaller number of desorpable molecules. This feature is known as localized sorption.

The traditional way of reporting sorption of condensable gases is as sorption versus the relative pressure, which is done in figure 51 and 52.

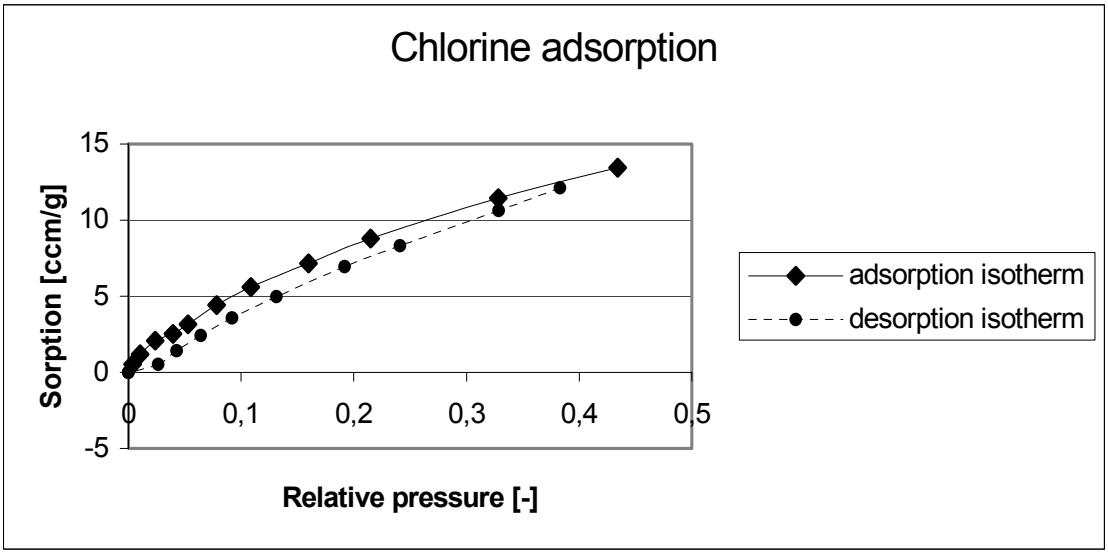

Figure 51: Adsorption and desorption at 30 °C given as [cm^3(STP)/g] as a function of the relative pressure. First run.

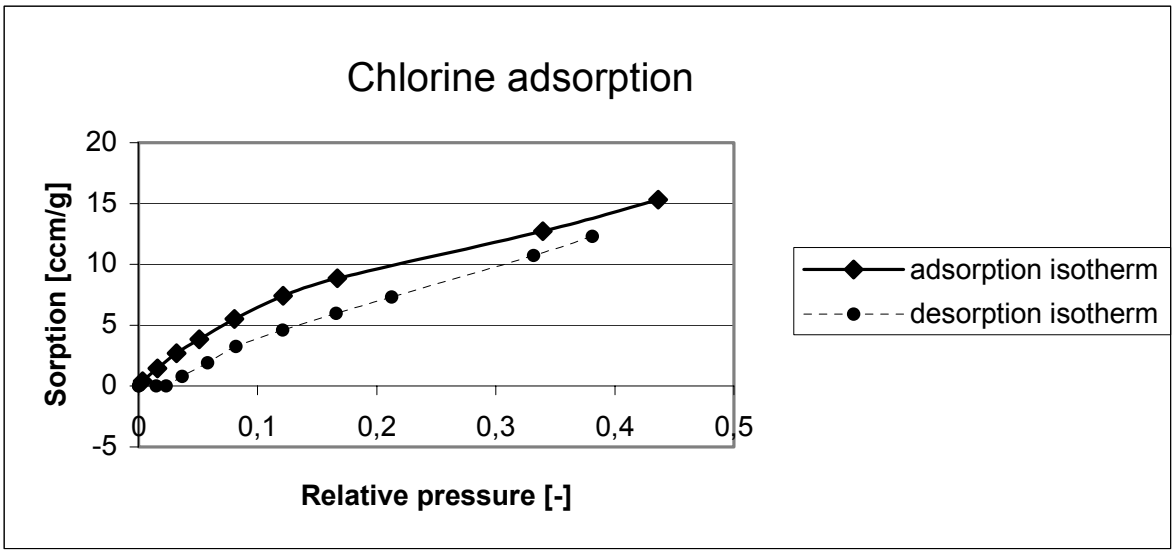

Figure 52: Adsorption and desorption at 30°C given as [cm³(STP)/g] as a function of the relative pressure. Second run.

A very interesting trend in figure 51 and 52 in is that contradictory to the "normal" situation the desorption branch is lower then the adsorption branch, which is also believed to be due to the localized sorption theory.

Temperature dependence of the chlorine adsorption

To be able to obtain a hint of the “strength” of the adsorption, adsorption enthalpy estimation has been performed. This enthalpy can be calculated from the adsorption temperature dependence which is believed to follow an Arrhenius equation:

$$A(T) = A_0 \cdot e^{\frac{E_a}{RT}} \tag{6.8}$$

Where A(T) is the temperature dependent adsorption [sccm/g], A_0= pre-exponential factor (or temperature independent adsorption) [sccm/g], E_a = energy of adsorption (adsorption enthalpy)[J/mol], R= ideal gas constant [8.314 J/(mol K)], T = (absolute)temperature [K].

This equation can be linearized by taking the logarithm of each side of the equation; thus leading to the following expression:

$$\ln(A(T)) = \frac{E_a}{R}\frac{1}{T} + \ln(A_0) \tag{6.9}$$

If equation 9 is compared to the general equation for a straight line: y = ax + b
Then if equation 8 is valid, a plot of ln(A(T)) vs. 1/T will yield a straight line with a slope equal to E_a/R and an intersection point with the y-axis equal to $\ln(A_0)$
This is attempted in figure 53:

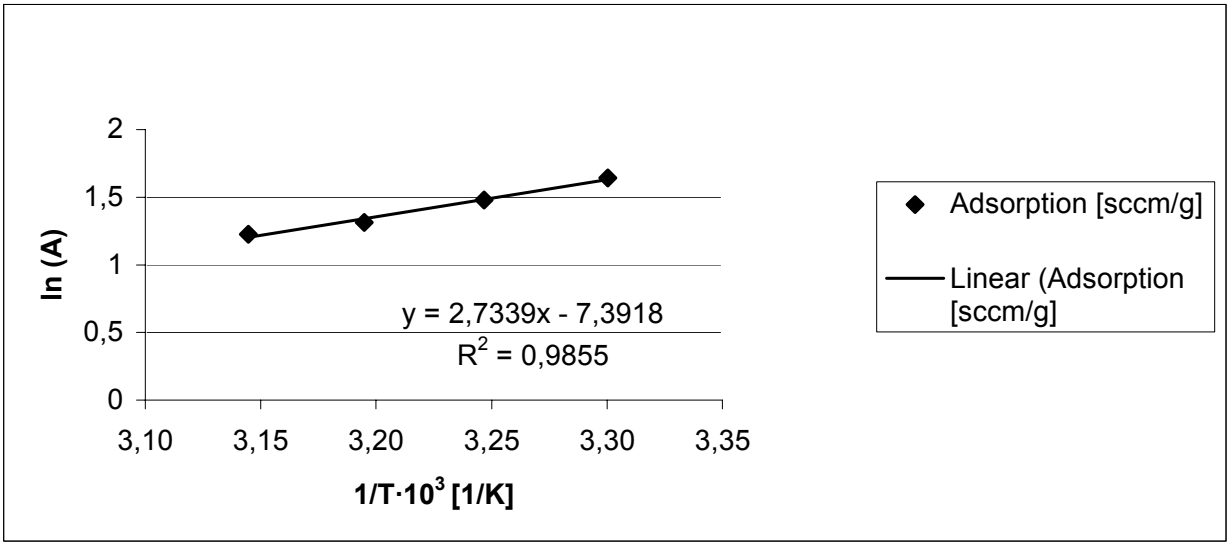

Figure 53: Arrhenius plot of the temperature dependence for chlorine adsorption on the Pf-C10 (2 nm) glass membrane, measured at 1.2 bar.

From the least-squares linear fit in figure 53, E_a/R=2733.9, which rearranges to yield Ea = 22.73 kJ/mol. Thus the best fit of the temperature dependence of the chlorine adsorption experiment yields the following result:

$$A(T) = 6.163 \cdot 10^{-4} \bullet e^{\frac{2733.9}{T}} \qquad (6.10)$$

This equation has a regression coefficient as high as 0.986, which is very high compared to the expected experimental errors that can be estimated to be approximately 10%.
The adsorption enthalpy is in good agreement with the tabulated heat of condensation for chlorine at 1 bar of 20.4kJ/mol. /Perry's/
The corresponding HCl results are reported on page 137.

Estimation of the degree of SSF

In section 3.5, based on the assumption that Knudsen and Surface flows were additive, the degree of surface selective flow (SSF) on the total transport was derived:

$$\psi_i = 1 - \frac{2 \bullet \sqrt{1/Mw_i}}{\alpha_{tot,i/He}} \qquad (3.16)$$

Where ψ is the degree of SSF which is equal to $(J)_{SSF}/(J)_{Tot}$ [-]

However, this derivation is based on the classical Knudsen mechanism and, as it has been shown previously in the "Knudsen flow" part of this session, the transport is much better described as activated Knudsen. This means the constant in the numerator has to be modified by a factor that equals $\frac{g_i}{g_{He}} \cdot e^{\frac{-(E_{a,i}-E_{a,He})}{RT}}$. However, this factor will not be included because of two reasons:

1. The intention of deriving the expression was to be able to predict the degree of surface selective flow from parameters that are easy to determine in practical experiments. The difference in the energy of activation according to the activated Knudsen flow will be very hard to obtain for gases other than helium and perhaps hydrogen, since it will be confounded with the activation energy of surface diffusion.
2. The activation energy for the Pf-C10 (2 nm) base membrane is only 50% of the activation energy in the C18 membrane. This indicates that neglecting the activated Knudsen contribution for the Pf-C10 membrane will have a smaller influence than in the C18 membrane.

Table 31 provides the necessary information to be able to calculate the degree of SSF according to equation 3.16.

Table 31: Permeances, selectivities, molar masses and adsorption for pure gases measured on the Pf-C10 (2 nm) surface-modified glass membrane at 30 °C.

Gas type	Permeance [m^3 (STP)/ (m^2 bar h)]	Selectivity [-] (Helium reference)	Molar masses [g/mol]	Adsorption [Sccm/g]	Tc [K]
N_2	0.00858	0.546	28.0	0.0975	126
O_2	0.0103	0.656	32.0	0.192	155
He	0.0157	1	4.00	0(calibr. gas)	5.3
HCl	0.0315	2.00	36.5	6.12	324
Cl_2	0.0402	2.56	70.9	5.85	417
Xe	0.0105	0.669	131	0.504	290
CO_2	0.0239	1.55	44.0	1.36	304
H_2	0.0222	1.42	2.02	0.0114	33.3
SF_6	0.0110	0.701	146	0.783	318
CO	0.00874	0.557	28.0	0.0971	133
R22 (CHF_2Cl)	0.0309	1.97	86.5	4.45	396

Figure 54 is showing the measured adsorption in the Pf-C10 surface-modified glass membrane for some gases as function of the degree of SSF, Ψ.

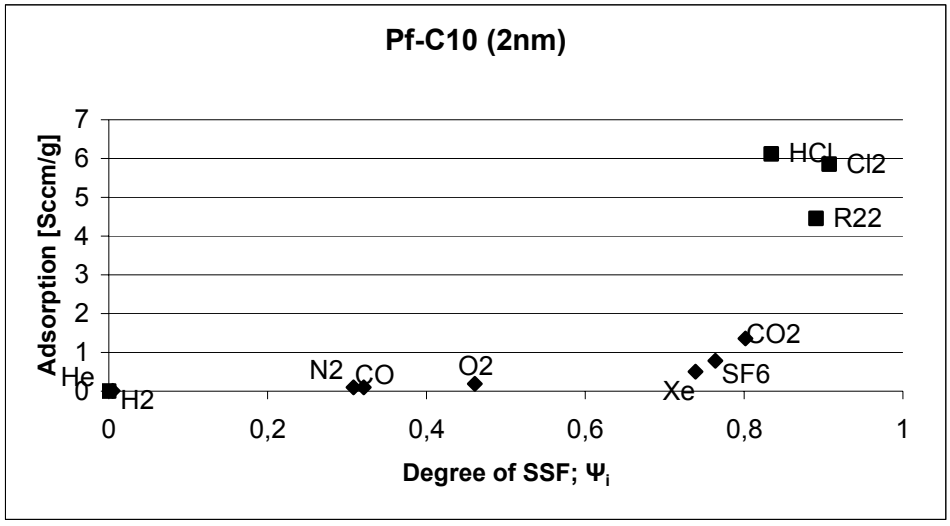

Figure 54: The adsorption as a function of the degree of SSF.

By a closer inspection of figure 54, two phenomena seem to be present simultaneously:

Cl_2, HCl, and R22 are clustering in the upper right corner of the diagram, and seem to be best described by a linear dependence. This is plotted in a least-square fit in figure 55 with He as reference.

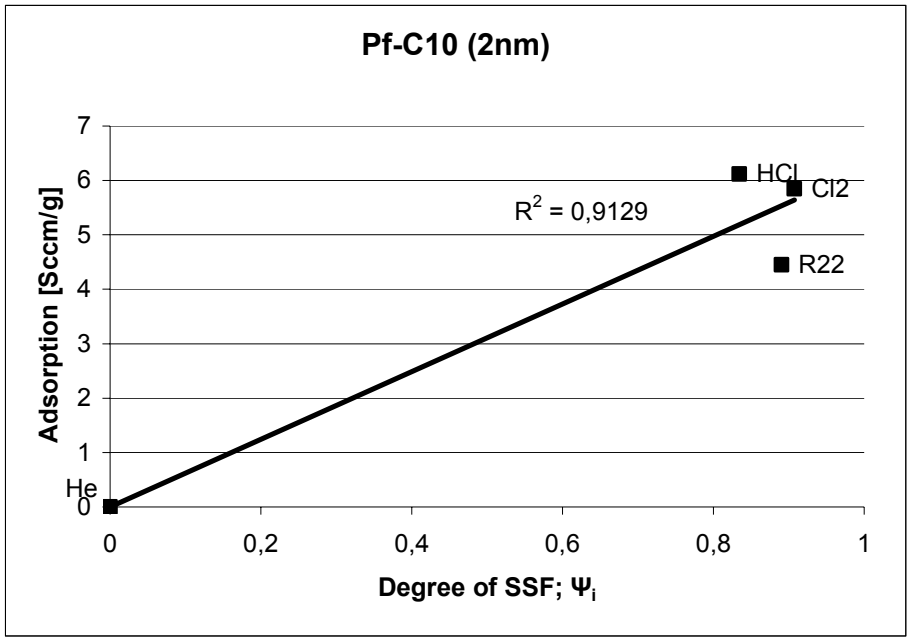

Figure 55: Least-square fit (linear) of selected parts of the data from figure 50.

As it can be seen in figure 55, the regression coefficient is fairly high (0.913) taken into account that two independent experiments are involved in obtaining the relation. (The helium gas was not measured, but serves as a reference both in the adsorption measurements and the evaluation of the degree of SSF.) The following dependency may be derived for these gases:

$$ad = 6.22 \bullet \psi \qquad (6.11)$$

Where: ad is the adsorption as a function of the degree of SSF, corresponding to a best fit of data.

From the slight curvature trend of the remaining gases in figure 54, an exponential fit was tried and the corresponding least-square fit is given in figure 56.

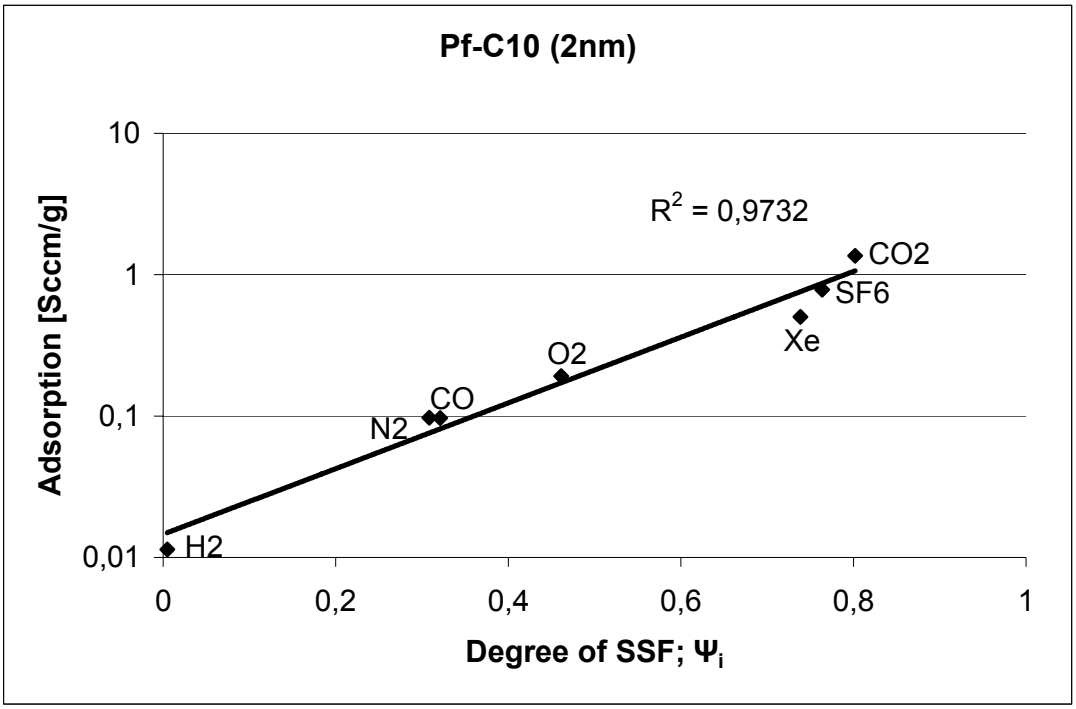

Figure 56: Least-square fit (exponential) of the remaining parts of the data from figure 54.

Figure 56 indicates that the guess of an exponential behavior seems to be very good. Thus from the least-square fit in figure 56, the relationship as is given in equation 6.12 is obtained:

$$ad = 0.0146e^{(5.3494 \cdot \psi)} \qquad (6.12)$$

An explanation of the two different adsorption behaviours found vs. the degrees of SSF (ψ), may be that Cl_2, HCl and R22 experience such strong interactions with the membrane that these gases are condensed on the pore surface and thus follow the "sliding layer" mode. This is further supported by the fair agreement between the measured heat of adsorption and the heat of condensation. The other gases have less interaction with the pore surface, and are thus transported by the 2D- gas and / or the hopping mode. For these gases, it should be remembered that the exponential contribution from the activated Knudsen mechanism was omitted. This means that the magnitude of the exponent may be too high.

A question to be raised: What is causing the greater affinity for the chlorine, hydrogen chloride and R22 on the glass surface? The first guess one may have is that the polarity of the gases is important. This is not the only factor involved because

then the CO gas should not been situated at such a low degree of SSF and having so low adsorption.

The second guess may be that the electronegativity of the atoms in the gas is important. This does seem to have a greater influence on the degree of SSF, but since fluorine is the most electronegative element and the SF_6 gas belongs to the lower branch of figure 54, this can not be the complete explanation.

A third guess would be that the ease of condensability (adsorption) could be estimated from the critical temperature of the gases (values given in table 31). As shown in figure 57, the critical temperature could be used as a measure for the degree of SSF but it will give no new information about why the three gases exhibit a different transport mechanism. It seems as if the element chlorine is an important factor in explaining the belonging of Cl_2, HCl and R22 to another mode of SSF than the other gases. The reason for why a chlorine atom is important is not known.

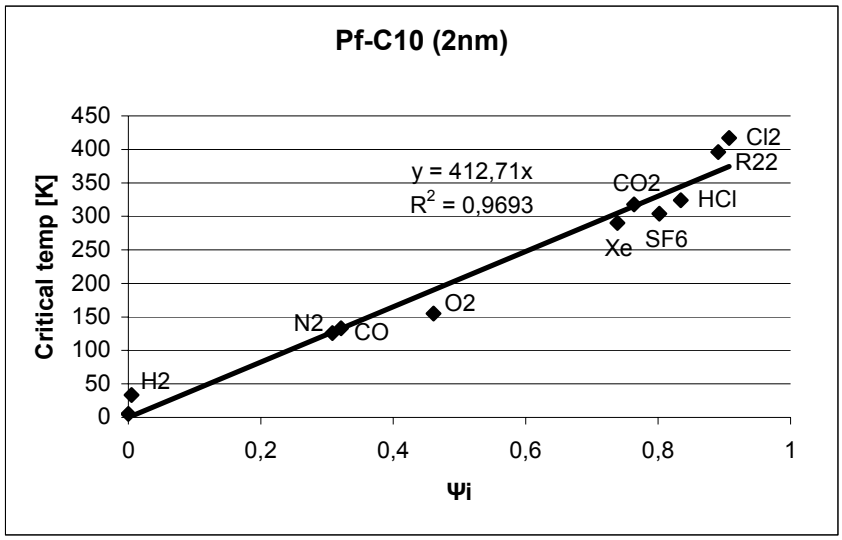

Figure 57: Least-square fit of the critical temperature versus the degree of SSF.

A consequence of the obtained linearity in figure 57 is the opportunity to predict the selectivities, relative to helium, from the molecular weight and critical temperature and only induce a 3% error. This could potentially save a lot of experiments required, if other gas selectivities (than those measured here) are wanted. However, since the least-square fit seems to be poorer as the critical temperature is increased, the obtained relation should not be used for gases with a critical temperature exceeding 350K. As a verification of this theory, additional gas selectivities have

been measured (with gases that have not been used in obtaining the relation) and the result is plotted in figure 58.

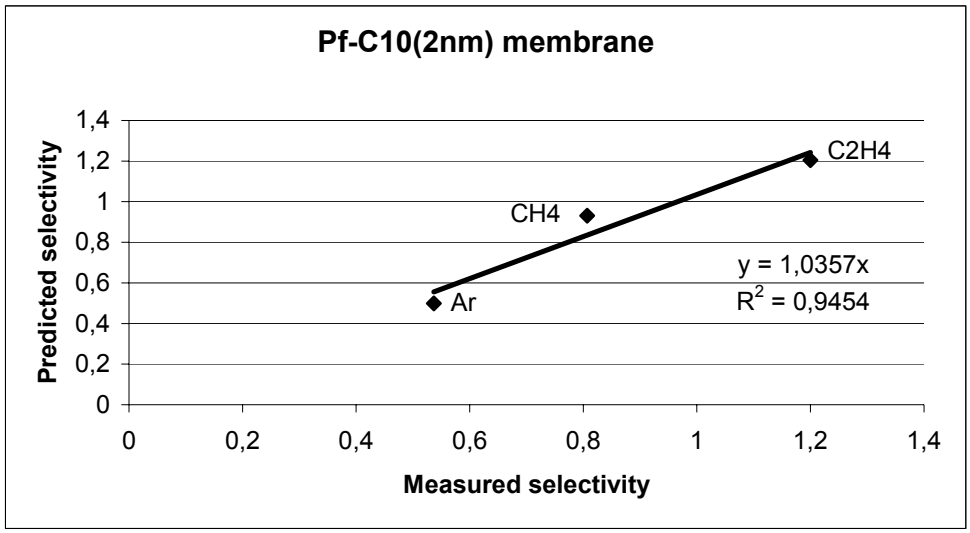

Figure 58: Predicted versus measured selectivities (helium reference) for the Pf-C10(2 nm) surface-modified glass membrane.

As can be seen from the regression coefficient in figure 58, the ability to predict the selectivity for gases, with a critical temperature below 350K, within 4 % accuracy (forced through zero) is taken as a support for the "selectivity theory". However, if the upper bound is challenged by trying to predict the selectivity for propane (Tc 370K), the deviation becomes very large. The measured selectivity is 1.8 whereas the predicted is 3.0.

.

Diffusion coefficient determinations

As described in chapter 5.6 the diffusion coefficient can be determined by two different methods, namely from the well known:

$$P = D \cdot S \tag{6.13}$$

Where P= permeability [m^3(STP)m/(m^2 bar h)], D is the diffusion coefficient [m^2/h] and S is the sorption coefficient [m^3(STP)/(m^3 bar)].

Thus the diffusion coefficient can be calculated as the ratio between P and S at a given pressure and temperature.

The diffusion can also be estimated from the time-lag at the start of the gas permeation measurement. The θ-value obtained from permeation measurement, relates to the diffusion according to /Mulder/:

$$\theta = \frac{l^2}{6D} \tag{6.14}$$

Where θ is the time-lag [s] and l is the membrane thickness [m].

Figure 59 gives a comparison of the diffusion coefficient obtained by the time-lag method vs. the calculated diffusion from the P/S ratio.

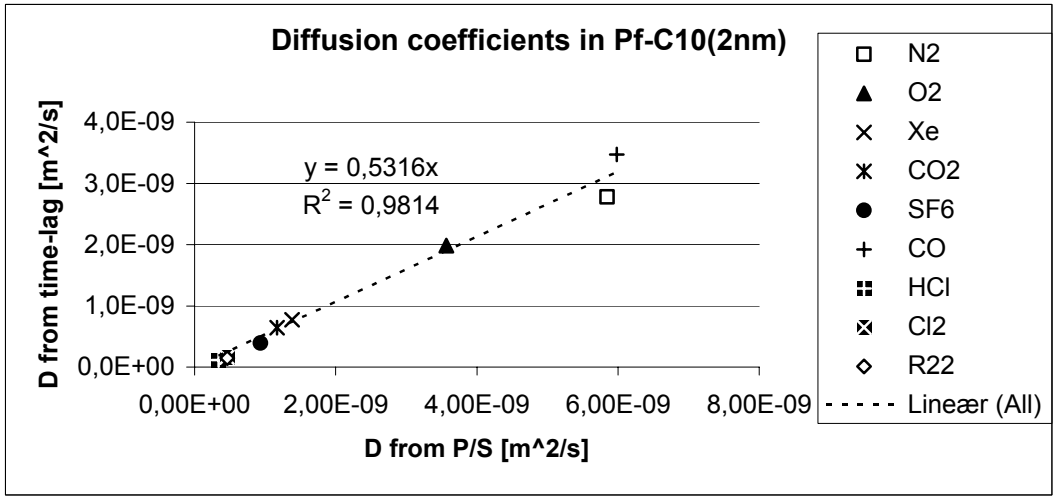

Figure 59: Comparison of diffusion coefficients obtained by the time lag vs. the P/S-ratio methods.

Initially one would expect the values obtained for the diffusion coefficient to be the same regardless of measuring method, thus the function of the regression line should be y = x. The reason for the discrepancy between the two values is not obvious. However, it should be noted that D is calculated from P/S at 1 bar from measured permeability and sorption values, while the D from the time-lag is estimated from the low-pressure side in the permeance apparatus.

6.1.11 Glass hollow fibre

The glass fibres are produced in fewer steps than the tubular membranes as discussed in chapter 2.3. The phase separation step lacks, leading to much smaller pore sizes by ion exchange of the sodium ions with protons during the acid leach. This means that both the pore size and the porosity is different than in the tubular membranes.

Permeance measurements

The permeance results are presented in table 32 and 33 for the short and long-term chlorine exposures, respectively.

Table 32: Permeance results for pure gases for the glass hollow fibre membrane at 30°C. (Tests performed with new module).

Parameter	Value [Unit]
P/l_{N2}	0.00239 [m^3 (STP)/(m^2 bar h)]
$\alpha_{O2/N2}$	0.76 [-]
$\alpha_{Cl2/N2}$	0.020[-]
PD(t)	0.48[10^{-5}/s]
Cl_2 exposure time	96500[s]

More detailed permeance data measured for this material is given in appendix 14-1

Since the fibres are produced by a different route where no extra phase separation is included, it is expected that the average pore size is smaller in the fibre than in any of the surface-modified membranes. This can easily be seen in the chlorine / nitrogen selectivity that is in favour of the N_2 molecule, which has the smallest kinetic diameter. This indicates activated Knudsen, molecular sieving or a combination of the two mechanisms.

Table 33: Permeance results for pure gases for the glass hollow fibre membrane at 30°C. Long exposure*. (Tests performed with new module)

Parameter	Value [Unit]
P/l_{N2}	0.0301[m^3 (STP)/(m^2 bar h)]
$\alpha_{O2/N2}$	0.61[-]
$\alpha_{Cl2/N2}$	0.054[-]
PD(t)	0.021[10^{-5}/s]
Cl_2 exposure time	4 690 600[s]

* The exposure was performed in the durability chamber.

The stability of the fibre seems to be at least as good as the average surface-modified glass membrane. As discussed in the experimental section, there are many pitfalls in the preparation of the fibre module and some of them may, at least partly, explain why there is an order of magnitude difference in the initial nitrogen permeance reported.

To investigate whether the fibres could be applied in chlorine separation at higher temperatures, screening tests have been performed at 80 °C. This is reported in table 34.

Table 34 Permeance results for pure gases for the glass hollow fibre membrane at 30 and 80 °C. (Tests performed with new module)

Parameter	Measured at 30 °C	Measured at 80 °C	[Unit]
P/l_{N2}	0.000299	0.000249	[m^3 (STP)/(m^2 bar h)]
$\alpha_{O2/N2}$	0.44	0.82	[-]
$\alpha_{Cl2/N2}$	0.22*	0.70*	[-]
PD(t)	0.31	0.14	[10^{-5}/s]
Cl_2 exposure time	170 000	190 000	[s]

* The selectivity is most likely lower, because the self leak rate of the apparatus is equal to the pressure change in the chlorine measurement (the raw data can be found in appendix 14-1)

If the pressure changes used to calculate the chlorine permeabilities in table 34 are compared to the corresponding self leak rates (appendix 14-1), then it is questionable whether the chlorine measurements are statistical significant (keep in mind that the accuracy of the equipment is ~7 % and that there are additional uncertainties in the trickiness of the fibre mounting into module). This means that the chlorine permeances are overestimates and that the chlorine / nitrogen selectivities are underestimates.

The detection problem arises since the available membrane fibre area in the module is too small. In order to improve the detection a new approach for mounting the fibres into a module should be sought. A possible mounting procedure is suggested in appendix 14-3 (the method has not been tested yet). If a module with a significantly increased (two orders of magnitude or more) membrane area could be prepared, then mixed gas experiments should be performed to validate whether the fibres are suitable in the chlorine air /separation or not.

6.1.12 Sum-up for the chlorine air separation

To be able to better evaluate and sum-up the different materials described in the chlorine – air separation, a Robeson plot is given in figure 60. In this plot the materials with the highest separation factor will be the ones at the upper-most right in the plot./Robeson/

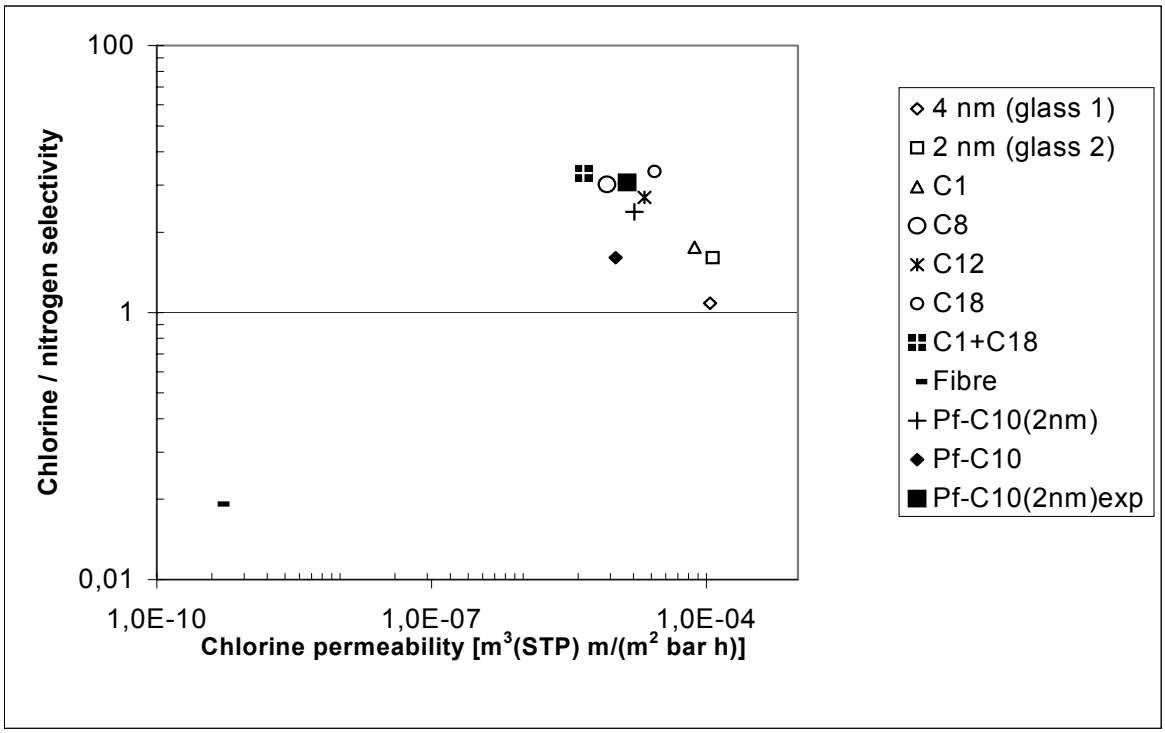

Figure 60: Robeson plot for the materials in the Chlorine –air separation, the air is modelled as nitrogen. Measured at 30 °C and 1 bar, pure gases.

From figure 60, it can be concluded that the best membranes are: C18, pure 2 nm glass, C1, C12 and the exposed Pf-C10(2 nm). The fibre is nitrogen selective, presumably a molecular sieving mechanism, and it can therefore not be directly compared to the other materials.

However, it has been shown in the previous sections that the stability of the materials vary considerably; hence a plot of the average nitrogen permeability decay rate as a function of the chlorine exposure time is given in figure 61. In this plot, if a line is drawn connecting the values given for the different membranes, the most stable material will have the most negative slope and simultaneously the lowest y-axis crossing point.

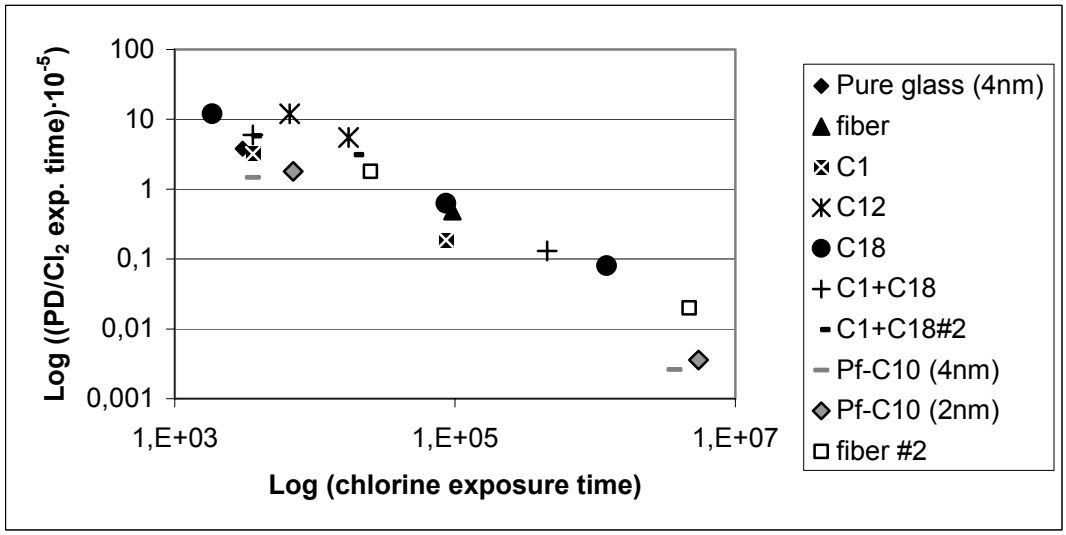

Figure 61: The average permeability decay for nitrogen after chlorine exposure as a function of the exposure time.

From the stability plot in figure 61, it can be concluded that the perfluorinated materials are the most chlorine-stable and that the C12 membrane has the worst stability.

If the information on the separation properties and stability are combined, it is evident that the Pf-C10 (2 nm) is the best combined choice for a chlorine selective membrane.

However, it should be mentioned that the fibres should not be excluded because of several reasons:

1. The available membrane area is small in the current set-up leading to very low permeances at the border of detection of the permeance rig.
2. The fibres are nitrogen selective, so even if the permeances are low, there may be gas compositions in other processes differing from the given example, where the fibres are the best choice. Membrane process simulations may reveal for which compositions the fibres are the best choice. Such simulations may also reveal if a combination of the fibres and tubes are preferable for some conditions.
3. Even in the cases were the fibre is not directly comparable to the tubes in the perm-selectivity, it should be noted that the packing density (membrane area / module volume) in a fibre module is usually much higher than in a tubular module, and that the process economy is largely dependent on the number of

modules required. Another argument in favour of the fibre is that the production of the fibres is simpler, involving fewer steps, making the fibre less costly than the Pf-C10 surface-modified membrane.

The fibre is separating according to a molecular sieving mechanism (or an activated Knudsen, the governing equations are almost identical, equation 3.5 and 3.13) and the selectivity and permeance may not be that vulnerable to an increase in temperature. For temperatures above about 80°C, the glue is not recommended, since it is not guaranteed to be temperature stable beyond this value. One possible solution of the sealant problem, as proposed by our Japanese research associate, is to use molten glass as a sealant. However, currently this method has a severe drawback since the available sealant glass and the fibre have such large differences in the thermal expansion coefficient, which would induce intolerable stresses leading to the breakage of the fibre. One possible, but very impractical solution might be to never cool the module down after it is produced.

Another, yet unexplored, approach is to use mixed matrix membranes (Organic inorganic hybrids where the organic polymer phase is continuous). This approach will require a lot of additional research in order to optimise both materials in the hybrid and the interface between them, but if successful, the mounting of the membrane could easily be based on existing flat-sheet mounting technology.

Some comments are also necessary about the sealing of the membrane (tubes or fibre) into a module. If a surface-modified Pf-C10 (2 nm) membrane is chosen, then the process temperature should be kept low in order to maintain a high degree of surface flow present in the membrane. Screening tests on a C18 membrane indicate that the chlorine permeance decreases by 50 % by increasing the temperature from 30 to 80°C, although no nitrogen permeances were recorded so the selectivity is unknown (appendix 9-3). In the pure 2 nm glass, the chlorine permeance also drops by 50% by increasing the temperature from 30 to 90 °C and the chlorine / nitrogen selectivity drops by 40% (appendix 6-3). This adds up to that the temperature must be kept low in order to maintain the highest possible separation power. Evaluation of the stability of the glue in chlorine environment has revealed the glue to be stable (for one week) up to 90 °C. Thus the Araldite® glue used in this thesis seems to be usable as a sealant.

The glass membrane tubes used in this work had a wall thickness of 0.5 mm which is too thick to be commercially viable. However, the Japanese glass template producer, Akagawa Hard Glass Co. Ltd., produces glasses with wall thicknesses down to 0.03 mm and corresponding diameter down to 0.2 mm. Thus the permeances can easily be increased by a factor of 17 and simultaneously the module pacing density increases as the tube diameter is reduced. Combined, this will increase the commercial potential of the membrane tubes significantly.

6.2 Hydrogen chloride – Hydrogen separation

Based on the results obtained in the chlorine separation evaluations, it was decided to focus on fewer materials in hydrogen chloride / hydrogen separation. This was based on the assumption that dry hydrogen chloride gas seems to be less aggressive (reactive) than chlorine gas.

All permeation measurements reported for HCl /H_2 were obtained using the new module

6.2.1 C18 surface-modified glass membrane (Low surface coverage)

As explained in section 6.1.5, a different preparation route was implemented for the precursor glass, leading to condensing surface OH groups. This will lead to fewer reaction sites on the membrane surface and possibly a more stable membrane.

Permeance measurements

Table 35 and 36 sum up the results obtained for the HCl / H_2 separation using the C18 (Low surface coverage) surface-modified glass membrane.

Table 35: Permeance results for pure gases for the C18 (low surface coverage) glass membrane at 30°C.

Parameter	Value [Unit]
P/l_{N2}	0.00106 [m^3 (STP)/(m^2 bar h)]
$\alpha_{O2/N2}$	1.7 [-]
$\alpha_{HCl/N2}$	21[-]
$\alpha_{HCl/H2}$	4.6[-]
PD(t)	4.3[10^{-5}/s]
HCl exposure time	3 600[s]

The raw-data can be found in appendix 9-2.

The initial durability seems to be better for hydrogen chloride than the durability reported for chlorine in table 10. Another issue to be addressed is that despite the relatively high HCl/ N_2 selectivity, the corresponding HCl /H_2 selectivity is over four times lower. This is due to the (activated)Knudsen and surface diffusion being additive. For hydrogen the degree of SSF is low (the degree of SSF in this membrane is assumed to follow the same general trends as the Pf-C10(2 nm) membrane in figure 49) so Knudsen flow prevails. The Knudsen flow is most favourable for the lightest molecules, since the diffusion coefficient is proportional to the square root of the inverse molecular weight of the gas. The permeance of HCl is high because of surface diffusion. In general, a conceptual plot of the selectivity as a function of the pore size, as given in figure 62, can be constructed for a membrane where HCl is transported according to a surface diffusion mechanism.

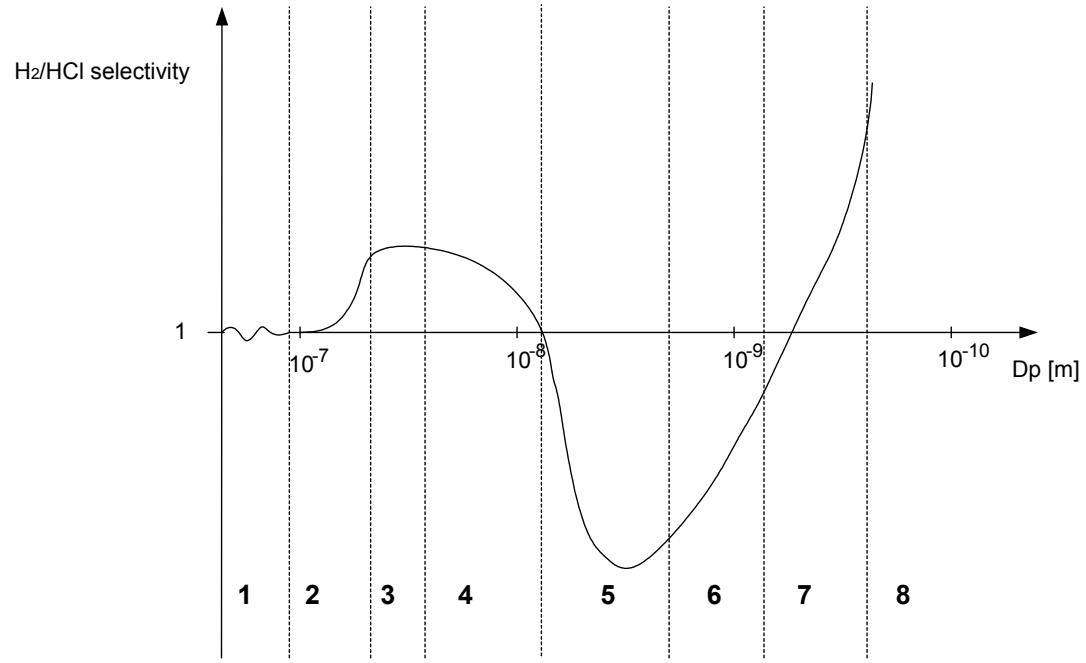

Figure 62: Conceptual plot of the hydrogen / hydrogen chloride selectivity as a function of the pore diameter. Most probable transport regimes indicated by numbers in the bottom of the figure.

In figure 62, the most probable transport mechanisms are the following:

1. For pore sizes larger than approximately 10^{-7} m, bulk flow with no selectivity prevails.
2. Knudsen flow is starting to become important, but still not dominating, meaning that the selectivity is increased towards the theoretical value, of 4.3 given as the root of the inverse ratio of the gases molecular weight.
3. Classical Knudsen with a constant selectivity of 4.3.
4. The selectivity is decreasing as the contribution of the surface flow is becoming more important.
5. Surface flow of HCl is causing the selectivity to reverse and approach a minimum. Thus, tailoring the pore size is of crucial importance in order to obtain the highest possible reversed separation factor.
6. Even more narrow pores are causing the contribution from the activated Knudsen mechanism to become more dominant and the selectivity will again be in favour of hydrogen.
7. Combination of activated Knudsen and molecular sieving.

8. Molecular sieving; the pore size of the membrane is smaller than the kinetic diameter for HCl, but larger than the kinetic diameter for hydrogen.

Table 36 gives the results of the medium-time exposure tests performed on the C18 (low surface coverage) surface-modified glass membrane.

Table 36: Permeance results for pure gases for the C18 (low surface coverage) glass membrane at 30°C. (Medium exposure time).

Parameter	Value [Unit]
P/l_{N2}	0.000896[m^3 (STP)/(m^2 bar h)]
$\alpha_{O2/N2}$	1.7[-]
$\alpha_{HCl/N2}$	34[-]
$\alpha_{HCl/H2}$	6.5[-]
PD(t)	0.070[10^{-5}/s]
HCl exposure time	86 400[s]

The membrane performance evaluated by the separation power, according to equation 6.1, is actually improved after the long-term exposure by 20 % ($SP_{\text{short time}}$ = 0.0049 and the $SP_{\text{medium time}}$ = 0.0058)

The stability of the C18 modification seems to be much better in contact with HCl than for chlorine (tables 10 and 11). This is not surprising since a chlorine substitution reaction with the glass most likely involves a substitution reaction of chlorine with one hydrogen or acyl group as indicated in figure 38. This reaction will produce HCl as a product and the process is most likely thermodynamically spontaneous at low temperature. Appendix 15 gives an example of calculating the spontaneity for a simple chlorination and a hypothetical HCl substitution in methane. In this appendix it is shown that a substitution chlorination reaction of methane to tetra-chloromethane, is thermodynamic spontaneous for almost all temperatures using chlorine as a reagent, whereas the use of HCl as a reactant is not spontaneous at any temperature.

It is assumed that the exact thermodynamic data for the surface modification in the glass will be very hard to obtain, therefore the actual stabilisation temperature can not be estimated.

The results obtained that the HCl does not attack the hydrocarbon at any temperature, does not include "acid –reactions" of the HCl, i.e. the HCl may react with the surface OH-groups or adsorbed water.

6.2.2 C1+C18 surface-modified glass membrane

Since it was found in the chlorine separation evaluations that the Cl_2 / N_2 selectivity was greatest for this membrane type, it would be interesting to investigate if this is the case for the HCl/H_2 selectivity as well.

Permeance measurements

Table 37: Permeance results for pure gases for the C1+C18 surface-modified membrane at 30°C. Short-time exposure.

Parameter	Value [Unit]
P/l_{N2}	0.00587[m^3 (STP)/(m^2 bar h)]
$\alpha_{O2/N2}$	1.3[-]
$\alpha_{HCl/N2}$	5.0[-]
$\alpha_{HCl/H2}$	2.1 [-]
PD(t)	0.83[10^{-5}/s]
HCl exposure time	4 700 [s]

The raw-data can be found in appendix 10-2.

By comparison of the selectivities reported in table 36 and 37, it is seen that the selectivity is lower by a factor of 2 in the C1+C18 membrane, compared to the low-surface coverage C18 membrane. However the permeance is increased by a factor of 4.

6.2.3 Pf-C10 surface-modified glass membrane

Permeance measurements

Ideally, based on the experience from the chlorine permeance measurements the optimum Pf-C10 membrane would be based on the 2 nm average pore size glass. However, the 2 nm base sample prepared for this purpose was unusable since the permeance was at least a magnitude too high and unstable (repeating the measurement of a particular gas would yield a different result). Luckily, a sample of

the 4 nm base was available and showing reasonable perm-selectivities. The results of the short time exposure are given in table 38.

Table 38: Permeance results for pure gases for the Pf-C10 surface-modified membrane at 30°C. Short-time exposure.

Parameter	Value [Unit]
P/l_{N2}	0.0115[m^3 (STP)/(m^2 bar h)]
$\alpha_{O2/N2}$	1.1[-]
$\alpha_{HCl/N2}$	1.6[-]
$\alpha_{HCl/H2}$	0.62[-] (0.23, classic Knudsen theory)
PD(t)	4.0[10^{-5}/s]
HCl exposure time	2 100[s]

Some additional pressure dependencies are given in the results summary in appendix 12-3.

If the measured selectivity for HCl / H_2 is compared to figure 62, it is clear that region 4 prevails (dominating Knudsen transport but surface diffusion is starting to be important). However, despite the pores being too large, valuable information may be obtained regarding the HCl stability of the perfluorinated surface modifying compound.

Table 39: Permeance results for pure gases for the g the Pf-C10 surface-modified membrane at 30°C. Long-time exposure. (Tests performed with new module)

Parameter	Value [Unit]
P/l_{N2}	0.0106[m^3 (STP)/(m^2 bar h)]
$\alpha_{O2/N2}$	1.1[-]
$\alpha_{HCl/N2}$	2.0[-]
$\alpha_{HCl/H2}$	0.8[-]
PD(t)	$9.8 \cdot 10^{-4}$[10^{-5}/s]
HCl exposure time	8 208 000[s]

*The exposure was performed in the durability chamber.

Additional experimental results can be found in appendix 12-3

The permeability decay reported in table 36 is the lowest found in this research, but the selectivity is of course much too low. It is expected that a 2 nm base perfluorinated membrane would have reversed, and possibly greater in magnitude, selectivity. One possible solution of obtaining the highest possible selectivity would be to use a longer chained perfluorinated surface modifying reagent. Sadly, there is a problem in getting a longer chained silane because the C10 chain is the longest chain commercially available. An inquiry to the Norwegian sales representative (Chiron) for the German especially chemicals company Gelest, revealed that in order to get a perfluorinated C18 equivalent specially synthesised, a cost of about 40 000Nok have to be spent in order to obtain the necessary 5g. This amount of money by far exceeds the available funding in this project. However, the stability of the C18 modification is much better in HCl than in Cl_2, as proven in table 32 and 33 compared to table 11 and 12. A detailed economic analysis of all operational and installation costs would have to be evaluated in order to determine how much cheaper a shorter-lasting membrane would be to have the same economical potential as a longer-lasting membrane.

6.2.4 Pf-C10 (2 nm) surface-modified glass membrane

Sorption measurements

The HCl adsorption measurements given in table 40 are performed by the same procedure as the chlorine measurements reported in chapter 6.1.9.

Table 40: Adsorption and desorption for HCl gas on the Pf-C10(2 nm) at 30 °C

Adsorption Pressure [bar]	Adsorption [cm^3(STP)/(g bar)]	Desorption Pressure [bar]	Desorption [cm^3(STP)/(g bar)]
0.0615	27.1	2.89	2.79
0.175	16.6	2.01	3.17
0.328	11.8	1.62	3.92
0.460	9.74	1.02	4.45
0.882	6.16	0.715	5.85
1.06	4.88	0.453	7.27
1.53	3.28	0.269	9.13
3.00	2.82	0.173	12.0
3.92	2.69	0.113	18.5
		0.0815	20.8
		0.0588	23.7
2.14	*3.74*		
3.5	*2.79*		

Figure 63 and 64 gives the adsorption and desorption as a function of the pressure and the relative pressure, respectively.

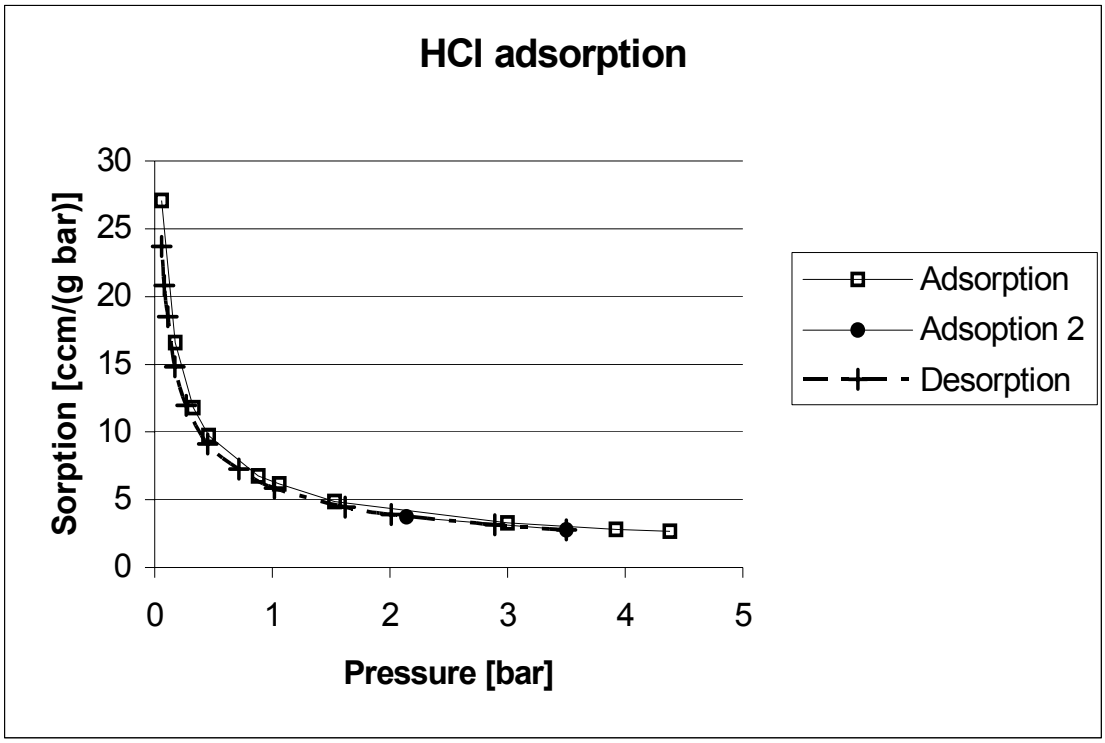

Figure 63: Adsorption and desorption as a function of the pressure for HCl gas

It is very interesting to compare the trends of the desorption branch in figure 63 with the similar curves for chlorine gas given in the figures 49 and 50. Contrary to what were experienced for chlorine in figures 49 and 50 the adsorption and desorption rates follow each other for HCl gas.

One plausible explanation for this may be that the sorption site association (that was strong for chlorine) is not present for the polar HCl gas on the polar glass. The HCl experiences a stronger (polar-polar interaction) potential, which levels of the differences in the weaker (polar- induced dipole) potential experienced by the chlorine molecules. As a consequence the adsorption and desorption for HCl is independent of the surface coordinates, a phenomenon known as delocalized adsorption.

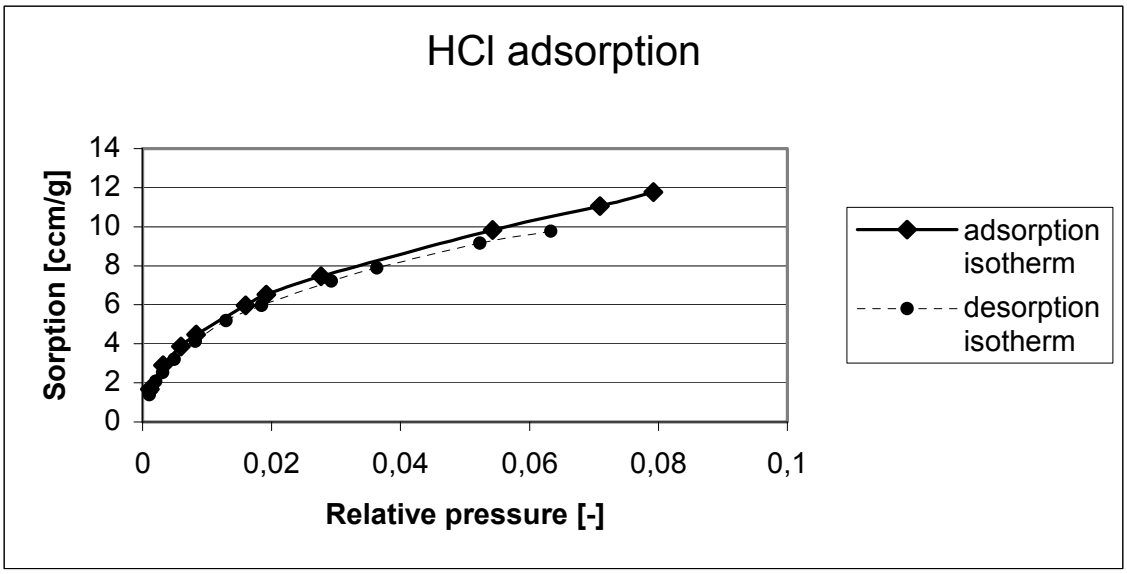

Figure 64: Adsorption and desorption as a function of the relative pressure for HCl on the Pf-C10 (2 nm) membrane.

Also, for HCl, the desorption branch is lower than the adsorption branch but the deviation seems to be smaller compared to the deviation experienced for chlorine.

Temperature dependence for the HCl adsorption

The adsorption enthalpy for HCl is fitted to equation 6.8 in figure 65.

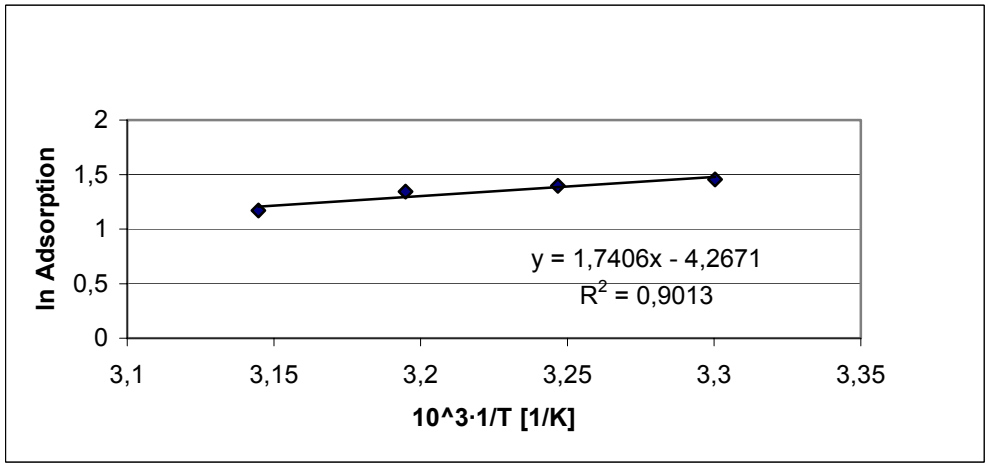

Figure 65: An Arrhenius plot of temperature dependence for the HCl adsorption on the Pf-C10(2 nm) glass membrane (P=1.8 bar)

According to figure 65 and equation 6.8, the following temperature dependence for the HCl adsorption can be determined:

$$A(T) = 1.402 \cdot 10^{-2} \bullet e^{\frac{14471.4}{RT}} \qquad (6.15)$$

The adsorption enthalpy is then 14.471 kJ/mol.
The adsorption enthalpy is in fair agreement with the tabulated heat of condensation for hydrogen chlorine at 1 bar of 17.6kJ/mol. /Perry's/
This indicates that the HCl is in a "condensed" state when adsorbed on the glass membrane surface and thus that the most likely transport mechanism is the sliding layer flow.

6.2.5 Glass hollow fibre

Permeation measurements

As discussed previously, the mounting of the fibres into the module is tricky and may possibly lead to a greater variance in the results. Table 41 reports the long-term HCl exposure of the fibres.

Table 41: Permeance results at 30°C for pure gases on the hollow glass fibres

Parameter	Value [Unit]
P/l_{N2}	$5.89 \cdot 10^{-5}$[m^3 (STP)/(m^2 bar h)]
$\alpha_{O2/N2}$	1.7[-]
$\alpha_{HCl/N2}$	0.37[-]
$\alpha_{HCl/H2}$	0.0082[-]
PD(t)	0.026[10^{-5}/s]
HCl exposure time	530 900[s] (Dynamic exposure)
$\alpha_{HCl/H2}$ (after exposure)	0.072[-]

The raw-data can be found in appendix 14-2.

It should be noted that the mounting of the fibres had to be redone after the first exposure because the breakage of some of the fibres during the exposure test. This means, that the error in the permeation measurements after the exposure may be different than before exposure and the error in the reported permeation decay is possibly larger than "normal".
A temperature dependency run was performed with a new sample to investigate if the fibres may be suitable at elevated temperatures. These results are reported in table 42.

Table 42: Permeance results for pure gases for the hollow glass fibre at 30 and 80 °C.

Parameter	Measured at 30 °C	Measured at 80 °C	[Unit]
P/l_{N2}	0.000229	0.000255	[m^3 (STP)/(m^2 bar h)]
$\alpha_{HCl/N2}$	0.25	0.75	[-]
$\alpha_{HCl/H2}$	0.024*	0.089	[-]
PD(t)	0.16	0.29 (at 80 °C)	[10^{-5}/s]
HCl exposure time	183 000	110 500	[s]

*The selectivity is possibly lower, because the self leak rate is equal to pressure change in this measurement.

The raw data can be found in appendix 14-2.

Two aspects should be discussed about the results in table 42:

1. The HCl / H_2 selectivity at 30 °C is too high, since the self leak rate is identical to the measured pressure change determined in this test. However, the leak rate at 80 °C was not determined, so it is possible that the HCl / H_2 selectivity at 80°C also is too high.
2. The increased temperature is seemingly worsening the separation slightly. As can be seen from the drop in the selectivities (the H_2 / N_2 selectivity is 11 and 8.5, at 30 and 80 °C, respectively) whereas the hydrogen permeance is approximately kept. This is not surprising since the molecular sieving is an activated transport, involving a threshold energy needed to be surmounted in order for a molecule can pass the obstacle (equation 3.14).

These aspects sum up to that the fibres have not been ruled out as a feasible option for the H_2/HCl separation, but a more stable mounting solution for the fibres into a module, as suggested in appendix 14-3, should be sought.

6.2.6 Sum up of the HCl / H_2 –separation

As for the chlorine separation a Robeson equivalent plot /Robeson/ for the HCl /H_2 separation has been prepared. Figure 66 gives this plot:

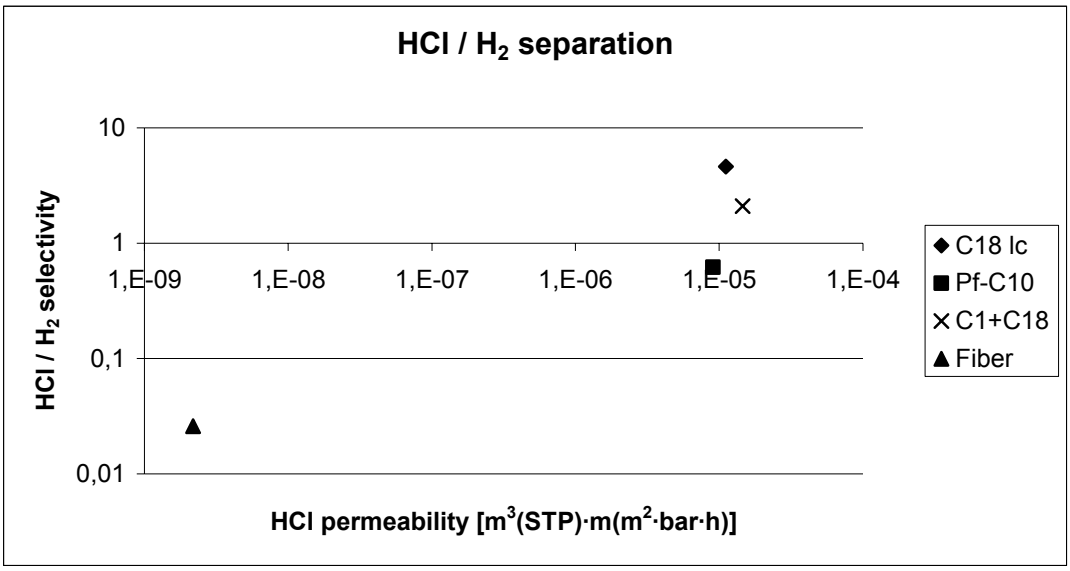

Figure 66: Robeson plot for the HCl /H_2 separation. Pure gases permeabilities at 30 °C

According to the process used as an example in this thesis, the feed contains ca. 93% (vol.) of HCl and the temperature can be as high 300°C. From the Robeson plot in figure 66 it is quite clear that none of the surface-modified glass membranes are very suitable to use in this process

A comparison of the stability of selected glass membranes is given in figure 67.

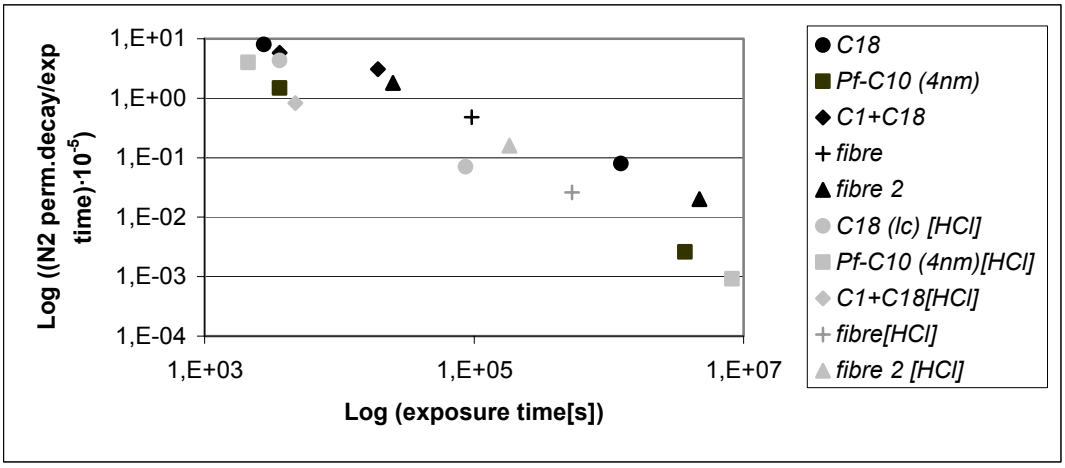

Figure 67 A comparison of the average permeability decay for nitrogen after chlorine exposure (black symbols) or hydrogen chloride exposure (grey symbol) as a function of the exposure time.

As can be seen from the stability plot given in figure 67, the stability of all the glasses is more or less identical and comparable to the stability of the perfluorinated glass experienced in the chlorine separation. Based on this, the optimum membrane would be the one found most suitable from the Robeson plot (figure 66). Thus, the most suitable surface-modified glass membrane in the HCl / H_2 separation seems to be the low-surface coverage C18 glass membrane.

In the current separation, the temperature should be as high as possible, preferably up to 300 °C. The glue can not sustain that high temperature and as discussed for the surface-modified glass membranes in the chlorine separation, the SSF- transport is believed to decrease as a function of the temperature. In order to keep a large separation power, it is necessary to keep the temperature low. This means that it is questionable whether the surface-modified membranes are suitable at all for the HCl / H_2 separation.

The fibre is H_2 selective and as the temperature is raised to 80° C, the hydrogen permeance is only slightly decreased, whereas the selectivity drops significantly as documented in table 42. However, the HCl permeance is on the border of detection, so the actual separation factors might be higher. The detection may be improved by using a larger membrane area module as described in section 6.1.11.

6.3 References

Aylward, G.H. and Findlay, T.J.V.:" SI chemical data", 2nd ed., John Wiley & sons 1974, p 101.

Kuraoka, K., Chujo, Y. and Yazawa, T.: "Hydrocarbon separation via porous glass membranes surface-modified using organosilane compounds" J. Memb. Sci., 182, (2001), pp 139-149.

Perry's, "Chemical Engineering Handbook", 6th ed. 1984, p3-120.

Robeson, L. M. "Correlation of Separation Factor versus Permeability for Polymer membranes", J. Membrane Sci., 62, (1991), 165-185.

Silverstein, R.M. and Webster F.X.: "Spectrometric identification of organic compounds", 6th ed., John Wiley & sons Inc, 1998.

7 CONCLUSION

Chlorine / air separation

Both pure glasses (including the fibre) and surface modified glasses have been tried out for their suitability in chlorine / air separation.

The pure glass tubes (4 and 2 nm average pore sizes) have too wide pores and therefore their perm-selectivities are too low, but their chlorine durability is acceptable.

The fibre separate according to a molecular sieving mechanism. The mounting of the fibres into the module is tricky, and the variance in these measurements is larger than for the glass tubes. This means that the perm-selectivity for this membrane is not directly comparable to the other membranes tested. However, the chlorine permeability is reduced by a factor of 10 000 and the reversed selectivity(N_2/Cl_2) is only 27. The chlorine permeabilities performed at both 30 and 80 °C lacked enough statistical accuracy to detect any flow beyond the leak rate of the cabinet, (oxygen /nitrogen selectivity is constant from 30 to 80 °C). This means that the chlorine permeances are an overestimates whereas the selectivity are most likely underestimates. Larger area modules should be produced in order rise the chlorine permeance above the leak rate of the cabinet. However, to find the possible compositions where the fibres could be an alternative to the chlorine permeating glass tubes, detailed process simulations would be required.

Among the five different aliphatic surface modifications (C1, C8, C12, C18 and C1+C18) initially tried out for their suitability in chlorine / air separation, the preferable order judged by the separation factor was: (ranged from best to worst) C18, C1, C12, C8 and C1+C18.

The membrane stability is also of vital importance in order to find the best suitable material. Based on the perm decay rate (permeability decay divided by the exposure time) the following order was obtained (best to worst): C1, C1+C18, C18, C8 and C12. Neither of the materials had entirely satisfactory stability, and a perfluorinated surface modification (based on a C10 chain, called Pf-C10) was tried out on both the 4 and 2 nm pore size pure glasses. This material was superior in stability and compatible in perm-selectivity (when used on the 2 nm glass). The Pf-C10(2nm) has a nitrogen permeability of $1.46 \cdot 10^{-6}$ m^3(STP) m /(m^2 bar h) and chlorine / nitrogen

selectivity of 9.4. Currently the membrane tubes come with a 0.5 mm wall thickness, but according to the template glass producer wall thicknesses down to 0.03 mm is available.

Hydrogen / Hydrogen chloride separation

Fewer materials were tested in the H_2 / HCl separation than in the Cl_2 / air separation, and the choice of materials tested in the H_2 / HCl separation were based on the experience gained in the Cl_2 / air separation. The following surface-modified glass membranes were tested: C18 (low surface coverage), C1+C18, and Pf-C10(4nm).

The stability of all glasses is almost identical and comparable to the stability of the perfluorinated glass experienced in the chlorine separation. Based on this, the optimum membranes would be those found most suitable, judging by the separation power. Thus, the most suitable surface-modified glass membrane in HCl / H_2 separation seems to be the low-surface coverage C18 glass membrane. This membrane has a hydrogen permeability of $2.44 \cdot 10^{-6}$ [m^3 (STP) m / (m^2 bar h)] and hydrogen chloride / hydrogen selectivity of 4.6 at 30°C. If the temperature is raised, the separation is expected to soon flip, and to become H_2 selective due to loss of surface flow.

The fibre is H_2 selective with a hydrogen permeability of $8.38 \cdot 10^{-8}$ [m^3 (STP) m / (m^2 bar h)] and hydrogen /hydrogen chloride selectivity of 38 at 30°C. As the temperature is increased to 80 °C, the hydrogen permeability drops by 10% whereas the hydrogen / hydrogen chloride selectivity drops from 38 to 11. However, as in the chlorine permeances in the chlorine separation, the HCl permeability is on the border of detection, so the actual separation factors might be higher.

FURTHER WORK

Several approaches should be pursued (valid for both separations in question) in further research.

- Since inorganic membranes in general are difficult to mount into modules, a mixed matrix membrane (MMM) approach should be investigated. Two approaches seem to be of particular interest:
    - Crushed surface modified glass tubes mixed into a perfluorinated rubber like Viton®, in search for a chlorine or hydrogen chloride selective material.
    - Crushed glass hollow fibres mixed into a perfluorinated glassy polymer (like Teflon® or Hyflon®), in search for a chlorine or hydrogen chloride retaining material.
- The experienced detection problems when measuring the permeances in the fibres may be prevented if longer fibre length can be acquired and the mounting technique proposed in appendix 14-3 is successful. If the membrane area can be increased by a factor of more than 100, mixed and pure gas permeation experiments for both separations should be tried out.
- Simulations should be performed in search for the optimum module combination (the simulated process should not be limited to the specifications of the process example used here). Simulation of whether a combination of both chlorine selective and chlorine retaining (or hydrogen chloride selective and retaining) modules in the same process could be feasible for a specific feed compositions at given process conditions.
- A longer perfluorinated silane chain (C18 chain) used as a surface-modifying agent may show improved perm-selectivities. This perfluorinated silane does not exist commercially, thus it would have to be special synthesised at a rather high cost.

LIST OF APPENDICES

Appendix 1 Reprint of article no.1 1
Appendix 2 Reprint of article no.2 22
Appendix 3 Permeance measurements 40
Appendix 4 Adsorption apparatus 46
Appendix 5 Pure 4 nm glass membrane 50
Appendix 6 Pure 2 nm glass membrane 51
Appendix 7 C1 surface-modified glass membrane 57
Appendix 8 C8 surface-modified glass membrane 58
Appendix 9 C18 surface-modified glass membrane 59
Appendix 10 C1+C18 surface-modified glass membrane 64
Appendix 11 C12 surface-modified glass membrane 69
Appendix 12 Pf-C10 surface-modified glass membrane 70
Appendix 13 Pf-C10 (2 nm) surface-modified glass membrane 77
Appendix 14 Glass hollow fibre 81
Appendix 15 Spontaneity estimations 88

Appendix 1 Reprint of article no.1

Glass membranes for purification of aggressive gases. Part I: Permeability and stability.

Arne Lindbråthen and May-Britt Hägg*

Norwegian University of Science and Technology, NTNU

Department of Chemical Engineering

N-7491 Trondheim, Norway.

Abstract

Chlorine gas is an aggressive chemical used in various industries. Standard separation processes, or purification of chlorine, are energy demanding and complicated. This work focuses on the use of glass membranes as an alternative to the existing separation methods. Three families of glass membranes were considered: pure glass tubes (pore diameters (2 – 4 nm), surface modified glass tubes (pore size ~1-2 nm), and glass fibres (pore size < 1 nm). Membrane performance for the gases Cl_2, N_2, O_2 was measured, as well as membrane stability towards chlorine exposure over time. A perfluorinated surface modified glass membrane showed the overall best performance and stability with a selectivity of ~9 for the gas pair Cl_2 – N_2 and a permeance of 3.45 [10^{-9} mol/(m^2 Pa s)]. It was however proved that longer acyl chains for the surface modifying component, will increase separation performance (a selectivity for Cl_2-N = 11 and permeance of 6.86[10^{-9} mol/(m^2 Pa s)] was achieved). Thinner capillary glass tubes of the same kind are available which will increase these permeances by a factor of 17. The selectivity is expected to increase for increased chain length of the perfluorinated compound, as documented in the current work. Hollow glass fibre membranes (not surface modified) are also promising candidates for the chlorine separation. A more detailed discussion of the governing transport mechanisms through the glass membranes is presented in part II of this paper.

Keywords: Glass membranes, permeability, UV-radiation, stability and chlorine gas

Introduction

Aggressive gases refer to chlorine (Cl_2) and hydrogen chloride (HCl) in the current work. Chlorine has the main focus in this paper, but aspects of HCl separation are also discussed. According to Ullmann's encyclopedia of industrial chemistry [1] the

* Corresponding author: *E-mail: may-britt.hagg@chemeng.ntnu.no*

total world wide capacity of chlorine in 1998 was $4.8 \cdot 10^9$ kg annually. It is also stated that in Western Europe, 1995:

- Almost two million jobs were related to chlorine.
- 55% of European chemical turnover depended on chlorine.
- 85% of pharmaceuticals are made using chlorine
- 98% of the drinking water is purified by chlorination
-

These numbers demonstrate the economical importance of the chlorine industry. In this variety of industries there is a great potential for improvement and simplification of the separation processes of chlorine from other gases. In the current work, chlorine – air separation has been studied, as well as (although to a less extent), HCl – hydrogen. The ultimate goal of this work is to incorporate membrane technology in process industry where these gases are in mixtures and need to be separated. The Cl_2 - air is often in a mixture at moderate temperatures (30°C-80°C), while a HCl – H_2 mixture may at times be present after a reactor, hence the temperature can be very high (300°C-400°C). These process conditions indicate clearly the demands that have to be met for a high efficiency, durable membrane material; likewise it indicates that the transport mechanisms which will be governing the two basic separations (Cl_2 – air and HCl – H_2) will be very different. Previously, different membrane materials have been tested for their suitability in the chlorine gas separation. The permeabilities and durability of the materials are reported by Hägg [2, 3 and 4] and Eikeland et al [5]. Based on the findings in these works, the focus was set on glass membranes in order to further optimise the separation properties of this material for the gases in question.

Preparation of the glass membranes

The tubular glass membranes (5 mm OD and 4mm ID) tested in the current work are produced by phase separation of a commercial sodium borosilicate glass (Akagawa Hard Glass, Osaka - Japan). Glass membrane can be produced with diameters as small as 0.2 mm and wall thickness 0.03 mm according to producer. For the current work, the thicker and larger ones were found to be easier to handle. The glass

membrane is formed by phase separation by heating the glass tubes to temperatures over 500°C for several days. When the phase separation is completed, the glass consists of two phases with different compositions; one rich in silica and one in boron. In the subsequent acid leaching, the boron rich phase is removed. The solubility of silica is however limited in the acid, hence the remaining silica in the phase where boron now is leached out, precipitates as colloidal sized particles on the silica rich phase (i.e. on the remaining network) of the glass. The glass / acid ratio is an important parameter which determines the diameter of the colloidal spheres and thereby indirectly the pore size of the membrane. (The membrane pore is the space between the randomly placed colloidal spheres.) If appropriate glass to acid ratio (less than 100 ml acid/g glass) [6] and phase separation temperature is chosen, a glass membrane is obtained with a peak at diameters 2 or 4 nm in the pore size distribution. These pore diameters are too large to achieve any significant separation factors beyond the Knudsen selectivities. In order to optimise the membrane performance, several chemical components of different chain lengths were tested as surface modification agents to tailor the pore size and thus improve separation. This process involves a site-specific reaction with the -OH surface groups inside the pores of the glass membrane [7]. This is shown in figure 1 a and b. For surface modification both organo silane compounds with different chain lengths of the acyl groups as well as a perfluorinated compound were tested. The components with longer acyl lengths will reduce the pore size. When the organo silane compounds are exposed to chlorine, a reaction will take place, and the surface modifying components become chlorinated. The pore size will thus be further reduced with the large chlorine atoms attached to the chain. This can be documented as reduced flux for the permeating chlorine gas. This chlorination reaction may be used as part of the pore tailoring, and is then important to control. If the surface modifying compound is wrongly chosen, the pores may become completely blocked due to this chlorination reaction. It was also tested out if the reaction could be speeded up by exposing the membrane to UV-radiation. The theory is that UV-radiation shorter than a specific wavelength (492 nm, estimated from the chlorine- chlorine bond energy) has the ability to break the chlorine-chlorine bond, hence giving two chlorine radicals (eq.1). The resulting chlorine radicals have a faster reaction rate in the substitution reaction than that of the chlorine gas.

$$Cl_2 + h\nu \rightarrow 2Cl\bullet \quad (1)$$

It has been documented that perfluorinated compounds are very stable towards chlorine [5]. By using such compounds as surface modifying agents, no substitution reaction will occur, and no reduction in flux can be observed.

From what is explained above, it can be understood that tailoring of the pore size for an optimised separation of the gases in question may have different approaches and is quite challenging. To understand and document how this can be done, is the main focus for the research reported in the current article, towards the goal of designing a stable, optimised membrane for the separation and purification of aggressive gases.

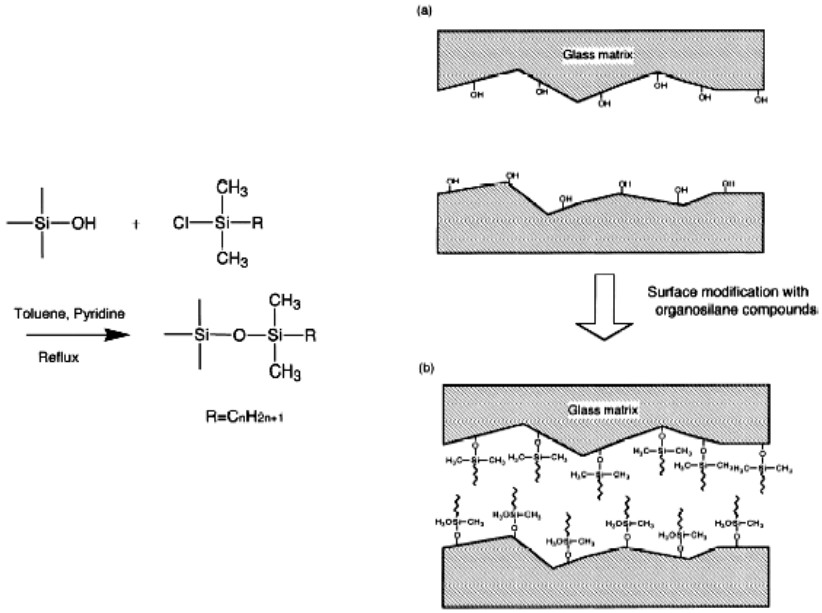

a)

b)

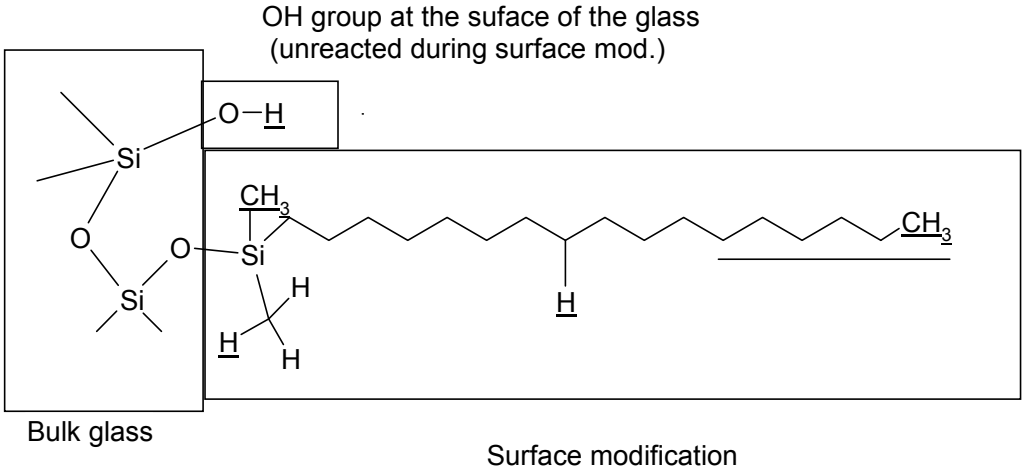

Figure 1: a) Principles of the surface modification. [7]

b) Details of how the surface modifying compound is attached.

Transport mechanisms

Three families of glass membranes were investigated in the current work: pure glass tubes (for reference), surface modified glass tubes and hollow glass fibres. These materials have an average pore size distribution from 4 nm down into the sub-nanometer range, respectively. The average pore diameter for each glass membrane gives an indication of which transport mechanism can be expected to be dominant for the given gas mixture. Figure 2 generalises the dependence of pore size and the transport mechanisms in microporous membranes.

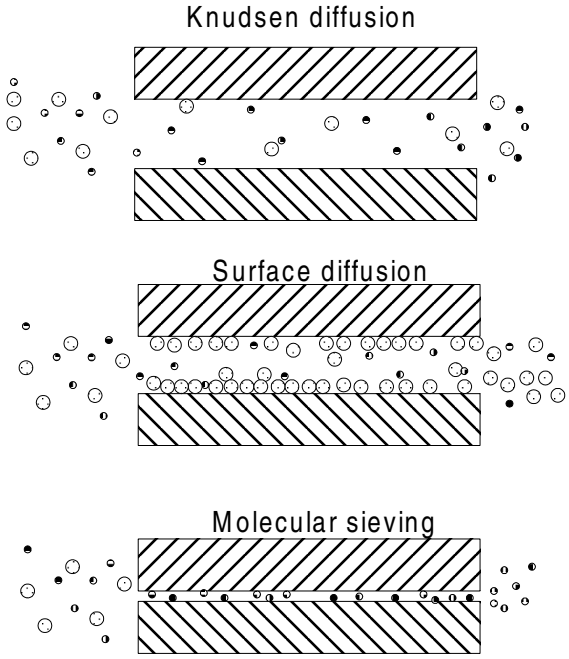

Figure 2: Transport mechanisms in microporous membranes

The mechanisms are briefly characterised as follows:

- Knudsen diffusion; the square root of the ratio of the molecular weights will give the separation factor.
- Selective surface diffusion (or flow, SSF); governed by a selective adsorption of the larger (non-ideal) components on the pore surface. For a mixed gas an increase in selectivity may be observed if the adsorbed monolayer covering the internal pore walls restricts the free pore entrance so that smaller non-adsorbed molecules cannot pass through.

- Molecular sieving; the smallest molecules will permeate, the larger being retained.

The preferred transport mechanisms for the gas separations in question, would be a selective surface diffusion for chlorine when Cl_2-air is considered, and molecular sieving for H_2-HCl. The microporous surface modified glass membranes should thus be suitable for Cl_2-air separation, while the hollow glass fibres with an average pore size < 1nm should be suitable for H_2-HCl separation. This conclusion is based on knowledge of the average pore sizes of the membranes, and on evaluation of the gas properties; see Table 1. The molecular size, shape and critical temperature (T_{crit}) are of special importance as a large non-ideal molecule with high critical temperature will more easily condense in the pore and may be transported according to a selective surface flow. Hence the pore size, process conditions, and physical properties of the relevant gases must be in focus for the optimised membrane separation.

Table 1: Some physical properties for the selected gases [8]

Gas	L-J diameter, σ[Å]	M_A [g/mol]	P_{Crit} [Bar]	T_{Crit} [K]
Cl_2	4.22	70.91	77.1	417
N_2	3.79	28.02	33.9	126.2
O_2	3.47	32.00	50.8	154.8
HCl	3.34	36.49	83.2	324.6
H_2	2.82	2.016	13.0	33.3

Fick's law gives the mass flux through an area perpendicular on the flow direction:

$$J_a = -D_{ab}\frac{dc_a}{dx} \tag{2}$$

where J_a is the mass flux [mol/(m^2 s)], D_{ab} is the diffusion coefficient [m^2/s] and dc_a/dx is the concentration gradient for component a over the length x [mol/(m^3·m)].
Fick's law integrated and applied for a membrane, yields dx = *l* (membrane thickness), and dc_a = concentration difference over the membrane. The $D_{a,b}$ will vary according to which transport mechanism is dominating (as indicated in figure 2).
The permeance P/l for a given gas (a) is defined by:

$$P_a/l = \frac{J_a}{\Delta p_a} \quad (3)$$

Where P/l is the permeance (also referred to as permeability flux) [mol/(m^2 Pa s)] and p_a is the partial pressure difference of component "a" over the membrane [Pa].

Knudsen Flow

Knudsen flow takes place when the mean free path (λ) of the molecules is larger than the pore size. A lower limit for the significance of the Knudsen mechanism has usually been set at $d_p > 20$ Å [9]. The classical Knudsen equation is:

$$D_{Kn,a} = \frac{d_p}{3}\bar{v}_a = \frac{d_p}{3}\sqrt{\frac{8RT}{\pi M_a}} = 48.5 \cdot d_p \sqrt{\frac{T}{M_a}} \quad (4)$$

Where d_p = average pore diameter [m], $\bar{v}_a$ = average molecular velocity [m/s], M_a = molecular weight [g/mol], and T = temperature [K].

However, recent findings of Gilron and Soffer [9] indicate that the Knudsen mechanism can be significant for pore sizes as small as d_p ~5Å. The Knudsen flow in this lower region takes a slightly different form as indicated in equation 5. This equation is derived as transport through a series of constrictions, and using a resistance in series model, hence indicating an activated Knudsen diffusion, $D'_{Kn,a}$:

$$D'_{Kn,a} = \gamma_d d_p \sqrt{\frac{8RT}{\pi M_a}} \exp(-\frac{\Delta E_a}{RT}) \quad (5)$$

where γ_d is the probability that a molecule can make a jump in the right direction given the jump length is d_p and the velocity is $\bar{v}_a$. In the current work, permeance measurements were performed at different temperatures for the membrane with the most narrow pore size (≤ 1 nm) in order to check if the inert gases were transported according to classical or activated Knudsen diffusion. Helium was used as a reference gas - this is further discussed in the results.

Surface diffusion

The mechanism of surface diffusion is disputed and several different approaches have been proposed in the literature. Theories are ranging from viewing the surface diffusion at low surface coverage of adsorbed gas as a 2D gas, through a hopping

model and further to a model where the adsorbed gas condenses into a liquid like "sliding layer". Which of the mechanisms is dominating, will be influenced by a number of factors such as: homogeneity of the surface, the temperature vs. the adsorption enthalpy and the surface concentration, c_s.[10]. All three regimes may be important to consider as well as pore size, pore structure and surface coverage. The three regimes can be described by a 2D analogue of Fick's law (equation 2, given for a single component, a). The flux, J_a, is then evaluated as molecules crossing a hypothetical line in the surface perpendicular to the direction x. The surface diffusion coefficient is then denoted D_s and dc_s/dx the surface concentration gradient in x-direction. When separation is strongly influenced by surface diffusion, it is called selective surface flow (SSF). This will often be the situation when large non-ideal gases are present in a gas mixture. Further details on the three regimes of surface diffusion are discussed in Article II of the current work; "Adsorption measurements and diffusion coefficient estimations."

Molecular Sieving

Molecular sieving is the dominating transport mechanism when the pore size is comparable to the molecular dimensions, 3-5 Å. For the glass membranes investigated, this would mean the hollow fibres. The dimensions of a molecule are usually described with either the Lennard-Jones radii (Table 1) or the Van der Waal radii. A shape factor should also be included [11].

The sorption selectivity has little influence on the separation when molecular sieving is considered. An Arrhenius type of equation is still valid for the activated transport, but attention should be drawn to the pre-exponential term, D_0. From the transition state theory this factor may be expressed as shown in equation 6 [12]:

$$D_0 = e\lambda^2 \frac{kT}{h} \exp\left(\frac{S_{a,d}}{R}\right) \tag{6}$$

Where k and h are Boltzmann's and Planck's constants, respectively; $S_{a,d}$ is the activation entropy for diffusion. A change in entropy will thus have a significant effect on the selectivity when molecular sieving is considered. This is thoroughly discussed by Singh and Koros [11]. The flux may be described as in equation 7 where $E_{a,MS}$ is the activation energy for diffusion in the molecular sieving media.

$$J_a = \frac{\Delta p}{RT \cdot l} D_0 \cdot \exp\left(\frac{-E_{a,MS}}{RT}\right) \quad (7)$$

The selectivity for separation will increase with increasing temperature because of increased diffusion rate for permeating component, while the larger ones are being retained.

Experimental

Permeance measurements.

The glass membranes were glued (using Araldite® AV138M) into a Pyrex® glass tube (8 mm OD, 5 or 6 mm ID). The Pyrex tube was then connected to the module with a Swagelok® 8mm union and the module closed using a dismantle-able glass slit coupling on the top of the module. The feed pressure could be varied between 1 to 5 bars, and was monitored by a MKS 121AA (5000 mbar) pressure transducer. The permeance was measured as pressure increase with a MKS Baratron 626 (100 mbar) pressure transducer on the vacuum side of the membrane. The closed set-up made it easy to keep track of the poisonous gases (Cl_2, HCl) at all times.

Detailed measurements of adsorption and diffusion coefficients were also performed; these results are presented and discussed in detail in Article II of the current work.

Durability of membranes

For measuring the durability of the glass membranes, they were exposed to pure chlorine gas over various length of time. The membranes were placed in a closed temperature regulated glass chamber which was filled with pure chlorine gas. The temperature was kept at 30 °C and pressure at 1 bar. The change in membrane properties was measured as change in flux before and after exposure. The chamber had the possibility of combining UV radiation with chlorine exposure of the membrane.

Results and discussion

Pure glass membranes (tubes and a hollow fibre) and glass membranes surface modified with different acyl-trichlorosilane, were investigated for their chlorine gas separation performance and stability. Different surface modifying components were

investigated for their ability to tailor the pores of the membrane (reduce the pore diameter to < 1 nm), and their stability towards the aggressive gases Cl_2 and HCl. To evaluate the performance (flux and selectivity) and the stability of the material towards chlorine gas, permeance was measured before and after varying exposure times.

Separation performance of the membranes

The economic potential for membrane application in the industry is closely related to the stability of the materials and required membrane area. The required area is a consequence of the trade-off between selectivity and permeance for a given material. If the permeance of one gas is plotted vs. the selectivity of a corresponding gas pair, the materials with the highest selectivity and permeance simultaneously, will cluster in the upper right corner of the diagram. This would be the best membrane judged by performance alone. This type of plot is often referred to as Robeson plot [13]. Figure 3 shows such a trade-off curve for all the glass membranes tested in the current work: tubes with or without surface modification and hollow fibres, with chlorine / nitrogen selectivity given as function of permeance [mol/(m^2 Pa s)]. It should be remembered that the glass membranes measured are tubes with an outer diameter OD = 5 mm, and wall thickness 0.5 mm. According to producer, the membranes can be delivered as tubes with diameter 0.2 mm and wall thickness 0.03 mm. With reference to the results reported here, this means an increase in performance times 17. For an industrial scale membrane module, the thinner capillary glass tubes with the higher performance will most likely be used.

The pure glass tubes had two different average pore sizes of 4 nm (here referred to as “Glass 1”) and 2 nm (here referred to as “Glass 2”) respectively. For the surface modified glass membranes the notation C1, C8, C12 and C18 refers to the chain length of the acyl part in the surface modifying compound (the R-group as shown in figure 1a). "Pf"-as a prescript indicates that the chain is perfluorinated. C1+C18 refers to a membrane that was first modified with C18 and subsequently with C1. Most of the surface modified glass membranes tested were based on “Glass 1” (4 nm average pore size). In figures 3 and 5 the surface modified glasses are identified with the alias names as explained here. (For conversion of permeance given as [mol/(m^2 Pa s)] to [m^3(STP)/(m^2 bar h)], multiply with $7.937 \cdot 10^6$)

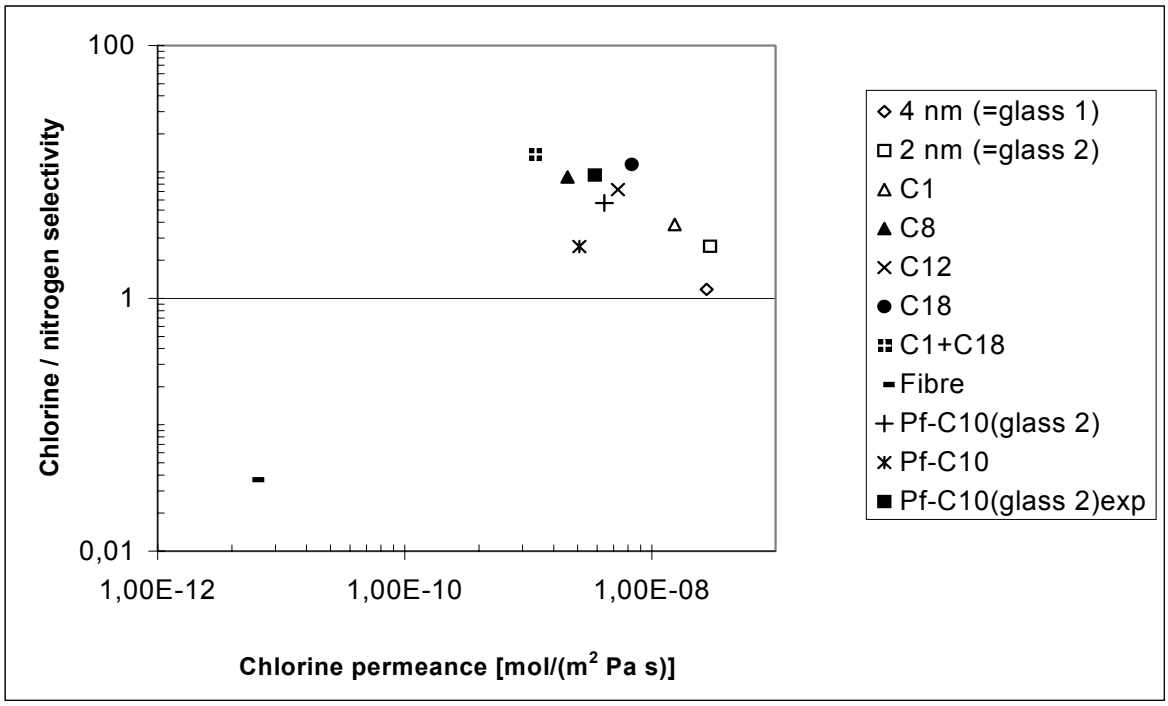

Figure 3: Selectivity of Cl_2/N_2 vs. chlorine permeance mol/(m^2 Pa s) for various glass membranes. The symbols identify different modifying components used for pore tailoring (see text). Pure gases, measured at 30 °C and 1 Bar

Figure 3 demonstrates that the fibres separate the gas mixture according to a different transport mechanism than the other membranes, showing a selectivity of $\alpha_{Cl2/N2}$ = 0.037 (lower left corner). The fibres were expected to separate according to a molecular sieving mechanism. This is consistent with the observed separation factor being below the theoretical Knudsen selectivity for the chlorine/nitrogen pair ($\alpha_{Kn,Cl2/N2}$ = 0.63); i.e. the smallest molecule, N_2, is permeating faster than the larger Cl_2 (see Table 1). For all the other surface modified membranes chlorine is the fastest permeating component (consistent with a selective surface flow, SSF mechanism as explained in the section on transport mechanism).

With reference to figure 3 it can be seen that the membranes modified with the longer acyl chains (C8 to C18) show the highest selectivities (~ 11 for C18). The permeance of chlorine is 6.86 [10^{-9} mol/(m^2 Pa s)] and a selectivity equal to 11. This would mean 116 [10^{-9} mol/(m^2 Pa s)] for a 0.2 mm diameter glass tube with wall thickness 0.03 mm. Also the perfluorinated Pf-C10 (Glass 2) should be noted, having a selectivity

of ~ 6 and a chlorine permeance of 4.13 [10^{-9} mol/(m^2 Pa s)]. The separation performance for the Pf-C10(Glass 2), is improved after chlorine exposure (9 weeks at 30°C and 1 bar), and the new test results are indicated as "Pf-C10(Glass 2)exp." in figure 3. The exposed Pf-C10(Glass 2) now has a selectivity of ~ 9 and a chlorine permeance of 3.45 [10^{-9} mol/(m^2 Pa s)]; hence the exposure has had a positive effect. This is believed to be caused by a more efficient selective surface diffusion of chlorine after exposure due to minor changes in the pore modification.

The chlorine permeances for the pure glasses (glass 1 and 2) are high, 27.7 and 29.6 [10^{-9} mol/(m^2 Pa s))], respectively, with corresponding selectivities of 1.2 and 2.6. Although the chlorine permeance is high, the selectivity is too low for these pure glasses to be of interest. The other materials fall somewhere between the two extremes described here.

For the C18 membrane, (the membrane with the most narrow pores) additional tests were performed within the temperature range (30°C-70°C). This was done to investigate how the inert gases in the mixture most likely were transported through the membrane. The mechanism would obviously be according to Knudsen diffusion, but it was not clear whether or not it would be a classical (eq. 4) or an activated (eq. 5) Knudsen mechanism. If this could be answered, temperature dependence of the separation could more easily be predicted.

Based on Fick's law (eq.2), flux equations for the two types of Knudsen diffusion could be derived. Integrating over the membrane thickness and substituting the ideal gas law for the concentrations, yield:

$$J_a = \frac{D_{a,(Knudsen)}}{RTl}\Delta p_a \qquad (8)$$

where $D_{a(Knudsen)}$ is the Knudsen diffusion coefficients [m^2/s] according to equations 4 or 5.

If the classical Knudsen diffusion equation (eq.4) is substituted into equation 8, the following temperature dependence for the permeance may be derived (eq.9):

$$J_a = \frac{48.5 \cdot d_p \sqrt{\frac{T}{M_a}}}{RTl} \Delta p_a = \frac{48.5 \cdot \Delta p_a \cdot d_p}{Rl \cdot \sqrt{M_a}} \cdot \frac{\sqrt{T}}{T} \Leftrightarrow \quad (9)$$

$$J_a = K_{Kn} \cdot \sqrt{\frac{1}{T}}$$

Thus, if the permeance is plotted as a function √1/T, a straight line with the slope K_{Kn} (collective term for the constants) should be obtained and the line should pass through origo.

For activated Knudsen diffusion, equation 5 is substituted into equation 8, and the following temperature dependence for the permeance is derived (eq.10):

$$J_a = \frac{\gamma d_p \sqrt{\frac{8RT}{\pi M_a}} \exp(-\frac{\Delta E_a}{RT})}{RTl} \Delta p_a = \frac{\Delta p_a \gamma d_p \sqrt{8R}}{R \cdot l \sqrt{\pi M_a}} \cdot \frac{\sqrt{T} \cdot \exp(-\frac{\Delta E_a}{RT})}{T} \Leftrightarrow \quad (10)$$

$$J_a = K_K \cdot \frac{1}{\sqrt{T}} \cdot \exp(-\frac{\Delta E_a}{RT}) \Leftrightarrow \ln(\sqrt{T} \cdot J_a) = -\frac{\Delta E_a}{R} \frac{1}{T} + \ln(K_K)$$

Thus, if activated Knudsen is obeyed, then a plot of ln(√T·permeance) versus the reciprocal temperature (1/T) should yield a straight line with a slope equal to -ΔEa/R and a constant (the crossing point of the line with the y-axis) equal to ln(K_K).

Helium gas was used as a reference for the inert gases, and helium permeance data was obtained as function of temperature. These permeance data were least-square fitted according to both the classical and activated Knudsen regime in the C18 membrane as shown in figure 4.

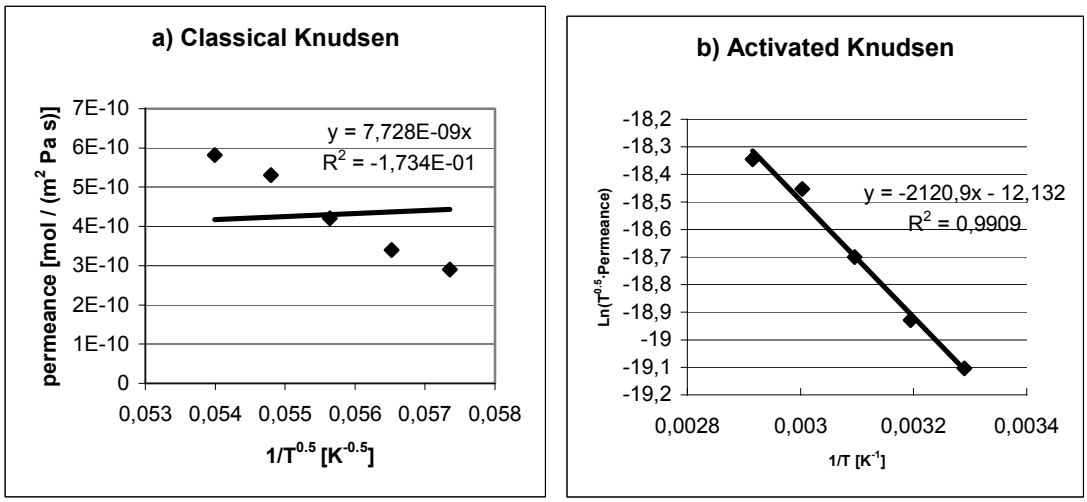

Figure 4: Fitting of the helium experimental permeances as function of reciprocal temperatures (1/T) to a) classical- and b) activated Knudsen flow.

It is obvious from the regression coefficients in figure 4 that the fit of the experimental permeances to the activated Knudsen mechanism is perfect (R^2=0.99). This means that the helium transport in the C18 modified glass membrane (d_p ~ 1nm) is according to the activated Knudsen mechanism. Depending on the pore size and molecular size, other inert gases (here N_2 and H_2 are considered) may also be transported according to an activated Knudsen diffusion. This knowledge is useful for evaluation of the separations in question ($Cl_2 – N_2$, $HCl – H_2$).

Separation results compared to the goal

With reference to previously documented chlorine separation results [3-6], the goal for performance of an industrial membrane was set to ~ 170 [10^{-9} mol/(m^2 Pa s)] with a selectivity Cl_2/O_2 of about 20, a goal which seems to be within reach. The best results achieved in the current work are with a C18 surface modified glass membrane; wall thickness 0.5 mm; with Cl_2 flux = 6.86 [10^{-9} mol/(m^2 Pa s)] and selectivity for Cl_2/N_2 = 11. Replacing the measured glass tube (diameter outer diameter of 5 mm, wall thickness of 0.5) with one of diameter 0.2 mm and wall thickness 0.03 mm (which can be supplied according to producer), the permeance will increase by a factor of 17, and a permeance of 116 [10^{-9} mol/(m^2 Pa s)] is achieved. In order to increase the flux and selectivity, further investigations are needed for pore tailoring. The road to follow for an optimised separation, seems however to be clear: A perfluorinated compound with longer (and more branched) chain, will be tried out as surface modifying component. An increase in selectivity and permeability is then expected (moving towards the upper right corner in figure 5). It should be noted that the goal for selectivity was set for chlorine with respect to oxygen, which will in any case be higher than for chlorine versus nitrogen.

A more comprehensive study of the adsorption and transport mechanisms through these glass membranes is presented in part II of this paper.

Stability towards chlorine exposure

In addition to good separation properties, the durability of the membrane towards chlorine exposure is vital. For durability measurements, a gas tight glass chamber

was used. From previous research it has been documented that the flux decreases to various extent when the surface modified membranes are exposed to chlorine [2-4]; this can be documented by measuring the nitrogen flux before and after exposure, as indicated in table 2. Table 2 is showing the permeability decay (PD) over time (equation 11); this is also plotted in figure 5. The nitrogen permeability decay [-] is calculated according to equation 11:

$$PD = \frac{\frac{P_{N_2,Before\ Cl2\_exposure}}{l} - \frac{P_{N_2,after\ Cl2\_exposure}}{l}}{\frac{P_{N_2,Before\ Cl2\_exposure}}{l}} \qquad (11)$$

where $(P/l)_{N2}$ is the permeance of nitrogen [10^{-9} mol/(m^2 Pa s)] measured at 30°C and 1 bar before and after chlorine exposure respectively.

Table 2: Nitrogen permeability decay (PD) as function of chlorine exposure time in glass membranes with or without surface modification

Type of glass membrane	Cl_2 Exposure time, t	PD/ t $[s^{-1}]\cdot 10^5$
Pure Glass 1 (4nm)	1.3 hour	2.4
Pure Glass 2 (2nm)	1 hour	-0.74
Glass fibre (~1nm)	26 hours	0.48
Glass 1 + C1	1 hour	3.2
Glass 1 + C12	5 hours	5.5
Glass 1 + C18	0.75 hour	8.0
Glass 1 + C18	14 days	0.080
Glass 1 + (C1+C18)	5.3 hours	3.10
Glass 1 + (C1+C18)	5 days	0.13
Glass 1 + Pf-C10	42 days	0.0026
Glass 2 + Pf-C10	63 days	0.0036

C1 to C18 is an abbreviation for the acyl length of the surface modifying silane used

Pf as a prescript indicates that the compound in perfluorinated.

It is quite obvious from these results that the perfluorinated compounds are very stable as they hardly show any decay. It was also documented that the original

permeance could be completely restored by regeneration with nitrogen at higher temperature when perfluorinated compounds were used for surface modification. This was also found to be true for the pure unmodified glasses (glass 1 and 2). The difference between performing regeneration or not for the pure glasses is illustrated in table 2: The negative value for the decay of the pure "Glass 2", Table 2, is explained by the fact that this particular membrane was exposed to higher temperature with nitrogen regeneration before the reported measurements in the table. Hence, the glass membrane was very efficiently regenerated, and the permeability for nitrogen actually increased after the treatment; a negative PD value was registered. Regeneration was not performed with "Glass 1" or the fibre, hence a decay is registered – some chlorine is most likely strongly adsorbed on the pore wall, and restricts the nitrogen permeance. None of the acyl surface modified membranes regained performance after regeneration, here permanent changes due to chlorination had obviously occurred. Details in table 2 are depicted in figure 5 for the surface modified glasses. Figure 5 illustrates that the decay in permeance is slowing down with increased chlorine exposure time. This is according to what should be expected as the reaction goes towards complete chlorination of the surface modifying agents (see Introduction). In figure 5 the most stable membranes are the ones closest to the bottom right corner.

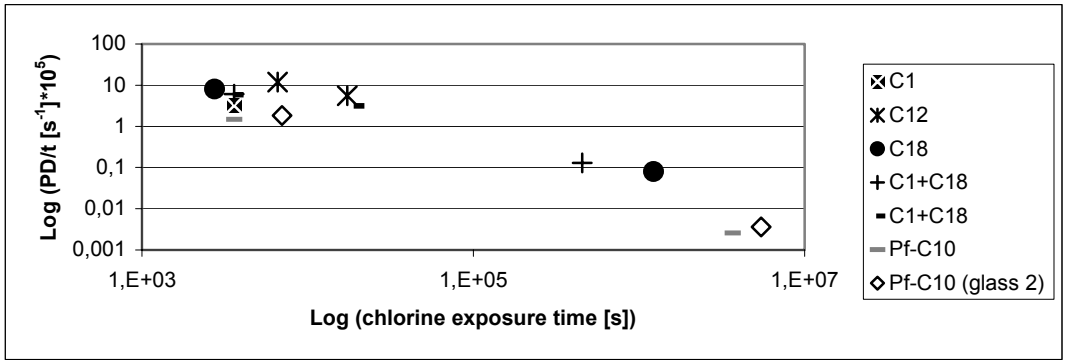

Figure 5: The average permeability decay for nitrogen after chlorine exposure as a function of the exposure time.

As can be seen from table 2 or figure 5, the C18 modified glass membrane is unstable towards chlorine exposure. Even after prolonged chlorine exposure tests the permeability decay is still significant. A combination of UV radiation and chlorine

gas exposure was tested both for C1 and C18 modified membranes as a method of speeding up the chlorination reaction, and make the membranes stable much faster - results are reported in table 3.

Comparing with the decay in table 2, the following may be observed: Chlorination of membrane with C1 is slightly slowed down, but the chlorination of the C1 component is not enough to block the pore and only minor changes in the perm-selectivity is observed from 1 – 6 hours exposure. For glass membranes modified with C18 it seems like the chlorination works in two steps: The short UV exposure (10 minutes) causes some of the surface modifying compound to be chlorinated, and it is believed that these chlorinated points act like "anchors" (obstacles) for the surface flow layer, thus effectively stopping the SSF contribution to the total transport. The permeance for chlorine goes down while nitrogen more efficiently goes through, and a negative decay (-1.84) is registered together with a major decrease in selectivity (1.3). As the reaction time is increased, the chlorination will effectively clog the pores, and thus decreasing the Knudsen flow contribution to the total transport. This is seen as a very low chlorine permeance and large permeability decay, simultaneously.

Although not yet exclusively proven, a chlorination substitution reaction of the hydrogen (or the end-methyl group) in the C18 surface modification, is believed to take place during the chlorine exposure. (Examples of different types of attack points for the chlorine substitution are indicated as underlined atoms or groups in figure 1b).

Table 3: Results of the combined chlorine and UV-exposures.

Modification	Reaction time	PD/t $[s^{-1}]\cdot 10^{-5}$	Chlorine permeance * $[10^{-9}$ mol/(m^2 Pa s)]	Selectivity Cl_2/N_2 (after reaction)
C18	6 hours	2.23	0.00760	0.27
C18 (Low surface coverage)	6 hours	4.20	0.000621	0.005
C18	10 minutes	-1.84	0.038	1.3
C1	1 hour	0.93	8.58	2.7
C1	6 hours	0.77	7.64	2.9

* The chlorine permeance is evaluated at the end of the combined UV- and chlorine exposure, after the UV – source was turned off.

C1 to C18 is an abbreviation for the acyl length of the surface modifying silane used

Some data on HCl-H_2 separation

For comparison, three glass membranes (C18, Pf-C10(Glass 2) and fibre) were also tested for the gas pair HCl –H_2. The initial pure gas permeabilities were measured and durability tests performed (see table 4 for results). For the C18 and Pf-C10(glass 2) it was assumed that HCl would permeate according to selective surface flow, and H_2 according to Knudsen diffusion. HCl is a significantly smaller molecule than Cl_2 (table1), and will not to the same extent be able to prevent the very small H_2 molecule from permeating. The fibres were expected to be separating according to a molecular sieving mechanism. The resulting selectivities are low, and being in favour of H_2 both in the Pf-C10(glass 2) and the fibre ($\alpha_{H2/HCl} \sim 1.4$ and 42 respectively), while the C18 membrane is HCl selective ($\alpha_{HCl/H2} = 5.9$). The pores in Pf-C10(glass2) are obviously too large for a separation in favour of HCl.

As table 4 indicates only initial exposure tests were performed on the Pf-C10 (glass 2). However, it is quite clear that the perfluorinated compound and the glass fibres

are stable, while the C18 is showing decay when exposed to yet another aggressive gas. A perfluorinated surface modification compound with longer chain, would be expected to show better performance. With respect to the registered negative permeation decay for PF-C10 (glass 2) shown in table 4, this membrane was regenerated after exposure and before last measurements, hence a negative value is obtained. As discussed for pure glass (table 2), permeance may easily be recovered for the perfluorinated membranes by regeneration. Small changes in permeance are believed to be caused by some sorption of molecules to the pore walls which can easily be removed. The fibres were not regenerated, and are showing a small decay.

Table 4: Permeability, selectivity and stability measurements in glass membranes for HCl – H_2 separation

Membrane type	HCl permeance $[10^{-9}$ mol /(m^2 Pa s)]·	H_2/HCl selectivity	PD/t $[s^{-1}]\cdot 10^{5}$ §
C18	2.82	0.17	4.3
Pf-C10 (glass 2)	1.85	1.4	-0.63*
Fibre	0.00753#	> 42	0.16

* This membrane was regenerated after exposure

§ According to eq. 11

This membrane is clearly HCl retaining and the measured permeance is at the detection limit of the permeance cabinet, this means that the reversed selectivity (H_2/ HCl) is most likely higher than reported here (42)

Conclusion

The Pf-C10 modified membrane has so far been documented to show the best performance; all aspects considered. A perfluorinated surface modifying compound with longer (branched) chain, is expected to increase the performance (Cl_2 flux and selectivity). The highest obtained chlorine flux with the tubular C18 surface modified glass membrane (diameter 5mm, wall thickness 0.5mm) was 6.86 [10^{-9} mol/(m^2 Pa s)], and Cl_2/N_2 selectivity 11. Diameter and thickness can according to the producer be reduced to 0.2 mm inner diameter and a wall thickness of 0.03 mm. This will increase the flux about 17 times compared to the values reported, and hence reduce

required membrane area significantly. Somewhat lower flux and selectivity was obtained for the stable perfluorinated (Pf-C10) membrane. This compound has however shorter acyl length, thus the results are in agreement with what could be expected. Comparing with the goals set for an industrial membrane (flux 170 [10^{-9} mol/(m^2 Pa s)] and Cl_2/O_2 selectivity 20), the goals are judged to be within reach.
The fibres are not yet sufficiently tested for long term stability, but they are very interesting candidates for chlorine / air separation due to their potential for molecular sieving separation. The greatest advantage of the fibres would be the very high packing density (membrane area / module volume). Pure gas permeance measurements using the fibres in the HCl-H_2 separation indicate a selectivity of in favour of H_2 which is considered to be rather low. Pore tailoring of the microporous glass membrane by using longer chain perfluorinated compounds may increase selectivity and flux in favour of H_2.

Acknowledgement

The authors want to thank Professor T. Yazawa at Himeji Institute of Technology, Himeji, Japan and Dr. K. Kuraoka at the Faculty of Maritime Sciences at the Kobe University, Kobe, Japan for preparing the various glass membranes and fibres.

References

1. Ullmann's Encyclopedia of Industrial Chemistry, Chlorine, Vol. 8, 6.ed. Wiley-VCH, 2000, 265-270.

2. M.-B. Hägg, Purification of chlorine gas with membranes- an integrated process solution for magnesium production, Sep.& Purif. Tech., 21, (2001), 261-278.

3. M.-B. Hägg, Membrane Purification of Cl_2 Gas I. Permeabilities as a Function of Temperature for Cl_2, O_2 N_2, H_2 in Two Types of PDMS Membranes, J. Membrane Sci., 170, (2000), 173-190.

4. M.-B. Hägg, Membrane Purification of Cl_2 Gas II. Permeabilities as a Function of Temperature for Cl_2, O_2 N_2, H_2 and HCl in Perfluorinated, Glass and Carbon Molecular Sieve Membranes, J. Membrane Sci.,177, (2000), 109-128.

5. M. S. Eikeland et al., Durability of Poly(dimethylsiloxane) When Exposed to Chlorine Gas, J. of Applied Polymer Sci., vol. 85, (2002), 2458-2470

6. H. Tanka, et al., Precipitation of colloidal silica and pore size distribution in high silica porous glass, Journal of non-Crystalline Solids, 65, (1984), pp301-309.

7. K. Kuraoka, Y. Chujo, T. Yazawa, Hydrocarbon separation via porous glass membranes surface- modified using organosilane compounds, J. Membrane Sci., 182, (2001), 139-149.

8. R.C. Reid et al., The Properties of Gases and Liquids, 4th Edition, McGraw-Hill, New York, 1987.

9. J. Gilron and A. Soffer, Knudsen Diffusion in Microporous Carbon Membranes with Molecular Sieving Character, J. Membrane Sci., Vol.209, (2002), 339-352.

10. E. R. Gilliland et al. Effect of concentration on the diffusivity of physically adsorbed gases, Ind. Eng. Chem. Fundam., Vol.13 no.2, (1974), 95-100.

11. A. Singh and W.J. Koros, Significance of Entropic Selectivity for Advanced Gas Separation Membranes, Ind. Eng. Chem. Res., 35, (1996), 1231-1234.

12. S. Glasstone, K.J. Laidler and H. Eyring, The Theory of Rate Processes, 1st Edition, McGraw-Hill Book Co., Inc. New York, NY, 1941.

13. L. M. Robeson, Correlation of Separation Factor versus Permeability for Polymer membranes, J. Membrane Sci.,62, (1991), 165-185.

Appendix 2 Reprint of article no.2

Glass membranes for purification of aggressive gases. Part II: Adsorption measurements and Diffusion coefficient estimations.

Arne Lindbråthen and May-Britt Hägg*

Norwegian University of Science and Technology, NTNU

Department of Chemical Engineering

N-7491 Trondheim, Norway.

Abstract

In the article part I of this work durability and separation properties for several types of glass membranes in aggressive gas environment have been evaluated. A surface modified glass membrane (modified with (Heptadecafluoro-1,1,2,2-tetrahydrodecyl) dimethyl chlorosilane, Pf-C10), proved to be the best choice with respect to stability, permeability and selectivity. For a better understanding of the gas separation taking place according to the governing mechanism, selective surface flow, the sorption and diffusion coefficients were investigated more closely. This is reported in the current paper for the gases Cl_2, HCl, R22 (CHF_2Cl), He, H_2, N_2, CO, O_2, Xe, SF_6 and CO_2. Temperature and pressure range focused on were 1 – 4 bar and 30°C–45°C respectively, as these ranges were judged to be most interesting with respect to possible changes in the transport through the Pt-C10 surface modified glass membrane. The degree of selective surface flow, SSF, relative to the Knudsen flow is also discussed in this work. When plotting the sorption coefficient vs. degree of SSF, there seems to be two distinct patterns: The Cl_2, HCl and R22 (all containing chlorine and have high critical temperatures) are described by exceptionally high sorption coefficients, while the other gases are best described by an exponential fit. The heat of adsorption for Cl_2 and HCl was found to be comparable to the heat of condensation at the same pressure. It was assumed that the adsorption of these gases corresponds to the proposed "sliding liquid layer" flow described in literature, while the exponential behaviour of the other gases correspond to the "site to site hopping" or 2-D gas flow.

Keywords: Glass membrane; Adsorption; Cl_2; HCl; Surface diffusion.

*Corresponding author: *E-mail: may-britt.hagg@chemeng.ntnu.no*

Introduction

In the current work, aggressive gases refer to chlorine (Cl_2) and hydrogen chloride (HCl). As chlorine is an important chemical within very many industrial processes, it would be of great interest to develop a high performance, durable membrane for chlorine gas separation. This has also been the focus over many years for the research performed in Norway by Hägg et al. [1-3]. Based on the reported findings, the most stable membrane material was found to be glass membranes, surface modified with perfluorinated compounds. The optimisation of separation properties by pore tailoring of the glass membranes is reported in Part I of this article [4]. A thorough understanding of the transport mechanisms governing the separation of Cl_2 and HCl in mixtures with more inert gases, were judged to be crucial for an optimised pore tailoring of the surface modified glass membranes – details around the transport mechanisms are therefore discussed in the current paper. Chlorine has the main focus in both articles, but aspects of the HCl separation are also discussed. A perfluorinated (Pf-C10) surface modified glass membrane is investigated in detail for the transport mechanisms. Pf-C10 is used as an acronym for the surface modifying compound (Heptadecafluoro-1,1,2,2-tetrahydrodecyl) dimethyl chlorosilane. Adsorption measurements have been performed, and diffusion coefficients estimated for the gases Cl_2, HCl, R22 (CHF_2Cl), He, H_2, N_2, CO, O_2, Xe, SF_6 and CO_2 in the membrane.

Transport mechanisms

Three families of glass membranes were investigated in the current work: pure glass tubes, surface modified glass tubes and a hollow glass fibre; all of them reported for separation properties and durability in Part I of the article [4]. Only the most favourable perfluorinated (Pf-C10) surface modified glass membrane was investigated with respect to governing transport mechanisms; results are reported in the current article. This glass membrane has an average pore size distribution 1 nm when it is surface modified (based on a pure glass membrane with pore size ~2nm). The average pore distribution is important since it gives an indication of which transport mechanism can be expected to be dominant for the gas mixture. The most probable transport mechanisms in our glass membranes were thus Knudsen diffusion

and/or selective surface diffusion. These mechanisms are briefly characterised as follows:

- Knudsen diffusion; the square root of the ratio of the molecular weights will give the separation factor.

- Selective surface diffusion (or flow; SSF); governed by a selective adsorption of the larger (non-ideal) components on the pore surface. For a mixed gas an additional increase in selectivity may be achieved if the adsorbed monolayer covering the internal pore walls restricts the free pore so the smaller non-adsorbed molecules cannot pass through.

The Knudsen diffusion is discussed in detail in part I and will not be covered here [4]. The various theories of surface diffusion are however of major interest, and are therefore also the focus for the current article. When process parameters like pressure and temperature are varying, a transition region may be observed between Knudsen flow and surface diffusion; hence a major change in separation properties may result.

Surface diffusion

The mechanism of surface diffusion is disputed and several different approaches have been proposed in the literature. Theories ranging from viewing the low surface coverage adsorbed gas as a 2D gas, through a hopping model into a more "liquid like" sliding layer theory exists. Which of the mechanism that is dominating the surface diffusion coefficient will be influenced by a number of factors, such as homogeneity of the surface, the temperature vs. the adsorption enthalpy and the surface concentration, c_s.[5].

All three regimes can be described by a 2D analogue of Fick's law (given here for a single component):

$$J_{x,s} = -D_s \frac{dc_s}{dx} \tag{1}$$

Where $J_{x,s}$= is the flux (evaluated as molecules crossing a hypothetical line in the surface perpendicular to the direction x) [mol/(m s)], D_s is the surface diffusion coefficient [m^2/s] and dc_s/dx is the surface concentration gradient in the x-direction [mol /(m^2·m)].

The following expression may be used to determine if the surface transport is dominated by the 2D-gas model:

$$q / RT < 1 / a \tag{2}$$

Where q is the adsorption enthalpy [J/mol] and a is an energy fraction factor. The factor a can be interpreted as the fraction of the adsorption energy required to loosen a molecule from its adsorption site. The energy barrier for surface migration, E, is then defined as:

$$E = a\,q \tag{3}$$

The 2D-gas is characterised by a surface mean free path (or interparticle distance), λ_s, inversely proportional to the surface concentration, c_s, and this λ_s value can be much larger than the spacing between adjacent surface sites.

If the q/RT part of eq. (3.7) is increased then λ_s will no longer be controlled by collisions between adsorbed molecules. As q/RT increases, λ_s decreases and approaches the spacing between adjacent sites, and a hopping mechanism is observed. If the c_s is low then a random walk diffusion of independent molecules can be expected and the D_s will be given as:

$$D_s = \frac{1}{4}\nu\lambda_s^2 \tag{4}$$

Where ν is a jump frequency factor (This factor has a temperature dependence according to Arrhenius law, $\nu=\nu_0 \cdot \exp(-aq/(RT))$ [1/s]).

When c_s is increased the chance of a molecule hitting another molecule increases and this interaction will bear some similarity to diffusion in liquid. Thus, the region of the sliding layer prevails. In this region the gas is condensed into a thin 2D liquid layer on the surface and the property of this layer approach those found in the corresponding "3D liquid".

The size and critical temperature of the gases in the mixture is a measure of how easily they condense on the pore wall and they can diffuse through the membrane according to a selective surface flow mechanism. For reference on the data for gases examined, please refer to Table 1

Table1: Some physical properties for the gases tested [6,7]

Gas	L-J diameter,σ [Å]	M_A [g/mol]	P_{Crit} [Bar]	T_{Crit} [K]
Cl_2	4.22	70.9	77.1	417
R22	-	86.5	49.7	396
HCl	3.34	36.5	83.2	325
SF_6	5.13	146	37.6	318
CO_2	3.94	44.0	73.8	304
Xe	4.04	131	58.8	290
CO	3.69	28.0	35.0	133
O_2	3.47	32.0	50.8	155
N_2	3.79	28.0	33.9	126
H_2	2.82	2.02	13.0	33.3
He	2.55	4.00		5.30

Combined mass transfer

The process conditions for separation (pressure, temperature) as well as membrane pore size, and physical properties of the gases may influence which flow regime is governing the gas separation. It is assumed that the selective surface flow (SSF) and the Knudsen flow are additive in the glass membrane. Using helium as a reference and assuming that helium is solely transported by Knudsen flow, hence the following expression may be derived:

$$\alpha_{Tot,i,He} = \frac{J_{Tot,i}}{J_{Tot,He}} = \frac{J_{Kn,i} + J_{ssf,i}}{J_{Kn,He}} = \alpha_{kn,i,He} + \frac{J_{ssf,i}}{J_{Kn,He}} \Leftrightarrow$$
$$1 - \frac{\alpha_{Kn,i,He}}{\alpha_{Tot,i,He}} = \frac{J_{ssf,i}}{J_{Tot,i}} \quad (5)$$

where J is the flux [mol/(m^2 s)], $\alpha_{Kn,i,j}$ is the selectivity based on the Knudsen flow [-] and $\alpha_{Tot,i,j}$ is the total selectivity [-]. From the general Knudsen transport mechanism theory the $\alpha_{Kn,i,j}$ is given as the square root of the inverse ratio of the molecular weights. This means that based on the assumptions above, an expression can be derived for the degree of contribution from SSF to the overall transport:

$$\psi_i = 1 - \frac{2 \bullet \sqrt{1/M_i}}{\alpha_{tot,i/He}} \quad (6)$$

Where ψ is the degree of SSF which is equal to $J_{SSF,i}/J_{Tot,i}$ [-] and M_i is the molar mass of the gas *i* [g/mol].

Experimental

Permeance measurements.

A closed experimental set-up for measurements of the poisonous and aggressive gases was used. Permeance was measured as pressure increase on the permeate side of the membrane. These measurements are described in detail in Part I of the paper.

Adsorption measurements

The adsorption tests were performed in a single chamber (volumetric) set-up as indicated in figure 1.

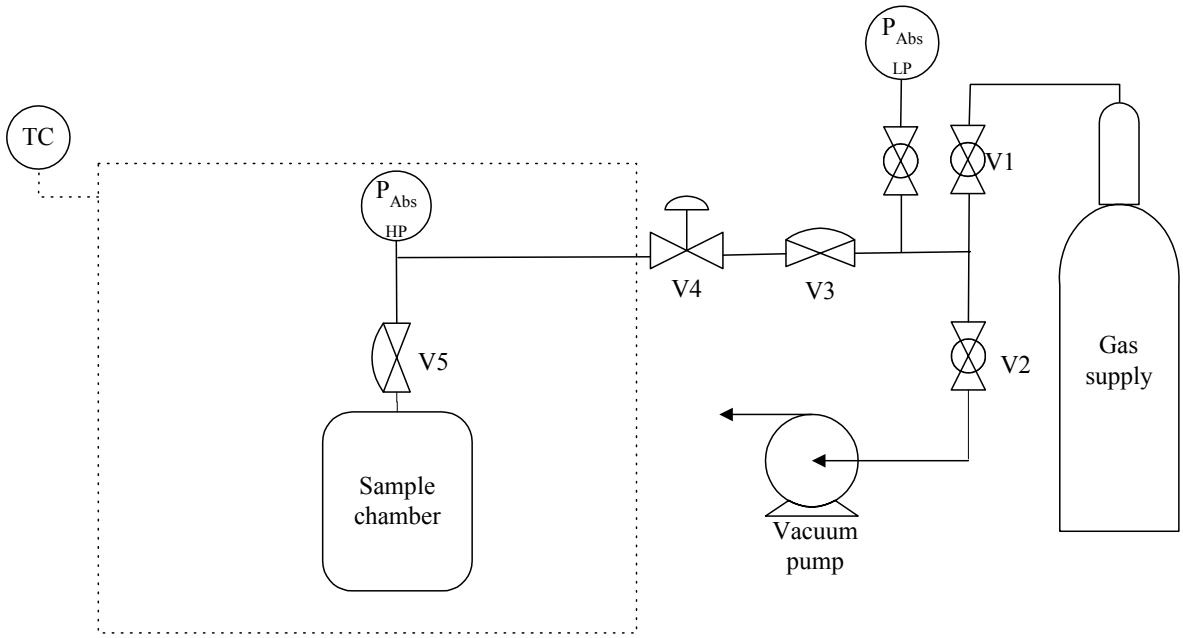

Figure 1: Flow scheme of the apparatus for the adsorption measurements.

For the adsorption measurements some important factors were considered:

- The volume of the sample cell, the pressure transducer, the tubes and valves were carefully volume calibrated. (see explanation in the following paragraph)
- The pressure transducer was kept inside the temperature-regulated chamber to minimize temperature gradients.

- The valve tagged as V4 in figure 1 must be of very high quality. Any leakage on V4 can erroneously be interpreted as adsorption.
- The amount of sample used was adjusted in relation to the cell volume, so that the resulting pressure decrease from the adsorption could be accurately detected with the pressure transducer.
- Sufficient desorption time was always applied, i.e. the evacuation time was as a rule of thumb at least twice the time it took to obtain stable adsorption measurement.

Volume calibration

The volumes of the empty sample chamber (vol 3) and the vis-à-vis tubing (the volumes of the tubing between valve 4 and 5 in figure 1(vol 2) including the internal volumes of those valves (when closed) were carefully volume calibrated in order to obtain stable sorption values. The remaining volume, (vol 1) consists of all pipes, valves and the low-pressure transducer between the valves V1, V2 and V4

The volume calibration was performed as follows:

- With all valves open, the apparatus was evacuated over-night,
- V2 was closed and the system filled with helium of ca.10mbar.
- V1 was closed and the established pressure was accurately measured (with $P_{abs,LP}$), and was denoted p_{start}.
- Valves V4 and V5 were then closed, while V2 and V3 were open, hence vol3 could be evacuated. V2 was closed; the resulting low pressure recorded (p_{evac}).
- Valve V4 was opened, and a new stable pressure recorded (p_1).
- ValveV5 was opened, and a new stable pressure, (p_2), recorded.

By applying the ideal gas law, it was then possible to calculate the ratios between the various volumes. The ratio between vol1 and vol2 is given by the expression:

$$\frac{vol\,1}{vol\,2} = \frac{p_{start} - p_1}{p_1 - p_{evac}} \tag{7}$$

The ratio between vol3 and vol2+ vol1 is calculated in a similar way:

$$\frac{vol\,3}{vol\,2 + vol\,1} = \frac{p_{stat} - p_2}{p_2 - p_1} \tag{8}$$

This allows the ratios of all the volumes to be calculated, but an additional known volume is needed to calculate the absolute volumes. This was done by inserting two

calibration spheres (known volume of 2.1544 cm^3) into the sample chamber. Then the volume of the sample chamber could be determined from the following equation:

$$vol3 = \frac{V_{cal,sphere}}{(1-\frac{R2}{R2'})} \quad (9)$$

Where R2 and R2' are the volume ratio without and with the calibration sphere, respectively.

Adsorption isotherms

The system (with the membrane sample in the chamber) was evacuated overnight prior to each test. The tests were performed in the pressure range of 1 – 4 bars, and temperature range 30°C - 45 C. From previous documentation [4] these regions were found to be most interesting with respect to possible changes in transport.

The adsorption isotherms (figure 3 and 5) were obtained by starting the measurements at lowest sorption pressure (here 0.1 bar), and adding new points for each chosen pressure increase up to 4 bars. The chamber (with membrane sample) was then evacuated for at least two days. This evacuation was very important for two reasons: 1) The error of measurement is propagated during the measurement of series, hence it is important to reinitialise the system conditions. 2) In order to determine the exact pressure starting point for adsorption (i.e. the pressure calculated from the flash into the chamber) the pressure transducer output must be readjusted to zero. Two adsorption experiments were carried out for this purpose only, and this is shown as bullet points on the adsorption curves in figures 3 and 5. The desorption curve was obtained by starting at the highest pressure and then reducing the pressure at chosen intervals.

<u>Diffusion coefficient estimation.</u>

Estimations of the total diffusion coefficient can be obtained by two methods:

1) The diffusion can be found by the following well known equation [8]:

$$P = D \cdot S \quad (10)$$

where P= permeability [mol·m/(m^2 Pa s)], D is the diffusion coefficient [m^2/s] and S is the sorption coefficient [mol/(m^3 Pa)]. Thus the diffusion coefficient can be calculated as the ratio between P and S at a given pressure and temperature.

2) The diffusion can be estimated from the time-lag in the start of the gas permeation measurement. Figure 2 gives a brief sketch of how this is done [8]. The θ-value obtained from the plot, relates to the diffusion according to equation 11 [8]:

$$\theta = \frac{l^2}{6D} \tag{11}$$

where θ is the time-lag [s] and l is the membrane thickness [m].

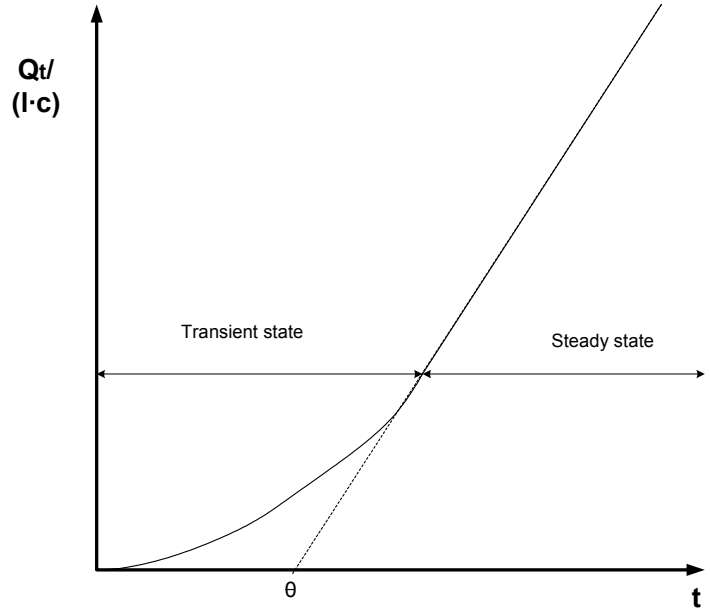

Figure 2: Time-lag measurements in gas permeation measurements [8]. (where $Q_t/(l \cdot c)$ is the amount of penetrant passing through the membrane divided by the product of the membrane thickness and feedside concentration)

Results and discussion

Based on the findings in part I of this work [4] the perfluorinated (2 nm base) surface modified glass membrane was found to exhibit the best combination of performance and stability. Further optimisation based on perfluorinated compounds for surface modifications is however needed. Adsorption tests were performed with the above mentioned membrane to fully understand the SSF-mechanism.

Chlorine adsorption measurements

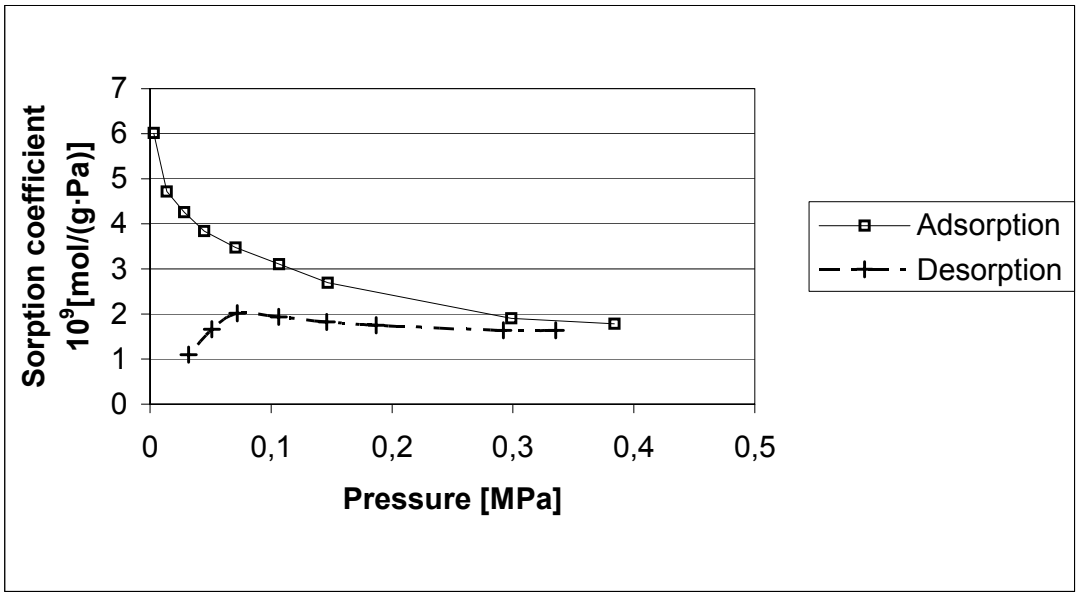

Figure 3: Adsorption and desorption isotherm (30°C) on a surface modified (Pf-C10, 2nm) glass membrane for chlorine as a function of the pressure.

The adsorption of chlorine was measured at 30°C; results are shown in figure 3.
The adsorption and desorption curve in this figure show an increasing deviation as the pressure is lowered. This behaviour was documented by repeated experiments. The explanation for this deviation is most likely that the surface has preferred sorption sites, and that chlorine molecules at low pressure adsorb to sites with the deepest potentials. This is known as "localized adsorption" [9]. During the desorption process, the sites associated to the shallowest surface potential will empty first leading to a progressively more energy demanding desorption. By additional experiments at temperatures from 30° to 45°C at 1.2 bars, the heat of adsorption (Ea) was found to be 22.7 kJ/mol (documented in figure 4, and calculated from eq.12):

$$ad(T) = A_0 \cdot e^{\frac{E_a}{RT}} \qquad (12)$$

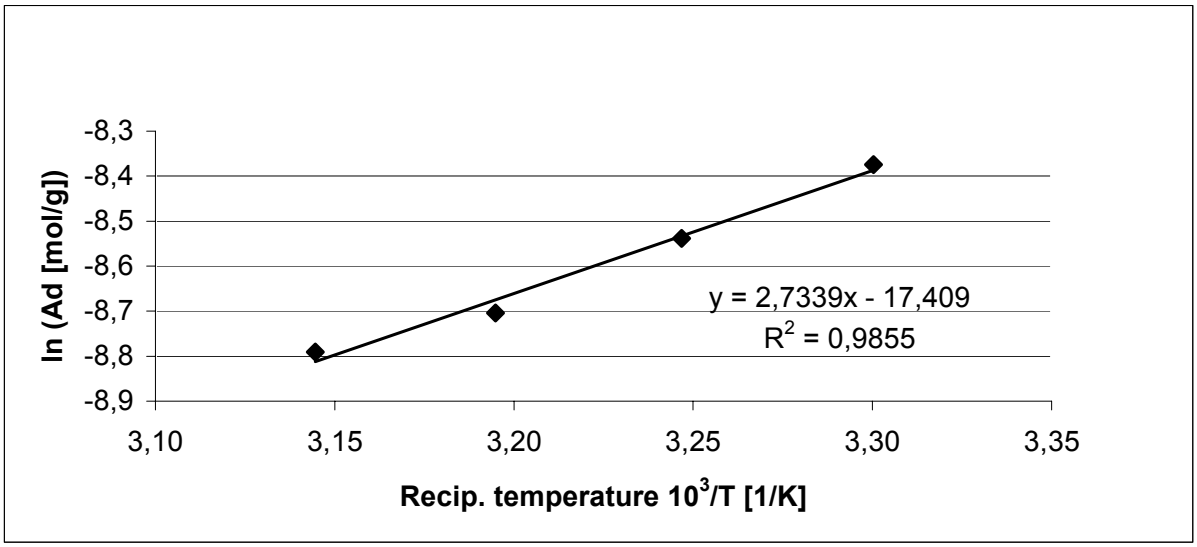

Figure 4: Arrhenius plot of the temperature dependence for chlorine adsorption on a surface modified (Pf-C10, 2nm) glass membrane, measured at 1.2 bar.

From the least squares linear fit (figure 4), $E_a/R=2734$ (see eq. 12) rearranges to yield Ea = 22.7 kJ/mol. Thus the best fit of the temperature dependence of the chlorine adsorption yield the following equation (where *ad(T)* stands for adsorption):

$$ad(T) = 2.75 \cdot 10^{-8} \bullet e^{\frac{22700}{RT}} \qquad (13)$$

This equation has a regression coefficient as high as 0.986 which is very high compared to the expected experimental deviation that can be estimated to be approximately 10% [1]. These results are in good agreement with the tabulated heat of condensation for chlorine which is given as 20.4kJ/mol at 1 bar [6].

Hydrogen chloride adsorption

The corresponding measurements for HCl at 30°C are given in figure 5.

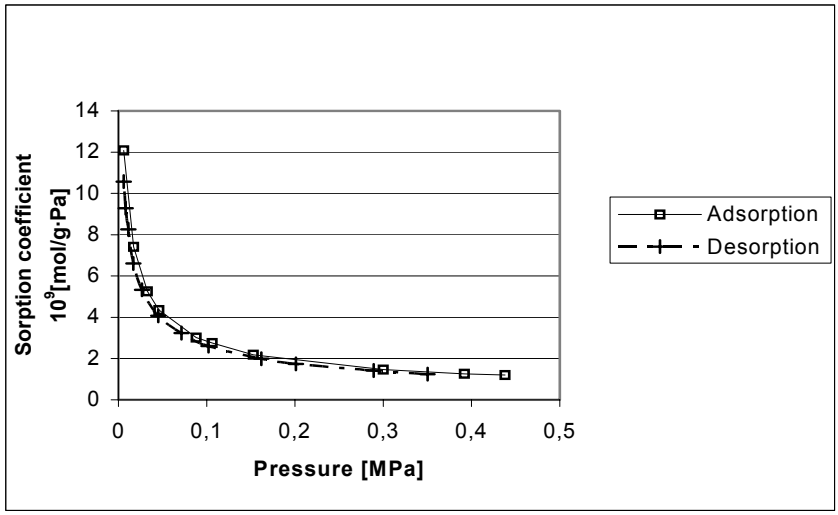

Figure 5: Adsorption and desorption isotherm (30°C) on a surface modified (Pf-C10, 2nm) glass membrane for HCl as a function of the pressure.

Figure 5 demonstrates that the adsorption and desorption curve coincide for all the measured pressures of HCl. It is believed that there is no sorption site association present for the polar HCl gas on the polar glass surface; and this is known as "delocalized adsorption" [9]. The heat of adsorption, Ea, for HCl on the Pf-C10 surface modified glass membrane, was measured to 14.5 kJ/mol, calculated from the values indicated in figure 5, and in the same way as for chlorine (Arrhenius plot).

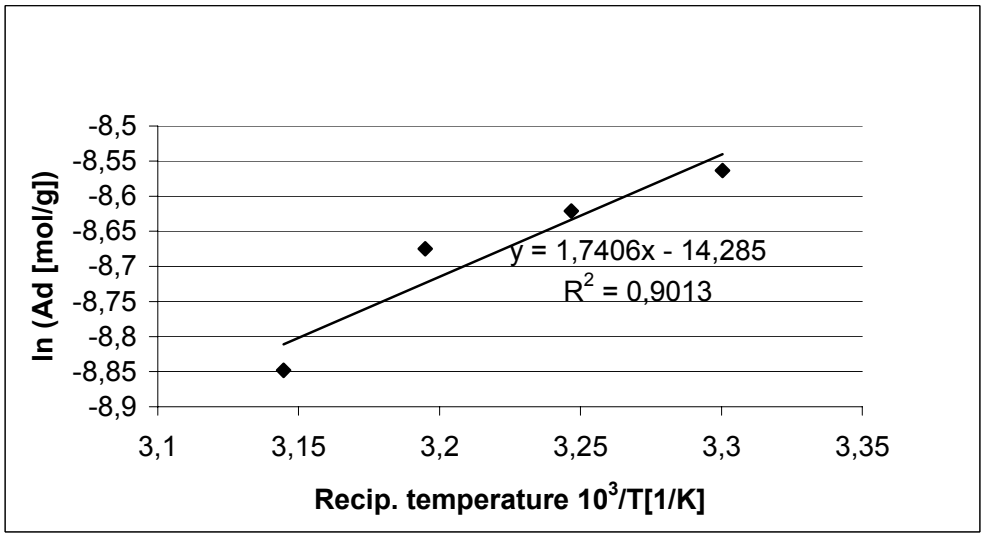

Figure 6: An Arrhenius plot of temperature dependence for the HCl adsorption a surface modified (Pf-C10, 2nm) glass membrane

According to figure 6 the following temperature dependence for the HCl adsorption was determined:

$$ad(T) = 6.25 \cdot 10^{-7} \bullet e^{\frac{14500}{RT}} \quad (14)$$

The adsorption enthalpy is 14.5 kJ/mol, which is in fair agreement with tabulated heat of condensation for hydrogen chloride at 1 bar (17.6 kJ/mol) [6].

Adsorption as a function of the degree of selective surface flow

Figure 7 is showing measured adsorption in the Pf-C10 surface modified glass membrane for some gases as function of degree of SSF (ψ) to overall transport. Equation 6 is applied in order to calculate ψ from data listed in table 2.

Table 2: Permeances, selectivities and molar masses for pure gases measured on a surface modified (Pf-C10, 2nm) glass membrane.

Gas type	Permeance 10^9[mol/(m^2 Pa s)]	Selectivity [-] Helium reference	Molar masses [g/mol]	Adsorption [μmol/g]
N_2	1.08	0.546	28.0	4.35
O_2	1.30	0.656	32.0	8.56
He	1.98	1	4.00	0
HCl	3.97	2.00	36.5	273
Cl_2	5.07	2.56	70.9	261
Xe	1.32	0.669	131	22.5
CO_2	3.01	1.55	44.0	60.7
H_2	2.80	1.42	2.02	0.509
SF_6	1.39	0.701	146	34.9
CO	1.10	0.557	28.0	4.33
R22 (CHF_2Cl)	3.89	1.97	86.5	198

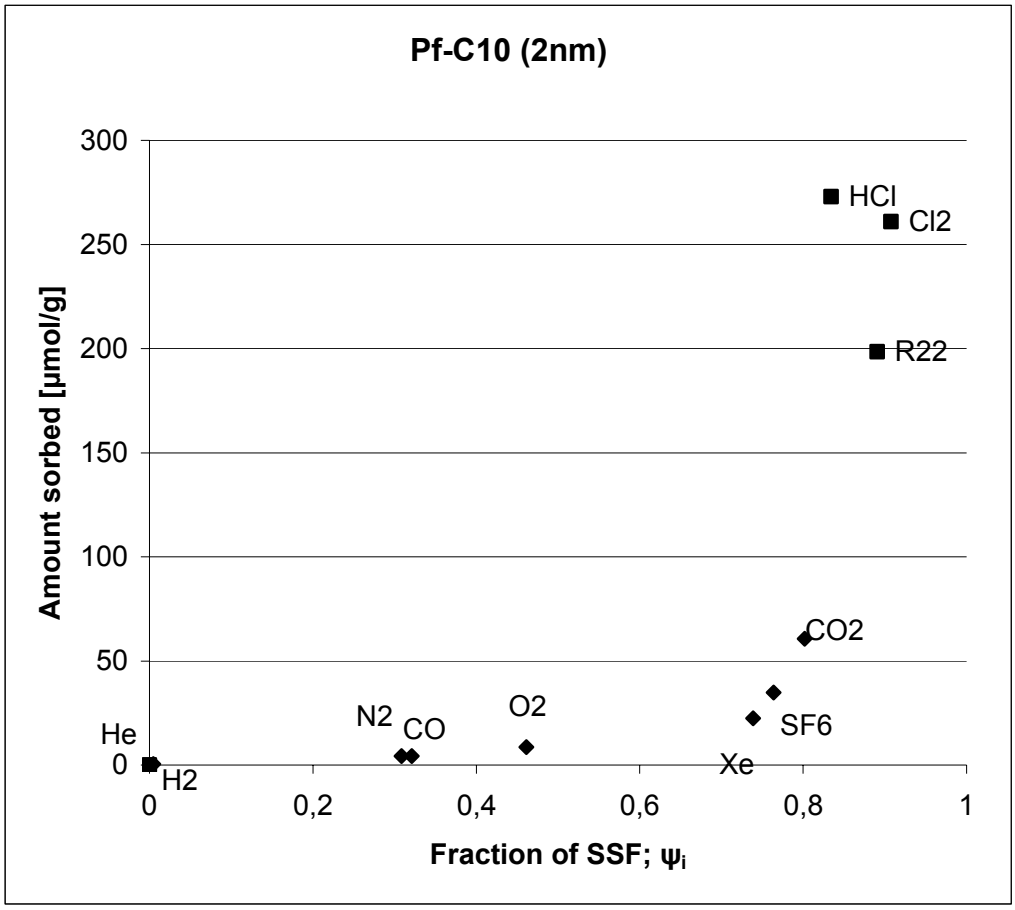

Figure 7: Adsorption as a function of the degree of SSF (ψ_i).

By a closer inspection of figure 7 two phenomena seem to be present simultaneously: There is a slight curvature trend of the gases: H_2, N_2, O_2, Xe, CO, CO_2, SF_6;, these are gases with a ψ_i value lower than ~ 0.8. An exponential fit was assumed for these gases, and the corresponding least square fit is given in figure 8.

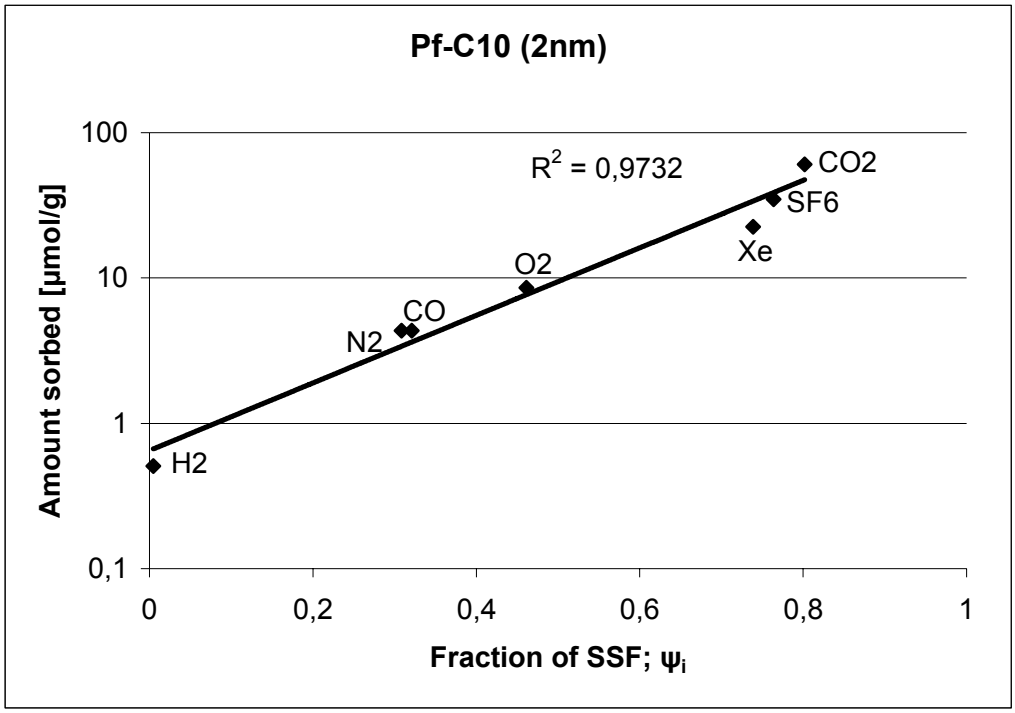

Figure 8: Least square fit (exponential) for gases with $\psi_i < 0.8$ (from figure 7).

Figure 8 indicates that the assumption of an exponential behaviour seems to be very good. Thus from the least square fit in figure 8 the relationship is given in equation 15:

$$ad = 0.65 \cdot e^{(5.3494 \cdot \psi)} \tag{15}$$

Cl_2, HCl, R22 are clustering in the upper right corner of the diagram, and having a ψ value exceeding ~0.8. If an average adsorption value for these three gases is calculated, it is found that: $\overline{ad}(Cl2, HCl, R22) = 244$ [µmol/g] and a corresponding average ψ-value of 0.877.

If the average ψ-value is substituted into equation 15, the resulting ad of 70[µmol/g] clearly indicates that Cl_2, HCl, R22 are adsorbing according to another mechanism than the other gases.

An explanation of the two different adsorption modes vs. the degrees of SSF (ψ), may be that Cl_2, HCl and R22 experience so strong interactions with the membrane that these gases are condensing on the pore surface and thus follows the "sliding layer " mode. (Note; they all contain chlorine.) This is further supported by the fair agreement between measured heat of adsorption and heat of condensation.

The other gases are assumed to have less interaction with the pore surface, and are thus transported by the 2D- gas and / or the hopping mode.

Diffusion coefficient determinations

Figure 9 gives a comparison of the diffusion coefficient obtained by the time-lag method (eq.10) vs. the calculated diffusion from the P/S ratio (eq.11).

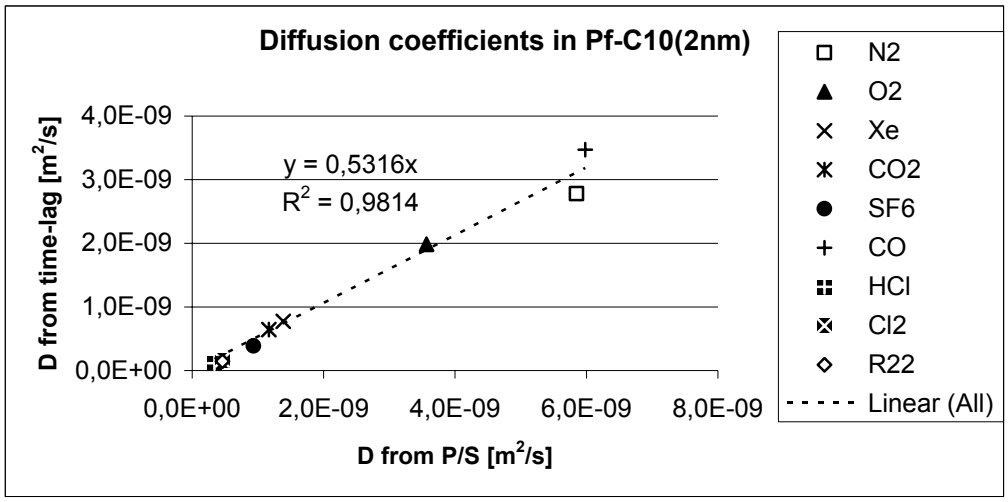

Figure 9: Comparison of diffusion coefficients obtained by the time lag vs. the P/S-ratio methods.

Initially one would expect the values obtained for the diffusion coefficient to be the same regardless of measuring method, thus the function of the regression line should be y = x. It can however be seen from the figure 9, that the diffusion coefficient calculated from P/S is consistently twice the value of those from timelag experiments. The reason for the discrepancy between the two values is difficult to explain. However, it should be noted that D from P/S is calculated at 1 bar from measured permeability and sorption values, while D from the time-lag is estimated from the low-pressure side in the permeance apparatus. The "time-lag D" may possibly be considered as an average diffusion coefficient through the membrane at the measured pressure difference (here the average Δp over the membrane is 0.5 bar).

Conclusion

The best surface modifying agent identified in part I of this work was the perfluorinated C10 modification. This paper has focused on if adsorption measurements could be used to predict the degree of selective surface diffusion in the surface modified glass membrane, and if so, be a tool for predicting separation properties of specific gas mixtures.

A comparison of the adsorption isotherms measured for HCl and Cl_2 indicates that these to gases seem to have different surface adsorption mechanisms. Cl_2 seems to obey a localized sorption site mechanism, while the HCl adsorbs according to a delocalized sorption mechanism. Heat of adsorption measurements indicate that both chlorine and hydrogen chloride are in a "liquid like" state on the surface, since the heat of adsorption is comparable to tabulated heats of condensation for pure compound at the same pressure. The localized / delocalized sorption for Cl_2 and HCl respectively, will explain a difference in need for regeneration of the membrane when these two gases are considered.

If the adsorption is plotted vs. the degree of SSF (ψ) two distinct dependencies emerge: The adsorption of H_2, N_2, O_2, Xe, CO, CO_2, SF_6 were found to be exponential with ψ. The Cl_2, HCl and R22 adsorption is 3.4 times higher than what could be estimated from an exponential behaviour, thus the Cl_2, HCl and R22 are clearly adsorbed by a different mechanism than the other gases. This dual nature might be explained according to the three modes of SSF described in the literature: 1) The liquid like sliding layer mode, 2) the site-to-site hopping mode and 3) the 2-D gas mode. Thus the Cl_2, HCl and R22 is transported according to the liquid sliding layer mode, while the other gases are transported according to the site to site hopping or 2-D gas mode.

Values for the diffusion coefficient show a good consistence between the two methods used for determination. The deviation between the two methods is difficult to explain, but is believed to be due to the pressure differences in the methods.

Acknowledgement

The authors want to thank Professor T. Yazawa at Himeji Institute of Technology, Himeji, Japan and Dr. K. Kuraoka at the Faculty of Maritime Sciences at the Kobe University, Kobe, Japan for preparing the various glass membranes and fibres

References

1. M.-B. Hägg, Membrane Purification of Cl_2 Gas I. Permeabilities as a Function of Temperature for Cl_2, O_2 N_2, H_2 in Two Types of PDMS Membranes, J. Membrane Sci., 170, (2000), 173-190.

2. M.-B. Hägg, Membrane Purification of Cl_2 Gas II. Permeabilities as a Function of Temperature for Cl_2, O_2 N_2, H_2 and HCl in Perfluorinated, Glass and Carbon Molecular Sieve Membranes, J. Membrane Sci.,177, (2000), 109-128.

3. M. S. Eikeland et al., Durability of Poly(dimethylsiloxane) When Exposed to Chlorine Gas, J. of Applied Polymer Sci., vol. 85, (2002), 2458-2470

4. A. Lindbråthen and M.-B. Hägg, Glass membranes for purification of aggressive gases. Part I: Permeability and stability, Submitted to J. Membrane Sci.

5. E. R. Gilliland et al., Effect of concentration on the diffusivity of physically adsorbed gases, Ind. Eng. Chem. Fundam., Vol.13 no.2, (1974), 95-100.

6. Perry's, Chemical Engineering Handbook, 6th ed. (1984), p3-120.

7. R.C. Reid et al., The Properties of Gases and Liquids, 4th Edition, McGraw-Hill, New York, 1987.

8. M. Mulder, Basic principles of membrane technology, 2nd ed. Kluwer Academic Publishers,1996.

9. J. R. Dacey, Surface diffusion of adsorbed molecules, Ind.&Eng. Chem, 57, no.6, (1965), 27-33.

Appendix 3 Permeance measurements

3-1 Permeation equations.

The high-pressure tank (on the feed side) and the low-pressure tank (on the permeate side) both have a volume of 1 dm^3. The volumes of the tubes and valves connecting the pressure tanks and the volume of the membrane module are neglectable compared to the pressure tanks. It is assumed that steady state permeation is achieved if constant gas pressures p_h (the high pressure side) and p_l (the low pressure side) are maintained at the membrane interface and that the driving force for the transport, $\Delta p = p_h - p_l$, through the membrane is constant (i.e. p_h=1 bar, $p_l=0.8\cdot10^{-3}$ bar (vacuum) give Δp=1 bar). The temperature is assumed constant inside the cabinet and measured by a temperature transducer. Figure A.3-1 gives a principal sketch of a membrane connected to two equal volumes.

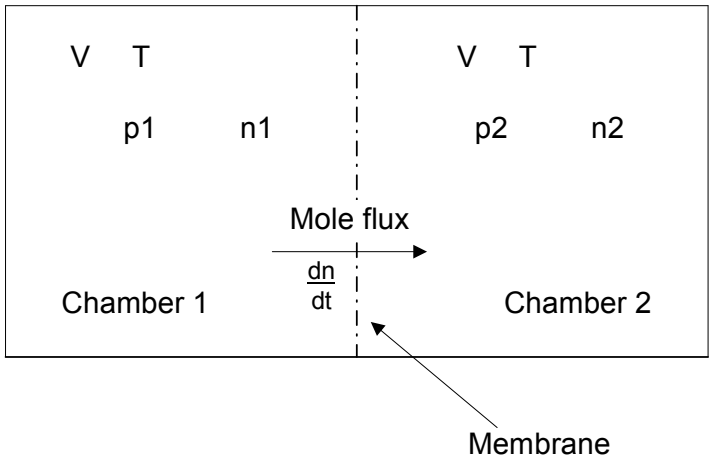

Figure A3-1: Principal sketch of a membrane permeation apparatus.

Both chamber 1 (high pressure side) and chamber 2 (low pressure side) have a relatively low pressure (where $p_1 > p_2$), and the ideal gas law is used as an initial description the system.

$$pV = nRT \qquad (A3.1)$$

Where: p = pressure [Pa], V= volume [m^3], n = number of moles [mol], R = gas constant [8.314 J /(K mol)] and T = temperature [K]

When the ideal gas law is applied on chamber 2, with constant T and V, the change in numbers of mol of gas in chamber 2 with time, $\frac{dn_2}{dt}$ is given as:

$$\frac{dn_2}{dt} = \frac{V}{RT}\frac{dp_2}{dt} \qquad (A.3.2)$$

In permeance measurements it is custom to convert the mole change to a gas volume change given at standard pressure and temperature;
Where: p_0= 1.0133 bar (1 atm) is the standard pressure, and T_0 =273.15 K (0°C) is the standard temperature.

Ideal gas law is time derived, yielding;

$$\frac{dV_{0,2}(n_2)}{dt} = \frac{T_0 R}{p_0}\frac{dn_2}{dt} \qquad (A.3.3)$$

Where: the subscript 0 indicates standard pressure and temperature conditions.
The flux is described as a flow through a given permeation area by:

$$J = \frac{dV_{0,2}(n)}{dt}\frac{1}{A} \qquad (A.3.4)$$

Where: A= Membrane area [m^2]
The flux can also be modelled as:

$$J_i = \frac{P_i(p_h - p_l)}{l} = \frac{P_i}{l}\Delta p \qquad (A.3.5)$$

This expression can be rearranged, yielding:

$$\frac{P_i}{l} = \frac{J}{p_1 - p_2} \qquad (A.3.6)$$

Combining equation 2, 3, 4 and 6 leads to the expression of the permeance P/l [m^3(STP)/(m^2 bar h)] as a function of the pressure change dp/dt:

$$\frac{P}{l} = \frac{1}{A}\frac{VT_0}{Tp_0(p_1 - p_2)}\frac{dp_2}{dt} \qquad (A.3.7)$$

If real gas behaviour is to be implemented, the pressure p_1 has to be corrected (should use camber 1 fugacity instead). This can be relatively easily done by implementing an appropriate equation of state like the viral equation. However, brief estimations of the compressibility factor, Z, shows that the deviation from the ideal gas law is in the range of maximum 1%.

3-2 Matlab m-files.

Permeance1.m:

```
clear all

%--------------------------------------------------
%                Input-values
filpath=input('Give file name with path: ','s');
min=input('Give start time value: ');
max=input('Give end time value: ');
filnr=input('Which pressure sensor (1, 2 or 3): ');
eval(['load ',filpath]);

%--------------------------------------------------
%       Saves filname as 'navn'
PFlagg=0;
N=length(filpath);
for i=1:N,
  if filpath(i)=='\'
    PFlagg=i;
  end;
end;

i=PFlagg+1;
while i>0,
  if filpath(i)=='.', i=0;
  else
    navn(i-PFlagg)=filpath(i);
    i=i+1;
  end;
end;
%--------------------------------------------------
%       Calculations

tid=0:1:(max-min);              %Creates a time vector step = 1sek, Hz=1

eval(['tabell=(',navn,'((min):(max),filnr));';]);
                                %Stores data into a vector table

tabell=1.*tabell;               %Transforming from volt into mbar
                                %(10mbar)


%--------------------------------------------------
%       Plot routine
figure
plot(tid,tabell);
xlabel('sec'),ylabel('mbar');

title(navn);
```

Permeance2.m

```
%       Input values

t1=input('Give start time for stable slope: ');
t2=input('Give end time for stable slope: ');
dim=input('Membrane diameter in cm: ');
Temp=input('Give temperature in °C: ');




%---------------------------------------------------------
%

eval(['tabell1=',navn,'((min):(max),2);']);
trykk=tabell1(t1);
trykk=trykk*0.5;        %transforms the high pressure from volt to bara
clear tabell1;




%---------------------------------------------------------
%
[p,s]=polyfit(tid((t1+1):(t2+1))',tabell((t1+1):(t2+1)),1);
avrund=polyval(p,tid((t1+1):(t2+1)));



%dpdt=(tabell(t2+1)-tabell(t1+1))/(t2-t1);
trykkl=tabell(t1+1)/1000;               %transforming mbar to bara
%---------------------------------------------------------
%       Calculates the permeance from dp/dt
%
%       -Transforms dp/dt from mbar per sec. to bar per hour
%        by multiplying dpdt by 3600/1000
dpdt=p(1,1);
dpdt=3600/1000*dpdt;

%
%-PVol = nRT, 22.414*dn/dt = dV/dt = Vol/(RT)*22.414*dp/dt
%dV/dt = konst/(T)*dpdt,konst = Vol*22.414/(R),Vol = 1 liter
%konst = 0.001*22.414/0.08314 = 0.26959


k=0.26959;
A=(pi*dim*dim)/4*10^(-4);           % Area of the membrane

PL=k*dpdt/(A*(trykk-trykkl)*(Temp+273.15))  ;
```

```
%-------------------------------------------------------
%       Places the figure caption
x1=0.9*(max-min);
y1=0.3*(tabell(max-min)-tabell(1))+tabell(1);
yt=(y1-tabell(1));
x2=0.6*x1;
y2=0.85*yt+tabell(1);
y3=0.7*yt+tabell(1);
y4=0.55*yt+tabell(1);
y5=0.4*yt+tabell(1);

%-------------------------------------------------------
%       Plot routine

hold on;
plot(tid((t1+1):(t2+1)),avrund,'r-')
plot(t1,tabell(t1+1),'*',t2,tabell(t2+1),'*')
text(x2,y1,'dpdt[mbar/s]=');
text(x1,y1,num2str(dpdt));
text(x2,y2,'P/L[m^3/(m^2*bar*h)]=');
text(x1,y2,num2str(PL));
text(x2,y3,'T(°C)=');
text(x1,y3,num2str(Temp));
text(x2,y4,'D(cm)=');
text(x1,y4,num2str(dim));
text(x2,y5,'Ph(bara)=');
text(x1,y5,num2str(trykk));
hold off
```

Permeance3.m

```
%This script calculates the time-lag in the start of an ordinary permeation curve.
t3=input('Give start time for stable base line: ');
t4=input('Give end time for stable base line: ');
[p2,s2]=polyfit(tid((t3+1):(t4+1))',tabell((t3+1):(t4+1)),1);
baseline=polyval(p2,tid((t3+1):(t2+1)));
avrund=polyval(p,tid((t3+1):(t2+1)));

%calculation of intersection point.
cross=(p2(1,2)-p(1,2))/(p(1,1)-p2(1,1))

hold on;
plot(tid((t3+1):(t2+1)),avrund,'g--')
plot(tid((t3+1):(t2+1)),baseline,'b-.')
hold off;
```

3-3 Equipment accuracy

In the permeability measurements, a MKS Instrument type 626A(0-10 mbar) pressure transducer was used on the low pressure side. The accuracy of this transducer is 0.15% of the measured value. On the high-pressure side, a MKS Instrument (type 121A(0-5000 mbar)) pressure transducer with an accuracy of 0.5 % of measured value was used.

The effect of variations in the temperature is estimated to be 0.3 % based on given accuracy for the temperature controller.

As discussed in previous section, the deviation from ideal gas law is inducing an error in the order of 1 % depending on which gas measured (and temperature and pressure of that gas).

The main error in the calculated permeabilities is caused by variations in the thickness of the membrane and not by the system or permeation procedures.

The thicknesses used for calculating the permeabilities i.e. in the Robeson plots are simply the average thickness stated by our Japanese research associate. Since the glass tubes are hand drawn, they are estimated to have a relative uncertainty of ±5% in the thickness.

For the fibres, the estimation of the relative accuracy is harder, since no data are known for the thickness variation: However, the mounting is difficult for the fibres and this is believed to be causing the largest uncertainty for these measurements.

Appendix 4 Adsorption apparatus

4-1 Volume calibration of sorption apparatus

The volumes of the empty sample chamber and the vis-à-vis piping have to be carefully volume calibrated in order to obtain stable sorption values. The volume calibration was performed as follows:

The apparatus was evacuated over-night, and then filled with ca.10mbar of helium and this pressure is called P_{start}. Figure A4.1 gives a principal sketch of the three volumes of the apparatus needed to be volume calibrated:

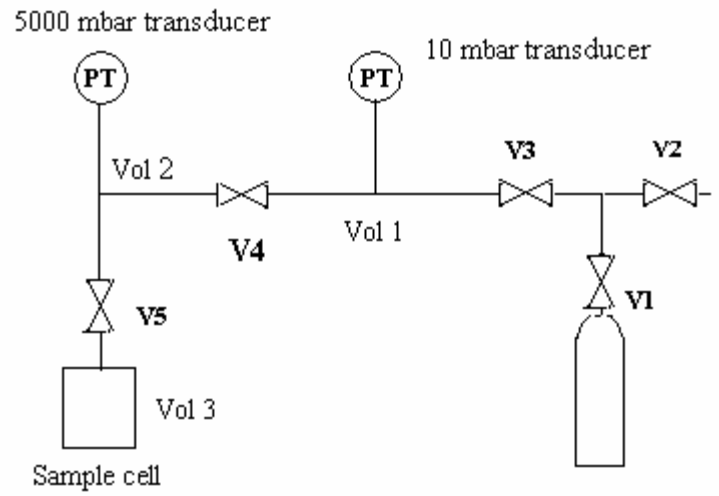

Figure A4-1: Volumes calibrated in the adsorption equipment.

All valves are then closed and V2 and V3 are opened and vol 1 is evacuated, the resulting low pressure is then recorded and called p_{vak}. Valve V4 is opened and the new stable pressure recorded as p1. By opening the valve (V5) the pressure p2, is recorded. By applying the ideal gas law, it is possible to calculate the ratios between the various volumes. The ratio between vol 1 and vol 2 is given by the expression:

$$\frac{vol\,1}{vol\,2} = \frac{p_{stat} - p_1}{p_1 - p_{vak}} \qquad \text{(A4-1)}$$

The ratio between vol 3 and vol 2+ vol 1 is calculated in a similar way:

$$\frac{vol\,2 + vol\,1}{vol\,3} = \frac{p_{stat} - p_2}{p_2 - p_1} \qquad \text{(A4-2)}$$

This allows the ratios of all the volumes to be calculated, but an additional known volume is needed to calculate the volumes absolutely. This can be done by inserting two calibration spheres (known volume of 2.1544 cm^3) into the sample cell. Then the volume of the sample cell can be determined from the following equation:

$$vol3 = \frac{V_{cal,sphere}}{(1-\frac{R2}{R2'})} \qquad \text{(A4-3)}$$

Where R2 and R2' are the volume ratio without and with the calibration sphere, respectively.

4-2 Sorption measurement

In determining the adsorption, the important parts of the equipment are the sample chamber and the vis-à-vis piping with the pressure transducer. These parts are sketched in figure A4-2

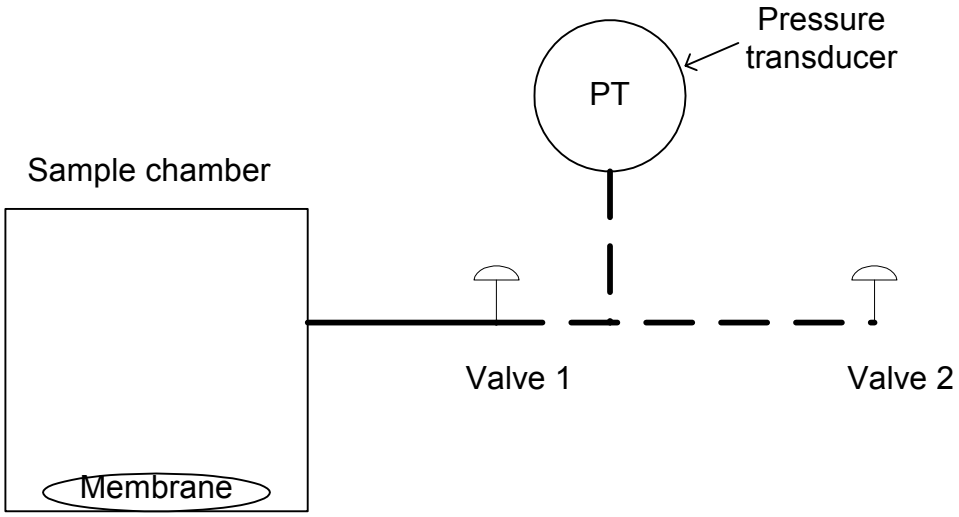

Figure A4-2: The sample chamber and the vis-à-vis piping of the sorption apparatus

The sorption can be calculated if the volume of the membrane sample is known, and the equipment can easily be used as a pycnometer if flashed with helium. The sample volume can in that case be calculated by equation 3 (applying the new volume ratio and $V_{membrane}$ substituted for $V_{cal,\ sphere}$).

The sample was evacuated at least overnight prior to each test. The maximum pressure test available in the set-up is a consequence of the pressure range of the pressure transducer. The flash resulting from having the sample chamber evacuated

and the vis-à-vis volume (the volume of the tube, including the pressure transducer between Valve 1 and Valve 2 in figure A4-2) at maximum detectable pressure gives a maximum test pressure of approximately 50 % of the maximum pressure. In the current set-up, this means that 3 bar is the maximum test pressure (in one single flash). The principle of calculating the sorption is to divide the calculation into two successive steps: First step is to calculate the "ideal" flash, treating the membrane as an inert body occupying a given volume. Second step is to calculate the sorption from the change in the total pressure as the pressure stabilises at a new level. In more detail:

Before valve 1 is opened, the following situation applies:

$$n_{tot} = \left((V_{sc} - V_{mem}) \cdot P_{vac} + V_{V-A-V} \cdot P_{feed}\right) \Big/ RT \qquad \text{(A4-4)}$$

Where: n_{tot} = total number of moles [mol], V_{sc} = volume of empty sample chamber [cm^3], V_{mem} is the volume of the membrane sample [cm^3], $V_{V\text{-}A\text{-}V}$ is the volume of the piping and the pressure transducer [cm^3], P_{vac} is the vacuum pressure [bar] , P_{feed} is the applied pressure of the measuring gas [bar], T = temperature [K] and R is the gas constant [8.314 J/(K mol)]

Then as valve 1 is opened, but "before" any adsorption takes place the total number of moles is preserved:

$$n_{tot} = \left((V_{sc} - V_{mem}) + V_{V-A-V}\right) \cdot P_{Flash} \Big/ RT \qquad \text{(A4-5)}$$

Thus by combining equation 4 and 5, the following expression for the flash pressure, P_{flash}, is obtained:

$$P_{Flash} = \frac{\left((V_{sc} - V_{mem}) \cdot P_{vac} + V_{V-A-V} \cdot P_{feed}\right)}{\left((V_{sc} - V_{mem}) + V_{V-A-V}\right)} \qquad \text{(A4-6)}$$

The end pressure is determined from the pressure transducer log file (evaluated by a Matlab script), and the adsorption is then calculated from this pressure difference:

$$\Delta n_{ads} = -\left((V_{sc} - V_{mem}) + V_{V-A-V}\right) \cdot (P_{Flash} - P_{End}) \Big/ RT \qquad \text{(A4-6)}$$

Where Δn_{ads} is the number of moles adsorbed [mol].

4-3 Accuracy

A MKS 121A, (0- 5000 mbar) pressure transducer with a 0.5 % accuracy (relative to the measured value) was used. The temperature regulator had a stability of ± 1°C. The balance had a precision of ± 0.00005 g which is negligible compared to other measurement errors.
The density measurement was performed in the same equipment and will have the same errors as the sorption measurement.

For absorption measurements, errors in the registered data will mainly be caused by possible inaccuracy in the volume estimation for tubes and sorption chamber in the experimental set-up (estimated to ± 5%). The volumetric errors will have to be counted for twice since the error is involved in determining both the density and the flash.

Appendix 5 Pure 4 nm glass membrane

The following tests were performed at 30 °C (old module)

Gas	**Permeance** [m^3(STP)/(m^2 bar h)]	**Selectivity** (gas/N_2)	**Comment**
N_2	0.1907		1st parallel
N_2	0.1745		2nd parallel
N_2	0.1721		3rd parallel
N_2	0.211		4th parallel An average of these four measurements is used in the selectivity calculations (0.1871)
O_2	0.1516	0.81	1st parallel
O_2	0.1521	0.81	2nd parallel
Cl_2	0.2205	1.18	1st parallel Evacuated for 6 hours Exposed for 450 s
Cl_2	0.2330	1.25	2nd parallel, Exposed for 600 s
Cl_2	0.2710	1.45	1st parallel Evacuated overnight Exposed for 500 s
Cl_2	0.2725	1.46	2nd parallel Exposed for 500 s
Cl_2	0.2727	1.46	3rd parallel Membrane exposed to Cl_2 for 0.5 hour between the last tests Exposed for 500 s
Cl_2	0.2660	1.42	4th parallel Exposed for 500 s
N_2	0.1655	0.88	1st parallel
N_2	0.1655	0.88	2nd parallel

Total exposure time: 3500 s at 30 C.

Appendix 6 Pure 2 nm glass membrane

Appendix 6-1: Nitrogen adsorption isotherm.

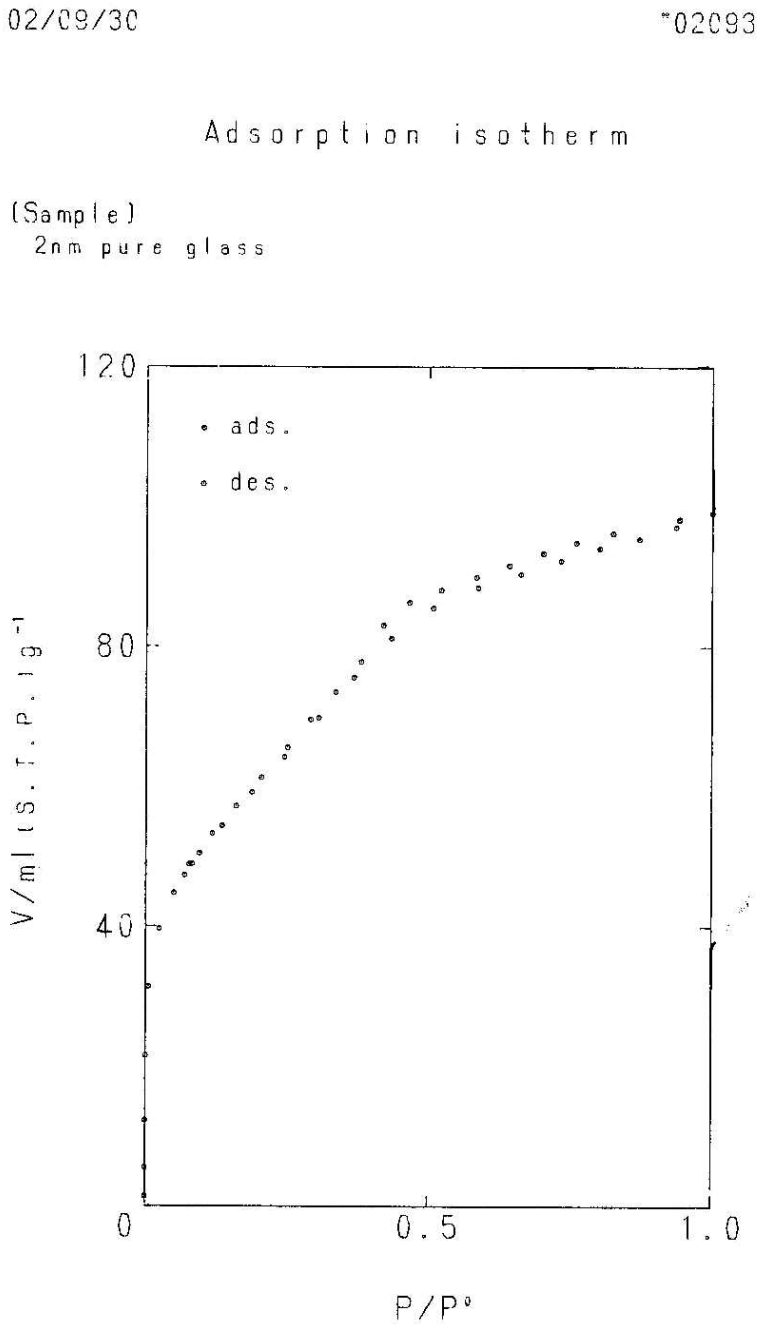

Appendix 6-2: Nitrogen adsorption BET plot

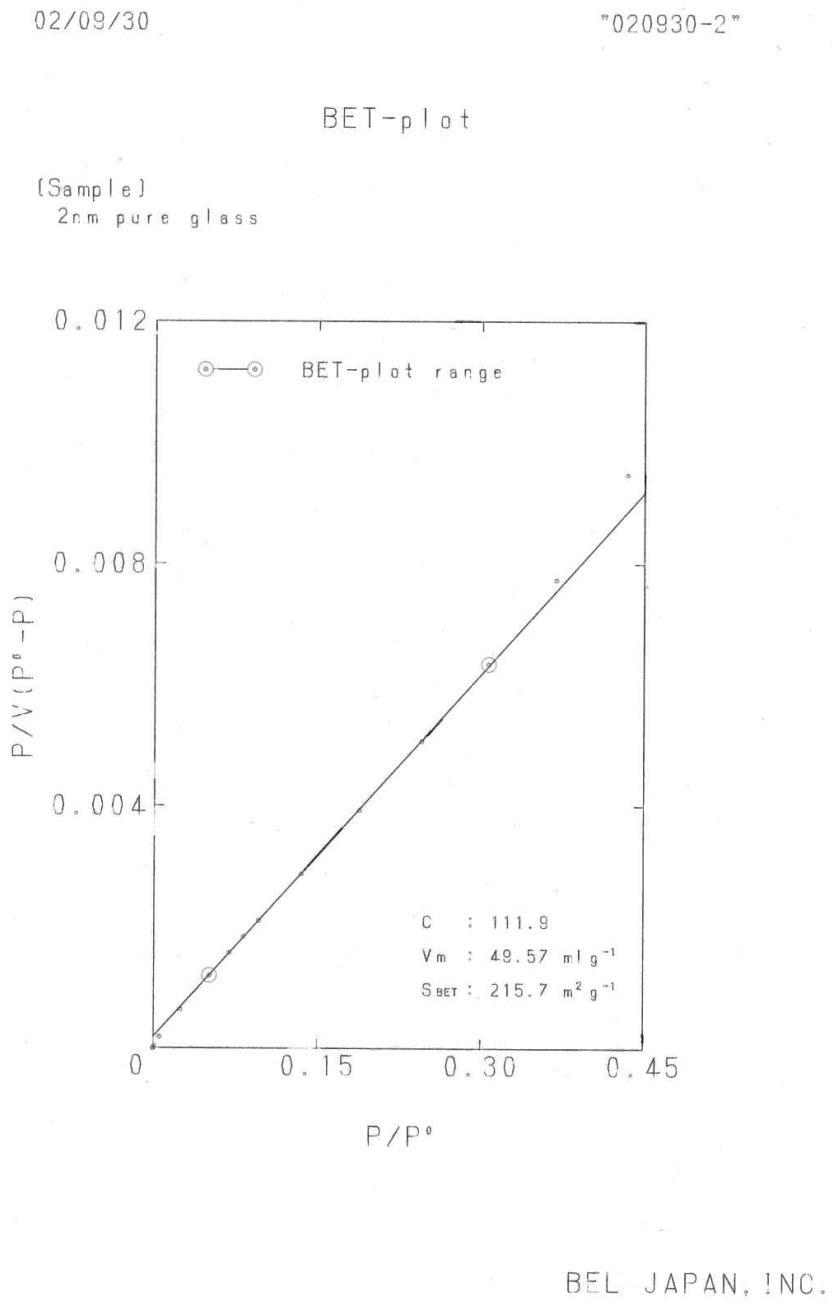

Appendix 6-3: Permeance measurements.

The tests are reported in the order as they were performed. Between each parallel at least 30 minutes long evacuation was performed and between each pressure an evacuation for at least 1.5 hours has been performed. (old module)

Pressure [bar]	**Gas**	**Temperature** [°C]	**Permeance** [m^3(STP)/(m^2 bar h)]	**Selectivity** (gas/N_2)	**Comment**
1	N_2	30	0.0888	-	1st parallel
1	N_2	30	0.0907	-	2nd parallel
1	N_2	30	0.0897	Mean: 0.0897	3rd parallel
2	N_2	30	0.0935	-	1st parallel
2	N_2	30	0.0936	Mean: 0.0935	2nd parallel
3	N_2	30	0.0945	-	1st parallel
3	N_2	30	0.0952	Mean: 0.0950	2nd parallel
1	N_2	60	0.0836	-	1st parallel
1	N_2	60	0.0845	Mean: 0.0841	2nd parallel
2	N_2	60	0.0848	-	1st parallel
2	N_2	60	0.0840	Mean: 0.0844	2nd parallel
3	N_2	60	0.0850	-	1st parallel
3	N_2	60	0.0856	Mean: 0.0853	2nd parallel
1	N_2	90	0.0741	-	1st parallel
1	N_2	90	0.0740	Mean: 0.0741	2nd parallel
2	N_2	90	0.0752	-	1st parallel
2	N_2	90	0.0760	Mean: 0.0756	2nd parallel
3	N_2	90	0.0755	-	1st parallel
3	N_2	90	0.0761	Mean: 0.0758	2nd parallel
1	N_2	30	0.0915	[1.02]	1st parallel
1	N_2	30	0.0924	[1.03]	2nd parallel
2	N_2	30	0.0948	[1.01]	1st parallel
2	N_2	30	0.0945	[1.01]	2nd parallel
3	N_2	30	0.0951	[1.00]	1st parallel
3	N_2	30	0.0948	[1.00]	2nd parallel

The selectivities in the following tables are calculated with reference to the corresponding nitrogen condition in the pervious table. The selectivities given in brackets refer to the internal stability of the two different 30 °C tests for each gas and they are calculated from the corresponding parallel of each pressure. (old module)

Pressure [bar]	**Gas**	**Temperature** [°C]	**Permeance** [m^3(STP)/ (m^2 bar h)]	**Selectivity** (gas/N_2)	**Comment**
1	O_2	30	0.0869	0.97	1st parallel
1	O_2	30	0.0863	0.96	2nd parallel
2	O_2	30	0.0883	0.94	1st parallel
2	O_2	30	0.0884	0.95	2nd parallel
3	O_2	30	0.0888	0.93	1st parallel
3	O_2	30	0.0889	0.94	2nd parallel
1	O_2	60	0.0770	0.92	1st parallel
1	O_2	60	0.0774	0.92	2nd parallel
2	O_2	60	0.0785	0.93	1st parallel
2	O_2	60	0.0786	0.93	2nd parallel
3	O_2	60	0.0789	0.92	1st parallel
3	O_2	60	0.0796	0.93	2nd parallel
1	O_2	90	0.0694	0.94	1st parallel
1	O_2	90	0.0698	0.94	2nd parallel
2	O_2	90	0.0710	0.94	1st parallel
2	O_2	90	0.0717	0.95	2nd parallel
3	O_2	90	0.0718	0.95	1st parallel
3	O_2	90	0.0715	0.94	2nd parallel
1	O_2	30	0.0865	0.96 [1.00]	1st parallel
1	O_2	30	0.0854	0.95 [1.01]	2nd parallel
2	O_2	30	0.0878	0.94 [1.00]	1st parallel
2	O_2	30	0.0880	0.94 [1.00]	2nd parallel
3	O_2	30	0,0885	0.95[1.00]	1st parallel
3	O_2	30	0,0885	0.95[1.00]	2nd parallel

Pressure [bar]	**Gas**	**Temp.** [°C]	**Permeance** [m^3(STP)/ (m^2 bar h)]	**Selectivity** (gas/N_2)	**Comment**	**Exposure time [s]**
1	Cl_2	30	0.216	2.41	1st parallel	400
1	Cl_2	30	0.215	2.40	2nd parallel	400
2	Cl_2	30	0.218	2.33	1st parallel	200
2	Cl_2	30	0.217	2.32	2nd parallel	200
3	Cl_2	30	0.205	2.16	1st parallel	150
3	Cl_2	30	0.207	2.18	2nd parallel	150
1	Cl_2	60	0.153	1.82	1st parallel	450
1	Cl_2	60	0.153	1.82	2nd parallel	450
2	Cl_2	60	0.155	1.84	1st parallel	250
2	Cl_2	60	0.155	1.84	2nd parallel	250
3	Cl_2	60	0.153	1.79	1st parallel	180
3	Cl_2	60	0.154	1.81	2nd parallel	180
1	Cl_2	90	0.106	1.43	1st parallel	600
1	Cl_2	90	0.105	1.42	2nd parallel	600
2	Cl_2	90	0.103	1.36	1st parallel	350
2	Cl_2	90	0.103	1.36	2nd parallel	350
3	Cl_2	90	Leakage in sealing*	-	1st parallel	-
3	Cl_2	90	Leakage in sealing*	-	2nd parallel	-
1	Cl_2	30	0.133	1.48 [0.62]	1st parallel	600
1	Cl_2	30	0.129	1.44 [0.60]	2nd parallel	700
2	Cl_2	30	0.130	1.39 [0.60]	1st parallel	350
2	Cl_2	30	0.130	1.39 [0.60]	2nd parallel	350
3	Cl_2	30	0.135	1.42 [0.65]	1st parallel	250
3	Cl_2	30	0.135	1.42 [0.65]	2nd parallel	250

* The module was disconnected and the sealing was exchanged before the tests proceeds. Since the 1 and 2 bar tests at 90 °C seems to be logic compared to the other chlorine tests, the 3 bar tests at 90 °C was omitted.

Total chlorine exposure time: 7 660 s, (1500+2500 s at 30 C)

Pressure [bar]	**Gas**	**Temp.** [°C]	**Permeance** [m^3(STP)/ (m^2 bar h)]	**Selectivity** (gas/N_2)	**Comment**
1	N_2	30	0.0531	0.59	1st parallel
1	N_2	30	0.0524	0.58	2nd parallel
2	N_2	30	0.0546	0.58	1st parallel
2	N_2	30	0.0547	0.59	2nd parallel
3	N_2	30	0.0555	0.58	1st parallel
3	N_2	30	0.0553	0.58	2nd parallel
1	N_2	60	0.0515	0.61	1st parallel
1	N_2	60	0.0518	0.62	2nd parallel
2	N_2	60	0.0529	0.63	1st parallel
2	N_2	60	0.0532	0.63	2nd parallel
3	N_2	60	0.0539	0.63	1st parallel
3	N_2	60	0.0541	0.63	2nd parallel
1	N_2	90	0.0505	0.68	1st parallel
1	N_2	90	0.0507	0.68	2nd parallel
2	N_2	90	0.0514	0.68	1st parallel
2	N_2	90	0.0514	0.68	2nd parallel
3	N_2	90	0.0515	0.68	1st parallel
3	N_2	90	0.0518	0.68	2nd parallel
1	N_2	30	0.0632	0.70 [1.19]	1st parallel
1	N_2	30	0.0632	0.70 [1.21]	2nd parallel
2	N_2	30	0.0639	0.68 [1.17]	1st parallel
2	N_2	30	0.0637	0.68 [1.16]	2nd parallel
3	N_2	30	0.0635	0.67 [1.14]	1st parallel
3	N_2	30	0.0639	0.67 [1.16]	2nd parallel

Appendix 7 C1 surface-modified glass membrane

Tests performed with the new module.

Permeances are reported as [m^3 (STP) /(m^2 bar h)] performed at 30 °C

Gas type	Permeance	Selectivity (N_2 ref)	Chlorine exposure time [s]	Permeability decay [10^{-5}/s]
N_2	0.0290	1		
O_2	0.0280	0.97		
Cl_2	0.0750	2.6	3.26	3 600
N_2	0.0256	0.88 [1]		
O_2	0.0258	0.89 [1]		

New membrane sample

Gas type	Permeance	Selectivity (N_2 ref)	Chlorine exposure time [s]	Permeability decay [10^{-5}/s]
N_2	0.0484	1		
O_2	0.0456	0.94		
Cl_2	0.149	3.07	0.187	86 400
N_2	0.0406	0.83 [1]		
O_2	0.0401	0.83 [0.99]		

Appendix 8 C8 surface-modified glass membrane

All the tests are performed at 30 °C.

The tests are reported in the order as they were performed. Between each parallel there has been an evacuation for at least 30 minutes and between each pressure an evacuation for at least 1.5 hours has been performed. (Old module)

Pressure [bar]	**Gas**	**Permeance** [m^3(STP)/(m^2 bar h)]	**Selectivity** (gas/N_2)	**Comment**
1	N_2	0.00175	-	
3	N_2	0.00181	-	
1	O_2	0.00226	1.29	
3	O_2	0.00240	1.32	
1	Cl_2	0.0165	9.42	Exposed for 2800 s
2	Cl_2	0.0148	-	Exposed for 2300 s
3	Cl_2	0.00889	4.90	Something happened Exposed for 1350 s
1	N_2	0.000302	1 [0.17]	
1	O_2	0.000295	0.98	
1	Cl_2	0.00541	17.92	Exposed for 500 s

Total exposure time 6950 s

Appendix 9 C18 surface-modified glass membrane

Appendix 9-1: Chlorine separation

The tests are reported in the order as they were performed. Between each pressure an evacuation for at least 1.5 hours has been performed. (Old module)

Pressure [bar]	**Gas**	**Temp.** [°C]	**Permeance** [m^3(STP)/ (m^2 bar h)]	**Selectivity** (gas/N_2)	**Comment**
1	N_2	30	0.00255	1	
3	N_2	30	0.00258	1	
1	O_2	30	0.00433	1.70	
3	O_2	30	0.00461	1.81	
1	Cl_2	30	0.0605	23.73	Exposed for 700 s
2	Cl_2	30	0.0794	-	Exposed for 500 s
3	Cl_2	30	0.0816	32.00	Exposed for 650 s
1	N_2	30	0.00199	1 [0.78]	To check exp. depend.
1	O_2	30	0.00383	1.92	To check exp. depend.
1	N_2	60	0.00378	1	
1	O_2	60	0.00622	1.65	
1	Cl_2	60	0.0497	13.15	
3	Cl_2	60	0.0495	13.10	
1	N_2	60	0.00262	1 [0.69]	To check exp. depend.
1	O_2	60	0.00443	1.69	To check exp. depend.

Total exposure time: 1850s at 30 C.

Second round, same membrane sample

Gas	Temp [°C]	Pressure [Bar]	Permeance [m^3(STP)/(m^2 bar h)]	Selectivity (gas/N_2)
N_2	30	1	0.00130	1
O_2	30	1	0.00257	1.98
HCl	30	1	0.0241	18.5
HCl	30	3	0.0281	-
N_2	30	1	0.00166	1 [1.28]
H_2	30	1	0.00450	2.71
H_2	30	3	0.00465	-
N_2	60	1	0.00288	1
O_2	60	1	0.00469	1.62
H_2	60	1	0.00805	2.80
H_2	60	3	0.00813	-
N_2	60	1	0.00304	1 [1.06]
HCl	60	1	0.0179	5.89
HCl	60	3	0.0250	-
N_2	80	1	0.00339	1
O_2	80	1	0.00524	1.55
H_2	80	1	0.0102	3.01
H_2	80	3	0.0106	-
N_2	80	1	0.00365	1 [1.07]
Cl_2	80	1	0.0187	5.12
Cl_2	80	3	0.0190	-
N_2	80	1	0.000495	1 [0.136]
N_2	80	1	0.000557 *	1 [1.13]
HCl	80	1	0.00555	9.96
HCl	80	3	0.00786 **	-
N_2	80	1	0.00098	

The selectivities for N_2 given in the brackets refer to the change of the selectivity relatively to the permeability obtained for nitrogen previously at the same pressure and temperature.

* The membrane was evacuated for 80 hours before this test was performed. The membrane has been discoloured during the chlorine test; this might be due to degradation of the sealing (some kind of silicone rubber) used in the mounting of the membrane in the module.

** The sealing broke under this test, but fortunately the test had been performed long enough so that a result was obtained. It was necessary to clean the module with a mixture of acetone / ethanol due to degradation products in the module. The membrane was so brown that it also was flushed with the mixture. Every part of the module (Except the membrane itself) was dried with paper before the module was assembled. The membrane was evacuated for 2 hours before the last nitrogen measurement was performed

Second sample

Pressure [bar]	**Gas**	**Temp** [°C]	**Permeance** [m^3(STP)/ (m^2 bar h)]	**Selectivity** (gas/N_2)	**Comment**
1	N_2	30	0.00479	-	
3	N_2	30	0.00393	-	
1	N_2	30	0.00465	-	
1	N_2	30	0.00440	-	
3	N_2	30	0.00369	1	
1	N_2	30	0.00452	1	
1	O_2	30	0.00555	1.23	
3	O_2	30	0.00494	1.34	
1	Cl_2	30	0.0545	12.1	Exposed for 1500 s
3	Cl_2	30	0.0564	15.3	Exposed for 1500 s
1	N_2	30	0.000188	1 [0.04]	After two weeks (1209600 s) of Cl_2 exposure at 30 °C and 1.05 bar
3	N_2	30	0.000145	1 [0.04]	
1	O_2	30	0.000183	0.97 [0.04]	
1	Cl_2	30	0.00168	8.94 [0.37]	Exposed for 4000 s
3	Cl_2	30	0.00218	15.0 [0.59]	Exposed for 11000 s
1	N_2	30	0.0000761	0,5	
1	N_2	30	0.0000714		After 1st regen.
1	N_2	30	0.000323		After 2nd regen.

Total exposure time: 1 227 600s at 30 C.

The selectivities are calculated with reference to the nitrogen tests performed under the same conditions.

The first regeneration: The module and membrane were heated to 80 °C and pressurised to 1 bar of N_2 gas. Evacuating the low-pressure side insured a stable pressure gradient over the membrane. This regeneration lasted for 16 hours, and then the permeability was measured the usual way. As it can be seen from the table of results, this procedure had no significant effect. It is believed that the silicone sealing used in the module are not stable for temperatures beyond 80°C. It seems like that the regeneration procedure had induced a slight discolouring of the membrane.

The second regeneration: The membrane was disassembled from the module, and put into an external heating camber. In here the membrane was heated up to 120 °C, put under vacuum and left for 16 hours. The temperature was allowed to decrease slowly, to avoid any crack formations in the glass. When the glass was removed from the heating chamber, it was noticed that the discolouring had become serve.
It looks like the temperature as much as the silicone sealing used might cause the colour change. None of the regeneration procedures tried here seems to be sufficient enough, although the last procedure gives a four-time increase of the flux.

Appendix 9-2: HCl separation (Low surface coverage membrane)

All tests are performed at 30 °C and 1 bar.
(New module)

Gas type	Permeance [m^3 (STP)/(m^2 bar h)]	Selectivity N_2 reference	HCl exposure length [s]	Permeability decay [10^{-5}/s]
N_2	0.00106	1 ref		
O_2	0.00181	1.7		
H_2	0.00488	4.6 {1 ref}		
HCl	0.0224	21 {4.6}		
N_2	0.000896	1 ref.0.85	3600	4.3
O_2	0.00151	1.7		
H_2	0.00463	5.2 {1 ref}		
HCl	0.0301	34 {6.5}	86400	0.070
N_2	0.000842	0.94		

Appendix 10 C1+C18 surface-modified glass membrane

Appendix 10-1: Chlorine separation

All permeances are measured at 30 °C and given in m^3(STP)/(m^2 bar h).

(old module)

Gas	Permeance at 1 bar	Selectivity at 1 bar, N_2 as reference	Comments
Nitrogen	0.000657	1	
Oxygen	0.000960	1.5	
Nitrogen	0.000795	1 [1.2]	
Nitrogen	0.000818	1	Ref.
Oxygen	0.000906	1.1	
Chlorine	0.00906	11	Exposed for 3600 s
Nitrogen	0.000641	1 [0.81]	
Oxygen	0.000770	1.2	
Chlorine	0.00772	12	Exposed for 3600 s
Nitrogen	0.000515	1 [0.80]	After 48 hours of evacuation. New sealing in the module
Oxygen	0.000710	1.4	
Chlorine	0.00940	18.2	Exposed for 4500 s
Nitrogen	0.000694	1 [1.3]	
Nitrogen	0.000689	1.0	
Oxygen	0.000731	1.05	
Chlorine	0.00925	13.2	Exposed for 3800 s
Nitrogen	0.000541	1 [0.78]	New sealing in the module
Oxygen	0.000870	1.6	
Chlorine	0.00889	16	Exposed for 4000s
Nitrogen	0.000592	1 [1.1]	
Oxygen	0.000491	0.83	The reason for this sudden drop is not discovered.
Nitrogen	0.000522	1[0.88]	
Oxygen	0.000634	1.21	

The sealing showed a slight degradation on the high-pressure side each time the module was remounted. This degradation was in an early stage and only an area around the metal pipe was attacked. By visual inspection the dept of the degraded layer was estimated to be approximately .5 mm.

After the membrane had been stored in a desiccator for 14 days, (The time the other parallel were measured) it was remounted. The nitrogen and oxygen permeabilities

were measured twice, to see if the storage had affected the membrane. The glass membrane was then demounted and placed in a glass durability chamber.
The chamber was evacuated over night and then filled with 1.1 bar Cl_2 at 30 °C. After 5 days the chamber was emptied, flushed with N_2 and evacuated over night. The membrane was remounted in the module and the module was evacuated over night before the last permeation tests were performed.

All permeability fluxes are measured at 30 °C and given in $m^3(STP)/(m^2\ bar\ h)$.

Gas	Permeance at 1 bar	Selectivity at 1 bar, N_2 as reference	Comments
Nitrogen	0.000751	1 [1.4]	
Oxygen	0.000919	1.2	
Nitrogen	0.000774	1 [1.03]	
Oxygen	0.000954	1.2	
Nitrogen	0.000329	1 [0.42]	After 5 days Cl_2 exposure (432000)
Nitrogen	0.000332	1.0	
Oxygen	0.000332	1.0	
Chlorine	0.00205	6.2	Exposed for 3750 s
Nitrogen	0.000325	0.98	
Oxygen	0.000330	1.0	
Nitrogen	0.000555	1[1.7]	After 5 days Cl_2 exposure (432000)
Nitrogen	0.000531	1 [0.95]	
Oxygen	0.000508	0.96	
Nitrogen	0.000530	1.0	Evacuated for 60 hours
Oxygen	0.000502	0.96	
Chlorine	0.000195 0.00155	2.9	Exposed for 4300 s The first flux is measured after 1000s, the last one is measured after 15000 s
Nitrogen	0.000644		Error in measurement, too short evacuation
Nitrogen	0.000539	1.0	
Oxygen	0.000503	0.96	
80 %O_2 20 %Cl_2	0.000477 0.000573		The first flux is measured after 1000s, the last one is measured after 15000 s Estimated; exposed for 4200s (pure Cl_2)
Nitrogen	0.000586	-	Short evacuation (2 hours)
Nitrogen	0.000536	1.0	
Oxygen	0.000518	0.97	
55%O_2 45 %Cl_2	0.000447 0.000756	-	The first flux is measured after 500s, the last one is measured after 15000 s Estimated; exposed for 7900s (pure Cl_2)

Gas	Permeability flux at 1 bar	Selectivity at 1 bar, N_2 as reference	Comments
Nitrogen	0.000532	1.0	
Oxygen	0.000507	0.95	
28 %O_2 72 %Cl_2	0.000384 0.00111		The first flux is measured after 500s, the last one is measured after 15000 s Estimated; exposed for 18700 (pure Cl_2)
Nitrogen	0.000550	1.0	
Oxygen	0.000513	0.93	
13 %O_2 87 %Cl	0.000388 0.00118		The first flux is measured after 500s, the last one is measured after 7000 s Estimated; exposed for 6950s (pure Cl_2)
Nitrogen	0.000538	1 [0.98]	
Oxygen	0.000506	0.94	
Chlorine	0.000382 0.00129	2.4	The first flux is measured after 500s, the last one is measured after 4000 s Exposed for 4000
Nitrogen	0.000533	1.0	
Oxygen	0.000505	0.95	
Nitrogen	0.000528	1 [0.99]	After 19 days Cl_2 exposure (1641600 s)
Nitrogen	0.000509	1 [0.96]	
Oxygen	0.000471	0.92	
Nitrogen	0.000506	0.99	
Oxygen	0.000472	0.92	
Chlorine	0.000325 0.000811	1.6	The first flux is measured after 1000s, the last one is measured after 7000 s Exposed for 7000
Nitrogen	0.000510	1.0	
Oxygen	0.000459	0.90	
Nitrogen	0.000183	1 [0.36]	After 14 days Cl_2 exposure (1209600 s)
Oxygen	0.000181	0.99	
Chlorine	0.000134 0.000384	2.1	
Nitrogen	0.000208	1 [1.1]	
Oxygen	0.000196	0.94	

Second sample

All permeability fluxes are measured at 30 °C and given in m^3(STP)/(m^2 bar h).(old module)

Gas	Permeance at 1 bar	Selectivity at 1 bar, N_2 as reference	Comments
Nitrogen	0.00192	1	
Oxygen	0.00230	1.2	
Nitrogen	0.00194	1.0	
Oxygen	0.00209	1.1	
Chlorine	0.0118	6.1	Exposed for 3600 s
Nitrogen	0.00190	1.0	
Oxygen	0.00210	1.1	
Chlorine	0.0115	6.0	Exposed for 4000 s
Nitrogen	0.000614	1.0 [0.32]	After 8 hours of evacuation. New sealing in the module. Module exposed to air for 24 hours
Oxygen	0.000775	1.3	
Chlorine	0.00907	15	Exposed for 3700 s
Nitrogen	0.000676	1.0[1.1]	
Oxygen	0.000778	1.2	
Chlorine	0.0110	16	Exposed for 3900 s
Nitrogen	0.000650	1.0 [0.96]	
Oxygen	0.000721	1.1	
Chlorine	0.0105	16	Exposed for 4100s
Nitrogen	0.000771	1 [1.2]	New sealing in the module
Oxygen	0.000877	1.1	
Nitrogen	0.000795	1.0	
Oxygen	0.000924	1.2	

Total chlorine exposure time is 19300 seconds.

The sealing showed a slight degradation on the high-pressure side each time the module was remounted. This degradation was in an early stage and only an area around the metal pipe was attacked. By visual inspection the dept of the degraded layer was estimated to be approximately .5 mm.

Appendix10-2: HCl separation

(New module)

Gas	Permeance [m^3(STP)/(m^2 bar h)]	Selectivity (N_2 ref, H_2 ref in {})	N_2 perm. decay [10^{-5}/s]	HCl exposure time [s]
N_2	0.00587	1 {0.42}		
O_2	0.00764	1.3 {0.56}		
H_2	0.0137	2.3 {1}		
HCl	0.0291	5.0 {2.1}		4 700
N_2	0.00564	0.96	0.83	
H_2	0.0138	2.3 {1}		

Appendix 11 C12 surface-modified glass membrane

All permeability fluxes are measured at 30 C and given in [m^3(STP)/(m^2 bar h)].

(Old module)

Gas	Permeability flux at 1 bar	Permeability flux at 3 bar	Permeability flux at 1 bar	Selectivity at 1 bar (Averaged) with N_2 as reference	Selectivity at 3 bar with N_2 as reference
Nitrogen	0.00580	0.00594	0.00570	1	1
Oxygen	0.00716	0.00741	0.00735	1.26	1.25
Chlorine	0.0422 Exposed for 3600 s	0.0412 Exposed for 1500 s	0.0410 Exposed for 1500 s	7.23	6.94
Nitrogen	0.00130	0.00135	0.00116	0.21 [New reference]	0.23 [New reference]
Oxygen	0.00164	0.00167	-	1.33	1.23
Chlorine	0.0147 Exposed for 3500 s	0.0164 Exposed for 2800 s	-	12.0	12.1
Nitrogen	0.000579	0.000545	-	0.47 [New reference]	0.40 [New reference]
Nitrogen	0.000574	0.000622	-	1	1.1
Chlorine	0.0129 Exposed for 2500 s	0.0114 Exposed for 2000 s	-	22.5	20.9
Nitrogen	0.000295	0.000309	-	0.51	0.57

The second results for the permeabilities at one bar are performed after the three bar tests. Since the results seem relatively pressure stable, the second run were only performed in the first screening test (the upper four rows in the table). The corresponding selectivities at one bar are based on the average value of the involved gases.

Between increasing pressures, only a short evacuation have been performed. When the test pressure is lowered the evacuation were extended to at least two hours.

Between the different gases, evacuation over night has been used.

The thicker solid line above the three last rows in the table indicates that the sealing of the module were changed prior to these tests.

Total chlorine exposure time: 17400 s at 30 C

Appendix 12 Pf-C10 surface-modified glass membrane

Appendix 12-1: Nitrogen adsorption isotherm, unexposed sample.

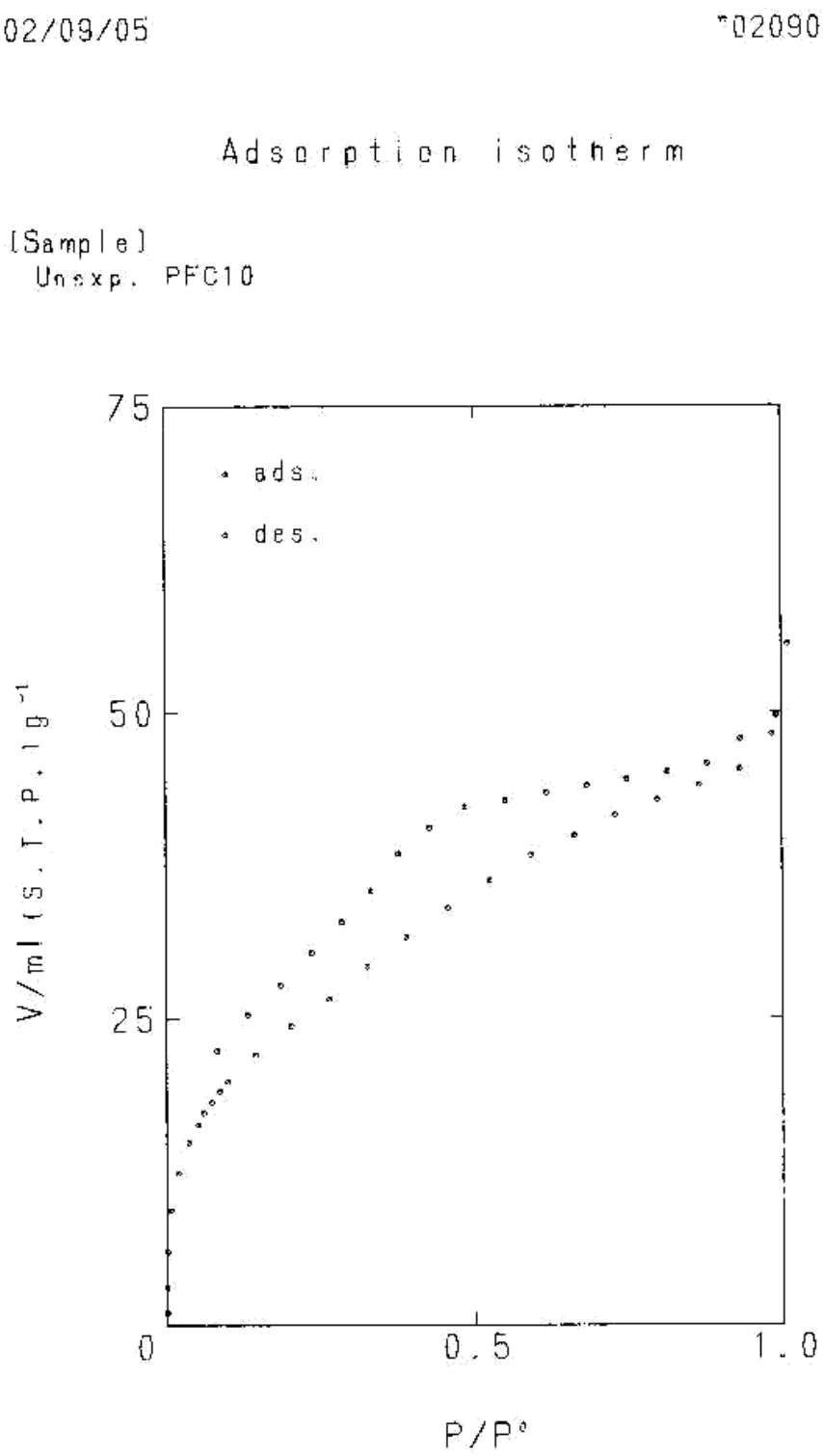

Nitrogen adsorption isotherm, chlorine exposed sample.

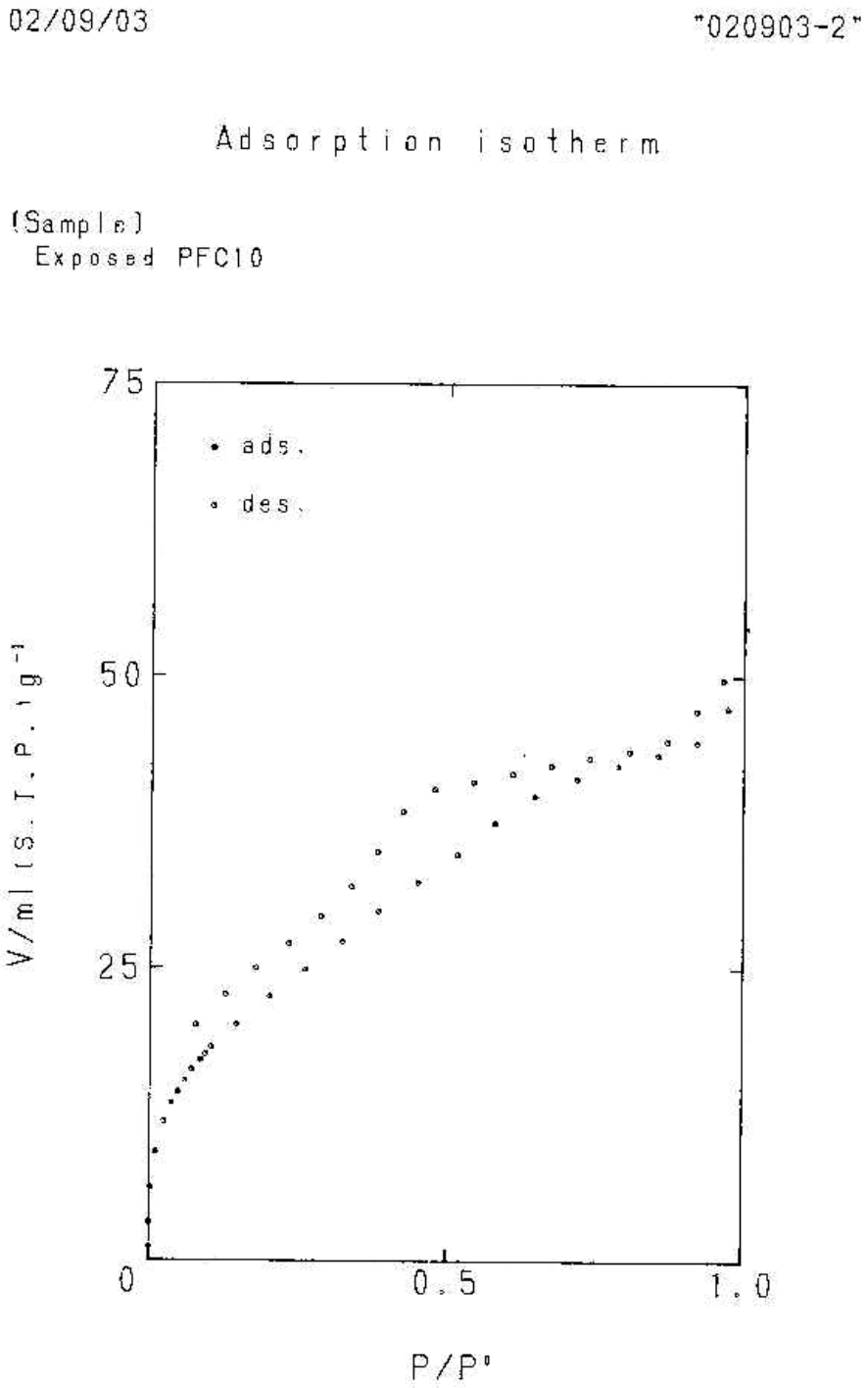

Appendix12-2: BET-plot, unexposed sample.

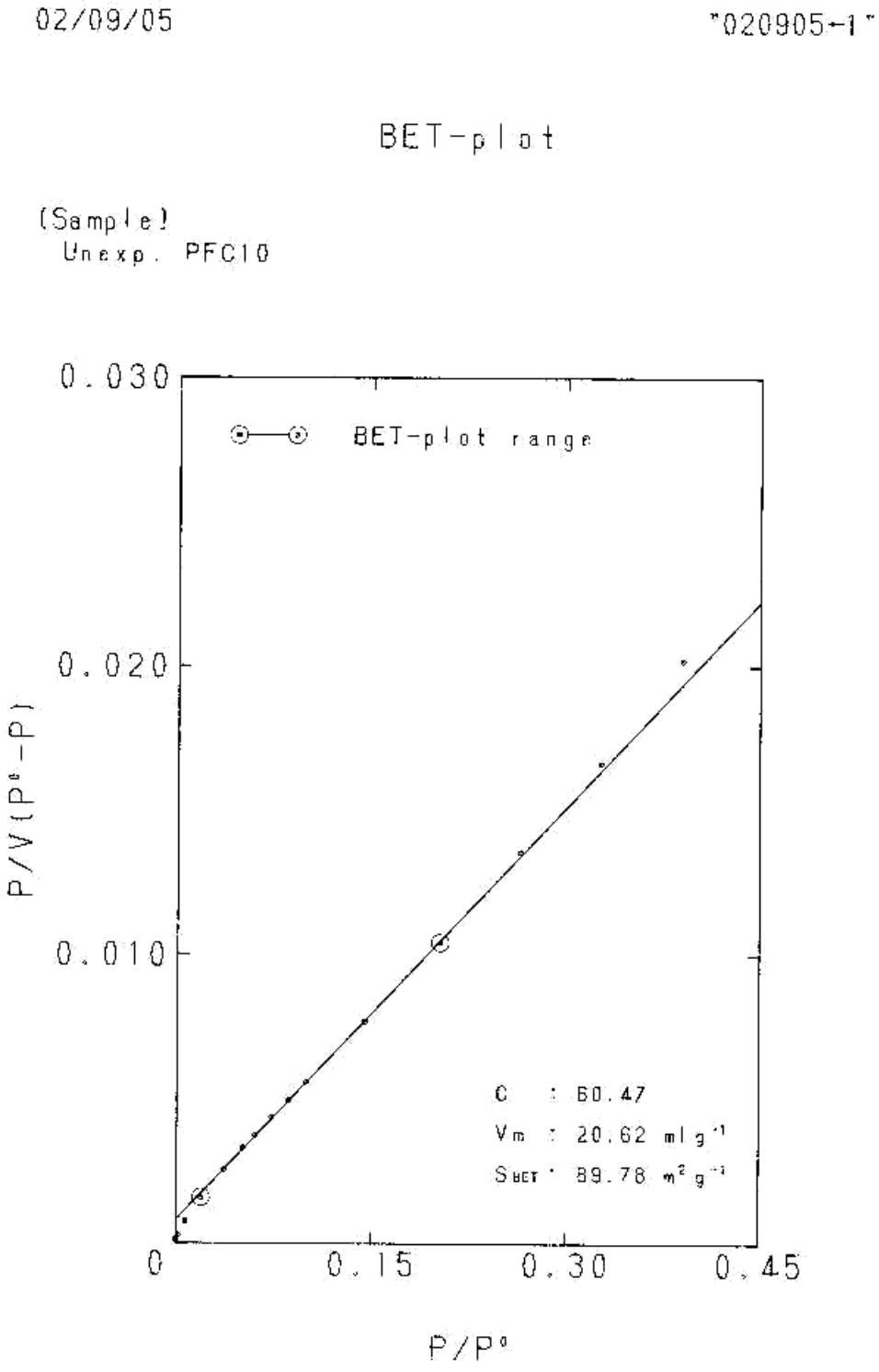

BET-plot, chlorine exposed sample.

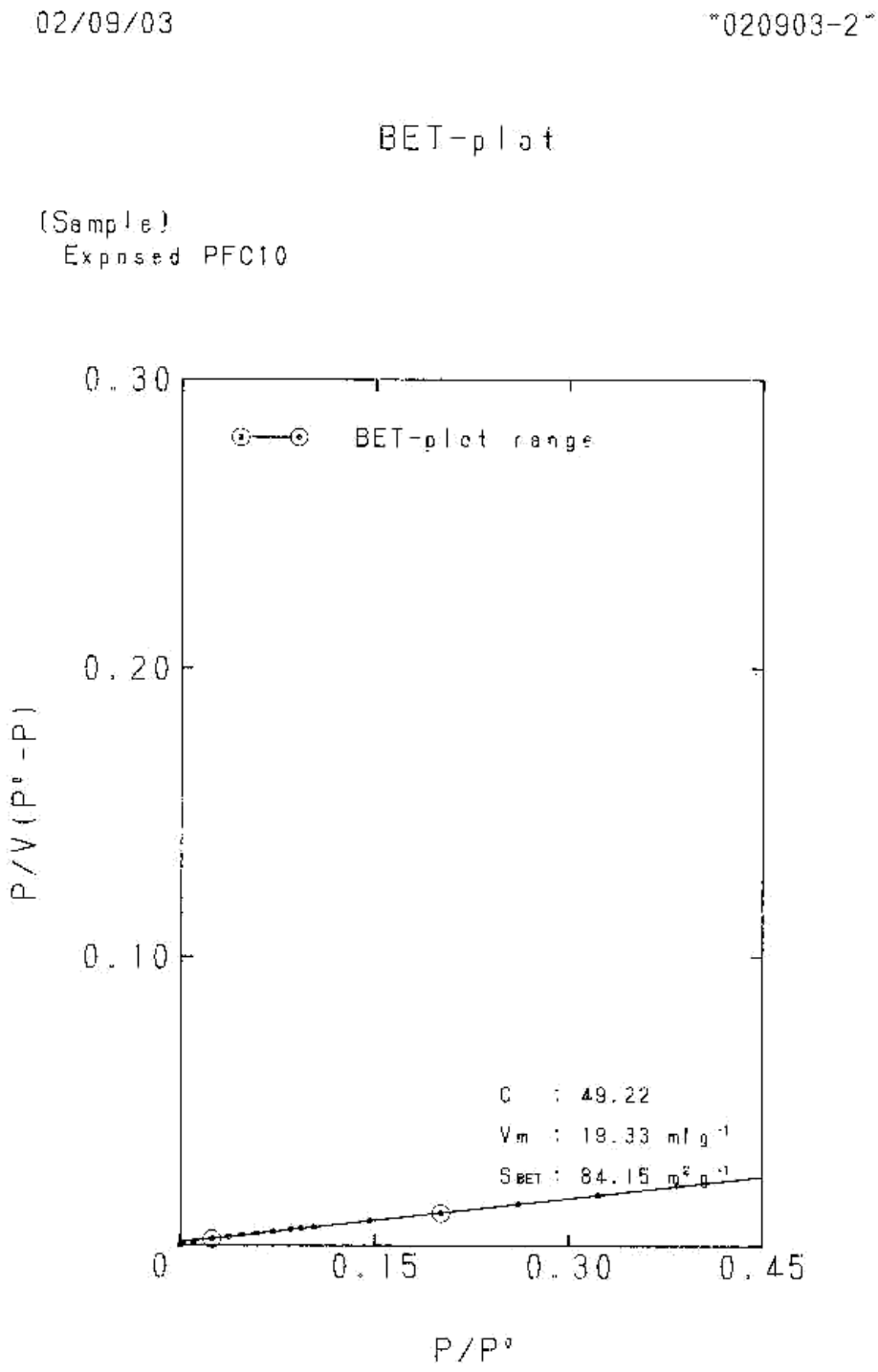

Appendix12-3: Permeance measurements.

Cl_2 separation

All fluxes are measured at 31-34 °C and given in [m^3 (STP)/(m^2 bar h)]

(New module)

Type of gas	Pressure difference [Bar]	Permeability flux	Selectivity (gas /nitrogen)	Chlorine exposure time*	$\Delta(P/l)_{N2,(relative)}$ / exposure time [1/s]·10^5
N_2	1	0.00803	-		
N_2	1	0.00796	1 (reference)		
O_2	1	0.00927	1.2		
Cl_2	1	0.02051	2.6	1h	
N_2	1	0.00752	0.94		1.48
N_2	1	0.00752	1 (New reference)		
O_2	1	0.00883	1.2		
N_2	1	0.00745	1.0		
Cl_2	1	0.02153	2.9	10h	
N_2	1	0.00752	1.0		-0.014
N_2	3	0.00745	1 (reference)		
O_2	1	0.00876	1.2		
O_2	3	0.00876	1.2		
N_2	1	0.00752	1.0		
N_2	1	0.00759	1.0		
			Static chlorine exposure	168 h	
N_2	1	0.00657	0.87		0.021
N_2	3	0.00657	0.87		
O_2	1	0.00788	1.0 (1.2 §)		
O_2	3	0.00796	1.1 (1.2 §)		
Cl_2	1	0.02029	2.7 (3.1 §)	1h	
Cl_2	3	0.02146	2.9 (3.3 §)	1.5h	
N_2	1	0.00672	0.89 (1.0 §)		
N_2	3	0.00679	0.89 (1.0 §)		
			Static chlorine exposure	336h	
N_2	1	0.00847	1.1		-0.022
N_2	3	0.00745	1.0		
N_2	1	0.00861	1.1		
O_2	1	0.01000	1.3 (1.2§)		
O_2	3	0.00883	1.2 (1.2§)		
Cl_2	1	0.02380	3.2 (2.8§)	1h	
Cl_2	3	0.02248	3.0 (3.0§)	0.5h	
N_2	1	0.00839	1.1 (0.99§)		

Type of gas	Pressure difference [Bar]	Permeability flux	Selectivity (gas /nitrogen)	Chlorine exposure time*	$\Delta(P/l)_{N2,(relative)}$ / exposure time $[1/s]\cdot 10^5$
			Static chlorine exposure	504h	
N_2	1	0.00888	1.2		-0.00305
N_2	3	0.00764	1.0		
O_2	1	0,01082	1.4 (1.2§)		
O_2	3	0.00907	1.2 (1.2 §)		
NB	see	below			
N_2	1	0.00582			
N_2	3	0.00598			
O_2	1	0.00730	1.3		
O_2	3	0.00730	1.3		
Cl_2	1	0.02016	3.5		
Cl_2	3	0.02139	3.6		
N_2	1	0.00650	1.1		0.00263 (total)
N_2	3	0.00645	1.1		

The chlorine exposure times are given for the duration of each experiment (cumulative total chlorine exposure time is 1023 hours)

§ "local selectivity based on the first nitrogen permeances measured after each long-term chlorine exposure

Prior to the "gap" in the table some problems with one union on the module was encountered. There might have been a leakage there for some time, possible causing the pressure dependency for the O_2 and N_2 experienced in the "middle" of the table

HCl separation

All permeances are measured at 30 °C.

Permeances given in [m^3 (STP)/(m^2 bar h)] (New module)

Gas	Pressure [bar]	Permeance	Selectivity (N_2 reference)	HCl exp time [s]	Perm. Decay [10^{-5} 1/s]
N_2	1	0.0115	1		
H_2	1	0.0291	2.5 [1 |H2]		
H_2	3	0.0291	- [1 |H2]		
O_2	1	0.0124	1.1		
HCl	1	0.0181	1.6 [0.62 |H2]	1500	
HCl	3	0.0217	- [0.75 |H2]	600	
N_2	1	0.0106	0.92 (new ref.)		4.0
H_2	1	0.0276	2.6 [0.95 |H2]		
H_2	3	0.0277	-[0.95 |H2]		
HCl	1	Static exposure	-	8 208 000 (95 days)	
N_2	1	0.00975	1(new ref.) 0.92		$9.8 \cdot 10^{-4}$
O_2	1	0.0106	1.1		
H_2	1	0.0247	2.5 [1 |H2]		
H_2	3	0.0250	- [1 |H2]		
HCl	1	0.0197	2.0 [0.80 |H2]	5000	
HCl	3	0.0202	- [0.81 |H2]	1500	
N_2	1	0.00920			
N_2	1	0.00913			NB! Regenerated@ 80°C and 1 mbar for 2 hours prior to this measurement.

Appendix 13 Pf-C10 (2 nm) surface-modified glass membrane

Appendix13-1: N2-adsorption isotherm.

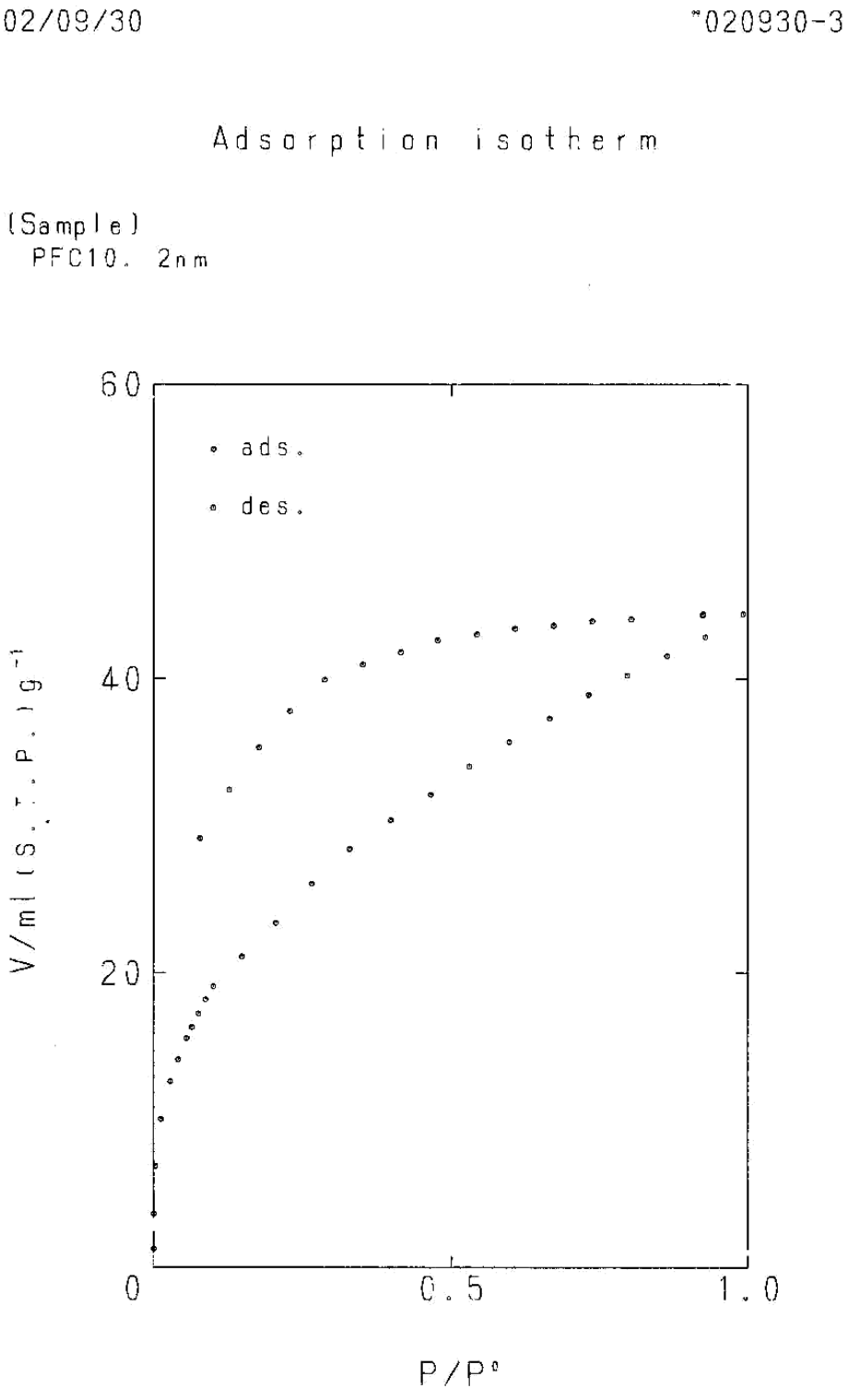

Appendix13-2: BET-plot.

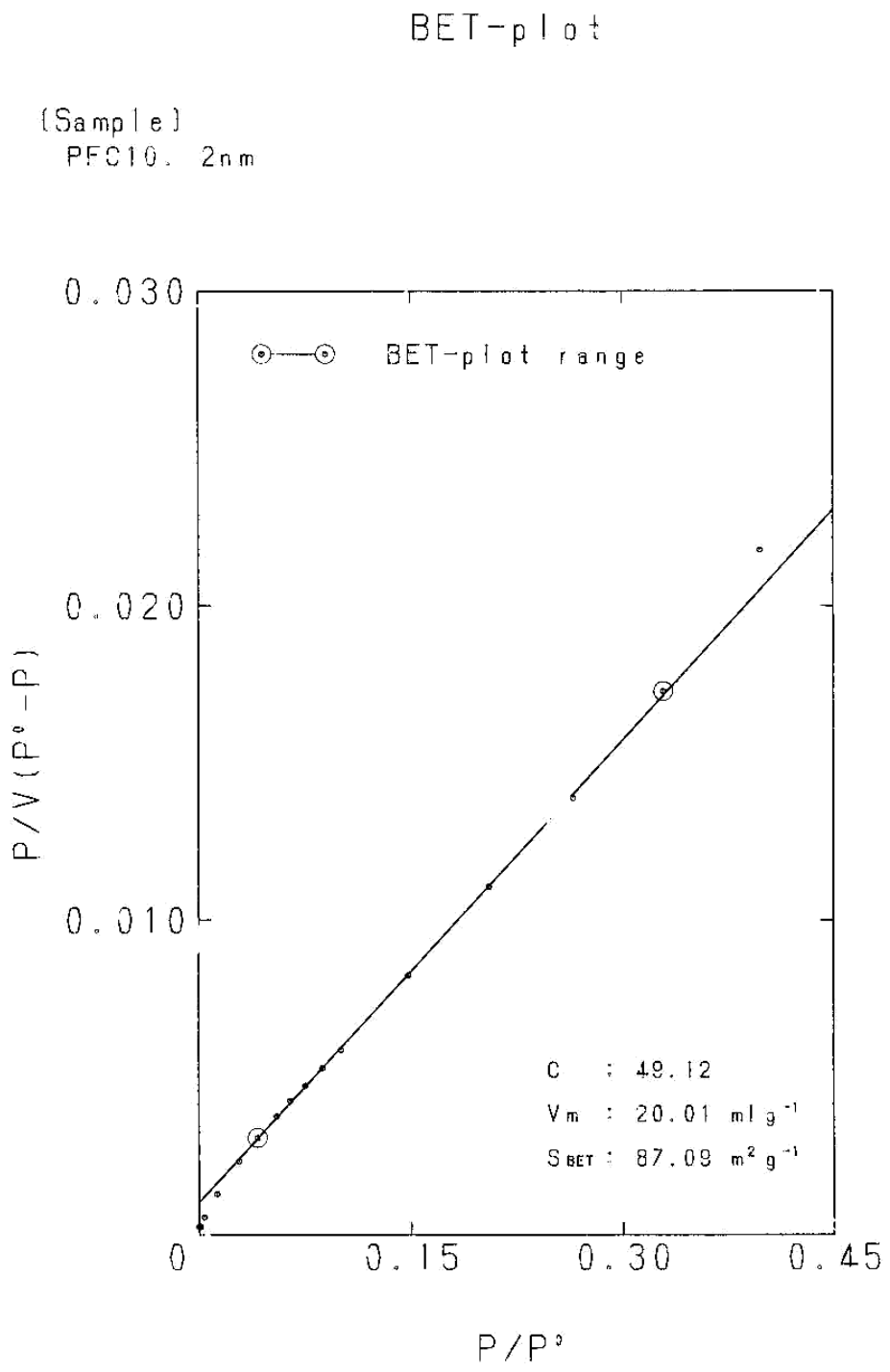

Appendix13-3: Permeance measurements.

All permeances are given in [m^3 (STP)/(m^2 bar h)] and measured at 30 °C

Gas type	Pressure [bar]	Permeance	Selectivity (Gas / N_2) [-]	Perm. Decay [1/s]
N_2	1	0.00576	-	
N_2	3	0.00694	-	
O_2	1	0.00752	1.3	
O_2	3	0.00905	1.3	
Cl_2	1	0.0328	5.7	Cl_2 exp. Time: 4000s
Cl_2	3	0.0327	4.7	Cl_2 exp. Time:3000s
N_2	1	0.00503	0.87	$1.81 \cdot 10^{-5}$
N_2	3	0.00516	0.74	
		Stored 1 month in the desiccator		
N_2	1	0.00496	1 (0.86)	
N_2		0.00491	1 (0.70)	
O_2	1	0.00688	1.4	
O_2	3	0.00690	1.4	
		Static chlorine exposure	63 days at 30 °C and 1 bar	Cl_2 Exp Time: $5.44 \cdot 10^6$s
N_2	1	0.00122	0.24	
N_2	3	0.00135	0.27	
O_2	1	0.00292	2.4 (0.58)	
O_2	3	0.00315	2.3 (0.64)	
N_2	1	0.00266	0.54	$8.52 \cdot 10^{-8}$
N_2	3	0.00269	0.55	
N_2	1	0.00290	1 (0.58)	
N_2	3	0.00296	1 (0.60)	
O_2	1	0.00417	1.4	
O_2	3	0.00427	1.4	
Cl_2	1	0.0274	9.4	Cl_2 Exp Time: 2500s
Cl_2	3	0.0250	8.4	Cl_2 Exp Time: 2400s
N_2	1	0.00398	1 (1.4)	$(3.63 \cdot 10^{-8})$ See comment
N_2	3	0.00407	1 (1.4)	
HCl	1	0.0147	3.7	
HCl	3	0.0229	5.6	
HCl	0.5	0.018		
HCl	0.5	0.00591/0.00219/ 0.0223		See comment on next page
HCl	1	0.0269	3.7	
N_2	1	0.00439	1.1	$(2.11 \cdot 10^{-8})$
N_2	3	0.00442	1.1	

Comments to the table

- The permeability decays displayed in brackets are calculated with the permeability prior to the 63 days long chlorine exposure as the before reference.
- The three flux values given for the 0.5 bar HCl test are given as a curiosity, since the pressure vs. time plot used to determine the permeability flux was showing four regions with a stable dp/dt as indicated by the numbers 1 to 4 in figure A13-1:

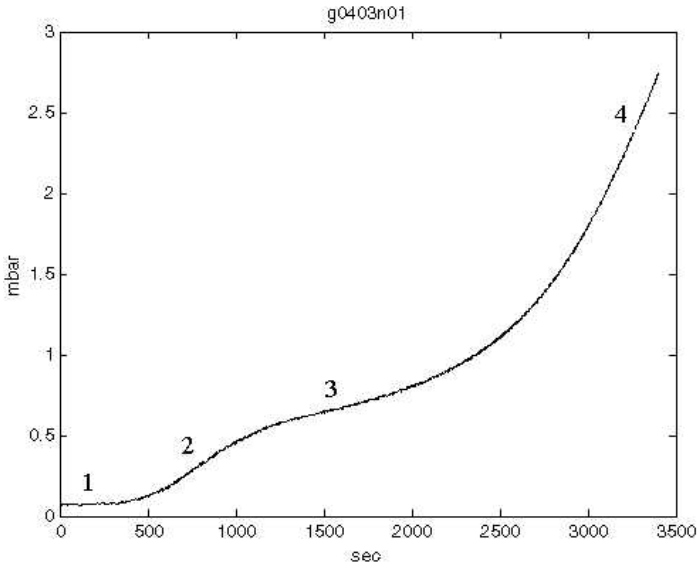

Figure A13-1: Experimental p vs. t dependence for HCl permeability at 0.5 bar (absolute).

As can be seen from the first gap in the table, storage in a desiccator does not significantly alter the membrane performance.

After the long-term chlorine exposure no mis-coloring of the membrane could be detected visually. However, a blurry layer had deposited on the surface. The (partial) removal of this layer as a consequence of several evacuations between the succeeding tests after the chlorine exposure may explain the rise in the permeability flux for nitrogen after the oxygen (and HCl) measurement.

Appendix 14 Glass hollow fibre

Appendix14-1: Cl_2 separation (New module)

All tests are performed at 30°C and are given in the unit [m^3 STP/(m^2 bar h)]

Gas	Permeance	Selectivity [-] (N_2 base)	N_2 perm. decay [10^{-5} /s]	Cl_2 Exposure time [s]
N_2	0.00241	-		
N_2	0.00239	1		
O_2	0.00181	0.76		
O_2	0.00186	0.78		
He	0.00795	3.3		
He	0.00723	3.0		
H_2	0.00984	4.1		
H_2	0.0101	4.2		
Cl_2	$4.73 \cdot 10^{-5}$	0.020		96000
N_2	0.00129	0.53	0.48	
HCl	0.00145	0.61		85000(HCl)
N_2	0.00129	0.53		

Temperature dependence

First parallel:

Gas type	Temp. [°C]	Permeance [m^3 STP / (m^2 bar h)]	Selectivity (N_2 ref.)	Exposure time [s]	Perm. decay [10^{-5} s]
N_2	30	0.00363	-		
N_2	30	0.00348	1		
Cl_2	30	0.000785	0.22	96000	
		(0.00140*)	0.40		
N_2	30	0.00308	1 [0.86]		1.41
N_2	80	0.00139!	-		
N_2	80	0.000428!	-		
N_2	80	0.000239	1		
Cl_2	80	0.000185	0.77	200 000	
		0.000271!	1.1 #		
N_2	80	0.000293	1.2		-
N_2	30	0.000103			0.48
leak	30	dp/dt = $2.1 \cdot 10^{-6}$ [bar/h]			

* Speeding up as a function of time

! Slowing down as a function of time

Selectivity lost, most likely is the self leakage of the cabinet the dominant flux. dp/dt = $6.9 \cdot 10^{-6}$ [bar/h]

Second parallel

Gas type	Temp. [°C]	Permeance [m^3 STP / (m^2 bar h)]	Selectivity N_2 ref	Perm. decay 10^{-5} [1/s]	Exp. time [s]	dp/dt [bar/h]
N_2	30	0.000232	1			
leak	30	-				$1.90 \cdot 10^{-6}$
O_2	30	0.0001943	0.84			
Cl_2	30	0.00006602	0.28	0.24	170 000	$1.97 \cdot 10^{-6}$
N_2	30	0.0001376	0.59			
N_2	80	0.0002489	1			
O_2	80	0.0002049	0.82			
Cl_2	80	0.0001759	0.71	0.14 (at 80 °C)	190 000	$5.11 \cdot 10^{-6}$
N_2	80	0.0001838	0.74			
leak	80	-				$4.52 \cdot 10^{-6}$
N_2	30	0.000650*				
leak	30					$2.04 \cdot 10^{-6}$

* The glue seal seems to be leaking gas and bypassing the membrane since the outside-in leakage, measured in the last measurement, is similar to the start-up leakage.

Appendix14-2: HCl separation

All tests are performed at 30 °C and 1 bar. The permeances are given in $[m^3(STP)/(m^2\ bar\ h)]$

(New module)

Gas	Permeance $\cdot 10^5$*	Selectivity [-]	N_2 perm decay $[10^{-5}$ /s]	HCl Exposure time [s]
N_2	5.89	1 [Ref]		
O_2	10.1	1.7		
H_2	267	45		
HCl	2.19	0.37 {122; H_2}		530900 (Dynamic)
N_2	5.09	1 [0.86]	0.026**	
H_2	72	14		

* A single fibre was mounted in the module so the membrane area is small leading to low permeation values. The HCl permeance value is so small that it can not be distinguished from the leakage of the cabinet.

** This perm decay is possibly an underestimate since the nitrogen measurements are having a great variance. The change in the H_2 flux as a consequence of the HCl exposure is much greater (27 % of original flux for H_2 compare to 86% of original flux for N_2)

Temperature dependence.

Permeances given in: [m^3(STP)/(m^2 bar h)]

Gas type	Temp. [°C]	Permeance	Selectivity N_2 ref [H_2 ref]	Perm. decay 10^{-5} [1/s]	Exp. time [s]	dp/dt [bar/h]
N_2	30	0.000229	1 [0.092]			
H_2	30	0.00248	11 [1]			
HCl	30	0.0000598	0.25 [0.024]	0.16	183 000	$1.94 \cdot 10^{-6}$
N_2	30	0.000162	0.71 [-]			
N_2	80	0.000255	1 [0.12]			
H_2	80	0.00217	8.5 [1]			
HCl	80	0.000193	0.75 [0.089]	0.29 (80°C)	110 500	$5.6 \cdot 10^{-6}$
N_2	80	0.000173	0.68			
N_2	30	0.000232		$-4.4 \cdot 10^{--3}$ (Total)		
leak	30					$1.90 \cdot 10^{-6}$

Appendix14-3: Mounting of fires into a larger sized module

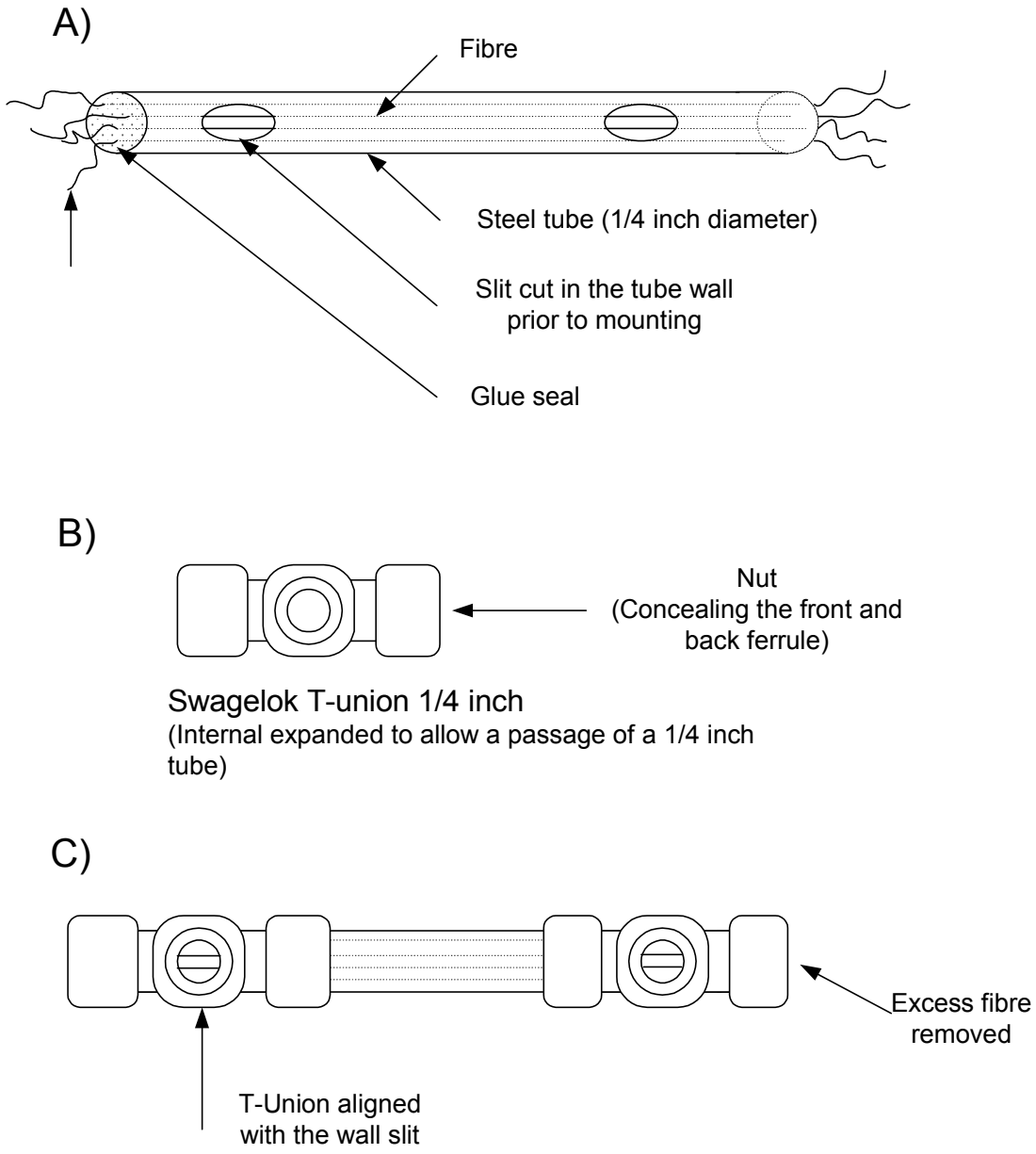

Figure A14-1: Three step procedure for making a larger scaled fibre module.

The mounting is planned as a three step procedure as sketched in figure A14-1:

A) A ¼ inch (diameter) steel tube is cut ca 3 cm shorter length than the available fibre length. Approximately 2 cm from each end a ca 0.5x 1.0 cm slit is cut in the tube wall. The internal gradients have to be grinded off using a grinding paper in order to prevent possible accidental fibre rupture during mounting. The fibres are threaded into the tube and each side is glue sealed using epoxy glue. (I.e. Araldite ® AV 138M). The glue is left for hardening for some hours (as will be discussed in section C, it is important that the glue is not completely hardened).

B) The two Swagelok ¼ inch tee-unions have to be modified, because their original internal diameter in the length direction is 0.19 inch. The diameter must obviously be greater than 0.25 inch in order to be able to slide the union onto the tube. The internal diameter may be increased by drilling using a proper sized bore (i.e. 9/32 inch).

C) Before the glue is completely hardened, the unions with the ferrules should be slid onto the tube and the unions should be aligned with the wall slit (In such a manner that it is possible to see the fibres through the perpendicular part of the tee) both ferules on each union (lengthwise) are then tightened according to the manufacturer recommendation. The tightening of the ferules will cause the tube wall to be slightly deformed, therefore the glue must still have some flexibility left; otherwise the glue may crack, or squeeze the fibre into fracture.

Appendix 15 Spontaneity estimations

Chlorine substitution

The following simple substitution reaction is used to describe the stability of an alkane when exposed to chlorine gas:

$$CH_4 + 4Cl_2 \rightarrow CCl_4 + 4HCl$$

From /Zumdahl/ the following thermodynamic data of formation is found:

Table A-15.1 Standard enthalpy of formation, $\Delta H°_f$, and standard entropy $\Delta S°$.

Compound	$\Delta H°_f$[kJ/mol]	$\Delta S°$ [J/(mol·K)]
CH_4	-75	186
Cl_2	0	223
CCl_4	-135	216
HCl	-92	187
H_2	0	131

Given the Hess' summation law, for the reaction enthalpy:

$$\Delta H^0_{Rx} = \sum_{i=products} n_i \cdot \Delta H^0_{f,i} - \sum_{j=reactants} n_j \cdot \Delta H^0_{f,j}$$

Where $\Delta H°_{rx}$ is the reaction enthalpy [kJ/mol] and n is the stoichiometric coefficient [-]. This law can also be applied to calculate the entropy change for the reaction.

$$\Delta S^0_{Rx} = \sum_{i=products} n_i \cdot \Delta S^0_i - \sum_{j=reactants} n_j \cdot \Delta S^0_j$$

By inserting the corresponding values from table A-15.1 the following results are obtained:

$\Delta H°_{Rx}$, = -428 kJ/mol and $S°_{Rx}$=-114 J/(mol·K).

The spontaneity is evaluated by the familiar thermodynamic relation

$$\Delta S_{universe} = -\frac{\Delta G^0}{T} = -\frac{\Delta H^0}{T} + \Delta S^0$$

A spontaneous process requires that the $\Delta S_{univ}>0$; Thus, $\Delta H/T>\Delta S$ leading to $T<\Delta H/\Delta S$

Inserting the calculated values, yields: T<3754 K

"The chlorination is "always" thermodynamic spontaneous"

HCl substitution

Consider the following (hypothetic!) substitution reaction:

$$CH_4 + 4HCl \rightarrow CCl_4 + 4H_2$$

By inserting values from table A-15.1, $\Delta H°_{Rx}$, = 308 kJ/mol and $S°_{Rx}$=-194 J/(mol·K) are obtained.

Thus, this process is spontaneous if T< -1587 K. Meaning it never will happen since the absolute temperature has to be positive.

“The Hydrogen chloride substitution is “never” thermodynamic spontaneous”

Ref: Zumdahl, S. S.:”Chemical principles” C.C. Heath and company, 1992.